Imperial College
London

Process Development using Organic Solvent Nanofiltration (OSN) for Oligonucleotide Synthesis

A thesis submitted in fulfillment of the requirements for the Doctor of Philosophy degree

Jeong Kim

March 2014

Department of Chemical Engineering

Imperial College of Science, Technology, and Medicine

Abstract

Following the discovery of RNA interference (RNAi) and its exquisite control of protein expression, oligonucleotide (oligos) based drugs have been considered as the next generation of therapeutics, as they can deliver the treatment at the protein expression level. Oligos are short chains of nucleotides, typically 15-28 base-pairs long, synthesized in an iterative manner by sequential addition of nucleotide monomers. As of year 2014, there are currently 3 FDA approved oligo-based drugs, and over 100 candidates are going through clinical trials. The current mainstream synthesis platform is solid-phase oligo synthesis (SPOS) which is fast and efficient, but difficult to scale-up. This thesis discusses work to develop a versatile liquid-phase oligo synthesis (LPOS) platform to manufacture oligos at large scale using emerging Organic Solvent Nanofiltration (OSN) technology. By attaching the growing oligos chain to a soluble, monodisperse, and branched polyethyleneglycol (PEG) support and operating entirely in liquid-phase, excess reagents and impurities can be filtered out using polybenzimidazole (PBI) OSN membranes. This process neatly solves cumbersome purification problems while allowing high reaction rates and a large reaction volume. With the proposed process, 5-mer and 9-mer 2'-OMe oligoribonucleotides have been successfully synthesized. The synthesis chemistry and membrane purification procedures have been modified to suit the LPOS platform. The transport of solutes through the PBI membranes has been studied in detail which revealed both size-exclusion and ion-exchange behavior. An economic analysis showed the competitiveness of the LPOS-OSN process, but also the necessity for a solvent recovery unit. Several key challenges, both expected and unexpected, have been identified, and appropriate solutions have been implemented. One of the main challenges was the low process yield, which was overcome through the use of membrane cascades. An adsorptive solvent recovery unit was also investigated to reduce the overall solvent consumption. Notably, employing a membrane reactor combined with a smaller protecting group (methoxyisopropyl ether, *i.e.* MIP, MW 74 Da) significantly simplified the overall process (9 to 3 unit operations per chain extension cycle). It is envisaged that the proposed LPOS platform can be used synergistically with the current SPOS platform to stimulate further growth in the field of oligo therapeutics. Furthermore, through the process development work using OSN technology, an effort was made to understand the gap between membrane science in academia and membrane technology in industry.

Declaration of Originality

I hereby certify that the work reported herein was originated mainly from me and this thesis was written by me. All of the process design and membrane separation experiments were carried out by me, the chemical syntheses of oligonucleotides were carried out together by Dr. Gaffney and me, the chemical synthesis of MIP building blocks was done together by Mr. Alex G. Molina and me at the University of Turku, Finland, and the polybenzimidazole membranes used in this work were fabricated by Ms. Irina Valtcheva. Deprotected oligonucleotides have been characterized by Dr. Glynn Williams. Information derived from the published and unpublished work of others has been acknowledged in the text, and a list of references is given.

Jeong Kim



March 2014

Copyright Declaration

The copyright of this thesis rests with the author and is made available under a Creative Commons Attribution Non-Commercial No Derivatives license. Researchers are free to copy, distribute or transmit the thesis on the condition that they attribute it, that they do not use it for commercial purposes and that they do not alter, transform or build upon it. For any reuse or redistribution, researchers must make clear to others the license terms of this work.

Acknowledgement

The past years in London have been an exciting journey. It passed by so fast that it is hard to believe the end is near. I have truly enjoyed this project and made memories I will cherish forever. I have met a lot of new people, all of whom helped me to grow as a person and as a researcher.

First and foremost, I am deeply grateful for Professor Andrew Livingston for giving me this Ph.D opportunity at Imperial College London under his supervision. His continual guidance, limitless support, and insightful advices throughout this project have been, and will always be, deeply appreciated.

Very special thanks to Dr. Piers Gaffney, my mentor, colleague, and a friend. We for sure had countless heated arguments and discussions, some a bit off the chart, but such debates really helped me to think more objectively and critically. His incomprehensible knowledge in chemistry has always been the key element in this project to obtain tangible results. Thank you Piers!

I would like to acknowledge EC Marie Curie FP7 grant (PITN-GA-2008-238291-MEMTIDE) for funding this project, and I thank all the project partners involved, especially to Irina Valtcheva, a great colleague and an amazing friend. I will remember our frequent breaks to get "unbored" during difficult moments in our Ph.D. I also thank Alex G. Molina for helping me to synthesize MIP monomers in freezing Turku with fantabulous steaming saunas.

I thank the group members for many helpful discussions during our group meetings and fun nightouts with countless pints of beer. I can't miss out Dr. Ludmilla Peeva for her help and her "magic hands" in the lab, Dr. Gyorgy Szekely for unbelievable motivation and drive he showed to inspire me, Mr. Marc Hagenschlagen for his generous scone offers and evening music selections. I am grateful for friendly office gang whom I met almost every day, and special thanks to Ms. Raluca Leonte for her help and assistance with everyday matter.

I must thank all the Imperial College Korean Society friends for many unforgettable memories (among the ones I remember). This society was basically my so-called "social life" during my time in London and undoubtedly *the* vitamin to keep my sanity. I thank you all!

Last but not least, I thank my parents for showing me the definition of endless love and altruistic support. After many years of living abroad, I may finally be coming home soon!

This thesis is dedicated to you all.

Table of Contents

List of Figures XI

List of Tables XVI

List of Acronyms and Symbols XVI

List of Publications XVIII

Chapter 1: Project Motivation, Thesis Structure, and Literature Review

1.1. Project Motivation & Objectives 2

1.2. Thesis Structure 5

1.3. Literature Review 7

1.3.1. Membrane Technology 7

1.3.1.1. Background 7

1.3.1.2. Membrane Classification 8

1.3.1.3. Organic Solvent Nanofiltration (OSN) 11

1.3.1.4. OSN Membrane Types 12

1.3.1.5. OSN Membrane Fabrication 13

1.3.1.6. Membrane Performance Characterization 14

1.3.1.7. Performance Prediction and Transport Models 16

1.3.1.8. Concentration Polarization and Mass Transfer Coefficient 18

1.3.1.9. Process Configuration and Scale-up Parameters 20

1.3.2. Oligonucleotide Chemistry 21

1.3.2.1. Basic Chemistry 21

1.3.2.2. Phosphodiester Method 23

1.3.2.3. Phosphotriester Method 25

1.3.2.4. Phosphite triester Method and Phosphoramidite Method 26

1.3.2.5. H-phosphonate Method....28
1.3.3. Summary....29

Chapter 2: New Liquid-Phase Platform for Oligonucleotide Synthesis using Organic Solvent Nanofiltration (OSN) Technology

2.1. Summary....31
2.2. Introduction....32
2.3. Experimental....38
2.3.1. Materials....38
2.3.2. PBI 17DBX Membrane Fabrication & Testing Rig....38
2.3.3. Justification for Using a Branched Hub: Linear PEG versus Branched PEG Homostar Support....39
2.3.4. Overall Process Schematic & Oligonucleotide Synthesis Chemistry....43
2.3.4.1. Initial Loading....44
2.3.4.2. Chain Extension & Detritylation procedure....46
2.3.4.3. Membrane Purification – Constant Volume Diafiltration (CVD)....47
2.3.4.4. Final deprotection and purification....48
2.3.5. Analytical Method....48
2.3.5.1. High Performance Liquid Chromatography (HPLC)....48
2.3.5.2. Nuclear Magnetic Resonance (NMR) & Mass Spectrometry (MS)....49
2.4. Results and Discussion....49
2.4.1. Membrane Screening & Characterization....49
2.4.2. Chain Extension & Detritylation (combining reaction and diafiltration)....50
2.4.2.1. Identification of Compounds in the Post-Reaction Crude Mixture....50
2.4.2.2. Ion Exchange Transport through PBI membranes....53
2.4.2.3. Synthesis of 9-mer....54

2.4.2.3. Solubility of the Growing Oligonucleotidyl Homostar 55
2.4.2.4. LPOS-synthesized oligonucleotide yield 56
2.4.4. Final Deprotection and Purity Analysis 57
2.4.5. Economic Analysis 59
2.4.6. Further Discussions: advantages and current challenges 63
2.5. Conclusions 64

Chapter 3: Developing a Membrane Cascade

3.1. Summary 67
3.2. Introduction 68
3.3. Experimental 71
3.3.1. Materials 71
3.3.2. Preparation of Polyimide and Polybenzimidazole (PBI) Membranes 71
3.3.3. Membrane Screening 72
3.3.4. Process Modeling 73
3.3.5. Single-Stage Diafiltration 75
3.4. Results and Discussion 77
3.4.1. Constant Volume Diafiltration (CVD) Parameters 77
3.4.3. Single-Stage Diafiltration 79
3.4.4. Model Predictions and Effect of Recycle Ratio (r_C) 80
3.4.5. Effect of Operating Pressure 82
3.4.6. Two-Stage Cascade Diafiltration 83
3.5. Conclusions 88

Chapter 4: Membrane Cascade with Solvent Recovery: Pharmaceutical Separation Case Study

4.1. Summary 91

4.2. Introduction....92
4.3. Experimental....94
4.3.1. Materials....94
4.3.2. Preparation of Polybenzimidazole (PBI) Membranes....94
4.3.3. Membrane Rejection Test....94
4.3.4. Single Stage Diafiltration....95
4.3.5. Two Stage Diafiltration....96
4.3.6. Charcoal Isotherm Determination & Solvent Recovery....96
4.3.7. Analytical Methods....98
4.4. Results and Discussion....98
4.4.1. Membrane Selection & Single Stage Diafiltration (SSD)....99
4.4.2. Two Stage Diafiltration (TSD)....101
4.4.3. Solvent Recovery – Adsorption Isotherm & Feasibility assessment....104
4.4.4. Economic & Green Metrics Analysis....108
4.5. Conclusions....115

Chapter 5: Process Intensification of Liquid-Phase Oligonucleotide Synthesis (LPOS) Platform Through Membrane Reactor and New Protecting Group Chemistry

5.1. Summary....117
5.2. Introduction....118
5.3. Experimental....122
5.3.1. Materials....122
5.3.2. Membrane Fabrication and Membrane Diafiltration Rig....122
5.3.3. Oligonucleotide Synthesis Protocol....124
5.3.4. Solving the First Challenge: Complete Removal of Excess Monomers....124
5.3.4.1. Modification of Chain Extension Reaction Protocol (Figure 5.1a)....124

5.3.4.2. Acid Doping of PBI Membranes....126
5.3.5. Solving the Second Challenge: Bulky 5'-O Protection....126
5.3.5.1. Synthesis of 5'-O-MIP Phosphoramidite Monomer....126
5.3.5.2. Oligo synthesis with 5'-O-MIP....127
5.3.5.3. Deprotection Equilibrium Study (Effect of Solvent and Acid)....127
5.3.5.4. In-situ Deprotection in the Rig: Concept of Membrane Reactor....128
5.3.6. Solving the Third Challenge: Improving the Yield....129
5.3.7. Global Deprotection and Final Purity Analysis....130
5.3.8. Analytical Methods....130
5.4. Results and Discussion....130
5.4.1. Solving the First Challenge: Incomplete Removal of Excess Monomers....130
5.4.1.1. Effect of Water and BDT on Oligos Synthesis....130
5.4.1.2. Effect of PBI Membrane Doping with Acid....133
5.4.2. Solving the Second Challenge: Bulky 5'-O-protection....133
5.4.3. Effect of Cascade, Yield and Purity Analysis....139
5.5. Conclusions....143

Chapter 6: Conclusions, Critical Assessment, and Future Direction

6.1. Overall Conclusions....145
6.2. Critical Assessment and Future Direction....148

References....152

Appendix is attached as a separate PDF file.

List of Figures

Figure 1.1. A schematic of the solid-phase oligonucleotide synthesis (SPOS) platform. The growing oligos is anchored onto a solid bead in a packed-bed reactor, and the reaction proceeds at the solid-liquid interface. After each reaction, the excess reagents are washed away from the bead using neat solvent. The cycle is repeated until the desired sequence is obtained.

Figure 1.2. Basic schematic of a membrane separation process: typically smaller component(s) selectively pass through the membrane, driven by a chemical potential gradient (**Δμ)**, *i.e.* pressure or concentration gradient.

Figure 1.3. Summary of filtration processes and their operating size range shown with respective solutes.

Figure 1.4. Two fundamental transport mechanisms of membrane processes: pore-flow and solution-diffusion, discussed in further detail later.

Figure 1.5. Cross-sectional view of common types of filtration membranes: a) symmetric membranes with uniform morphology throughout the thickness; b) asymmetric membranes with active skin layer on the top and porous support layer below made out of same material; c) TFC membranes with thin active layer on top of a support layer made out of different material. Typically, the active layer performs the actual separation while the support layer provides mechanical support.

Figure 1.6. A standard MWCO curve of a membrane where different MW solutes are plotted versus their corresponding rejection values.

Figure 1.7. Illustration of the concentration polarization layer on the feed side of a membrane surface. The notation used for film theory derivation: C_b, C_m, and C_p refer to the solute concentrations at the bulk, membrane, and permeate, respectively.

Figure 1.8. a) Basic nucleotide structure and five bases. R = H (in DNA), OH (in RNA); b) structure of poly(nucleotide).

Figure 1.9. General oligonucleotide synthesis scheme with appropriate protecting groups. One monomer is added sequentially to the 5' position. For RNA synthesis, the R group in the 2' position is –OH and it's protected with appropriate group.

Figure 1.10. First published example of the phosphodiester approach, only coupling step is shown using *N,N′*-Dicyclohexylcarbodiimide (DCC).

Figure 1.11. Dimethoxytrityl (DMT) protecting group on 5' hydroxyl group.

Figure 1.12. Nucleoside base protecting groups suggested by Khorana.

Figure 1.13. Phosphotriester method. One of the oxygen atoms in the P atom is protected to prevent branching and build-up of anionic charge.

Figure 1.14. Example of P(III) and P(V) oxidation state compound.

Figure 1.15. Phosphite triester method. The P atom is in the more reactive P(III) state until oxidation step.

Figure 1.16. Phosphoramidite method, the chloride leaving group in the P(III) state monomer is replaced with an amine group, allowing more robust handling with similar efficacy.

Figure 1.17. H-Phosphonate method scheme in solution, all reactions proceed *in situ*

Figure 2.1. Basic schematic of the proposed LPOS-OSN process composed of 4 unit operations per cycle: a) chain extension; b) first membrane diafiltration to wash out excess reagents; c) deprotection of 5'-*O* using acid; and d) second membrane diafiltration.

Figure 2.2. Diagram of membrane testing & diafiltration rig. Four membrane cells (effective membrane area of 51 cm^2 per cell) were connected in series (N = 4). The feed tank was pressurized using nitrogen, and the system level was maintained by constant addition of pure solvent back into the

feed tank.
Figure 2.3. The effect of rejection on the overall concentration profile (*i.e.* diafiltration yield *versus diavolumes* at different solute rejections).
Figure 2.4. Comparison between linear *versus* branched PEG rejection on PBI 17DBX membranes. Linear PEG rejection, regardless of the PEG MW, do not exceed 95%. Branched PEG compounds exhibit higher rejections and approach 100% above 3,000 Da.
Figure 2.5. The proposed LPOS platform: overall process flowchart. The process is split into three phases: initial loading, chain extension cycle, and final purification. Each phase of the protocol is discussed in detail in the experimental section.
Figure 2.6. The proposed LPOS platform: overall chemistry scheme for the same three phases.
Figure 2.7. Excess monomers identified during the chain extension cycle. Thioamidate (**6a,** Dmtr or H) and amidate (**6b,** Dmtr or H) are neutral species, whereas monothioate (**6c,** Dmtr or H) and dithioate (**6d,** Dmtr or H) are charged species.
Figure 2.8. Analysis of a typical chain extension cycle, from mU loaded homostar **3** to 5'-*O*H dinucleotidyl homostar **8**. HPLC of feed, retentate and permeate **a)** after chain extension, but before detritylation, and **b)** after detritylation. Small molecule reagents – PADS, ETT, and pyridine – permeate through the PBI membrane in a), but monomer-related species are retained; after detritylation excess monomers permeate, but Dmtr-pyrrole only permeates partially. **c)** ^{31}P NMR of retentates in a), red, and b), blue. Three classes of monomers (except thioamidate **6a**) are present before detritylation, but are absent after detritylation. **d)** MALDI-TOF+ MS confirming the presence of compound **7** and **8**. Also, N-deacetylation of cytosine base for **8**, a common impurity, is identified ([**8**−Ac+2H]$^+$ = 3495.6, calc. $C_{142}H_{212}N_{18}O_{71}P_3S_3^+$ = 3495.2).
Figure 2.9. Transport of anionic thioate monomers (**6a, 6b**, R=H) through PBI membranes via the ion-exchange mechanism. The cationic imidazole backbone allows anionic species to exchange between the sites, pushing out the thioates to the permeate side via concentration gradient.
Figure 2.10. HPLC chromatograms up to 7-mer oligos (from 9-mer preparation). Tritylated (-*O*Dmtr) compounds have longer retention times than detritylated (-*O*H) species. The peaks became too broad to be detected by HPLC after 7-mer.
Figure 2.11. Summary of chain extension yield and the corresponding overall yield, starting from the mononucleosidyl homostar **3** as the basis of calculation: The yield is calculated from the mass data and reported as molar yield, assuming 100% purity.
Figure 2.12. Final purity analysis by HPLC after global deprotection: a) 5-mer oligo prepared by LPOS-OSN using 1*vol*% DCA; and b) 5-mer oligo by LPOS-OSN using 1*vol*% Py.DCA; c) 9-mer by LPOS-OSN, then purified by ion exchange; d) 9-mer by SPOS after desalting. Purity is roughly estimated by integrating the product peak.
Figure 2.13. Overall breakdown of the cost of API purification: (left) with solvent disposal and (right) with 90% solvent recovery. The two largest fractions are the solvent and phosphoramidite monomer. Implementing a distillation solvent recovery unit significantly reduces the overall cost.
Figure 2.14. Sensitivity analyses to understand how changes in key parameters affect the overall cost: a) effect of monomer excess; b) effect of overall yield; c) effect of membrane area; and d) effect of monomer cost.
Figure 3.1. Calculation using the pore-flow model of the rejection of uncharged solutes by a membrane with uniform pore sizes (r_p) between 0.75 nm and 1.5 nm. This range covers molecular weights of most nanofiltration solutes (approximate MW shown). If the product and impurity solutes give indicated rejection values, the separation efficiency is too low to be

practical due to the broad rejection curve.
Figure 3.2. System diagrams of single-stage diafiltration and two-stage cascade diafiltration. For two-stage cascade diafiltration, the permeate from the first stage is directly connected to the feed of the second stage. The symbols in parentheses are the variables used in the process model (*Section 3.3.4*).
Figure 3.3. Single-stage CVD using M4-A(2) membrane. Dotted curve: Predicted solute mass in retentate using rejection from the screen. Solid curve: Best fit of model to experimental data. The differences in rejections between the screening results and the preparative CVD may be due to membrane aging. The yield of PEG-2000 after 13 *diavolumes* was 59%. The temperature stayed approximately constant at 22 ^{o}C.
Figure 3.4. Simulated effect of recycle ratio, r_C, on the yield and purity of PEG-2000 using M4-A in a two-stage cascade after 12 *diavolumes*. The parameters were obtained from the screening experiment. For comparison, single-stage purity and yield after 12 *diavolumes* are indicated.
Figure 3.5. The change of PEG rejection with pressure in M4-A(1) and M4-A(2) membranes. PEG-400 rejection is a strong function of pressure, whereas PEG-2000 rejection is not.
Figure 3.6. Total normalised mass of PEG-400 and -2000 during two-stage diafiltration using M4-A membranes, with recycle ratio, $r_C = 0.5$. Dotted curve: Predicted solute mass in the total retentate using rejection values from the screen. Solid curve: Best fit of model to PEG-2000 experimental data (PEG-400 is omitted for clarity). The yield of PEG-2000 was 94% at the same purity as from the single-stage diafiltration (i.e. 98%). The effective overall rejections of PEG-400 and PEG-2000 were 65.5% and 99.8%, respectively. Overall rejection values are back-calculated rejection for the entire system (including both first and second stage membranes).
Figure 3.7. Retentate concentration profiles for individual stages during two-stage CVD, with the recycle ratio, $r_C = 0.5$: **a)** Profile of the first stage using M4-A(1); **b)** Profile of the second stage using M4-A(2).
Figure 3.8. Comparison of PEG-2000 yield and purity between single- and two-stage diafiltrations over 12 *diavolumes*. The yield increased from 59% to 94% at the purity of 98% at $r_C = 0.5$.
Figure 4.1. System diagrams of single-stage diafiltration and two-stage cascade diafiltration. For two-stage cascade diafiltration, the permeate from the first stage is directly connected to the feed of the second stage. The symbols in parentheses are the variables used in the process model (Appendix A).
Figure 4.2. Chemical structure of the model compounds: roxythromycin (Roxi, 837 Da) API, ethyl tosylate (EtTS, 200 Da) and 4-dimethylaminopyridine (DMAP, 122 Da) GTI impurities.
Figure 4.3. Single stage diafiltration (SSD) normalized concentration profile using PBI membranes. Both GTIs were removed at virtually the same rate. Less than 5 ppm GTI purity has been achieved after 10 diavolumes with final yield of 58%.
Figure 4.4. Two-stage diafiltration (TSD) normalized concentration profile using PBI membranes. Recycle ratio (r_C) was set at a value of 0.5. GTI concentrations less than 5 ppm were again achieved after 10 *diavolumes* with the final API yield of 95%, a substantial improvement from SSD yield of 58%.
Figure 4.5. Predicted yield improvement after 10 *diavolumes* for different product rejection. The TSD configuration achieves significant yield improvement, overcoming the membrane limitation inherent in the SSD for rejection less than 99%. As long as the product rejection is above 90%, the process promises high product yield, making the process competitive to other

traditional unit operations.
Figure 4.6. Log-log plot of adsorption isotherm of GTIs on charcoal in methanol at 21°C. The Freundlich isotherm describes the adsorption behavior of two GTIs well.
Figure 4.7. (**a**) GTI permeate concentration at each *diavolume* before adsorption and the respective amount of charcoal used to extract pure solvent. Approximately 90% of GTI permeate in the first three *diavolume*, requiring over 70% of the overall charcoal used. (**b**) A typical UV-HPLC chromatogram of crude permeate (1st *diavolume* data shown) and recovered solvent, which shows no remaining impurity (C_{GTI} < LOD). Arrows show the extent to which initial permeate GTI content is reduced via solvent recovery.
Figure 4.8. Calculated economic benefit from solvent recovery plotted versus percentage of solvent recovered curve shows an optimum for solvent recovery. The calculation is based on the cost of solvent, charcoal, and waste disposal.
Figure 4.9. (left) Total purification cost per unit of API calculated for single-stage diafiltration (SSD) and two-stage diafiltration (TSD). The calculation includes the cost of API loss, solvent, membrane, charcoal, and waste disposal. **(right)** Summary of cost reduction for API purification compared to SSD by implementing TSD and TSD with 70% solvent recovery. The cost reduction is most significant when the cost of API is high. The difference between TSD and TSD+SR becomes considerable at lower API cost.
Figure 4.10. Mass Intensity (MI) comparison. The majority of fractions of MI comes from solvent use. TSD achieves lower MI than SSD in all cases.
Figure 4.11. Comparison of CO_2 footprint with and without solvent recovery, and of energy consumption for distillation and adsorption for solvent recovery, for commonly used organic solvents, for TSD.
Figure 5.1. Concept diagram illustrating the potential improvement from the **a)** original LPOS-OSN process to the **b)** simplified process using a membrane reactor with MIP protecting group. Application of a membrane reactor should reduce the number of unit operations from 9 to 3 per chain extension cycle (counting each solvent exchange step).
Figure 5.2. A concept diagram illustrating the use of membrane reactor for oligo synthesis. As the reaction is an equilibrium reaction, it can be pushed to completion by removing the compounds on the right-hand side of the equilibrium. However, the rejection of Dmtr group was too high to achieve 100% completion. The use of the smaller MIP group allows 100% deprotection and purification, combining reaction and separation into one unit operation.
Figure 5.3. Membrane diafiltration rig schematics: 1-stage configuration is the conventional mode, whereas the 2-stage cascade configuration (N=4 per stage) is employed to improve the process yield.
Figure 5.4. Overall chemistry scheme employed in this work: Initial loading and final purification procedures stayed the same as Chapter 2, but the chain extension cycle has been modified.
Figure 5.5. Synthesis protocol for 5'-*O*-MIP cytidine phosphoramidite. A bulk-scale synthesis was carried out until **12e**; the last step, phosphitylation to synthesize cytidine phosphoramidite **12f**, was carried out prior to each chain extension reaction.
Figure 5.6. Four types of phosphoramidite (PA) monomers after chain extension (**11a-d**). The 5th type, H-phosphonate **11e**, is only generated when the phosphoramidite comes in contact with water. Conventional chain extension method in Chapter 2 generates all four types of PA monomers, shown in black box. With the modified protocol, adding water then BDT/PADS converts all excess PA to monothioate **11c**, shown in green box.
Figure 5.7. Stacked ^{31}P-NMR spectra to illustrate the effect of water and BDT. Addition of water hydrolyzes all the monomers to H-phosphonate **11e**. As the peak shift for H-

phosphonate **11e** was the same with the amidate **11b** peak, ^{1}H NMR was used to identify the presence of H-phosphonate (Appendix D). Addition of BDT turns all the H-phosphonate into monothioate **11c**. Upon diafiltration after detritylation (***P*** = H), all monothioates were removed from the reaction mixture.

Figure 5.8. a) Speculated PBI polymer structures showing the effect of HCl doping, only one benzimidazole ring in the monomer was modified in the diagram to illustrate the concept. b) ^{31}P-NMR of retentate after diafiltration without HCl doping; c) ^{31}P-NMR of retentate after diafiltration with HCl doping.

Figure 5.9. HPLC chromatogram summarizing the membrane reactor in action for: a) Dmtr protection and b) MIP protection. Dmtr deprotection reaction proceeds to 5th *diavolumes* but reverts back as the acid concentration decreases. MIP deprotection reaction reaches completion due to the small size of MIP.

Figure 5.10. Yield improvement through 2-stage cascade configuration. 3-mer oligos was synthesized using MIP protection. The actual yield improvement in the 2-mer was lower than expected because a normal phase column was run on the final retentate. Nevertheless, the yield improved to near 100% in the 3-mer chain extension cycle.

Figure 5.11. HPLC chromatogram of each 3-mer synthesized after global deprotection, compared to a SPOS-prepared 3-mer. 3-mer synthesized before the HCl doping shows the lowest purity, with peak profiles significantly different compared to the chromatogram of SPOS-prepared 3-mer.

List of Tables

Table 2.I. Overall cost breakdown per 1kg batch of oligo
Table 3.I. Membrane compositions and preparation conditions
Table 3.II. PEG separation performance of the membranes. Tests were conducted in MeCN at 10 bar at 22 ^{o}C. Two coupons per membrane batch were tested
Table 3.III. Summary of comparison between single-stage and two-stage diafiltration for M4-A and M4-B membranes. All values are given in percentages
Table 4.I. Rejection and flux data at different transmembrane pressures
Table 5.I. Acid screening for MIP deprotection

List of Acronyms and Symbols

A/V	Area-to-Volume ratio	MWCO	Molecular Weight Cut-off
API	Active Pharmaceutical Ingredient	NF	Nanofiltration
BDT	3*H*-1,2-benzodithiol-3-one	NMI	*N*-methylimidazole
CVD	Constant Volume Diafiltration	NMR	Nuclear Magnetic Resonance
DBX	Dibromoxylene	oligos	Oligonucleotide
DCA	Dichloroacetic acid	OSN	Organic Solvent Nanofiltration
DCC	*N,N'*-Dicyclohexylcarbodiimide	PA	Phosphoramidite
DCM	Dichloromethane	PA	Polyamide
DLC	Diamon-like Carbon	PADS	Phenylacetyl disulfide
DMAc	*N,N*-Dimethylacetamide	PAN	Polyacrylonitrile
DMAP	4-Dimethylaminopyridine	PBI	Polybenzimidazole
DMF	*N,N*-Dimethylformamide	PEEK	Polyetheretherketone
Dmtr	Dimethoxytritylphenylmethyl ether	PEG	Polyethyleneglycol
ELSD	Evaporative Light Scattering Detector	PFM	Plate and Frame Membrane Module
Et_2O	Diethyl ether	PI	Process Intensification
EtOH	Ethanol	PIM	Polymers-of-Intrinsic-Microporosity
ETT	Dthylthiotetrazole	PS	Polysulfone
EtTs	Ethyl tosylate	Py.DCA	Pyridinium dichloroacetate
GTI	Genotoxic Impurity	r_C	Recycle Ratio
HCl	Hydrochloric acid	RO	Reverse Osmosis
HDA	Hexanediamine	Roxi	Roxythromycin
HFM	Hollow Fiber Membrane Module	SI	Solvent Intensity
HPLC	High Pressure Liquid Chromatography	SLM	Standard Liters per minute
IP	Interfacial Polymerization	SPOS	Solid-phase Oligonucleotide Synthesis
LOD	Limit-of-Detection	SR	Solvent Recovery
LPOS	Liquid-phase Oligonucleotide Synthesis	SRNF	Solvent Resistant Nanofiltratio
MeCN	Acetonitrile	SSD	Single Stage Diafiltration
MeOH	Methanol	SWM	Spiral Wound Membrane Module
MF	Microfiltration	TFA	Trifluoroacetic acid

MI	Mass Intensity	TFC	Thin Film Composite
MIP	Methoxyisopropyl ether	TM	Tubular Membrane Module
MMM	Mixed Matrix Membranes	TMA.Cl	Tetramethylammonium chloride
MOF	Metal Oragnic Framework	TSD	Two Stage Diafiltration
MS	Mass Spectrometry	UF	Ultrafiltration
MWCO	Molecular Weight Cut-off	CSTR	Continuously stirred tank reactor

Jv	Solvent Flux	$L.m^{-2}.hr^{-1}$
A	Membrane Area	m^2
B	Membrane Permeability	$L.m^{-2}.hr^{-1}.bar^{-1}$
Cb	Bulk Concentration	$g.L^{-1}$
Ce	Equilibrium concentration	$mg.L^{-1}$
$C_{p,i}$	Permeate Concentration of Component i	$g.L^{-1}$
$C_{R,i}$	Retentate Concentration of Component i	$g.L^{-1}$
C_m	Membrane Concentration	$g.L^{-1}$
C_o	Adsorbate initial concentration	$mg.L^{-1}$
D_i	Diffusion Coefficient of Component i	$m^2.s^{-1}$
F	Flowrate	$L.hr^{-1}$
k	Mass transfer coefficient	$m.s^{-1}$
K_F	Sorption Capacity - Freundlich Isotherm	--
m	Mass of the adsorbent	g
n	Sorption Intensity - Freundlich Isotherm	--
q_e	Amount of adsorbate in the adsorbent at equilibrium	$mg.g^{-1}$
Ri	Rejection of Component i	%
t	Filtration time	hr
V_{system}	System Volume	L
ΔP	Transmembrane Pressure	bar
$\Delta\pi$	Osmotic Pressure	bar

List of Publications

In Chronological Order

Szekely, G.; Valtcheva, I.; Kim, J. F.; Livingston, A.G., Molecularly imprinted organic solvent nanofiltration membranes – Revealing molecular recognition and solute rejection behavior, *React. Funct. Polym.*, **2014**, accepted.

Valtcheva, I.; Kumbharkar, S. C.; Kim, J. F.; Bhole, Y.; Livingston, A. G., Beyond polyimide: Crosslinked polybenzimidazole membranes for organic solvent nanofiltration (OSN) in harsh environments, *J. Membr. Sci.,* **2014**, *457,* 62-72.

Kim, J. F.; Szekely, G.; Valtcheva, I. B.; Livingston, A. G., Increasing the sustainability of membrane processes through cascade approach and solvent recovery-pharmaceutical purification case study, *Green Chem.,* **2014**, *16*, 133

Kim, J. F.; Freitas da Silva, A. M.; Valtcheva, I. B.; Livingston, A. G., When the membrane is not enough: A simplified membrane cascade using Organic Solvent Nanofiltration (OSN), *Sep. Purif. Technol.,* **2013,** *116*, 277-286.

Stawikowska, J.; Kim, J. F.; Livingston, A. G., Pore-flow calculations based on pore size distributions in polyimide membranes determined by a nanoprobe imaging technique, *Chem. Eng. Sci.,* **2013,** *97*, 81-95.

Imperial College London

Chapter 1

Project Motivation, Thesis Structure, and Literature Review

The overall objectives and the structure of the thesis are presented. Relevant current literatures on organic solvent nanofiltration (OSN) and oligonucleotide synthesis chemistry are compiled.

1.1. Project Motivation & Objectives

The field of oligonucleotide (oligo) therapeutics is expanding at an unprecedented rate, with over 100 oligo-based drug candidates currently undergoing clinical trials[1]. Following the recent FDA approval of Kynamro (mipomersen) in 2013, it is expected that more oligo-based drugs will soon obtain FDA approval, suggesting that at some point it will be necessary to produce such drugs at a scale of metric tons per year. However, there are as yet no synthesis platforms to manufacture oligo drugs in >10 kg per batch scale. Hence, to meet the forecast demand, there is a pressing need to develop a scalable manufacturing platform to synthesize such drugs at the metric ton scale per annum[2, 3].

The current state-of-the-art platform is solid-phase oligonucleotide synthesis (SPOS), where oligos are grown sequentially on solid supports in a packed-bed column. After each round of chain extension reaction, any excess reagents are simply washed away from the solid bead, leaving the growing oligos ready for the next step (illustrated in Figure 1.1). The synthesis procedure is completely machine-automated and highly efficient, such that a small-scale synthesis of a 23-mer oligo can be done within a day. Hence, the SPOS platform has been an excellent tool for small-scale users in research laboratories and clinical trials. However, due to its heterogeneous nature, the process suffers from high mass intensity (E-factor) and requires a large excess of oligo building blocks, the main cost element in the oligo synthesis[1]. These restraints place an economic burden when it comes to SPOS scale-up to commercial manufacturing scale, and the general consensus is that cost-effective SPOS scale-up is inherently difficult, if not impossible[4, 5].

To overcome this challenge, there have been many works on developing a liquid-phase oligonucleotide synthesis (LPOS) platform, as the liquid-phase processes are more readily scalable. The main challenge for LPOS lies in the separation of excess reagents during the cyclic protocol, as the growing oligo products are chemically similar to the oligo building blocks. Commonly employed separation techniques are precipitation[6, 7] and extraction[8], but none of the processes have yet taken off to commercial scale. In this work, it was envisaged that Organic Solvent Nanofiltration (OSN) technology could be an effective separation unit to develop a scalable LPOS platform.

An FP7 EC project named Membrane-Enhanced TIDE Synthesis (PITN-GA-2008-238291-MEMTIDE) was initiated in 2010 to develop a scalable TIDE synthesis platform. Project partners include Imperial College (*UK*), University of Turku (*Finland*), University of

Barcelona (*Spain*), Evonik-MET (*UK*), Lonza (*Switzerland*), and Janssen (*Belgium*). The roles of Imperial College were to develop a suitable membrane and process for TIDE (oligos and peptides) synthesis platform, with the help of oligo chemistry experts from University of Turku, peptide chemistry experts from University of Barcelona, membrane experts from Evonik-MET, and pharmaceutical process experts from Janssen and Lonza. I started at Imperial with a task of developing a LPOS-OSN platform; and Irina Valtcheva, Ph.D student from Imperial, was given a task to develop a suitable membrane for the platform.

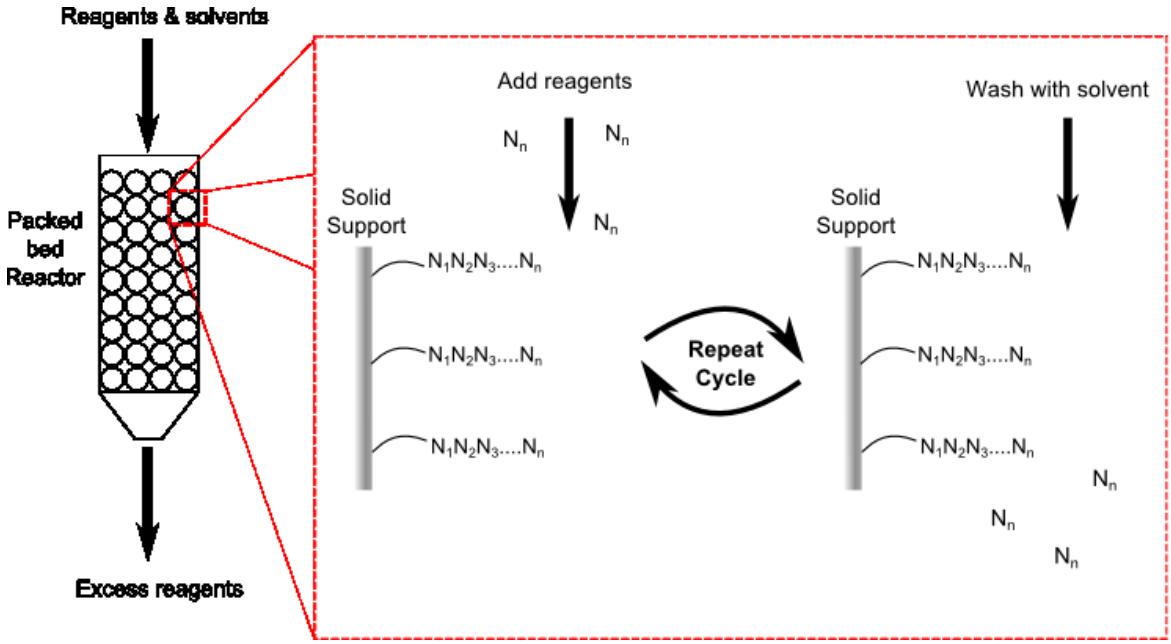


Figure 1.1. A schematic of the solid-phase oligonucleotide synthesis (SPOS) platform. The growing oligos is anchored onto a solid bead in a packed-bed reactor, and the reaction proceeds at the solid-liquid interface. After each reaction, the excess reagents are washed away from the bead using neat solvent. The cycle is repeated until the desired sequence is obtained.

OSN technology is a nanofiltration process that separates molecules in organic media in nano-range, primarily by exploiting the differences in size. In the past decade, OSN membranes have improved tremendously in regard to the solvent stability, longevity, separation performance, and flux[9]. Various types of OSN membranes with tailored performances can now be fabricated[10]. Boosted by such improvements, OSN has shown potential in wide range of applications such as pharmaceutical, fine chemicals, petroleum, and food industries[11-14]. However, only a few applications have actually taken off to commercial scale[15-17].

Albeit the promising potential of OSN has been shown with experimental evidence in the literature, there seems to be a considerable gap between membrane science in academia and

the actual membrane technology employed in industry. The technology transfer from the academia to industry appears slower than anticipated (and desired), which may be due to several interacting reasons, both business-related and technical limitations. For instance, OSN processes mainly target application-specific niche markets which are inherently risky from the business perspective. Blockbuster membrane markets such as water industry have not yet emerged in the OSN field. Also, many of the commercially available OSN membranes do not seem to give satisfactory performance, often making the process development stage longer than estimated.

Hence, one of the core objectives of this work was also to understand the reason for this gap through a LPOS process development project, and to narrow the identified gaps through process innovations. In short, the main objectives of this work were to:

1) Develop a scalable LPOS platform using OSN as the separation unit;
2) Understand the technical challenges of OSN which impede smooth commercialization;
3) Improve the OSN technology to reduce the gap between innovations in academia and realized capability in industry.

1.2. Thesis Structure

This thesis is composed of six chapters followed by a Bibliography and Appendix section. The first chapter is an introduction chapter justifying the main objectives and summarizing the overall contents of the thesis. The introduction chapter also covers the current literatures on the two main topics of this thesis: OSN membrane technology and oligonucleotide synthesis. More in-depth and detailed literature is discussed in the appropriate chapters. The next four chapters, Ch. 2~5, are the main body chapters where each chapter is written as a full paper format. A deliberate attempt was made to make each body chapter stand on its own. Hence, some crucial parts of the chapters are repeated. To keep the body chapters concise and succinct, supporting information has been compiled in the Appendix section of the thesis. Each body chapter is briefly summarized below.

Chapter 2 discusses the main objective of this work: developing a liquid-phase oligonucleotide synthesis (LPOS) platform. An extensive membrane screening was carried out to identify a suitable membrane, and the chemistry and purification procedures were developed to fit the overall scheme. An economic analysis was carried out to understand the competitiveness of the proposed platform and to identify the key economic parameters. Several key challenges were identified with possible solutions.

Chapter 3 proposes a solution to the low yield challenge of membrane processes through the use of membrane cascades. One of the key challenges with the LPOS platform was low yield. The concept of membrane cascades were proposed a long time ago but never fully exploited mainly due to the delicate control of interacting flows. An innovative cascade configuration that simplifies the control is proposed and tested on polyethyleneglycol (PEG) mixture. The key process parameters were identified and an appropriate process model has been developed.

Chapter 4 takes the cascade configuration proposed in Chapter 3 to the next level by implementing an adsorptive solvent recovery unit to recycle the solvent. Combining the cascade configuration with a solvent recovery unit improved the overall yield and reduced the solvent consumption significantly. The process was tested with a practical pharmaceutical application for genotoxins removal.

Chapter 5 tackles the key challenges identified in Chapter 2 by employing a membrane reactor concept combined with a new protecting group chemistry (methoxyisopropyl ether,

i.e. MIP protection). Understanding the transport of solutes through the polybenzimidazole (PBI) membrane elucidated the ion exchange behavior of anionic solutes through the PBI membranes. Yield and purity improvements as well as achieved process intensification are summarized.

Following the body chapters, the last chapter (Ch. 6) is a conclusion chapter reiterating the key findings with critical assessment of the overall work, and suggesting future directions.

1.3. Literature Review

1.3.1. Membrane Technology

The field of membrane technology is vast covering multiple disciplines and wide range of applications. In this review, the basic background knowledge in membrane technology is compiled with a particular focus on liquid applications and OSN. Also, to narrow the scope of the review, only solid polymeric membranes are considered.

1.3.1.1. Background

Selective separations of liquids and gases are commonly carried out using membranes. A general definition of membrane is: a layer of material that acts as a selective barrier between two phases[18], as shown in Figure 1.2. The transport and separation occurs using a difference in chemical potential as the driving force, which are typically pressure and/or concentration gradient.

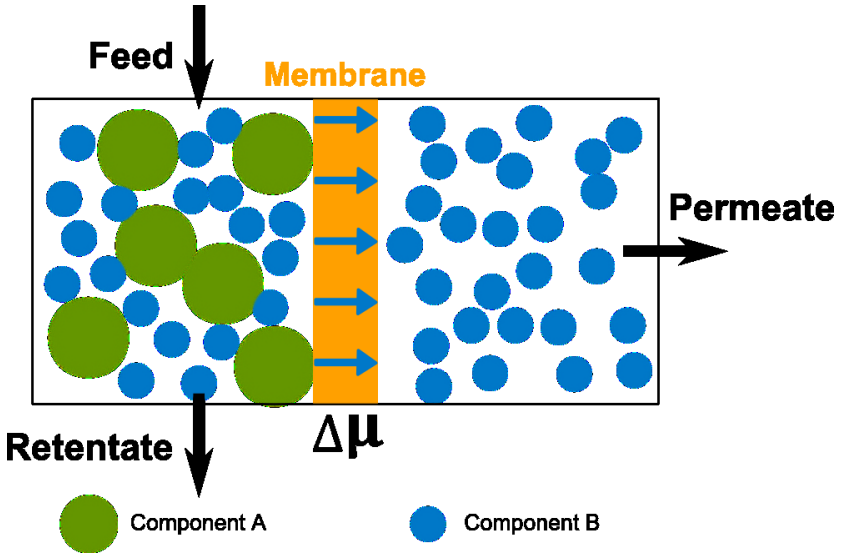


Figure 1.2. Basic schematic of a membrane separation process: typically smaller component(s) selectively passes through the membrane, driven by a chemical potential gradient (**Δμ**), *i.e.* pressure or concentration gradient.

In a typical membrane process, what gets fed into the membrane unit is called the "feed"; what goes through the membrane is called the "permeate"; what gets retained (or rejected) by the membrane is called the "retentate." The desired product(s) could either be in the permeate, retentate, or both.

Membrane processes have several unique advantages over other conventional separation units such as distillation, adsorption, extraction, and chromatography. A notable advantage is the energy efficiency, as in many cases a pressure gradient is all it takes to achieve a desired

separation. In chemical industries, separation processes now account for 40 – 70% of the operating cost[19, 20], a large fraction of which is associated with the energy cost; and with the current energy prices soaring at an unsustainable rate, membrane processes are becoming an attractive alternative. In addition, membranes are especially useful in separating: chemically similar compounds, thermally sensitive compounds, and azeotropes[21]. Also, the inherent simplicity and scalability are distinctive characteristics. As the operating simplicity of membrane processes allows easy integration with other unit operations, they are frequently used in conjunction with conventional separation processes to increase the yield and efficiency, and to decrease operating cost[22]. In terms of scalability, membrane processes can be scaled-up relatively easily by increasing the membrane area (*e.g.* add membrane modules).

1.3.1.2. Membrane Classification

The main types of filtration membranes for liquid applications, and their respective operating ranges, are summarized in Figure 1.3. In addition, membranes can be roughly classified by the mode of transport mechanism, which can be either pore-flow and/or solution-diffusion mechanism, shown in Figure 1.4. Both microfiltration (MF) and ultrafiltration (UF) membranes function as pore-flow membranes, and reverse osmosis (RO) membranes function primarily by solution-diffusion mechanism. Nanofiltration (NF) membranes, interestingly, exhibit both pore-flow and solution-diffusion transport behavior, depending on the solute's size and chemical properties. The theoretical backgrounds for both transport mechanisms will be discussed later.

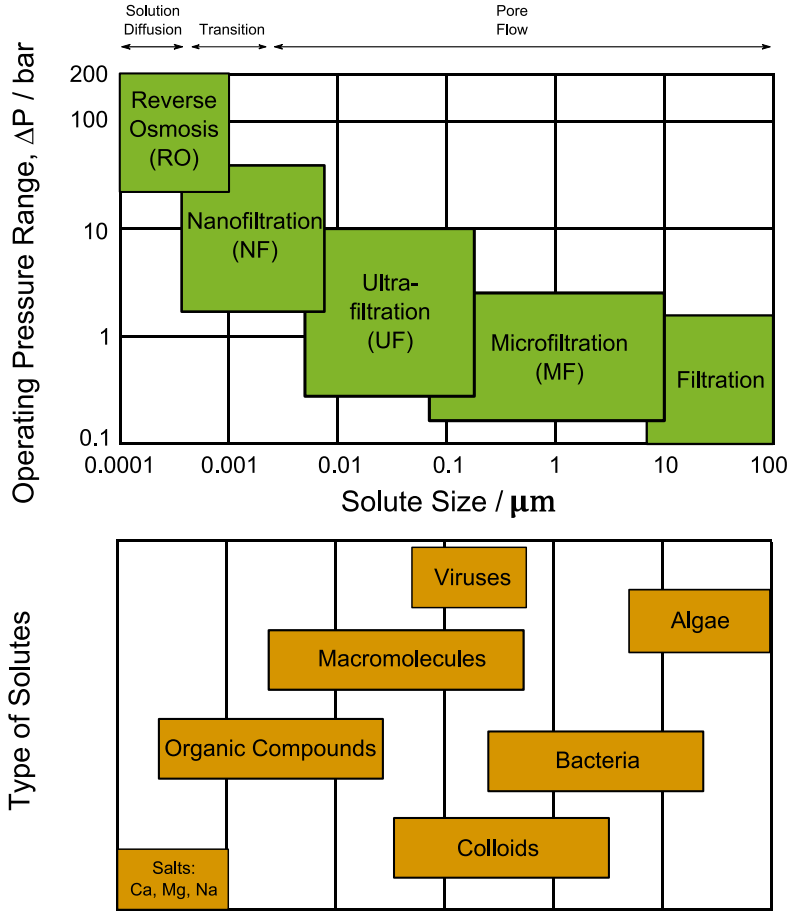


Figure 1.3. Summary of filtration processes and their operating size range shown with respective solutes.

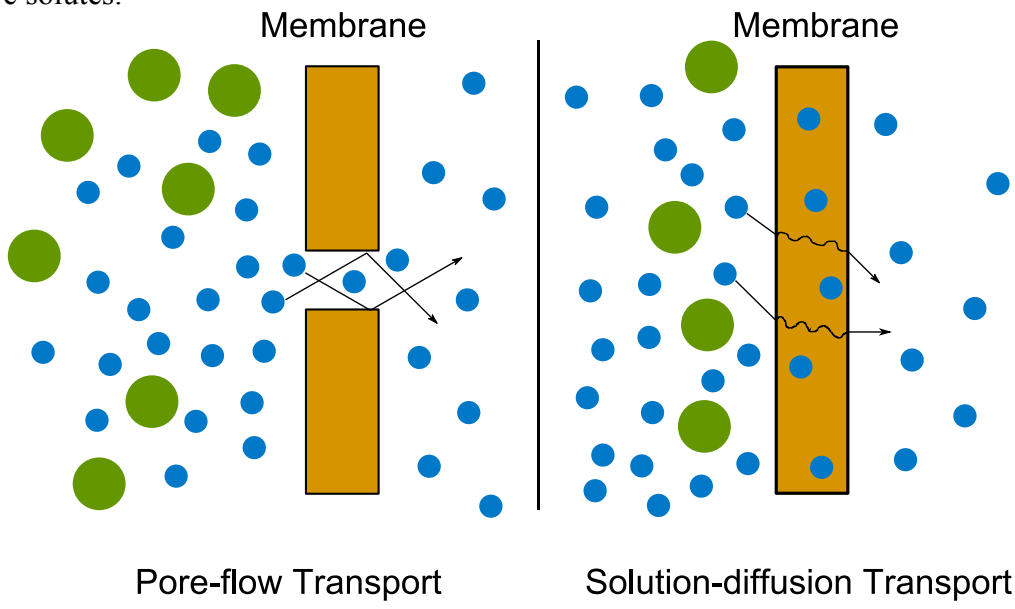


Figure 1.4. Two fundamental transport mechanisms of membrane processes: Pore-flow and solution-diffusion, discussed in further detail later.

MF membranes typically exhibit symmetric structure: uniform morphology throughout the thickness (illustrated in Figure 1.5a). They mainly act as depth filters, capturing solute

particles *within* the membrane by several mechanisms such as size sieving, adsorption, and electrostatic interaction[22]. MF membranes in a form of disposable cartridges secured variety of lucrative markets, mainly for pharmaceutical and electronic industries for sterilization purposes. For instance, 200 nm MF membranes can remove virtually all viruses and bacteria in injectable drug solutions[23].

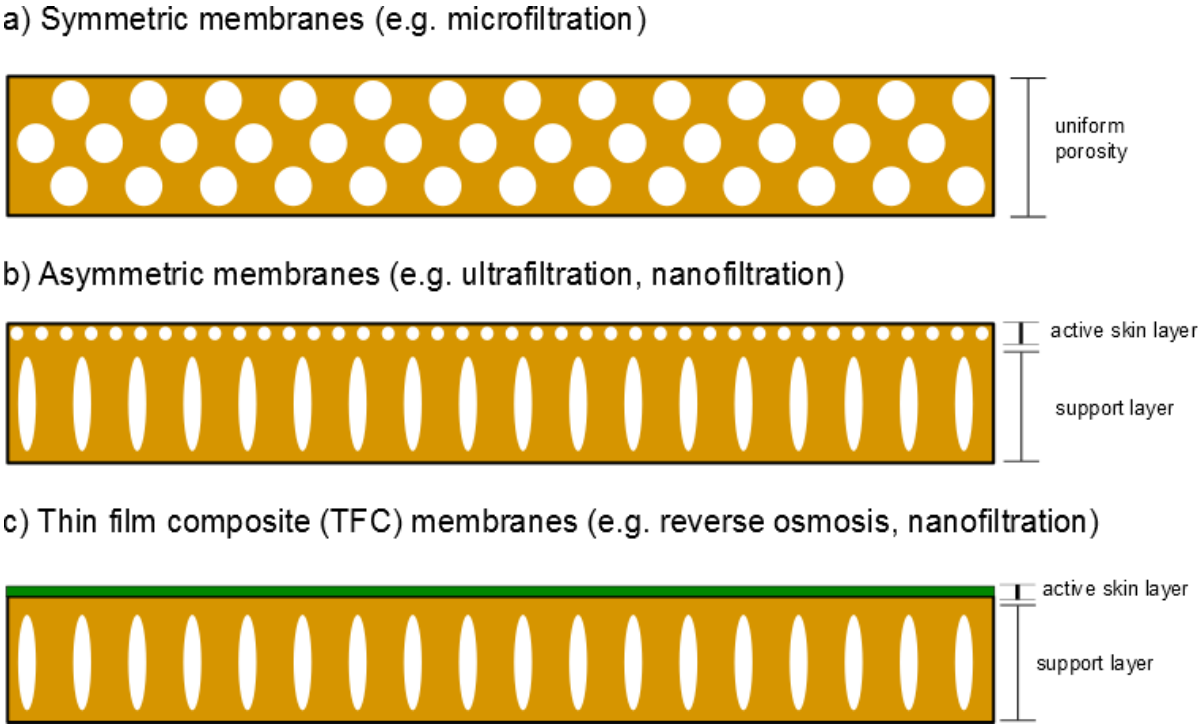


Figure 1.5. Cross-sectional view of common types of filtration membranes: a) symmetric membranes with uniform morphology throughout the thickness; b) asymmetric membranes with active skin layer on the top and porous support layer below made out of same material; c) TFC membranes with thin active layer on top of a support layer made out of different material. Typically, the active layer performs the actual separation while the support layer provides mechanical support.

In contrast to MF membranes, UF membranes exhibit an asymmetric structure: gradient morphology composed of thin and dense layer on the top (active or skin layer) overlaying a thick and open layer below (Figure 1.5b). The top-most layer, the "active layer," is where the actual separation takes place. This layer is usually a few microns thick and has the highest mass-transfer resistance. The layer beneath the active layer is called the "support layer." This part of the membrane provides the necessary mechanical support to withstand high operating pressures, and is usually few hundred microns thick. As the two layers are made of the same membrane material, they are often referred as integrally skinned asymmetric membranes.

UF membranes are found in a variety of markets including food and beverage industries[24].

RO membranes were initially asymmetric cellulose acetate membranes[25] but the current state-of-the-art membranes are thin-film composite (TFC) membranes (Figure 1.5c). TFC membranes are composed of a thin film layer on the top, usually made up of a different material to that of a support layer. Similar to the integrally-skinned asymmetric membranes, the actual separation takes place in the thin film layer. As a general rule of thumb, the thinner the membrane, the higher the permeability; and TFC membranes' top layer, as the name suggests, are typically thinner than asymmetric membranes' skin layer. Another unique advantage of TFC membranes is that each layer can be optimized independently[9].

NF membranes were initially developed to fill the market niches between RO and UF membranes, mainly for water softening applications[26]. NF membranes do not have as high monovalent salt rejection as RO membranes, but have much higher flux with high rejections for multivalent salts, effectively softening water with lower energy consumption. The current mainstream NF membranes are mainly the asymmetric membranes, but TFC membranes are increasingly becoming more popular.

1.3.1.3. Organic Solvent Nanofiltration (OSN)

Organic Solvent Nanofiltration (OSN), also called solvent resistant nanofiltration (SRNF), is an emerging separation platform competitive to other commonly-known processes such as distillation, chromatography, adsorption, and extraction. OSN membranes separate solutes mainly based on their size and MW, ranging between 100 - 2000 Da. Although it is relatively a young technology, it holds a tremendous potential with its ability to perform molecular separations in organic media using a simple pressure gradient[9].

Since many polymeric membranes are not stable in aggressive organic solvents, the liquid-phase application of membrane technology has been somewhat limited to aqueous systems such as reverse osmosis and wastewater treatment. However, OSN technology now allows inexpensive polymeric membranes to be used in various organic solvents, greatly expanding nanofiltration applicability into many fields. For instance, cases such as de-waxing process in the petroleum industry[27], organometallic catalyst recovery in the fine chemicals industry[28], and solvent-exchange process in the pharmaceutical industry[29] have shown the potential of the OSN technology. In addition, OSN membranes now make continuous *in-situ* separation feasible within a chemical reactor, where reaction medium is usually an organic solvent. This unique concept of a membrane reactor holds a lot of promise and is an active area of research[18, 30].

1.3.1.4. OSN Membrane Types

There are mainly three classes of OSN membranes: organic (*e.g.* polymeric, carbon), inorganic (*e.g.* ceramic, metal), and composite (mixture of organic and inorganic) membranes. Among all types, polymeric membranes are the dominant type as they are relatively inexpensive, flexible, and easy to fabricate; most importantly, their flexibility allows them to be tightly packaged into membrane modules, which will be discussed later. Polymeric membranes are, however, more prone to solvent swelling as well as chemical and thermal degradation, rendering their performance difficult to predict[22]. Their performance also varies with pressure and time (*i.e.* aging), as the polymer network gets compacted over time. The choice of polymer mainly depends on the chemical stability, ease of handling, and performance of the cast membrane. Some commonly used OSN polymers are polyimide (PI), polyamide (PA), polyacrylonitrile (PAN), polyether-ether-ketone (PEEK), and polybenzimidazole (PBI)[31-35] mostly used as integrally-skinned asymmetric membranes. A recent work using polymers-of-intrinsic-microporosity (PIM-1)[36] as TFC membranes also showed promising results for OSN applications. In comparison to polymeric membranes, carbon membranes such as graphene[37] and diamond-like carbon (DLC) membranes[38] have shown excellent performance and stability (chemical, mechanical, and thermal). However, their economic viability in large scale is still an unanswered question and it is yet uncertain whether such membranes can be fabricated into a membrane module with high membrane area to volume ratio.

On the other hand, inorganic (*i.e.* ceramic) membranes are typically fabricated from Al_2O_3, TiO_2, ZrO_2, SiO_2, or a combination of these materials[18]. Ceramic membranes offer superior chemical and thermal stability, and are free from solvent swelling, securing them an indispensable position in the membrane market; however, ceramic membranes typically need to be coated (and sintered) with an additional layer to exhibit nanofiltration characteristics. Hence, they are generally more expensive and difficult to fabricate reproducibly[39]. Also, their brittleness makes their use at large scale impractical. Nevertheless, considerable improvements have been made on ceramic membranes in the past decade and their market share is likely to increase[22].

Composite membranes, also called mixed-matrix membranes (MMM), are typically composed of polymer with metal additives such as TiO_2, zeolite, or metal-organic-framework (MOF)[40]. MMMs have shown to improve the membrane flux and reduce the polymer

swelling and compaction; however, the exact transport pathway of solutes, whether it is through the inorganic network or via the void defects between the organic-inorganic interfaces, has not been fully elucidated, rendering their performance unreliable. In addition, at the moment, their high fabrication cost is a hindering factor for MMM membranes.

Overall, polymeric membranes are the most wide-spread type in the OSN technology[9], and will be covered in this review.

1.3.1.5. OSN Membrane Fabrication

Polymeric membranes can be fabricated in several different ways, e.g. phase inversion, extrusion, controlled stretching, and track etching, to name a few[22]. Depending on the method, membranes assume different morphologies and characteristics. The most commonly used method is the phase inversion method, which in turn, can also be classified into several different techniques such as immersion precipitation, controlled evaporation, and thermal precipitation; and the immersion precipitation technique, sometimes referred as the Loeb-Sourirajan process, is by far the most popular technique due to its simplicity and versatility[22]. To fabricate a membrane using the immersion precipitation technique, the polymer of interest is first dissolved in a suitable solvent until a homogeneous solution is obtained. Then, the dope solution (viscous liquid) is cast onto a suitable support (*e.g.* non-woven polypropylene) and subsequently immersed into a non-solvent (*e.g.* water) in which the solvent is miscible but the polymer is not. The non-solvent then diffuses into the cast film, precipitating out the polymer into solid, hence the term *phase inversion*. The membranes fabricated with this technique exhibit asymmetric membrane morphology (Figure 1.5b), which can be used directly, or as a support for TFC membranes.

It is important to note that during membrane fabrication, membrane morphology and performance can vary significantly depending on several factors such the non-solvent bath temperature, humidity, evaporation time prior to immersion, and casting speed[21]. The immersion precipitation technique has been studied extensively and many theoretical models have been proposed[41]. However, the practice is still largely empirical requiring a trial-and-error approach. Interesting work by Vankelecom *et al.* to apply genetic algorithm to optimize casting condition is noteworthy[32]. In addition, the membrane performance can be roughly manipulated by varying the polymer concentration[31] and/or the dope solution solvent mixture[10].

Recently, high flux thin-film composite (TFC) membranes have been reported for OSN[42, 43]. To fabricate TFC membranes, the support layer is usually prepared via the phase inversion method and a thin film layer is subsequently coated on top via dip-coating or interfacial polymerization (IP) method. In contrast to the RO TFC membranes which typically employ polysulfone (PS) support, OSN TFC membranes have been fabricated on different supports such as cross-linked PI or PEEK, to ensure stability in organic solvents. The employed thin-film chemistry was adapted from the RO membrane: trimesoyl chloride (TMC) and *m*-phenyldiamine (MPD) *in-situ* polymerization. The reported TFC membranes show quite remarkable performances with 4-5 folds higher fluxes than commercially available OSN membranes[42, 43].

Once membranes are prepared, additional post-treatment steps are typically employed either to improve the membrane performance or to enhance their chemical stability. For instance, cross-linking PI and PBI membranes with hexanediamine (HDA) and dibromoxylene (DBX), respectively, provides stability to the membranes to the solvent in which they were initially cast[44, 45]. Also, immersing PI and PBI membranes in a PEG solution allowed them to be handled in dry state, a very useful treatment in practice (they become brittle and crack without PEG impregnation)[31]. Notably, a recent publication by Jimenez et al.[42] showed that immersing the TFC membranes in DMF drastically improved the membrane flux, effectively *activating* the membrane by dissolving away small MW oligomers. Other post-treatments reported in the literature are UV treatment, thermal annealing, and grafting[9].

1.3.1.6. Membrane Performance Characterization

Membranes can be characterized using structural parameters and performance-related parameters. Structural parameters include pore size, pore shape, membrane thickness, polymer type, and chemical functional groups[22].

More practical parameters, from the end-user perspective, are the performance-related ones such as the membrane permeance and its separation performance. An ideal membrane should have high permeance and a sharp separation between solutes of interest. The membrane flux, J_v, can be calculated using the following equation:

$$J_v \left[\frac{L}{m^2.hr}\right] = B(\Delta P - \Delta\pi) \qquad \text{(Eq. 1.1)}$$

where B represents the membrane permeance ($L.m^{-2}.hr^{-1}.bar^{-1}$) and ΔP and $\Delta\pi$ refer to pressure gradient and osmotic potential gradient across the membrane, respectively.

On the other hand, the separation performance of a membrane is assessed by its rejection profile. For example, if a solute has 100% rejection, none of it goes through the membrane; if it has 0% rejection, all of it goes through the membrane and nothing gets retained. The term rejection is mathematically defined in Equation 1.2.

$$R_i(\%) = \left(1 - \frac{C_{p,i}}{C_{R,i}}\right) \times 100\% \qquad \text{(Eq. 1.2)}$$

where $C_{p,i}$ and $C_{R,i}$ represent the concentrations of solute *i* in the permeate and retentate, respectively.

There has been a long-debate on the actual threshold of the term rejection. Currently, a widely accepted characterization parameter for membranes is the molecular weight cut-off (MWCO). The MWCO of a membrane represents the molecular weight of a reference solute that has a 90% rejection[26]. However, this definition is rather arbitrary and not applicable in many areas including pharmaceutical applications, as a rejection of 99.99% is typically required to obtain pure products with reasonable yields[12]. Thus, membrane separation performance should be defined according to the specific application and product requirements.

In most cases, the mixture of interest contains at least two solutes with different rejections. Therefore, a more convenient way to represent the membrane separation performance is by using a MWCO curve, or rejection curve, which plots a series of reference solutes of different molecular weights against their respective rejections[46]. A typical MWCO curve is shown in Figure 1.6 below.

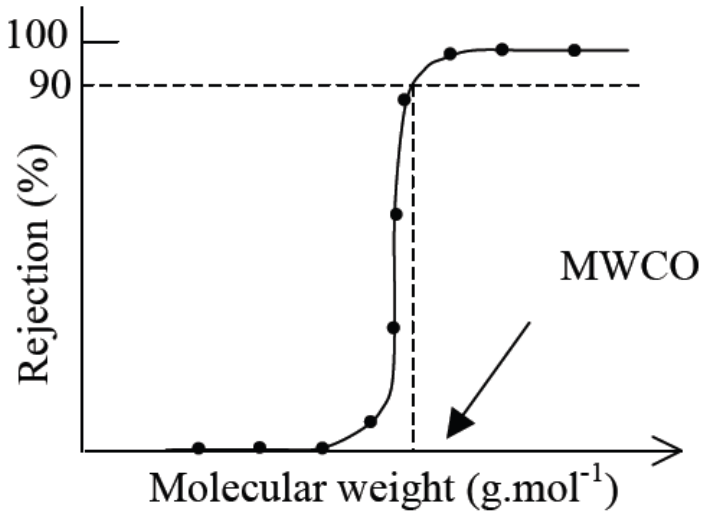


Figure 1.6. A standard MWCO curve of a membrane where different MW solutes are plotted versus their corresponding rejection values.

As illustrated in Figure 1.6, the MWCO curve gives a rough estimation of membrane performance over a wide range of molecular weights. However, it should be stressed that MWCO itself is a poor estimation of membrane performance, as the molecular shape, charge, and functional groups also affect the rejection[46], particularly in the nanofiltration range (100 – 2000 Da). As expected, choosing the right reference components to assess the membrane performance has been under a constant debate and it is also very application-dependent. Nevertheless, MWCO curve is a good starting point when screening for suitable membranes.

At present, an extensive and lengthy membrane screening step is usually required to determine a suitable membrane for a potential application[47]. This step is usually the bottleneck step and it is often difficult to identify an ideal candidate. This challenge will be discussed in more detail in Chapter 3.

1.3.1.7. Performance Prediction and Transport Models

Predicting the performance of membranes is crucial from the end-user perspective to appropriately implement membrane units to fit the overall process design. However, due to the complex pore network and irregular flow path of filtration membranes, understanding the transport mechanism has not been an easy task, and it is still an active area of research; and in the past few decades, many models have been proposed and debunked[48, 49].

It is widely accepted now that membrane transport mainly occurs through two fundamentally different mechanisms: pore-flow and solution-diffusion, as illustrated in Figure 1.4. In the pore-flow model, solutes permeate by pressure-driven convective flow through the membrane pores. Separation occurs as one of the solutes permeates more slowly or is excluded by the membrane pores. On the other hand, the solution-diffusion model assumes that the membranes have no pores. Instead, solutes first *dissolve* into the membrane and subsequently *diffuse* through the membrane down a concentration gradient, hence the name solution-diffusion[22, 48].

The difference between the two models comes from the relative size of the pores. It has been computationally predicted that fluctuations between polymer chains due to the thermal motion is approximately 0.5 nm for dense polyimides[50]. In other words, transient voids between 0 - 0.5 nm continuously appear and disappear within a dense polyimide membrane due to the thermal motion of atoms. The time-scale at which the pores appear coincides with the random motion of the permeating solutes[48]. Such observations match with the validity of the model. For instance, the pore-flow models are widely applied for UF and MF membranes

where the membranes are clearly microporous with pore sizes bigger than 1.5 nm diameter. On the other hand, the solution-diffusion model is universally applied for RO membranes which exhibit dense morphology with no visible pores (only transient pores).

Nanofiltration, however, lies in a transition region where the transport occurs through both solution-diffusion and pore-flow mechanisms. Roughly, this transition range is between 0.5 – 1 nm pores[22]. Naturally, performance of NF membranes is generally more difficult to model and to predict, as both pore-flow and solution-diffusion properties should be considered. In addition, as the size of the pore is of the same scale as the solute size, the electric potential interactions become significant. Furthermore, macroscopic description of transport hydrodynamics begins to break down at this scale, a phenomenon commonly referred to as *hindered transport*[49]. For instance, the idea of viscosity needs to be re-conceptualized in sub-nanometer sized pores[51].

An ideal transport model should provide quantitative prediction with minimal experimental input. Among the proposed models, the extended Nernst-Plank equation best describes the NF transport process as it captures both convective and diffusive flow, as well as electrical potential interactions[52]. Also, the model is flexible with respect to implementing hindrance factors within NF pores. The extended Nernst-Plank equation may be written as the following:

$$J_i = -K_{i,d} D_{i,p} \frac{dc_i}{dx} + K_{i,c} c_i J_v - \frac{z_i c_i D_{i,p}}{RT} F \frac{d\varphi}{dx} \qquad \text{(Eq. 1.3)}$$

where three terms on the right hand-side of the equation represent transport due to diffusion, convection, and electrical field gradient, respectively; J_i (mol.m^{-2}.s^{-1}) represents the solute flux, $D_{i,p}$ (m^2.s^{-1}) the solute diffusivity through membrane pores, c_i (mol.m^{-3}) the solute concentration, J_v (m^3.m^{-2}.m^{-1}) the volumetric flux of the solution, z_i the valence of ion (0 for neutral solute), F (C. mol^{-1}) the Faraday constant, φ (V) the electrical potential, and $K_{i,d}$ and $K_{i,c}$ the diffusive and convective hindrance factor within the pore, respectively.

Assuming neutral solute (z_i = 0) and rearranging, the concentration gradient across the membrane can be obtained,

$$\frac{dc_i}{dx} = \frac{J_v}{K_{i,d} D_{i,p}} (K_{i,c} c_i - C_{i,p}) \qquad \text{(Eq. 1.4)}$$

where $J_i = J_v C_{i,p}$ in which $C_{i,p}$ represents the concentration of solute *i* in the permeate.

This expression can be integrated over the membrane thickness (Δx) with the following boundary conditions

$$x = 0, c_i = C_{i,retentate} \; and \; x = \Delta x, c_i = C_{i,p} \qquad \text{(Eq. 1.5)}$$

to calculate membrane solute rejection (R_i defined in Eq. 1.2) as function of flux (J_v).

The extended Nernst-Plank model described above has been improved by many membrane researchers recently[51, 53, 54]. However, the model still requires essential input data such as the membrane thickness and effective pore radius, which are difficult parameters to obtain experimentally (hence resort to fitting).

In addition, modeling membrane transport is further complicated when several key interactions such as membrane-solvent, solute-solvent, and solute-solute interactions are taken into account. Notably, polymeric membranes can swell or shrink in organic solvents, and the degree of swelling and shrinking varies with the type of solvent[55, 56]. A recent work by Marchetti *et al.* proposed a phenomenological model that only requires the physical parameters to predict solvent flux through ceramic membranes[57], isolating the swelling parameter.

In summary, predicting OSN performance is a challenging task, as the membrane performance varies quite significantly depending on the operation conditions such as solvent, temperature, concentration, and pressure. At the moment, similar to the membrane preparation step, the practice is largely empirical with a heuristic approach being adapted. Current OSN technology is severely hindered by the fact that membrane performance needs to be experimentally validated prior to implementation[58], a main bottlenecking step during the process development. Hence, it is crucial to develop a suitable model to predict the OSN membrane performance with reasonable precision. A recent work by Peshev *et al.*[59] to couple OSN membrane performance with the Aspen platform (*i.e.* OSN Designer) is the right direction forward.

1.3.1.8. Concentration Polarization and Mass Transfer Coefficient

In membrane separation processes, feed mixture components permeate through the membrane at different rates creating a concentration gradient near the membrane surface, a well-known phenomenon called concentration polarization (Figure 1.7). The concentration polarization phenomenon can cause significant adverse effects on the overall membrane flux and separation; hence, it is a crucial parameter to control and to minimize[60, 61].

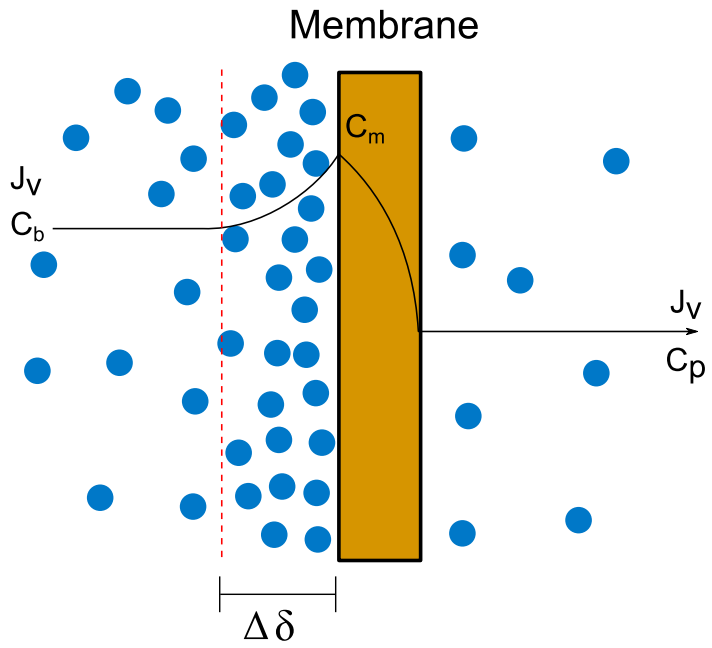


Figure 1.7. Illustration of the concentration polarization layer on the feed side of the membrane surface. The notations used for film theory derivation: C_b, C_m, and C_p refer to the solute concentrations at the bulk, membrane, and permeate, respectively.

The extent of concentration polarization is often modeled using film theory, in which a boundary layer with a thickness of δ is assumed on the membrane surface. A solute mass balance around the boundary layer may be written as:

$$J_v c_i - D_i \frac{dc_i}{dx} = J_v c_p \qquad \text{(Eq. 1.6)}$$

where D_i represents the diffusion coefficient, and c_i represents the solute concentration as a function of x (coordinate perpendicular to the membrane surface).

Equation 1.6 can be integrated over the boundary layer thickness (δ) to yield the following concentration profile.

$$\frac{c_m - c_p}{c_b - c_p} = \exp\left(\frac{J_v \delta}{D_i}\right) = \exp\left(\frac{J_v}{k}\right) \qquad \text{(Eq. 1.7)}$$

The crucial parameter here is the mass transfer coefficient ($k = D_i/\delta$), which is an intrinsic parameter relative to the process configuration: typically, the lower the k, the lower the J_v. A typical mass transfer coefficient in a flat-sheet membrane for a cross-flow configuration is in a range of $10^{-4} \sim 10^{-5}$ $m.s^{-1}$.[60] The effect of mass transfer coefficient is perhaps best illustrated by its effect on the observed solute rejection. The observed membrane rejection may significantly deviate from the real rejection depending on the mass transfer coefficient. For instance, if the mass transfer coefficient is low, the observed rejection may seem considerably lower than the intrinsic membrane rejection. The implication of such a deviation becomes

significant when a membrane unit is implemented into a full-scale process, as the performance prediction and control deviates from the actual data.

The importance of high mass transfer becomes evident in tightly-packed membrane modules, where the flux can sometimes be limited by the mass transfer to the membrane surface rather than through the membrane (due to the osmotic pressure gradient across the membrane)[62]. One way to enhance the mass transfer coefficient is to induce better mixing by increasing the liquid circulation rate. Alternatively, the process configuration can be modified to alter the flow-path of the circulating solution. Unfortunately, the work to understand and improve the overall process design and mass transfer coefficient has not kept pace with the membrane improvement itself[20, 63] and it is an area that urgently requires more attention.

1.3.1.9. Process Configuration and Scale-up Parameters

A membrane application development commences by first identifying a suitable membrane at lab-scale. Then, the process is validated in pilot-plant tests and eventually scaled-up to industry scale. Each step along the way requires a larger membrane area; hence, it is necessary to fabricate the selected membrane into a suitable membrane module with a high area-to-volume (A/V) ratio. Notably, many potential applications have been unsuccessful because the membranes could not be fabricated into membrane modules[22].

There are mainly four types of membrane modules: spiral wound membrane (SWM), hollow fiber membrane (HFM), plate and frame membrane (PFM), and tubular membrane (TM) module[9]. Among the four types, SWM module is the dominant type in the field of OSN. SWM module consists of several membrane leaves (flat sheet membranes), separated by a spacer, wound around a central collection pipe. Logically, the design and geometry of the spacer is crucial to control the axial (and radial) pressure drop and mass transfer. The packing density of SWM modules ranges from 300 – 1000 m^2 per m^3.

It is important to stress that for OSN applications, all other module components such as spacer, adhesive, and O-rings, need to be resistant to the operating solvent media. Currently, OSN membranes are now commercially available as SWM up to 8'' module[64, 65], but 16'' module has recently been standardized in RO industry[66].

1.3.2. Oligonucleotide Chemistry

As the objective of the project is to develop a scalable oligonucleotide synthesis process, the history of oligonucleotide synthesis chemistry is covered in this section. The literature on manufacturing platform such as solid-phase and liquid-phase are covered in Chapter 2.

1.3.2.1. Basic Chemistry

Oligonucleotides (oligos) are short chains, typically 15-28 monomer length, of nucleotides, which are the building blocks of DNA and RNA. Nucleotide, shown in Figure 1.8a, is made up of a nucleoside and a phosphate group joined by ester bond at the 3' position. Nucleoside, in turn, is made up of a base and a pentose sugar.

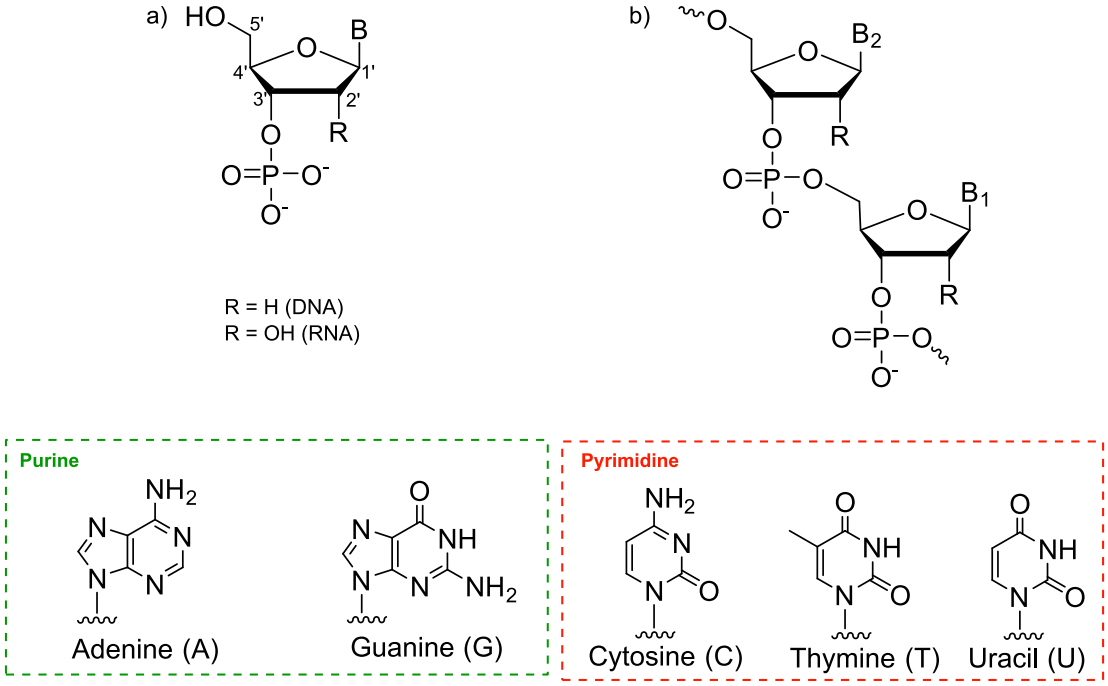


Figure 1.8. a) Basic nucleotide structure and five bases. R = H (in DNA), OH (in RNA); b) structure of poly(nucleotide).

There are five types of bases, which can be divided into two groups: purine — adenine (A) and guanine (G) — and pyrimidine — cytosine (C), thymine (T) and uracil (U). While A, G and C are found in both DNA and RNA molecules, T is almost exclusively in DNA, while U replaces T in RNA. Another major difference between the DNA and RNA is the functional group in the 2' carbon position in the pentose sugar: DNA has an *–H* group attached to the 2' carbon, whereas RNA has an *–OH* group. This extra *−OH* group in RNA makes the molecule more reactive compared to DNA.

Nucleotides can covalently bond to form phosphodiester link and polymerize as shown in Figure 1.8b. Since the groundbreaking publication by Watson and Crick that revealed the

structure of DNA[67], the fundamental units of life, synthetic oligonucleotides have been the backbone of molecular biology[68]. As the significance of genetics with respect to biology becomes elucidated, the importance of oligonucleotides in therapeutics has long been foreseen.

In the strictest sense, the definition of an oligo is a short piece of nucleic acid less than 50 nucleotides in length. Typical oligos with therapeutic potentials are generally 15 – 28 nucleotides long[69]. Oligos can be synthesized in several different ways and the chemistry has improved significantly since Michelson and Todd first reported a synthetic dinucleotide in 1955[70]. Since DNA and RNA are polymers consisting of a small number of possible monomers, a logical way to assemble an oligo is by stepwise addition of one monomer at a time with appropriate protecting groups as shown in Figure 1.9. Typically, oligonucleotides are synthesized in 3' → 5' direction.

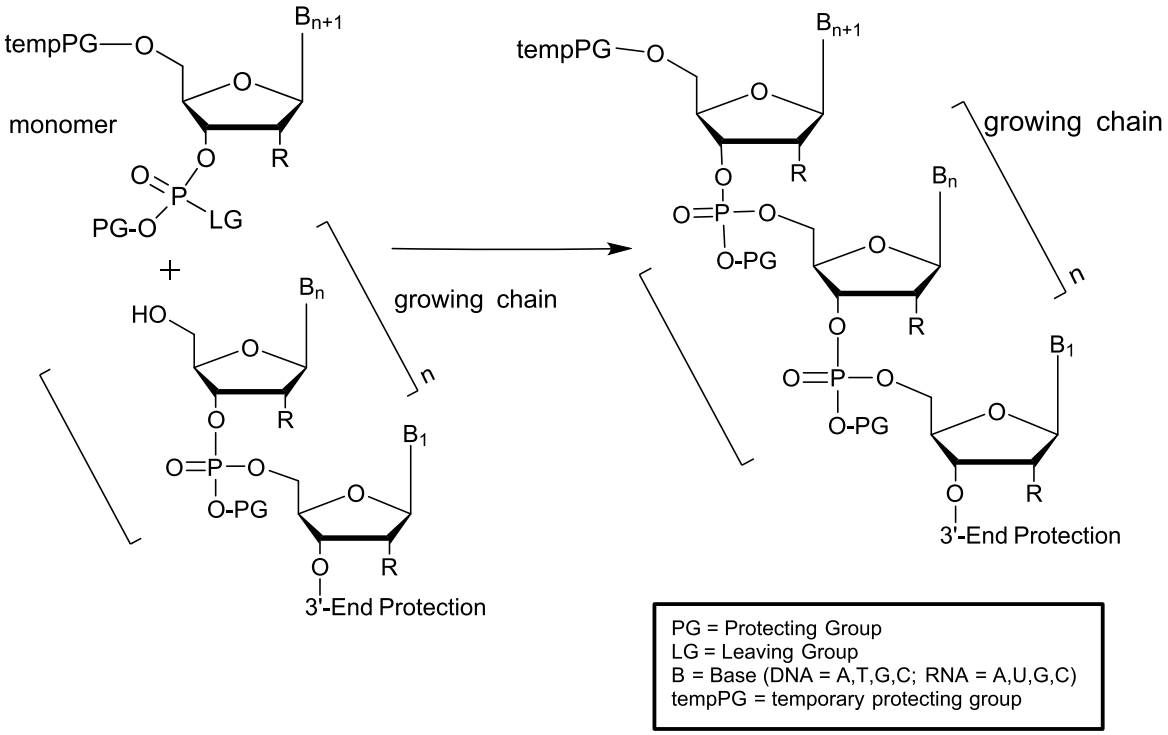


Figure 1.9. General oligonucleotide synthesis scheme with appropriate protecting groups. One monomer is added sequentially to the 5' position. For RNA synthesis, the R group in the 2' position is –OH and it's protected with appropriate group.

Two important considerations for oligo synthesis are the chain extension yield and the necessary chemical modifications. Firstly, since the oligonucleotides are grown sequentially, a simple mathematical equation (Eq. 1.8), so called the "arithmetic demon," shows that each chain extension yield is crucial and needs be almost quantitative to achieve reasonable overall yields.

$$\text{Overall yield} = (\text{Chain extension yield})^{n} \qquad \text{(Eq. 1.8)}$$

where *n* is the number of coupling steps required.

For example, to grow a 21-mer oligonucleotide, a chain extension yield of 95% would result in 36% overall yield and 99% chain extension yield results in 82% overall yield. To compensate for this, one can devise an alternative route such as the convergent synthesis method, or fragment condensation method, where short chains are synthesized independently and linked together. For instance, a 21-mer oligonucleotide can be synthesized by linking seven independently-prepared trimers together sequentially.

Another important consideration when developing oligo therapeutics is the chemical modification of the oligos. It is well known that the oligos in their native form cannot be delivered to their targets due to enzymatic degradation by endo- and exonucleases. Significant progress has been made to develop nuclease-resistant oligonucleotides such as phosphorothioate analogues, phosphoroselenate, and arylphosphonate[71-73]; In addition, the PEGylation approach to enhance pharmacokinetics of drugs is also an active research area[74].

To understand the important points in oligonucleotide synthesis such as protecting group and phosphate chemistry, a short history of how synthetic oligonucleotide chemistry developed over the past 50 years is discussed.

1.3.2.2. Phosphodiester Method

The first published method, the phosphodiester approach (Figure 1.10), developed by Khorana and co-workers, introduced the very important concept of cyclic scheme with an on-off protections procedure.

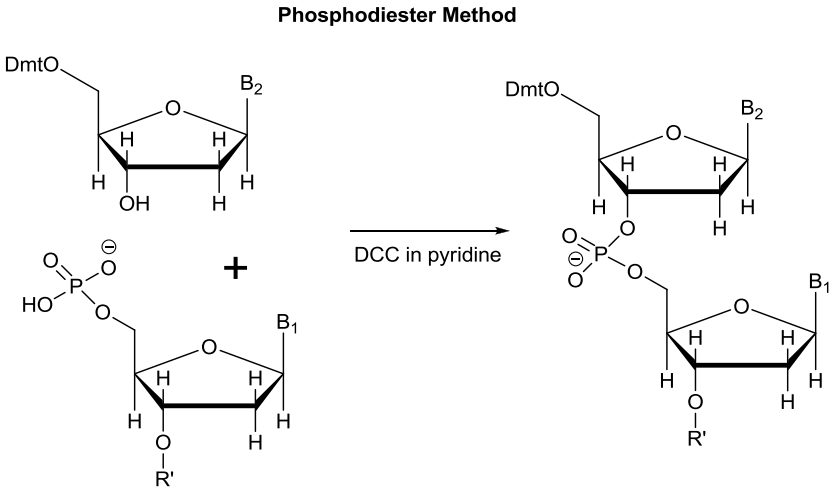


Figure 1.10. First published example of the phosphodiester approach, only the coupling step is shown using *N,N'*-dicyclohexylcarbodiimide (DCC).

To avoid any undesired side reactions which could lower the final yield, it is crucial to protect reactive functional groups such as 5' hydroxyl groups, the phosphate group, and nucleoside bases. An ideal protecting group should: 1) be efficient, fast, and quantitative; 2) allow selective removal at the desired time; 3) be stable during other reactions.

Khorana's lasting legacy comes from the protecting groups he suggested. The protecting groups and the on-off cyclic scheme he proposed more than 40 years ago have been virtually unmodified since[75-77]. This convenient process has made it possible to synthesize oligos more than just a few bases long.

During the chain extension step, it is necessary to protect the 5' hydroxyl group of the monomers while that of the growing chain is deprotected (tempPG in Figure 1.9). The dimethoxytrityl (Dmt) protecting group suggested by Khorana offers both good stability and easy removal with mild acid. In addition, the distinctive orange color that appears during the removal step allows optical analysis of the extent of deprotection possible. The Dmtr protecting group, shown in Figure 1.11, is practically ubiquitous in oligo chemistry today.

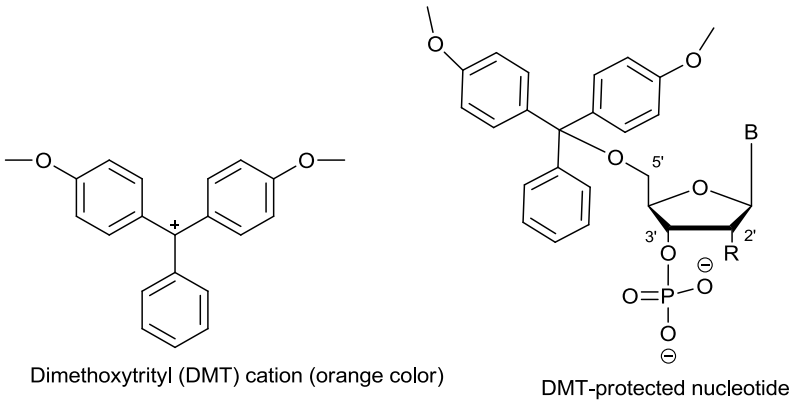


Figure 1.11. Dimethoxytrityl (Dmt) protecting group on 5' hydroxyl group.

Khorana also suggested very effective protecting groups for all the nucleoside bases: isobutyryl group for G, and benzoyl group for A and C, shown in Figure 1.12. It is particularly difficult to protect purines (adenine (A), guanine (G)) as they are susceptible to depurination even at moderately acidic conditions.

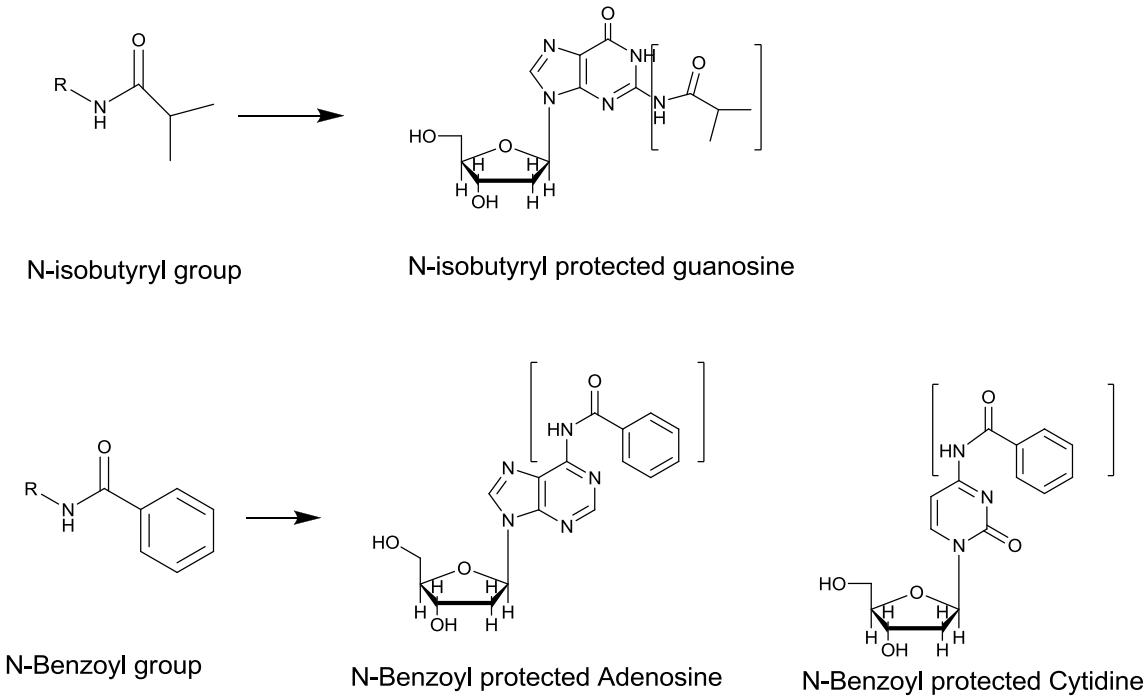


Figure 1.12. Nucleoside base protecting groups suggested by Khorana.

Although the nucleoside base protecting groups suggested by Khorana are the most commonly used ones, alternatives exist such as acetyl-protected cytidine and *O*(6)-acylated guanine[78, 79]. Although thymine and uracil bases are usually left unprotected, it is usually recommended to protect uracil residues for oligoribonucleotide synthesis[78].

One drawback of the phosphodiester method was the branching effect during the coupling step due to the unprotected phosphate group. Also, the build-up of charged phosphodiester groups decreased the yield as the chain elongated. On the other hand, Khorana believed exploiting the polyelectrolyte character for the downstream purification was the phosphodiester group's most important property, and protecting the phosphate group would be meaningless unless the coupling yields were quantitative. This idea has turned out to be invalid with the phosphotriester method. Nevertheless, the phosphodiester approach was quickly replaced by other methods due to its uncontrollable side reactions and low yields.

1.3.2.3. Phosphotriester Method

Subsequent to Khorana's work, the group led by Letsinger developed the phosphotriester method[80, 81] shown in Figure 1.13. The key improvement of this method was the protection of the phosphate group to prevent undesired side reactions such as branching while preventing the charge build-up. It later became clear that employing the phosphotriester approach brings more gain than loss, as the chain extension yield was significantly higher than phosphodiester

method[78]. A commonly used protecting group nowadays is the β-cyanoethyl (Cne) group which is easily removable with base. In addition, to push the efficiency of the reaction to near-completion, the role of activator became crucial and many different activators such as mesityl sulfonyl chloride (MSCl) and mesityl sulfonyl nitrotriazole (MSNT) were investigated. Unfortunately, even with this method and activator, a critical drawback was the coupling efficiency, as it often failed to reach over 95%, limiting the length of oligos[79].

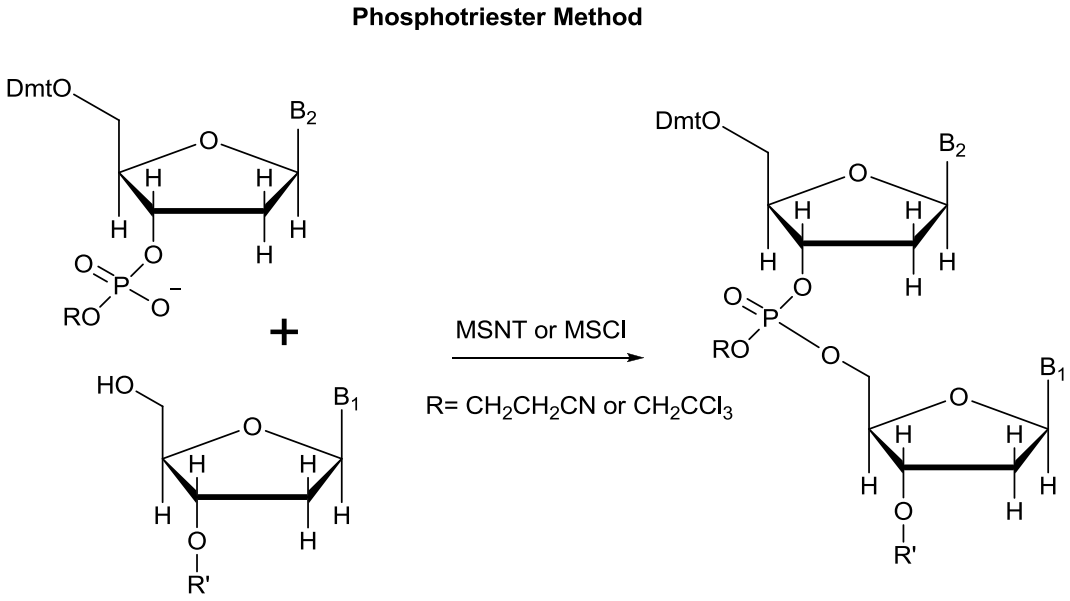


Figure 1.13. Phosphotriester method. One of the oxygen atoms in the P atom is protected to prevent branching and build-up of anionic charge.

1.3.2.4. Phosphite triester Method and Phosphoramidite Method

In 1976, Letsinger published a very crucial finding in oligonucleotide chemistry with the phosphite triester method. Letsinger and his co-workers have shown that P(III) oxidation-state compounds are far more reactive than those in P(V) oxidation state[82] (Figure 1.14).

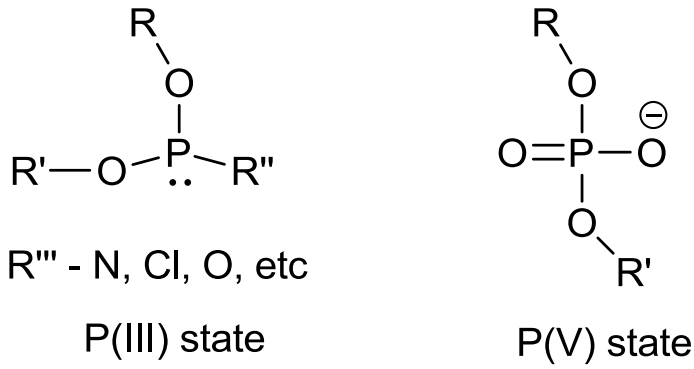


Figure 1.14. Example of P(III) and P(V) oxidation state compound.

It turns out that the transitional energy of the intermediates is much lower with P(III) species than that of P(V) species, increasing the rate of reaction drastically.

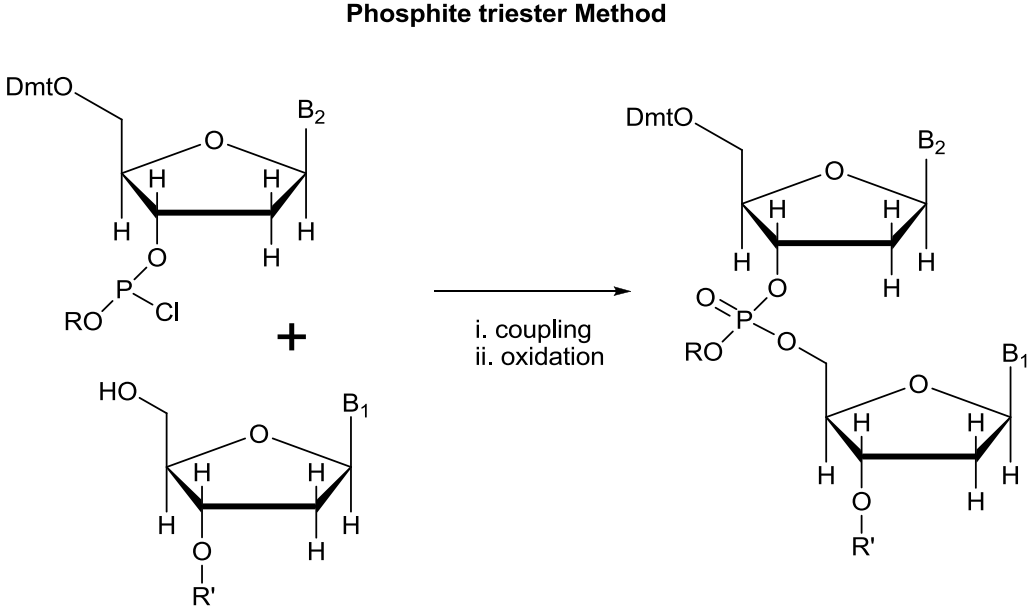


Figure 1.15. Phosphite triester method. The P atom is in more reactive P(III) state until oxidation step.

As shown in Figure 1.15, although this chemistry required an additional oxidation step after coupling, it drove the coupling efficiency close to completion and reduced the coupling time significantly. In addition, the subsequent *in-situ* oxidation step can be achieved in *seconds* with a simple mixture of iodine, water, and base. However, the most significant problem was its high reactivity, the very feature that distinguished the phosphite triester method from other methods. A critical problem arose during the preparation of phosphitylated monomers, as it was very difficult to prevent many undesired side-products from forming. Even after its successful synthesis, the intermediate compound was extremely susceptible to hydrolysis, leading to a short shelf-life. Such disadvantages removed all of the advantages brought about by using the P(III) species.

However, such problem was solved by Caruthers by simply exchanging the leaving group from a chloride to an amine[83] (Figure 1.16), hence the name phosphoramidite method. This subtle and almost trivial modification resulted in major changes to the properties of the molecule. First of all, the synthesis of phosphitylated nucleoside monomers became much easier and they could be isolated and stored until needed. In addition, Caruthers suggested a very powerful and efficient activator, tetrazole, which is acidic enough to activate the

reaction but not too acidic to deprotect the DMT group. Equipped with this activator, the method guaranteed reliable reproducibility with almost quantitative coupling efficiency.

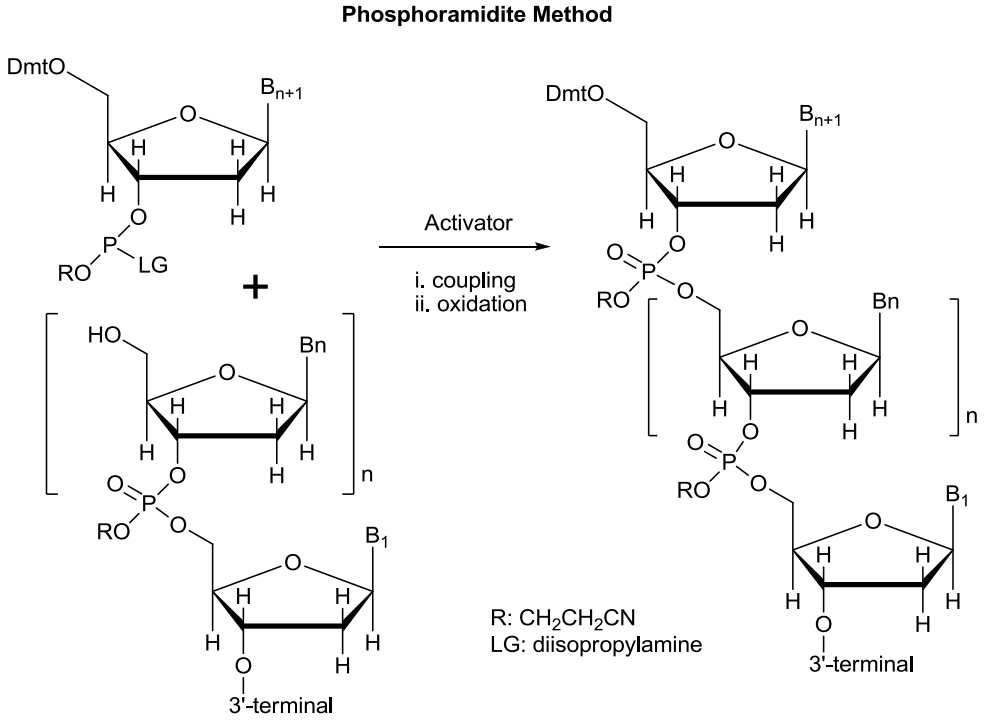


Figure 1.16. Phosphoramidite method, the chloride leaving group in the P(III) state monomer is replaced with an amine group, allowing more robust handling with similar efficacy.

The phosphoramidite method was so effective and simple that it has remained virtually unmodified for almost two decades. Some of the notable improvements are the replacement of explosive tetrazole[84] and replacement of chlorinated solvent to toluene[85]. With the phosphoramidite method in hand, the synthesis of oligos was completely automated and became an indispensable tool for the biologists who could fully exploit it.

1.3.2.5. H-phosphonate Method

Contrary to the aforementioned methods, the H-phosphonate approach has been pursued and developed rather independently. This method was first reported in 1957[86], modified and applied to solid phase synthesis using a diphenyl phosphorochloridate as an activator[87], then re-modified to solution phase synthesis with protected phosphate group[88]. The monomeric building blocks can be readily prepared and the reaction proceeds almost quantitatively.

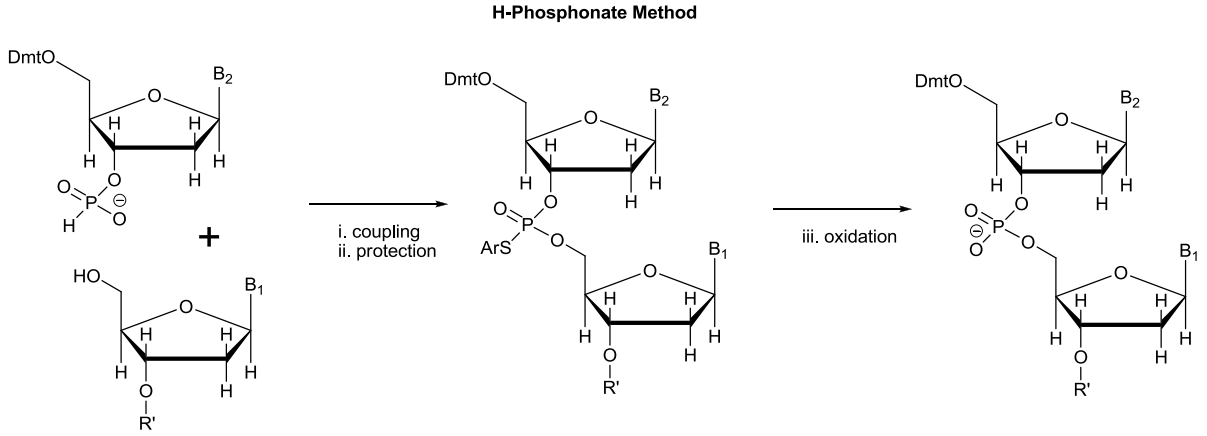


Figure 1.17. H-Phosphonate method scheme in solution, all reactions proceed *in situ*.

Since the H-phosphonate diesters are quite susceptible to hydrolysis in solution, a phosphonate protection step became necessary after the coupling step and prior to oxidation (Figure 1.17), which can be done easily and quantitatively. However, one drawback of this method is the low reaction temperature, as the usual reaction temperature is below -40 ^{o}C; reactions at room temperature have been attempted but resulted in low yields[89]. Nevertheless, the preparation of H-phosphonate monomers is very easy and the coupling yield is virtually quantitative, rendering the method very attractive.

1.3.3. Summary

In summary, synthetic methods to make oligonucleotides have been actively researched for the past 50 years and there are many synthesis routes available to choose from. Apart from the synthesis routes, several practical parameters must be taken into account when synthesizing oligos at a large scale. First, the reagents and monomers must be readily available, inexpensive, and chemically robust. Also, the reaction conditions should be mild and easy to control. And most importantly, purification of intermediates after each coupling step must be fast, efficient, and economically feasible.

Imperial College London

Chapter 2

New Liquid-Phase Platform for Oligonucleotide Synthesis using Organic Solvent Nanofiltration (OSN) Technology

This chapter discusses the process research aimed at oligonucleotide synthesis using OSN. A suitable membrane and appropriate chemistry were selected to match the separation platform. Several key challenges have been identified which will be tackled in subsequent chapters.

2.1. Summary

This chapter presents a versatile and scalable liquid-phase oligonucleotide synthesis (LPOS) platform that can potentially manufacture oligos on a large scale using Organic Solvent Nanofiltration (OSN) as the separation technique. By attaching the growing oligo chain to a soluble monodisperse polyethyleneglycol (PEG) branched support and operating in liquid-phase, excess reagents and impurities can be filtered out using polybenzimidazole (PBI) OSN membranes. Using this process, 5-mer and 9-mer 2'-*O*Me oligoribonucleotides were successfully synthesized, and their purities were compared to oligos synthesized from solid-phase oligonucleotide synthesis (SPOS). The synthesis chemistry and membrane purification procedures were modified to suit the LPOS platform. The transport of solutes through the PBI membranes was studied in detail to reveal both size-exclusion and ion-exchange behavior. The ability to analyze each coupling reaction adds a unique advantage to the LPOS platform. An economic analysis highlighted the competitiveness of the LPOS-OSN process, but also the necessity for a solvent recovery unit. Several key challenges, both expected and unexpected, were identified and possible solutions are suggested. It is envisaged that the proposed LPOS platform can be used synergistically with the current SPOS platform to stimulate further growth in the field of oligo therapeutics.

2.2. Introduction

Oligonucleotides (oligos) are short chains of DNA or RNA. In the 1980s and 1990s, DNA oligos were first considered as potential therapeutic agents for treatment of genetic disorders, through anti-sense therapy[90]. This concept built on the unique biological specificity and complementarity of oligos for their target sequences at the genetic level, but these original approaches failed to yield many viable therapies. However, since the discovery of RNA interference (RNA*i*), leading to the award of the 2006 Nobel Prize in Physiology or Medicine to Fire and Mello[91], there has been a renaissance in the search for oligo-based drugs built around RNA 15- to 28-mers[92]. Potential targets include viral infections, cancers, and chronic genetic disorders[69, 93].

The first antisense drug, fomivirsen (brand name Vitravene), a DNA phosphorothioate 21-mer to treat cytomegalovirus associated retinitis, was approved by the FDA and EMA in 1998. Its mechanism of action is simply to block the progress of the RNA translation complex moving along the mRNA strands, and so prevent protein expression. Later, with the realization of functional RNA and directed evolution, pegaptanib (brand name Macugen), a PEGylated 2'-modified RNA 28-mer, was developed to treat macular degeneration and received approval from FDA in 2004. This aptamer was developed to block the binding of vascular endothelial growth factor (VEGF) to its receptor. Recently, the second-generation anti-sense drug mipomersen (brand name Kynamro), a mixed DNA and modified RNA phosphorothioate 20-mer, received FDA approval in 2013. This gapmer functions by targeting RNAse-H to the mRNA which is then specifically digested to prevent protein expression. Following on from these successful entrances into the market, over 100 oligo-based drugs are now going through different phases of clinical trials[1].

However, as potent as they seem, anti-sense therapeutics are not without drawbacks. Unmodified phosphodiester oligonucleotides (native form) are prone to degradation by endo- and exonucleases, some side-effects have been reported, and drug delivery to the target cells is often a major hurdle[94]. Much research is currently dedicated to overcoming such limitations, from substitution of the backbone with nuclease resistant phosphorothioate analogues[71-73] to shielding of the oligo through PEGylation[74] and SNALP (stable nucleic acid-lipid particles) technology[95]. A recent demonstration by *Alnylam* of the safe and effective delivery of oligos in man has further heightened interest in the field of oligo-based drugs[96] .

Apart from the difficulties in drug delivery, another major practical challenge for the exploitation of oligo therapeutics is the large-scale production of these complex molecules. As more drugs are developed that target a broader range of patients, it is expected that metric tons per annum of such drugs will soon be required[2, 97]. Thus, there is a pressing need to develop economically viable processes to produce oligos on such scales[2, 3, 98].

The basis of the synthetic methodology has remained essentially the same for the last 40 years. Current designs of therapeutic oligo sequences are mainly between 15 and 28 base-pairs long. DNA and RNA are heteropolymers, with their mode of action defined by the sequence of the monomers. Therefore the synthesis employs step-wise addition of each nucleotide monomer, followed by separation of the reagent mixtures. The current state-of-the-art oligo synthesis platform is solid-phase oligonucleotide synthesis (SPOS). The key feature of SPOS is the use of a solid support to anchor one end of the growing chain. This facilitates rapid removal of the excess reagents after each step-wise coupling of the monomers, where the solid beads are simply washed with solvents. The growing chain on the solid support is then ready for the next step.

At first oligos were simply a versatile tool, used by biologists and chemists on small scales in their research. Since the early days much more research has been dedicated to improving the SPOS process. For small-scale synthesis, SPOS has been completely automated and has become an excellent tool for molecular biology, with a host of suppliers providing any desired DNA sequence, even in excess of a hundred base-pairs length with a short turn-around time. RNA is harder to prepare due to the molecular difference of possessing a 2'-hydroxyl, but shorter sequences are now also commercially available.

Despite its clear advantages of easy purification and rapid synthesis, the general consensus with regard to scaling up the SPOS process is that it is very difficult[4, 5, 98]. This is due to the heterogeneous nature of the SPOS process which creates high mass-transfer resistance between the bulk solution and the support surface, and steric hindrance between the growing chains within the support, as well as low polymer loading[99]. The SPOS process is highly mass intensive at large scale[1]. For instance, to produce 1kg of 20-mer phosphorothioate oligos, approximately 4,000 kg of solvents, reagents, and water are needed[100]. In addition, one of the main impediments for SPOS scale-up is the difficulty in intermediate analysis. As oligo batch synthesis proceeds within a packed-bed reactor, the final product can only be analyzed when material is removed from the bed. In practice, this means only after the entire

synthesis is complete. If one of the reactions fails, this will often not become apparent until the end of the synthesis and so, in the event of one poor step, the whole batch must be extensively purified, or even discarded. For small-scale syntheses, the process can quickly be repeated. But for a large-scale synthesis, loss of a batch is highly undesirable in terms of economics and operation time. Nevertheless, many significant breakthroughs have been made in SPOS scale-up recently, reviewed by Sanghvi[1].

Liquid-phase oligonucleotide synthesis (LPOS) has long been proposed as an attractive alternative to SPOS[101]. To date, the versatile SPOS platform has been able to meet the small-scale demands of research and there have been no fundamental changes to the LPOS process for the past 20 years. The major difference between the LPOS and SPOS processes is that a soluble support is used instead of the solid support, and so the reaction proceeds in liquid phase, as opposed to at the interface between liquid and solid. Owing to the homogeneous phase, this process does not suffer from mass-transfer resistance, allows high reaction concentrations, and occupies a lower reaction volume since the inert interior of the solid support no longer needs to be accommodated. In addition, anchoring the growing chain to a soluble support facilitates the downstream purification using different techniques such as precipitation, extraction, or membrane separation.

Among the reported LPOS processes, the majority have been built around precipitation to separate the growing oligo from reagents. One of the first and most developed is the high efficiency liquid-phase (HELP) process in which oligos are synthesized tethered to a soluble polyethyleneglycol (PEG-5000) support. The reaction was monitored by NMR, then the oligo-PEG conjugate was precipitated from diethyl ether and recrystallized in ethanol after each chain extension[6]. With this method, oligos were synthesized on a hundred milligram scale. A more recent related approach by Kungurtsev *et al.*[7] grew oligos around a small pentaerithritol core, synthesizing a 5-mer with near quantitative step-wise yields after precipitation from methanol. However, industrial scaling up of precipitation often requires extensive process development to control the precipitation rate and particle size, which may vary based on the desired compound[102, 103]. Instead, from the practical point-of-view, a more general downstream platform that can be used with any oligo sequences is highly desirable.

Apart from precipitation, extraction has also been explored as a method to separate growing oligos from the reaction mixture[8]. This process maximizes partition of the oligo into the organic phase using highly lipophilic protecting groups on the nucleobases, and ensures

that all the excess building block is converted to anionic species that can then be washed into the aqueous phase. With optimization, a 6-mer oligonucleotide was synthesized in 67% yield (92% coupling yield). This method is promising on a large scale, but extreme care had to be taken to prevent the hydrolysis of the phosphoryl backbone.

Bayer and Mutter[101] first identified membrane separation as a key adjunct to liquid phase synthesis for downstream processing, although in their case it was for peptide synthesis. Although ultrafiltration membranes are now routinely utilized for the final desalting step of oligo synthesis[97], until recently membranes could not be effectively employed for oligo purification: readily available polymeric membranes were not stable in organic solvents and lacked molecular discrimination. Organic Solvent Nanofiltration (OSN) membranes can now withstand harsh conditions, for instance aggressive solvents such as DMF and NMP, while being stable over a wide range of pH, as well as resilience to both organic acids and bases[45]. But most importantly, OSN membranes now have nano-separation capabilities[9], discriminating solutes in the range 100 to 2,000 Da.

With OSN technology as the separation platform, a new LPOS process exploiting OSN separation (LPOS-OSN) is explored in this work. A similar concept has previously been explored with liquid-phase peptide synthesis[104], whereby a large soluble mono-methoxy polyethylene glycol (mPEG-5000) support was attached to the growing peptide chain, and excess reagents and impurities were filtered out using OSN membranes. Building on this previous work, the use of a lower molecular weight, branched mono-disperse PEG support was explored, on which three oligo chains could grow simultaneously, increasing the atom efficiency of the process. A general schematic of the process is illustrated in Figure 2.1.

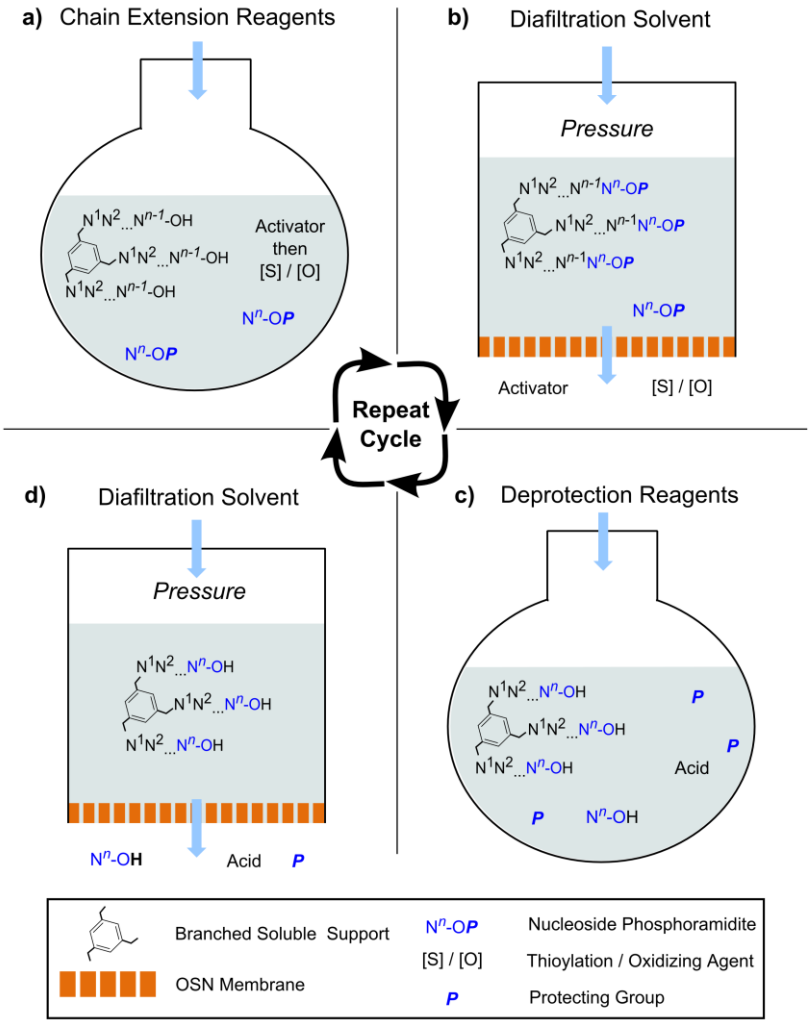


Figure 2.1. Basic schematic of the proposed LPOS-OSN process composed of 4 unit operations per cycle: a) chain extension; b) first membrane diafiltration to wash out excess reagents; c) deprotection of 5'-*O* using acid; and d) second membrane diafiltration.

As shown in Figure 2.1, the entire process proposed in this work proceeds in the liquid phase. The first nucleotide monomer, N^1, is attached to the soluble polymer support via a linker that is only cleaved at the end of the synthesis. To prepare a heteropolymer of *n* non-identical monomers, the iterative growth cycle then requires two synthetic steps, with membrane purification after each, to be repeated up to the desired length: A building block (N^n-*OP*), bearing a temporary protecting group (***P***), is first coupled to the chain terminus of the growing oligo (Figure 2.1a); the temporary protecting group ***P*** is then removed (Figure 2.1c) to commence the next chain extension cycle. After each reaction, the excess reagents are washed through the OSN membrane (Figure 2.1b, d), in a process known as constant volume diafiltration, CVD (discussed in more detail in the Experimental Section).

Nucleotide monomers are large molecules (MW > 800 Da), especially because the usual commercial ***P*** is a bulky 4,4'-dimethoxytriphenylmethyl ether (Dmtr, MW 302 Da). Thus, although most excess reagents were expected to pass through the OSN membrane, it was anticipated that immediately after chain extension (Figure 2.1a) the nucleotide monomer would not. However, after the second step, unblocking of the 5'-hydroxyl (Figure 2.1c), it was expected that the smaller fragments from the building block would then diafilter. The process is repeated *n*-1 times until the desired sequence is obtained.

Using the proposed process, a 5-mer and a 9-mer 2'-methoxy phosphorothioate oligoribonucleotides have been successfully synthesized. The sequence followed the M23D 2'-methoxy phosphorothioate anti-sense oligoribonucleotides 20-mer that have shown efficacy towards Duchenne muscular dystrophy (DMD)[105] (Sequence 5'-GGCCAAACCUCGGCUUACCU-3'). A cross-linked polybenzimidazole (PBI) membrane was identified as suitable for the process. The performance and stability of the membranes were excellent throughout the duration of the synthesis. The synthesis was carried out using commercially available phosphoramidite building blocks, employing the standard phosphoramidite coupling method[106]. Step-wise analyses were carried out using HPLC, NMR, and MS. The purity and identity were confirmed by comparing oligos from LPOS-OSN to the same species synthesized by SPOS. With the data obtained, an economic analysis has been carried out to assess the feasibility of the proposed LPOS process. It is shown that the LPOS-OSN process is highly competitive and scalable for large-scale synthesis. This new process has been designed to be generalized to any oligomeric compound constructed from suitably protected monomers (e.g. peptides, carbohydrates, PNA etc.). It is envisaged that the proposed LPOS-OSN process can stimulate synergy with the current SPOS technology to make large-scale (>100 kg) synthesis of oligonucleotides a reality.

2.3. Experimental

2.3.1. Materials

Acetonitrile (MeCN), methanol (MeOH), *N*,*N*-dimethylformamide (DMF), dichloromethane (DCM), *N*,*N*-dimethylacetamide (DMAc), diethyl ether (Et_2O), ethanol (EtOH), and isopropyl alcohol (IPA), were HPLC grade from *VWR, UK*. Anhydrous solvents were prepared by storing the solvents over baked 4Å molecular sieves. Celazole® S26 polybenzimidazole (PBI) solution (26 *wt*% polymer in DMAc containing 1.5 *wt*% LiCl) was purchased from *PBI Performance Products Inc, USA*. Non-woven polyolefin Novatexx 2471 was from *Freudenberg Filtration Technologies*, *Germany*. The crosslinker α,α'-dibromo-*p*-xylene (DBX) was purchased from *VWR*. Nucleoside phosphoramidite building blocks were purchased from *Chemgene Corp., USA* or *Fisher Scientific Ltd., UK,* ethylthiotetrazole (ETT, 0.25M solution in MeCN, *Proligo*), N-methylimidazole (NMI), phenylacetyl disulfide (PADS), pyridine, pyrrole, and dichloroacetic acid (DCA) were bought from *Sigma-Aldrich, UK*. PEG solutes were purchased from *VWR, UK*. The hub used in this work, *tris*-octagol homostar **1**, as well as different MW branched supports, were synthesized by Dr. Gaffney following the procedure reported in the literature[107].

2.3.2. PBI 17DBX Membrane Fabrication & Testing Rig

PBI membranes have been prepared and characterized by Irina Valtcheva using the procedures described in the literature[45]. PBI dope solutions were prepared by diluting the Celazole® S26 solution to 17 *wt*% with DMAc. Once a homogeneous solution had been obtained, it was cast on polyolefin non-woven support, setting the casting knife height to 250 μm. The supported film was placed in a deionized water coagulation bath for phase inversion. The resultant membrane was washed with IPA to ensure complete removal of water. To cross-link the polymer, the membrane was immersed in a well-stirred 3 *wt*% solution of DBX in MeCN and heated under reflux for 24 hours. The membrane was then removed from the cross-linking solution and washed with IPA. Finally, the membrane was immersed in a PEG-400:IPA (1:1 *v/v*) impregnation bath for 4 hours and then air-dried. This formulation of PBI membrane is referred to as PBI 17DBX (17 *wt*% PBI cross-linked with DBX).

For membrane testing and purification of oligos, membrane discs (effective area of 51 cm^2) were loaded into four cells connected in series. The diagram of the process rig is shown in Figure 2.2.

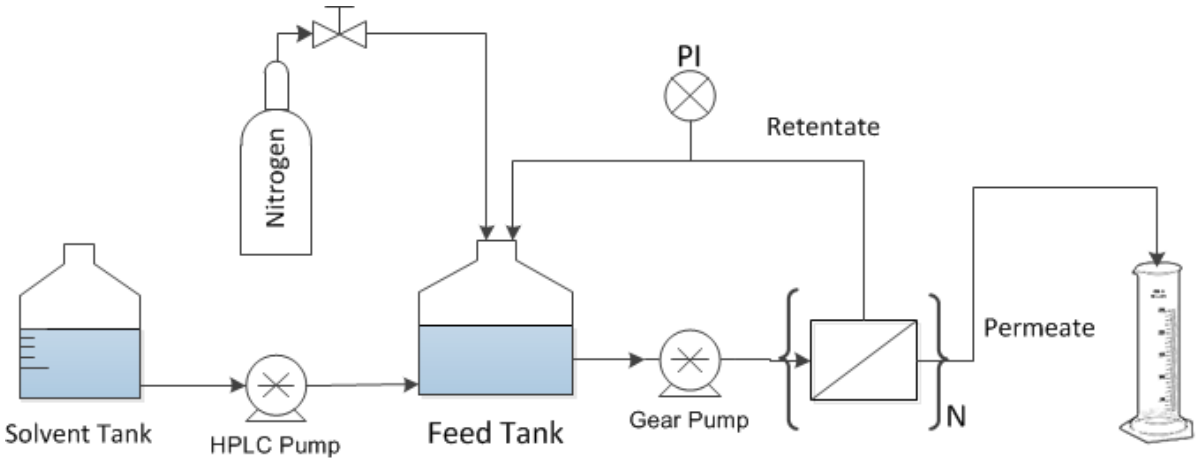


Figure 2.2. Diagram of membrane testing & diafiltration rig (a photo of the rig in Appendix A). Four cross-flow membrane cells (effective membrane area of 51 cm^2 per cell) were connected in series (N = 4). The feed tank was pressurized using nitrogen, and the system level was maintained by constant addition of pure solvent back into the feed tank.

The feed tank was pressurized to the desired pressure (typically 10 bar) with nitrogen. The gear pump (*Michael Smith Ltd.* GL Series) provided a flow rate of 66 $L.hr^{-1}$ to generate turbulence, and so to minimize concentration polarization (build-up of solute concentration at the membrane surface, leading to lower flux).

For preparative oligo purifications, the rig was charged with the crude mixture (Section 2.3.4.2), having an entire system volume of 0.4 L. The solvent was either neat MeCN or MeCN mixed with varying amounts of MeOH (explained in greater detail in Results and Discussion Section). To balance the loss of system volume from permeate, an equal volume of pure solvent was pumped into the feed tank using an HPLC pump (*Gilson* Model 305) to maintain a constant level in the feed tank. The temperature of the rig remained constant at 21 ± 1 ^oC. Whenever necessary, samples were taken from both the permeate and the feed tank which were then analyzed by HPLC.

2.3.3. Justification for Using a Branched Hub: Linear PEG versus Branched PEG Homostar Support

When performing a solute fractionation operation using membranes, the constant volume diafiltration (CVD) mode is usually employed, where the retentate volume is held constant by matching the permeate volume outflow with pure solvent input. In CVD, smaller solutes generally permeate through the membrane faster than bigger solutes. The slower the permeation rate of a solute, the higher its rejection by the membrane, and the higher the permeation the lower the rejection (mathematically defined in Eq. 1.2). Consequently, the

greater the difference in solute permeation rates (or rejections), the easier the separation becomes.

In this work the growing oligos are the product that must be highly rejected by the membrane, whereas it is desirable that everything else (excess building blocks and other reaction mixtures) permeates through the membrane.

By writing a mass balance around the system shown in Figure 2.2 (see Appendix A for derivation), it can be shown that to achieve a clean and efficient separation using diafiltration, two conditions need to be met: 1) the difference in rejection between the two solutes needs to be wide; and 2) the rejection of the larger compound should be as close to 100% as possible. The first condition determines the efficiency of separation, whereas the second condition determines the yield of the process. This is illustrated in Figure 2.3 where the normalized solute concentration (C/C_o) profile is plotted against *diavolumes*, a convenient *time-like* dimensionless variable (Eq. 2.2), also known as residence time, commonly used for CVD systems:

$$diavolume = \frac{J \cdot A \cdot t}{V_{system}} \qquad \text{(Eq. 2.2)}$$

where J represents the membrane flux ($L.m^{-2}.hr^{-1}$), A the membrane area (m^2), t the filtration time (hr), and V_{system} is the volume of the system (L). For instance, one *diavolume* means that the total permeated volume equals to the system volume, which is maintained at a constant level.

In Figure 2.3, it can be seen that the concentration falls rapidly with decreasing rejection. For instance, even with a seemingly high product rejection of 95%, the remaining concentration (*i.e.* diafiltration yield) after 20 *diavolumes* is only 38%. Notably, rejection of 0 % would resemble a CSTR residence time profile of a solute. At least one CVD is required for each chain extension. Therefore, to obtain a high diafiltration yield, the growing oligos must have near 100% rejection. On the other hand, deriving from the first condition, it is highly desirable for impurities to exhibit rejections as low as possible to achieve efficient separation: the lower the rejection of the smaller molecule, the faster the separation and the lower the number of *diavolumes* of solvent required to achieve the desired separation.

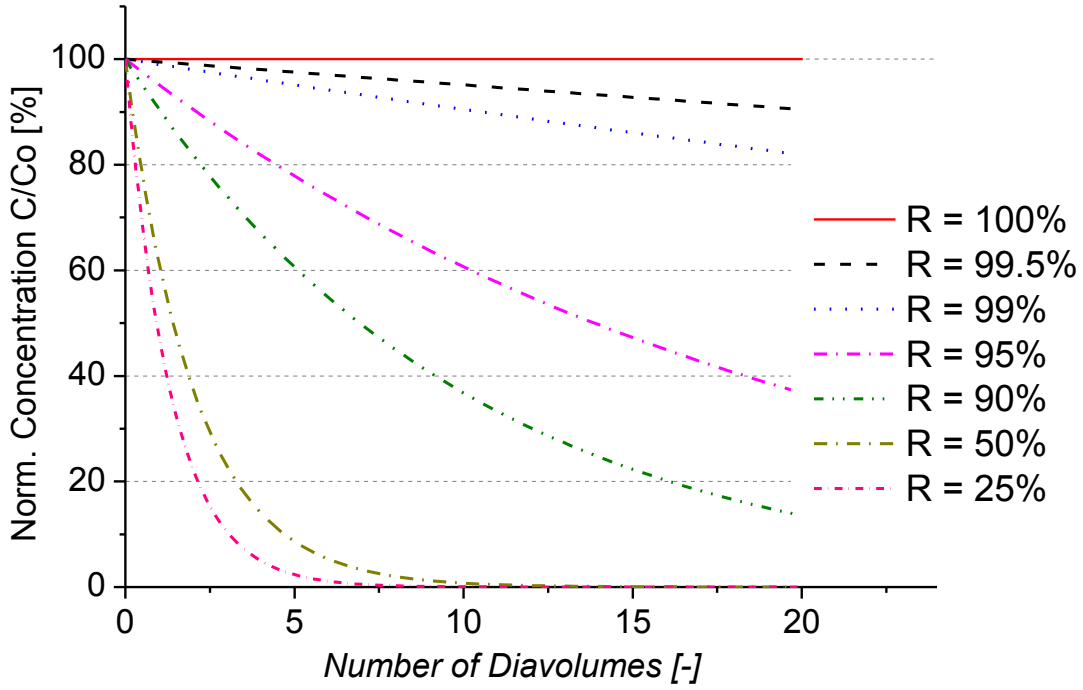


Figure 2.3. The effect of rejection on the overall concentration profile (*i.e.* diafiltration yield *versus diavolumes* at different solute rejections).

As a result of these considerations, to increase the oligo rejection and widen the rejection difference between the oligos and the excess reagents, in initial work the growing oligo was covalently attached to a long-chain linear PEG support to increase its overall size relative to the impurities. PEG was selected as the polymer support because of its high solubility, easy functionalization, and low cost. In addition, different molecular weights (MW) were readily available. However, it quickly became clear from early work of Vasconcelos[108] that it is difficult to obtain rejections higher than 95%, regardless of the MW of the PEG, which was again proven in this work as shown in Figure 2.4. It was hypothesized that because of PEG's highly flexible nature, it could thread through the membrane pores, lowering its rejection below that typically expected for more globular molecules of a similar MW.

Because of these initial observations, the use of a branched PEG support was investigated, as it has been shown that a branched solute exhibits higher rejection than linear ones of comparable MW[109]. The use of a branched support has the additional benefit of increased oligo loading per support molecule – from only two sites per linear PEG, to one site for every side-arm on a branched support.

The loaded PBI membranes were first characterized for rejection performance using a mixture of five linear PEGs (MW of 200, 400, 1000, 2000, and 8000 Da), 1 $g.L^{-1}$ of each

dissolved in MeCN (0.4 g each dissolved in 400 ml). The system (Figure 2.2) was pressurized to 10 bar and the permeate was recirculated back into the system. Both permeate and retentate samples (1 ml) were taken after 2 hours and analyzed by HPLC. Each branched PEG homostar was tested separately (1 $g.L^{-1}$) using the same system and procedures. The rejections of linear and branched PEGs are plotted against MW, Figure 2.4.

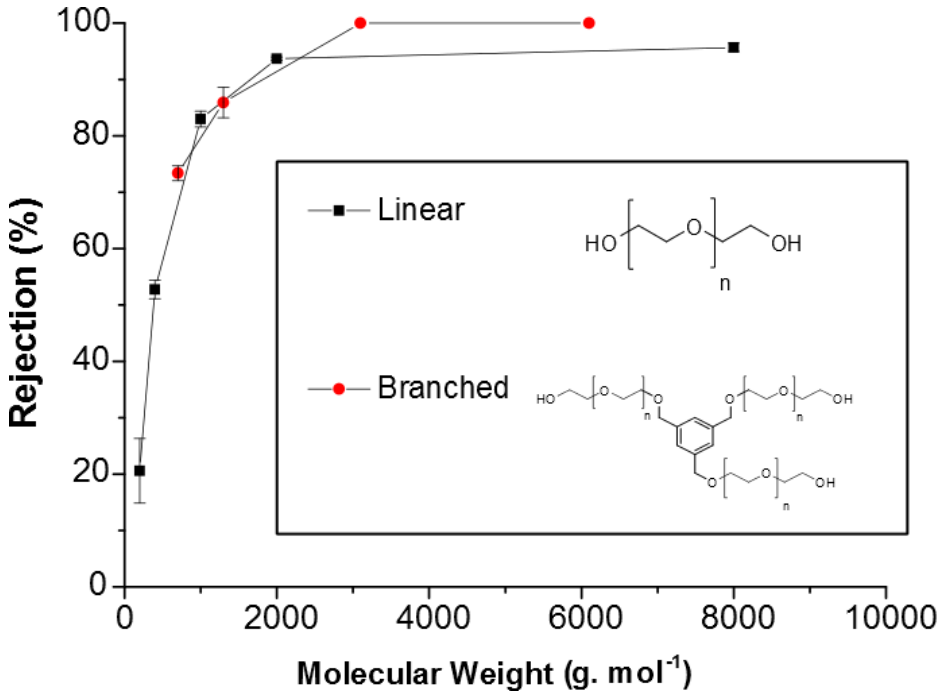


Figure 2.4. Comparison between linear *versus* branched PEG rejection on PBI 17DBX membranes. Linear PEG rejections, regardless of its MW, do not exceed 95%. Branched PEG compounds exhibit higher rejections and approach 100% above 3000 Da.

It can clearly be seen in Figure 2.4 that, in the case of PBI 17DBX, above *ca.* 3000 Da, the rejection of branched PEG homostars was virtually 100%, whereas that of the linear PEGs remained around 95% and did not rise higher. The significance of this apparently small difference should not be understated, as it makes a large difference in overall yield after many *diavolumes* have permeated, as illustrated in Figure 2.3.

Taking the homostar rejection effect as a general principle, it was then realized that a monodisperse PEG soluble support for oligo synthesis would have significant advantages over a more easily prepared polydisperse support: its complete monodispersity would ensure a discrete molecular entity, with a single MW (unlike a polydispersed support) facilitating convenient analysis by mass spectrometry (MS), as well as NMR and HPLC. A *tris*-octagol homostar (1224 Da, Compound **1** in Figure 2.6) was chosen as the monodisperse support[107] for this work because once the first nucleotide (cytidine in the present work) is attached, the

size of the dinucleotidyl PEG homostar conjugate has already become large enough (2245 Da) to be highly rejected by the PBI 17DBX membrane (>99%). In addition, as the oligo chains grow, the rejection is expected to approach 100%.

2.3.4. Overall Process Schematic & Oligonucleotide Synthesis Chemistry

Figures 2.5 and 2.6 summarize the overall process and the chemistry scheme for the LPOS platform developed in this work, respectively. The process is divided into three phases: initial loading of the support, the chain extension cycle, and release and purification of the final oligo. First, the first monomer (uridine) of the chosen sequence (20-mer anti-sense oligoribonucleotide[105] to treat Duchenne muscular dystrophy) was conjugated to the branched tris-octagol soluble support, via a succinate ester linkage. Then, the growing oligo was rotated through *n*-1 chain extension cycles, involving two synthetic procedures and two membrane diafiltrations per cycle, using the rig shown in Figure 2.2. The first pair of reactions (coupling and thioylation) constitutes *chain extension* where the next monomer is attached. After partially purifying the crude mixture using membrane CVD (procedure described in Section 2.5), the second synthetic procedure removes the 5'-*O*-(4,4'-dimethoxytiphenylmethyl) (Dmtr) protecting group from the terminus of the growing oligo, in preparation for the next round of chain extension, hereafter referred to as *detritylation*. After detritylation, the crude was again purified via membrane CVD, this time removing all the excess monomers. The detailed analysis of membrane purification efficiency is described in Results & Discussion section.

Using the proposed procedure in Figures 2.5 and 2.6, a 5-mer (pentamer) and 9-mer (nonamer) have been successfully synthesized, with the RNA sequence shown in Figure 2.6. The synthesis of 5-mer and 9-mer protected homostars started from 0.7 g (0.3 mmole) and 1.4 g (0.6 mmole) of mononucleosidyl homostar **3**, respectively. However, as the oligos became longer, the concentration varied depending on the yield after each step, and how much sample was retained for further analysis.

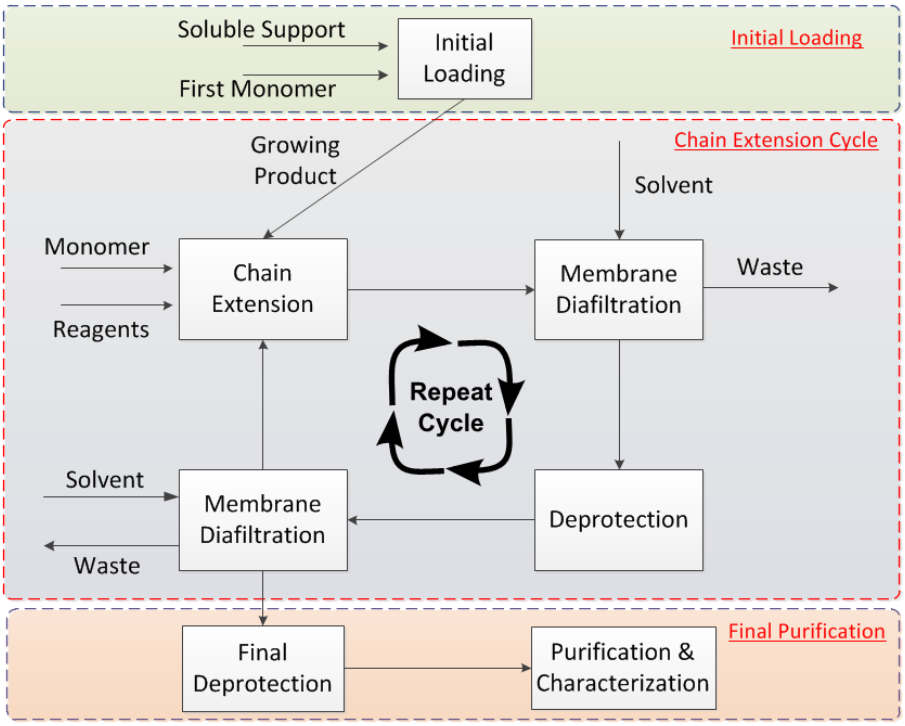


Figure 2.5. The proposed LPOS platform: overall process flowchart. The process is split into three phases: initial loading, chain extension cycle, and final purification. Each phase of the protocol is discussed in detail in the experimental section.

2.3.4.1. Initial Loading

Loaded homostar **3** was prepared by Dr. Gaffney using the following procedure. Homostar **1** (1 mmol, 1.125g) was first co-evaporated from MeCN (3 x 15 mL) then redissolved in DCM (7 mL). On a separate flask, 5'-*O*-Dmtr-2'-*O*-methyl-3'-*O*-succinyl uridine **2** (4 mmol, 3.047g) was also co-evaporated from THF (3 x 50 mL) then redissolved in DCM (14 mL) to which 2,6-dichlorobenzoyl chloride (DcbCl, 3.8 mmol, 0.54 mL) and N-methylimidazole (NMI) were added and stirred for 20 minutes. Then, the mixture was slowly added to the prepared homostar **1** solution over 45 minutes. The reaction flask was stirred overnight at 21 ^{o}C, diluted with DCM, and then extracted with saturated sodium bicarbonate. The organic layer was dried over sodium sulfate and the solvent stripped off *in vacuo*, yielding the loaded homostar **3**.

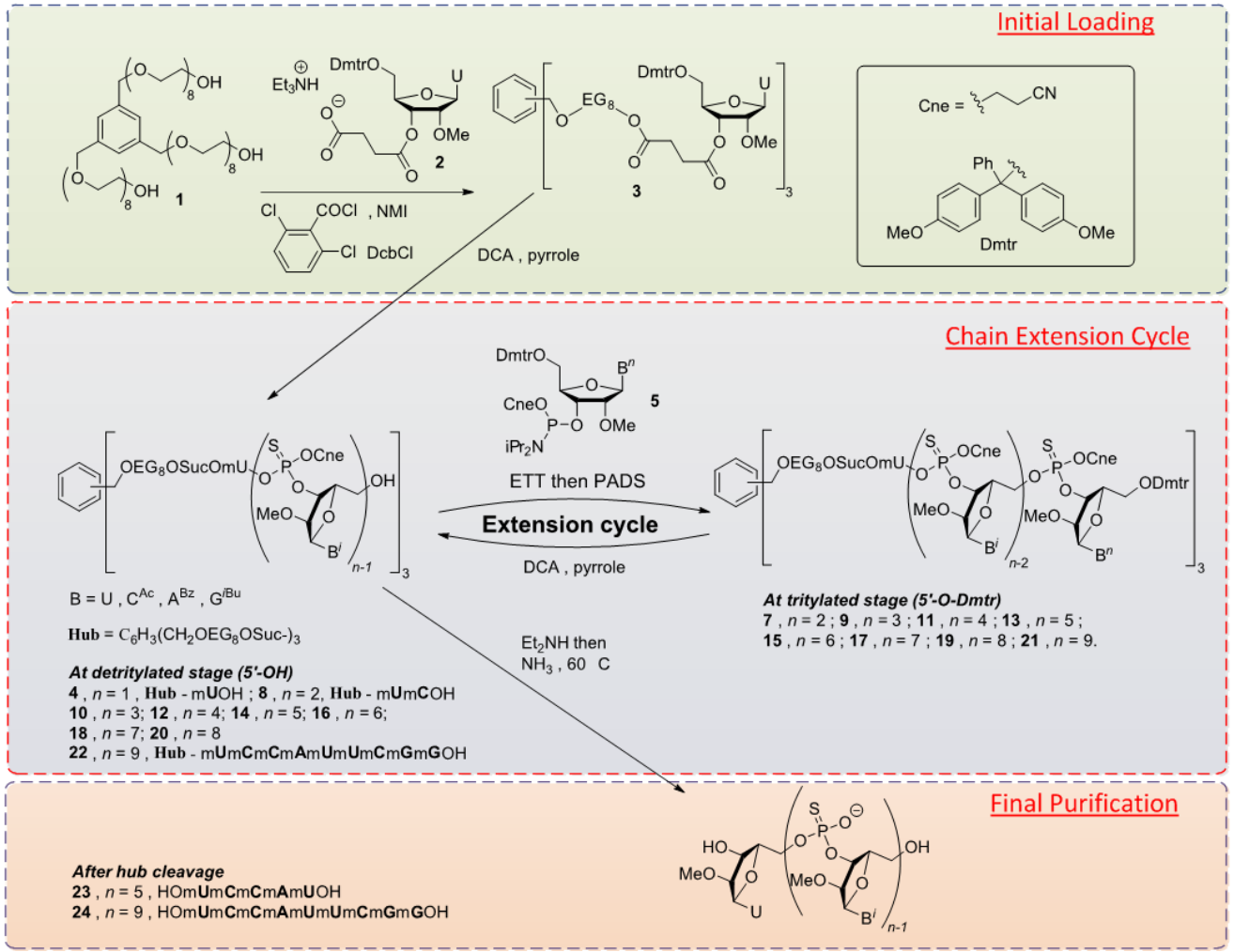


Figure 2.6. The proposed LPOS platform: overall chemistry scheme for the three phases. Each chemical species is given a unique number in the diagram.

2.3.4.2. Chain Extension & Detritylation procedure

Each reaction is slightly different due to the changing molecular weight and solubility of each substrate, a chain extension protocol to dimer is described: The starting oligonucleotidyl homostar (0.503 mmol, 1.130g) was dissolved in DMF (1 mL) under N_2 and co-evaporated from MeCN (3×20 mL). The next phosphoramidite monomer (1.5 eq. per OH, 2.26 mmol, 1.808g) was added as a dry solid, and the mixture was dissolved in 0.25M ETT in MeCN (3 eq. per OH, 4.53 mmol, 18.1 mL). After stirring for 0.5 hr at 21 ^{o}C, PADS (3 eq. per OH, 4.5 mmol, 1.36g) and pyridine (18.1 mL) were added, and stirring continued for another 0.5 hr. Notably, PADS was used as obtained, instead of allowing a solution of PADS in pyridine or 2-picoline to develop overnight (a common practice to increase the reactivity of PADS). It should again be noted that the scale of reaction varied with yield and chain length.

In SPOS, an additional capping step is usually included in the cycle, using acetic anhydride to cap any unreacted hydroxyl group. However, by HPLC and NMR, no incomplete reactions were detected. Also, since there is no mass transfer between the bulk liquid and a solid phase interface, there is a reason to postulate that couplings to the fully dissolved supported oligo will be faster and more complete than SPOS couplings. Hence, the capping step was deliberately omitted to shorten the chain extension cycle.

After chain extension and the subsequent membrane CVD in MeOH-MeCN (5-20% MeOH), the supported oligo was washed out of the membrane rig and the solvent evaporated *in vacuo*. The residue was re-suspended in dry DCM (62 mL) to which pyrrole (2 *vol*%, 1.05 mL) then DCA (1 *vol*%, 0.62 mL) were added; upon addition of DCA the substrate dissolved and an intense orange color appeared which dissipated over the next 10 minutes. Stirring was continued for a total of 30 minutes to ensure complete detritylation of the 5'-*O*-Dmtr protecting group. Upon completion of the reaction, 1 equivalent of pyridine was added per mole of DCA to neutralize the solution; with longer oligos a thick precipitate formed at this point, presumed to be the product. This re-dissolved when diluted into MeOH-MeCN (5-20% MeOH, 250 mL), and was then subjected to another CVD in MeOH-MeCN (5-20% MeOH). Initially, it had been anticipated that it would be possible to carry out only one CVD per cycle by detritylating immediately after chain extension. However this was not successful, and led to many unidentified side products of longer HPLC retention time

if left for any length of time (Appendix B). Accumulation of even low levels of such contaminants with repeated cycles of chain extension could not be risked, which is why the double CVD approach reported here was adapted.

2.3.4.3. Membrane Purification – Constant Volume Diafiltration (CVD)

After the chain extension (coupling and thioylation, described in section 2.4.2), the crude material was first diluted with either MeCN or MeOH-MeCN (250ml, 5-20% MeOH) and the rig (containing 150ml solvent) was charged with this solution. It was found that the choice of solvent (MeCN or MeOH-MeCN) had negligible effect on the membrane performance in terms of flux and rejection, but increasing proportion of MeOH with oligo chain length was essential to maintain the solubility of the supported oligos. The rig was then pressurized to 10 bar to commence CVD, and this continued until a total of 13-15 *diavolumes* had permeated, after which the retentate was washed out of the rig; the solvent was evaporated to provide a mass balance, and the residue analyzed by NMR, MS, and HPLC.

After detritylation in DCM (section 2.4.2), the reaction was quenched with an equal volume of pyridine to DCA (approximately equimolar amounts), then diluted with MeOH-MeCN (250 ml, 5-20% MeOH). Prior to CVD, to ensure that DCM did not damage the O-ring seals or membranes, the crude solution was concentrated on a rotary evaporator until the vapor pressure reached 20 mbar at a bath temperature of 30 °C, when DCM was assumed to have been removed. The crude solution was then charged to the rig, which was once more pressurized to 10 bar for the second round of CVD. This time, the solvent for the first 5 *diavolumes* contained 1*vol*% pyridinium dichloroacetate (Py.DCA) in MeOH-MeCN (5 – 20% MeOH, 400 mL per *diavolume*), followed by 10 *diavolumes* with neat solvent. The addition of Py.DCA was found to facilitate the removal of excess monomers, discussed in more detail in section 3.2.1. The purified retentate was washed out of the rig, the solvent evaporated to provide a mass balance, and the residue again analyzed by NMR, MS, and HPLC.

After chain extension and detritylation, with their associated two rounds of CVD, at this point the solution of supported oligo had only one detectable impurity, Dmtr-pyrrole which forms during the detritylation reaction. It is assumed that the bulky shape of Dmtr-pyrrole (despite a relatively low MW), and perhaps a contribution from its hydrophobicity as well, made it difficult for this molecule to permeate through the

membrane and to be removed by CVD. The retentate solution was evaporated to dryness, re-dissolved in DCM (15 mL). The solution was added dropwise to a stirred solution of diethyl ether (250 mL). The precipitate was filtered off and collected as a gray powder.

2.3.4.4. Final deprotection and purification

A sample of supported oligo (5-mer **14**, 20.2 μmol, 152 mg) was suspended in MeCN (4 mL) to which was added diethylamine (20*vol*%, 1 mL) and stirred. The oligos only dissolved upon addition of diethylamine. After 30 min the solvent was evaporated *in vacuo* and the residue dissolved in conc. ammonia (2 mL), filtering through a pad of cotton wool to remove any insoluble material using further 3 mL of conc. ammonia. The filtrate was placed in an ACE pressure tube fitted with PTFE screw top and O-ring seal. The solution was heated to 55 °C and stirred overnight and the next day filtered once more through a pad of cotton wool. The filtrate was evaporated to dryness, and the residue co-evaporated from ethanol (3×10 mL). Finally to remove protecting group and support fragments, the crude solids were added to a stirring solution of MeCN and the precipitate filtered off to afford the title compound **23**.The globally deprotected oligos have been analyzed by Dr. Glynn Williams offsite.

2.3.5. Analytical Method

2.3.5.1. High Performance Liquid Chromatography (HPLC)

All samples during the chain extension cycle were analyzed by HPLC using an *Agilent* 1100 Series system equipped with a UV detector and *Varian* 385-LC ELSD detector. The pump flow-rate was set at 1 $ml.min^{-1}$, the injection volume was 30 μL, the column temperature was 30 °C, and an ACE C18 RP column (*Hichrom Ltd, UK*) was fitted. The column was eluted with a gradient of MeOH and water buffered with 100 mM ammonium acetate. The UV wavelength was set at 260 nm, the ELSD evaporation temperature was set to 40 °C, nebulization temperature at 55 °C, and the nitrogen gas flow rate was at 1.5 SLM (standard liter per minute).

2.3.5.2. Nuclear Magnetic Resonance (NMR) & Mass Spectrometry (MS)

NMR spectra were recorded on Brüker AV-400 or Brüker AV-500 spectrometers. Mass spectra were recorded on *Micromass* MALDI micro MX, or *Micromass* LCT Premier (ESI) mass spectrometers.

2.4. Results and Discussion

2.4.1. Membrane Screening & Characterization

Among the available OSN membranes including polyimide, polyamide thin film composite, and ceramic membranes, a cross-linked polybenzimidazole (PBI) membrane was selected as the most suitable. The criteria for membrane selection were: 1) chemical and solvent stability, 2) high rejection of the product, 3) low rejection of the impurities, and 4) durability and longevity. Polyimide and polyamide membranes were not stable for prolonged periods under the oligonucleotide synthesis conditions[45] and thus were discarded. A set of PBI membranes cross-linked with DBX (PBI 17DBX) exhibited promising PEG rejection data, shown in Figure 2.4. Furthermore, the chemical stability of PBI membranes and their reproducible performance during OSN has already been demonstrated in the work of Valtcheva *et al.*[45]

PBI 17DBX membranes showed exceptional chemical and mechanical stability towards all the reagents used here, as well as long service time with excellent durability. It was determined that the threshold pressure of PBI 17DBX membranes is approximately 15 bar, *i.e.* above 15 bar the membrane underwent irreversible compaction and a permanent loss of membrane performance. Hence, the membrane was operated at 5-10 bar at all times, which ensured constant membrane performance for more than a year. The membrane permeance remained virtually constant at approximately 8 $L.m^{-2}.hr^{-1}.bar^{-1}$ over the entire duration of the 9-mer (nonamer) synthesis. Slight variations in flux were observed, depending on the solution concentration and solvent composition, but periodic testing of the PEG rejection by the membranes between preparative experiments confirmed that the performance was unchanged.

2.4.2. Chain Extension & Detritylation (combining reaction and diafiltration)

2.4.2.1. Identification of Compounds in the Post-Reaction Crude Mixture

As far as could be determined in the liquid phase oligo synthesis reactions presented here, the rate of reaction was fast (always complete after the first HPLC analysis) and efficient, requiring only a relatively low excess of phosphoramidite monomer (1.5 eq.). SPOS typically employs more than 2 equivalents excess monomer [5]. It should be stressed that in oligonucleotide synthesis, the main economic driver is the phosphoramidite excess (discussed in Section 3.5).

The post-reaction crude mixture at first seemed to contain more byproducts than had been expected. This resulted from conversion of the excess phosphoramidite monomer into not one, but a mixture of four different phosphoryl derivatives on addition of PADS to the coupling mixture, as shown in Figure 2.7. Apart from the monomer excess, the crude mixture also contained ETT and its diisopropylammonium salt, pyridine, and a large number of PADS-related species.

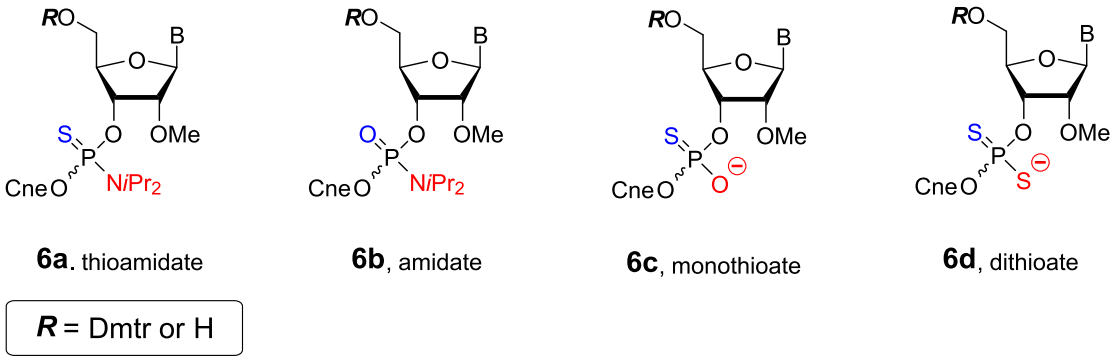


Figure 2.7. Excess monomers identified during the chain extension cycle. Thioamidate (**6a,** Dmtr or H) and amidate (**6b,** Dmtr or H) are neutral species, whereas monothioate (**6c,** Dmtr or H) and dithioate (**6d,** Dmtr or H) are charged species.

As the process developed in this work is a liquid phase method, it is possible to apply versatile and highly informative analytical techniques such as HPLC, NMR, and MS that are unavailable to SPOS. HPLC was used to determine if the reaction had reached completion or not (Appendix B), and also whether the impurities had been completely removed. Since ^{31}P NMR only detects phosphorus containing compounds, this was able to show what types of monomers were present, and also whether they had been removed or not. MS was mainly used to confirm the identity of the product, and for the dimer and trimer LC-MS could also be used to identify some minor

product-related impurities. The HPLC, ^{31}P NMR, and MS data of the dinucleotidyl homostar (tritylated **7**, and detritylated **8**) are presented in Figure 2.8.

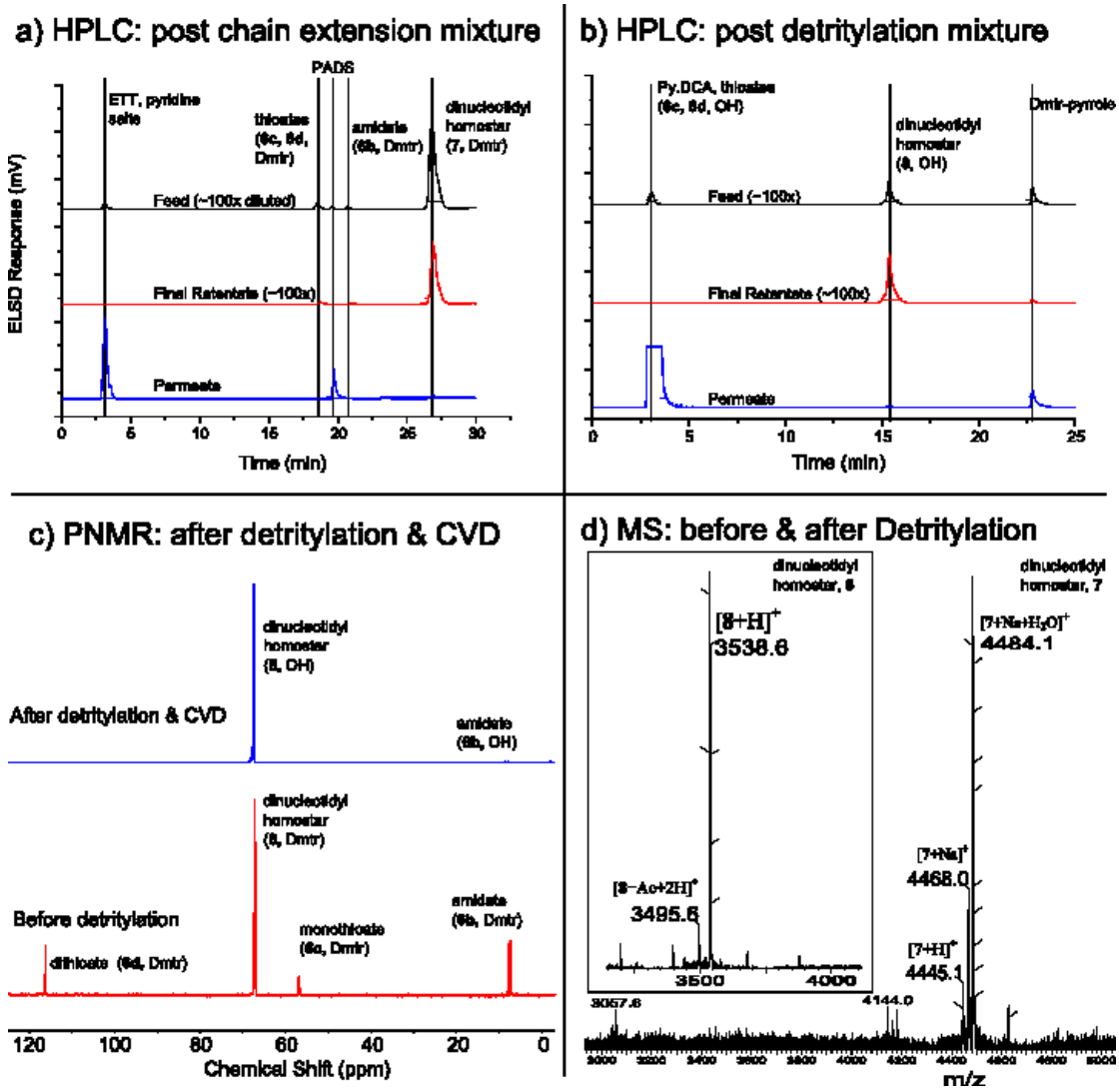


Figure 2.8. Analysis of a typical chain extension cycle, from mU loaded homostar **3** to 5'-*O*H dinucleotidyl homostar **8**. HPLC of feed, retentate and permeate **a)** after chain extension, but before detritylation, and **b)** after detritylation. Small molecule reagents – PADS, ETT, and pyridine – permeate through the PBI membrane in a), but monomer-related species are retained; after detritylation excess monomers permeate, but Dmtr-pyrrole only permeates partially. **c)** ^{31}P NMR of retentates in a), red, and b), blue. Three classes of monomers (except thioamidate **6a**) are present before detritylation, but are absent after detritylation. **d)** MALDI-TOF+ MS confirming the presence of compound **7** and **8**. Also, N-deacetylation of cytosine base for **8**, a common impurity, is identified ([**8**−Ac+2H]$^+$ = 3495.6, calc. $C_{142}H_{212}N_{18}O_{71}P_3S_3^+$ = 3495.2).

Figure 2.8 summarizes a typical set of data obtained for the first chain extension cycle; the ^{31}P NMR and MS are representative of later cycles, although the HPLC becomes weaker for longer oligos (explained in Section 2.4.2.3). Figure 2.8a depicts the HPLC traces of dinucleotidyl homostar **7** (5'-*O*-Dmtr) post-chain extension, both

before and after membrane CVD. All the HPLC peaks were resolved except for the thioamidate (**6a**, R=Dmtr) peak, which overlapped with the product **7** (5'-*O*-Dmtr). PADS showed more than one HPLC peak and their relative intensities varied with the batch. Figure 2.8a demonstrates that all the small reaction excess reagents, *i.e.* ETT, pyridine, and PADS, were completely removed in the first diafiltration. However, all four types of excess monomers (**6**, R=Dmtr) remained in the final retentate, as they were all highly rejected (>95%) by the PBI membranes. The main reason for such high rejections was assumed to be the bulky 5'-*O*-Dmtr protecting group.

Figure 2.8b shows HPLC traces for the same experiment, but post-detritylation to dinucleotidyl homostar **8** (5'-*O*H), where the thioamidate (**6a**, R=H) and amidate (**6b**, R=H) peaks overlapped with product **8**. After membrane CVD, only two peaks were present in the final retentate: dinucleotidyl homostar **8** (5'-*O*H), and Dmtr-pyrrole. Complementing the HPLC data, it can be seen in the ^{31}P NMR (Figure 2.8c) that after detritylation all the charged thioate monomers (**6c**, **6d,** R = H) were removed efficiently by diafiltration. However, thioamidate (**6a**, R=H) and small traces of amidate (**6b**, R=H) monomers were detected in the final retentate (thioamidate **6a** not shown in Figure 2.8, explained below). The measured rejection of amidate **(6b**, R=H) was 85%, but the rejection of thioamidate (**6a**, R=H) was significantly higher at >99%. Thus, the amidate **(6b**, R=H) was mostly removed by the second diafiltration, but the thioamidate **(6a**, R=H) could accumulate as a major component of the excess monomers.

Notably, the ratios of the concentrations of the four types of monomers varied considerably from one chain extension to the next. Since the relative amounts of excess monomers were only quantified (by ^{31}P NMR) after the first CVD, this variation may be partially explained by slight differences in the rejections of the monomers. However, it was found that reducing the excess of PADS from 10 to 3 equivalents consistently reduced the proportion of thioamidate generated to undetectable levels. Thus, it was beneficial to use the lower excess of PADS to minimize the amount of thioamidate generated, and so to maximize oligonucleotidyl homostar purity at the end of each chain extension cycle. Figure 2.8d presents the MALDI MS data for the tritylated and detritylated dinucleotidyl homostar (**7** and **8**, respectively), which clearly shows the expected peaks of $[\mathbf{7}+Na+H_2O]^+ = 4484.1$ and $[\mathbf{8}+H]^+ = 3538.3$.

The only significant contaminant remaining at this point, after the second CVD, was Dmtr-pyrrole. Although this molecule does permeate PBI 17DBX (see permeate in lower trace, Figure 2.8b), its absolute quantity and rejection is too high (>90%) to be removed completely. Although it probably does not interfere with the next chain extension, in order to obtain accurate mass data the growing oligonucleotidyl homostar was deliberately precipitated in diethyl ether to remove the remaining Dmtr-pyrrole. Undoubtedly, this step should be avoided or replaced in a scalable LPOS strategy, either by using a different membrane, or a different protecting group.

2.4.2.2. Ion Exchange Transport through PBI membranes

After detritylation, it was initially observed that the rejection of thioate monomers (**6c, 6d,** R=H) was over 95% in MeCN, making CVD impractical. Surprisingly, upon addition of 1*vol*% DCA, the thioate monomers began to permeate. However, significant capping of the 5'-*O*H by DCA esters was observed, as well as acid catalyzed deacetylation of the cytosine base (shown in Figure 2.8d). Therefore, the DCA was replaced by 1*vol*% Py.DCA (in 20% MeOH-MeCN), when it was observed that the anionic thioate monomers (**6c, 6d,** R=H) again permeated through the PBI membranes with rejections lower than 50%, although the higher rejections of neutral monomers (**6a, 6b**, R=H) were unaffected. Considering that the difference in MW between the thioate monomers and neutral monomers is less than 84 Da, the differences in rejections were quite remarkable. Even so, prolonged exposure of the oligo to mildly acidic Py.DCA still resulted in traces of cytosine *N*-deacetylation, although to a lesser extent.

From this behavior it was hypothesized that the anionic thioate monomers (**6c, 6d**), paired with ETT cation, permeated via an anion exchange mechanism. Such a mechanism would be consistent with the poly-basic structure of cross-linked PBI[45], which can deprotonate Py.DCA ($Py(+)H.DCA(-)$ pair). In addition, the PBI backbone may contain some permanent positive charges on cationic benzimidazolium rings that form during the membrane cross-linking step, shown in Figure 2.9. Addition of Py.DCA will also facilitate movement of membrane-associated thioates (**6a**, **6b**, R=H) through the membrane by exchange of anions between immobile benzimidazolium cations and pyridinium cations in solution. A postulated transport mechanism is illustrated in Figure 2.9. Notably, thioate monomers did not permeate at

the tritylated stage (**6c, 6d**, R = Dmtr), suggesting that permeation occurs through a combination of both ion exchange and sieving mechanisms.

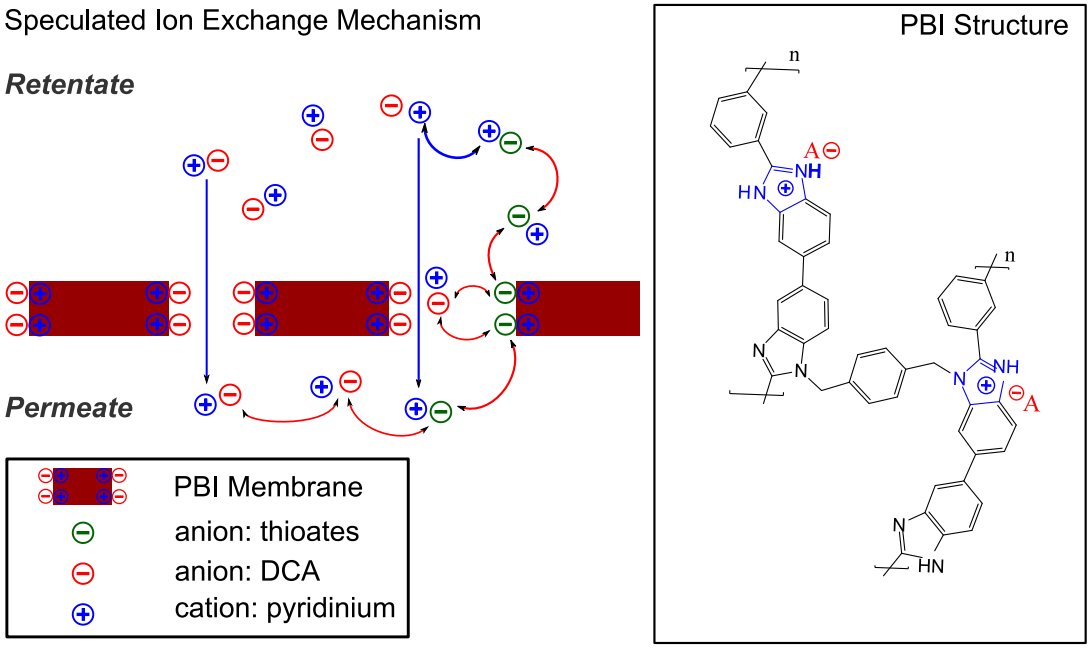


Figure 2.9. Transport of anionic thioate monomers (**6a, 6b**, R=H) through PBI membranes via ion-exchange mechanism. The cationic benzimidazole backbone allows anionic species to exchange between the sites, pushing out the thioates to the permeate side via concentration gradient.

2.4.2.3. Synthesis of 9-mer

From the outset, the choice of a mono-disperse support was seen as an opportunity to exploit HPLC throughout oligo synthesis. A stack of HPLC chromatograms of OSN retentates from dimer **7** up to 7-mer **17** is presented in Figure 2.10. Firstly, it can be seen that tritylated (-*O*Dmtr) oligo-homostars elute from the HPLC column later than detritylated (-*O*H) species, owing to the hydrophobicity of the Dmtr protection. Secondly, the peaks gradually get broader with longer chain length. The main reason for such peak broadening is the exponential increase in the number of diastereoisomers in the oligo-homostar's phosphate backbone. For instance, the number of diastereoisomers quadruples from 2-mer (four) to 3-mer (sixteen) (Appendix B).

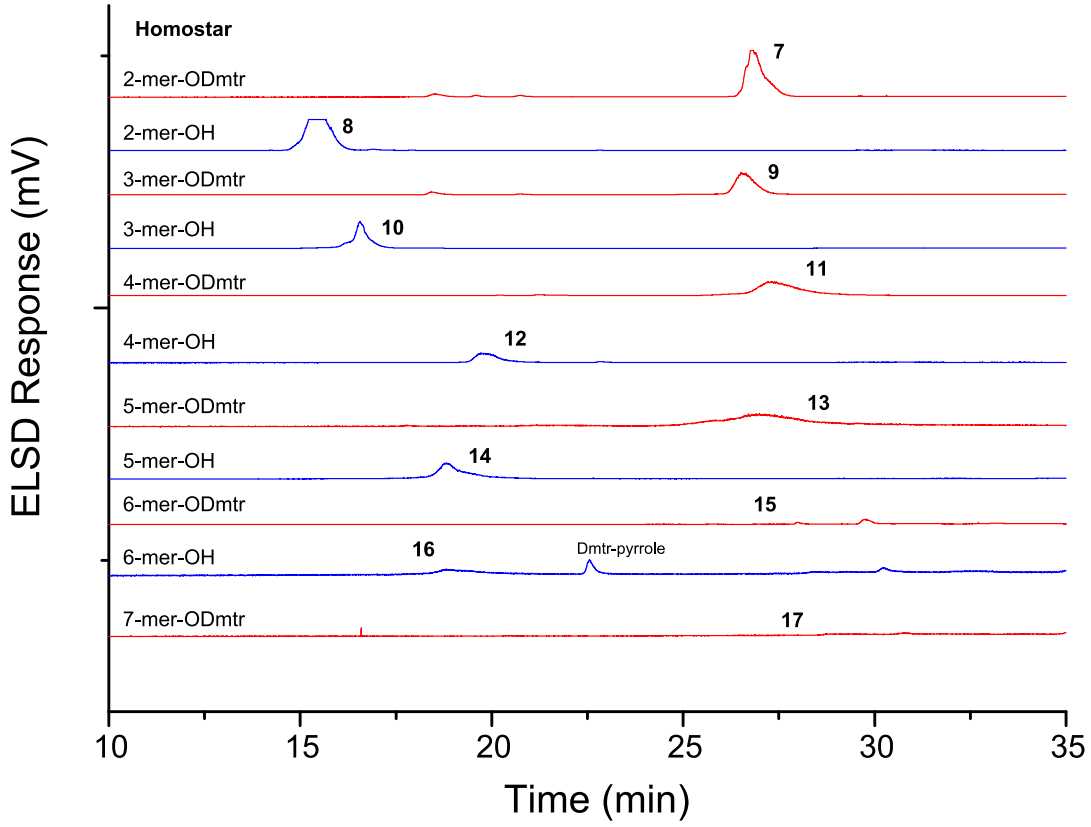


Figure 2.10. HPLC chromatograms up to 7-mer oligos (from 9-mer preparation). Tritylated (-*O*Dmtr) compounds have longer retention times than detritylated (-*O*H) species. The peaks became too broad to be detected by HPLC after 7-mer.

Thirdly, the solubility of the oligos in the HPLC mobile phase (MeOH-water) decreased with the chain length, and the samples had to be diluted leading to weaker peak intensity. Hence, from 7-mer **17** onward, it was not possible to analyze the oligos using HPLC, and the ^{31}P NMR was mainly employed for assessing the oligo purity. Nevertheless, HPLC has proved to be an effective analytical tool to monitor the extension reaction, as well as to detect the presence of impurities. In order to analyze the oligo-homostars beyond 7-mer, an effective destructive method to remove the diastereoisomeric artifact (*e.g.* global deprotection) should be employed.

2.4.2.3. Solubility of the Growing Oligonucleotidyl Homostar

The oligos' solubility changed drastically with the growing chain length. It was observed that their solubility in neat MeCN rapidly decreased with chain length, so that while 2-mer **8** had moderate solubility in MeCN, 4-mer **12** was almost insoluble. However, upon the addition of MeOH to the solution, the oligo solubility was markedly enhanced (5-20% MeOH in MeCN). Notably, the oligo-homostars were insoluble in both neat solvents, dissolving only in the mixture. The same was true for

chlorinated solvents, when the oligo-homostars only dissolved in mixtures of chloroform or dichloromethane and methanol. This suggests these species require a protic solvent, possibly to disrupt hydrogen bonding of the nucleobases, to be solvated. In addition, a higher fraction of MeOH was required with the increasing chain length, possibly due to greater opportunities for intermolecular H-bonding with larger molecules. Even so, the 9-mer **22** had an excellent solubility (above 10g.L^{-1}) in 20% MeOH-MeCN.

Apart from the MeOH-MeCN mixtures, the oligo-homostars also exhibited excellent solubility in neat DMF (above 100 g.L^{-1}) and DMF-MeCN mixtures. Even though oligonucleotide phosphoramidite couplings have been reported in DMF[7], there was some evidence that the chain extension reaction was not as fast in neat DMF as in MeCN. As the chemistry of the growing oligos is quite complex, it seems inevitable that a mixed solvent will be required for both synthesis and purification. Nevertheless, a single-solvent system for both reaction and separation is highly desired from the process perspective and will be explored further in Chapter 5.

2.4.2.4. LPOS-synthesized oligonucleotide yield

Chain extension yields and the corresponding overall yield for 9-mer synthesis are summarized in Figure 2.11 below. Yield values were calculated from the measured mass data assuming 100% product purity, and are reported as molar yield.

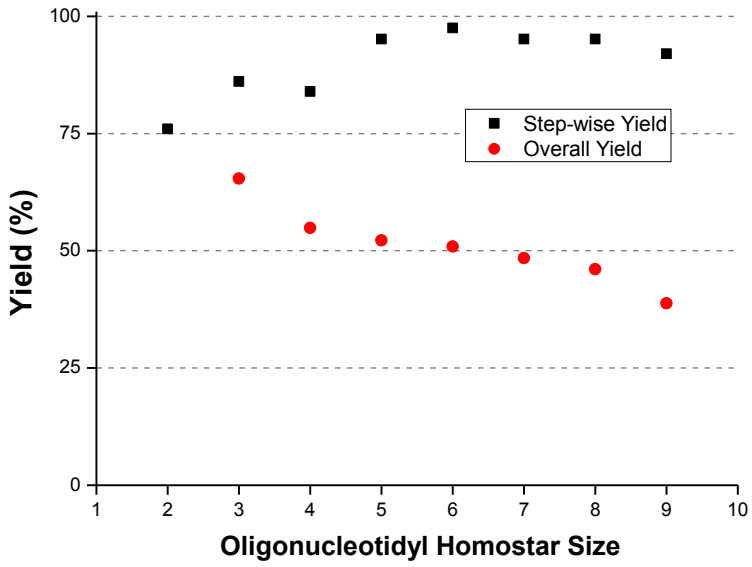


Figure 2.11. Summary of chain extension yield and the corresponding overall yield, starting from the mononucleosidyl homostar **3** as the basis of calculation: The yield is calculated from the mass data and reported as molar yield, assuming 100% purity.

Aligning with the expectations, it can be seen in Figure 2.11 that the step-wise yield improved with the chain length, as bigger oligo-homostars exhibited higher rejections by the membrane. Indeed, from the 5-mer onward the average step-wise yield was higher than 95%. It can also be seen that the major loss in the overall yield resulted from the first three chain extension cycles, contributing half the total decline. Although the rejection of the oligo homostars at the dimer stage was high at 99%, the isolated yield after 25 *diavolumes* was only 75%, as predicted from Figure 2.3. The rejection of the oligo-homostars rose to 99.8% after tetramer. However, it should be noted that the calculated yield was solely based on the mass data and the purity was not taken into account. Hence, the yield measurement is not entirely accurate. Nevertheless, the rejection of the product is approximately correct based on the HPLC integration, and the obtained yield values are likely to be within errors.

It is often difficult to obtain a complete rejection (100%) using membranes, and rejection values between 95 – 99.9% are commonly observed among tight membranes[22]. This is due to a low level of defects that inevitably arise during the fabrication process, and/or to the permeation mechanism through the membranes. Generally, the defect-related drop in rejection is eliminated when membrane modules are employed, due to the much larger area to system volume ratio. Nevertheless, it is anticipated that the maximum yield per chain extension is likely to be below 100% due to incomplete rejection. Thus, to compensate for the major losses in the first three chain extension cycles, a different membrane configuration needs to be applied, such as membrane cascades, which will be discussed in subsequent chapters.

2.4.4. Final Deprotection and Purity Analysis

Two different batches of pentanucleotidyl homostar **14**, and one batch of 9-mer homostar **22**, were cleaved from the core octagol-homostar support and analyzed for purity by HPLC (Figure 2.12).

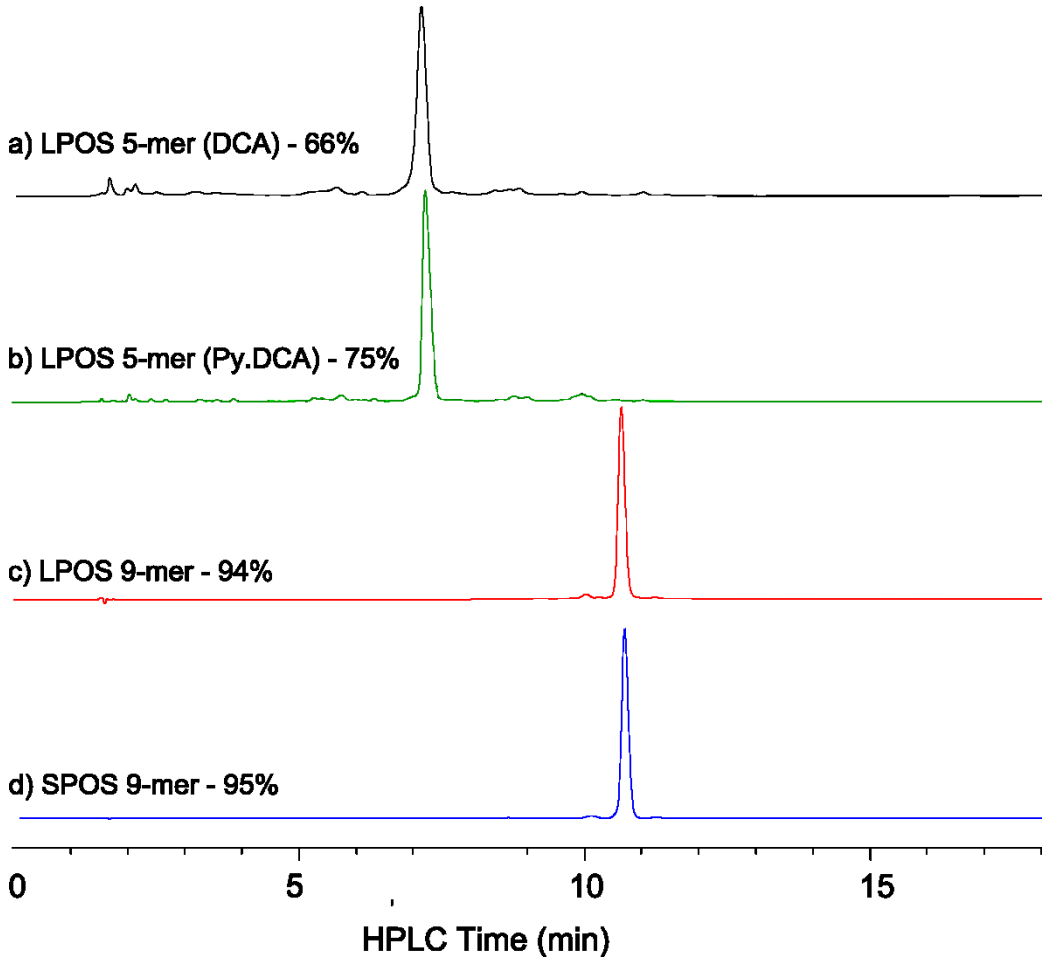


Figure 2.12. Final purity analysis by HPLC after global deprotection: a) 5-mer oligo prepared by LPOS-OSN using 1*vol*% DCA for deprotection; and b) 5-mer oligo by LPOS-OSN using 1*vol*% Py.DCA for deprotection; c) 9-mer by LPOS-OSN, then purified by ion exchange; d) 9-mer by SPOS after desalting. Purity is roughly estimated by integrating the product peak.

For comparison, a 9-mer oligo sample of the same sequence was also synthesized using standard automated SPOS. It can be seen in that the main peaks are indeed the desired 5-mer (**23**) and 9-mer (**24**) oligos; the purity is roughly assessed by integrating the product peak. The 5-mer purity was improved by switching from using DCA during OSN of the detritylated oligo-homostars (66%) to Py.DCA (75%), presumably because capping of the 5'-*O*H was prevented reducing the amount of short-mer contaminants (*n*-1, *n*-2, …and/or *n*-*i*). The peaks after the product suggest the presence of long-mer (*n*+*i*) impurities, which may be generated during chain extension reaction when a newly coupled Dmtr-nucleotide is detritylated by the mildly acidic ETT activator, leading to double chain extension. Also the *N*-deacetylated cytosines can serve as sites of chain branching to generate long-mers, although they are not very reactive. In general, the purity of oligos prepared by LPOS

was not as high as those prepared via SPOS. Another possible source of impurities may have arisen from deliberate omission of the capping step after each chain extension, although no incomplete reaction could be detected by HPLC. However, comparing the impurity profile of SPOS derived oligos (Figure 2.12d), where short-mers and long-mers peaks are clearly identifiable, to the impurity profile for the LPOS-prepared oligos (Figure 2.12a-c) exhibiting many irregular and unidentifiable peaks that do not overlap with the SPOS contaminants, it is possible that these peaks are not oligo-related. Thus, a simplistic HPLC purity comparison may not be precise. In the future, LC-MS techniques will be employed to understand this impurity profile.

Nevertheless, the final purity of 9-mer was lower than anticipated (49%), mainly because the last coupling reaction had not reached completion (17% of *n*-1 impurity observed, confirmed by LC-MS). It is possible that the chain extension did not reach completion because the 5'-mGmG dinucleotide is the most hindered internucleotide linkage to form. Even so, it can be seen that upon purification of the 9-mer using ion exchange chromatography, the purity can be increased up to acceptable standards (> 90%)[1].

2.4.5. Economic Analysis

Currently, the major impediments for SPOS scale-up are the costs associated with it, and the need for larger sizes of SPOS synthesizer depending on synthesis scale. For instance, the cost of a 1kg scale synthesizer is approximately £2 million. Also, the price of oligo therapeutics prepared by SPOS varies significantly depending on the synthetic routes and chemical modifications. On the other hand, the chief attraction of membrane-based processes is that they can be implemented on almost any scale. To understand the competitiveness of the LPOS-OSN platform, an economic evaluation of the proposed process was carried out from the data obtained in this pilot project.

The basis for calculations was the synthesis of 1 kg of a 23-mer oligoribonucleotide. The required reagents and solvents were back-calculated accordingly. Some crude assumptions were made: (i) initial capital investment on the membrane rig of £250,000 was amortized with a capital charge factor of 0.2 (split into 5 years); (ii) a total of 20 batches per year was assumed (based on the operation time and membrane flux); (iii) the system volume was fixed at 100L (based on the concentration); (iv) only acetonitrile was used as solvent; and (v) the labor and operation cost was not taken into account. Although the membrane process is

considered as low labor-intensive process[102], an exact operational cost was difficult to estimate at this stage. It was found that solvent accounts for a large proportion of the overall cost, and hence two different scenarios were considered: the case with solvent disposal, and a scenario with 90% solvent recovery. The overall cost breakdown is shown in Table 2.I and Figure 2.13 below.

Table 2.I. Overall cost breakdown per 1kg batch of oligos

Item	Calculations	Solvent Disposal	Solvent Recovery
Capital Cost	Amortize by 0.2, 20 batches.yr^{-1}	£2,500	£2,500
Phosphoramidite Monomer	1.5 eq., £10.2.g^{-1}	£53,000	£53,000
PADS, ETT, DCA, etc		£1,500	£1,500
Solvent	Acetonitrile, £0.8.L^{-1}	£60,700	£6,300
Membrane	18m^2, £1600.m^{-2}, 10 batches	£3,800	£3,800
Homostar support		£100	£100
TOTAL (kg^{-1})		£121,600	£67,200
TOTAL (g^{-1})		**£122**	**£67**

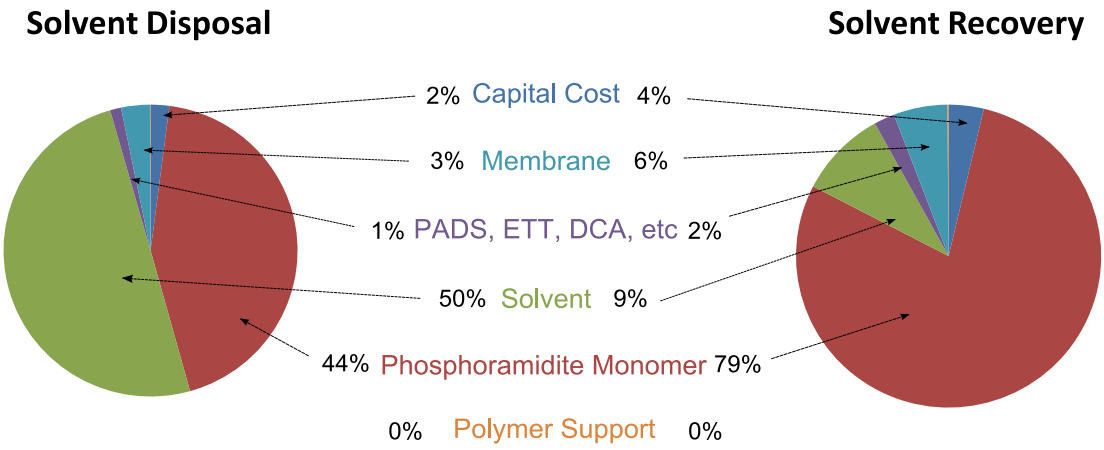


Figure 2.13. Overall breakdown of the cost: (left) with solvent disposal and (right) with 90% solvent recovery. The two largest fractions are the solvent and phosphoramidite monomer. Implementing a distillation solvent recovery unit significantly reduces the overall cost.

For the purpose of the calculation, the overall yield of 23-mer was assumed to be 50% (step-wise yield of 97%). In the first case of solvent disposal, it is quite clear from Table 2.I and Figure 2.13 that two main cost components are the

phosphoramidite monomers and the solvent; other parameters, such as capital cost and membrane modules, are relatively insignificant. The cost of phosphoramidite monomers has come down significantly in the past 10 years in the face of rising demand[84, 110], but it is still an obstacle to commercial oligo synthesis. In addition, the cost of phosphoramidite depends significantly on the scale.

However, it can be seen that the overall cost of solvent when it is not recovered is even higher than the phosphoramidite monomer itself. This is not very surprising considering the fact that membrane CVD is a highly solvent-intensive process and acetonitrile is one of the most expensive solvents. For this reason, several approaches have been reported that couple solvent recovery to membrane CVD[11, 102]. For the purpose of this calculation, an assumption of 90% solvent recovery via distillation with associated energy cost was implemented. Distillation was chosen as a suitable solvent recovery unit as the only other significant volatile compound employed in this project was pyridine. If 90% solvent recovery is now taken into account, the cost of the oligo drops by 50% and the biggest fraction of cost then become the phosphoramidite monomers.

Costs of oligos prepared by SPOS are difficult to gauge. Currently, there are many companies that offer custom made oligos[111-113]. The final price depends on several factors such as oligo lengths, synthesis scale, backbone modifications, nucleobase modifications, and desired purity. For instance, as a comparison, the price of 23-mer 2'-*O*Me RNA phosphorothioate oligos can be calculated as high as £23,000.g^{-1}, but only offered in 10 mg scale[111]. The price is likely to drop to below £10,000.g^{-1} when ordered in larger scales though.

Hence, it can be asserted that the proposed LPOS-OSN platform is highly competitive with the SPOS platform, but more easily scalable. However, it should be stressed that the labor and operation costs have not been considered. To understand which operation parameters affect the overall economics, different sensitivity analyses were carried out, as shown in Figure 2.14.

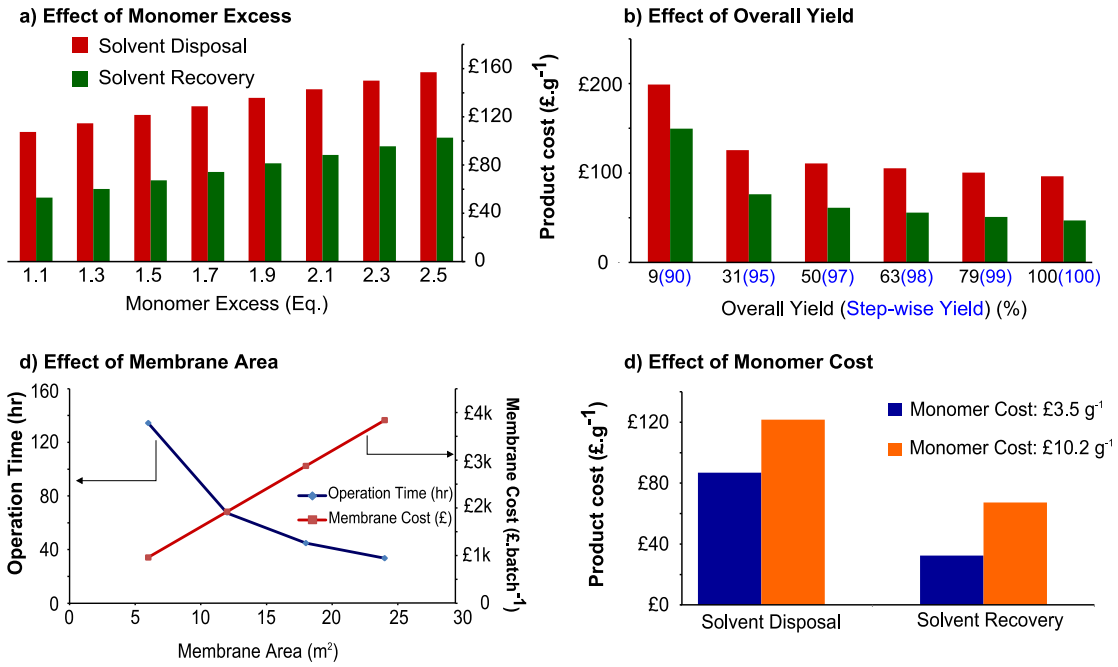


Figure 2.14. Sensitivity analyses to understand how changes in key parameters affect the overall cost: a) effect of monomer excess; b) effect of overall yield; c) effect of membrane area; and d) effect of monomer cost.

Several trends can be observed in Figure 2.14. First of all, it can be seen that recovering the solvent is economically beneficial, and environmentally necessary, for all cases. Secondly, it can be seen in Figure 2.14a that the monomer excess shows a linear relationship with the final oligo cost. For instance, decreasing the monomer excess from 1.5 to 1.1 eq. can reduce the final product cost by up to 21%, a possibility with the LPOS platform as the reaction proceeds in the homogeneous liquid phase. Thirdly, the overall yield has a steep inverse exponential relationship with the final cost (Figure 2.14b), and a steeper gradient for the solvent-recovery case. For instance, increasing the overall yield from 50% to 100% decreases the required monomer amount by 42%, and decreases the overall cost by 27%.

Fourthly, another very important parameter to optimize is the total operation time with respect to the membrane area (Figure 2.14c). As the membrane area can easily be increased with additional membrane modules, and the operation time drops exponentially with higher membrane area, the operation time is an independent variable under control. It should be stressed that the cost of membranes is only a small fraction (3-6%) of the overall breakdown of the cost (Figure 2.13). It is expected that the membrane area will be chosen based on the required campaign schedule considering the number of batches, reaction time, and available reactor schedule, etc. Lastly, as expected, the price depends significantly on the monomer price. If the

monomer cost can be reduced down from £10.2.g^{-1} to £3.5.g^{-1}, the final product cost drops by 52%.

2.4.6. Further Discussions: advantages and current challenges

The two batches of oligo synthesis here using the LPOS-OSN process clearly proved the expected advantages such as efficient reaction, low usage of phosphoramidite monomers, simple purification methodology, easy scalability, and *in situ* analysis. However, several challenges, both expected and unexpected, have been identified during the development stage, and the process needs to go through continuous improvement and optimization. The current challenges are: i) incomplete removal of excess monomers, especially the amidate **6b**, leading to lower purity; 2) low process yield; 3) incomplete removal of Dmtr-pyrrole requiring a separate precipitation step; and 4) redundant solvent exchange steps.

As for the first challenge, an equilibrium exists for excess phosphoramidite monomers, leading to formation of four different types upon addition of PADS (Figure 2.7). By understanding the mechanism of formation, the equilibrium should be pushed to the thioates (**6c, 6d**), which have been shown to permeate more easily than amidates (**6a, 6b**) through the PBI membranes via an ion exchange mechanism. The second challenge, low process yield, can be tackled through different membrane configurations, which will be discussed in Chapter 3 and 5. Also, further improvements in yield and purity can be made by parallel tuning of the size of the soluble support and the membrane separation performance, to make the purification more efficient. Notably, monodisperse PEG homostar has been prepared up to 8000 Da, and membrane separation performance can be roughly controlled using polymer fraction and solvent-to-cosolvent ratio[10]. It should be noted although a bigger soluble support may exhibit higher rejection, it also decreases the oligo loading (mmol.g^{-1} of PEG support) while increasing the solution viscosity.

The use of Dmtr protecting group has been extremely versatile and useful for the SPOS process, but it has proven to be too bulky for the proposed LPOS-OSN process, at least with the PBI 17DBX membrane, requiring a precipitation step after every chain extension cycle. Instead, other acid-labile protecting groups should be explored. For example, the acetal protecting group (MW 74) employed by Molina *et al.*[114] to synthesize 3-mer oligos on a cyclodextran support could be applied.

Lastly, the current chain extension protocol requires redundant solvent exchanges and a precipitation step, rendering the practical operation of the process cumbersome and time-consuming. From the process operation perspective, a single-solvent and single-pot synthesis protocol is preferred. One way to achieve significant process intensification is to bypass the detritylation reaction in DCM, and perform the deprotection reaction and membrane CVD in the rig. This is expected to significantly simplify the process, as the entire chain extension cycle can proceed with effectively a single CVD using a single-solvent system.

Apart from the practical challenges identified in this work, the LPOS-OSN concept still needs to prove its versatility and that it can produce other species apart from antisense oligos, for instance spieglmers, locked nucleic acid (LNA) among other types of oligo-based drugs. As rightly pointed out by Sanghvi[1], the large-scale synthesis of oligos is likely to occur through synergistic utilization of both SPOS and LPOS platform. As the versatility and efficiency of the SPOS is unparalleled, it is expected that the LPOS will be utilized for very large-scale batch process, or to perform a fragment condensation using short building blocks prepared via SPOS.

2.5. Conclusions

In this Chapter, a new liquid-phase oligonucleotide synthesis (LPOS) platform using organic solvent nanofiltration (OSN) was introduced as a scalable purification technology. By growing oligos on a soluble, branched monodispersed PEG support, purification after each reaction was performed using OSN membranes, exploiting the difference in size between the product oligonucleotidyl homostar and smaller reagent excess. Using this new platform, 5-mer and 9-mer 2'-methoxy phosphorothioate oligoribonucleotides have been successfully synthesized and characterized. The solubility of the oligo-homostars was excellent in mixed MeOH-MeCN solvent, as well as in DMF. The synthesis was carried out on a gram-scale, which could easily be scaled-up to kilo-scale using membrane modules. The main advantage of the proposed process is that its performance is not affected by the scale of synthesis. PBI membranes were chosen as they gave reliable and robust performance for over a year. An economic analysis was carried out for the LPOS-OSN platform to understand the main cost factors, as well as operation parameters.

Although this work has shown the potential of the new liquid-phase platform for oligo synthesis, continuous improvements and optimization steps must be taken. Several process challenges have been identified, and possible solutions suggested. These challenges and appropriate solutions will be further discussed in subsequent chapters. Nevertheless, the proposed LPOS-OSN platform presents a flexible alternative for the large-scale synthesis of oligos, and allows economical synthesis of oligo-based therapeutics on a metric-ton scale. With the ever-growing number of oligo-based drugs going through clinical trials, a scalable manufacturing technology is expected to further boost growth in this exciting new era of oligo therapeutics.

Imperial College London

Chapter 3

Developing a Membrane Cascade

One of the main challenges of the proposed LPOS process was low yield, which is tackled in this chapter. It is shown that employing a cascade configuration can significantly improve the yield without affecting the final purity.

3.1. Summary

In Chapter 2, a versatile Liquid-Phase Oligonucleotide Synthesis (LPOS) platform was proposed using Organic Solvent Nanofiltration (OSN) technology. Although the proposed platform has shown potential and economic feasibility, several challenges have also been identified. Mainly, the process yield was unacceptably low due to incomplete rejection of the product by the membranes. It should be stressed that a near-quantitative yield should be obtained for each step in order to obtain reasonable overall yield.

In fact, this low-yield challenge is prevalent throughout the membrane technology. Particularly for OSN, obtaining a sharp separation between two molecules which are both in the nanofiltration range from 100 to 2000 Da, remains a challenge. This is because the differences in rejection of the solutes by the membrane are often insufficient for them to be separated in a single filtration stage, resulting in either low purity or low yield. Membrane cascades can meet this challenge, and have potential for process intensification (PI), allowing more sustainable membrane units.

The membrane cascade concept was proposed in the early 1940s, but to date several implementation challenges such as control difficulties have presented major hurdles and only few experimental data have been reported. In this work a simplified-control cascade process is proposed that not only overcomes previous implementation issues, but also minimizes the product loss and maximizes the purity. The process operates using a single high pressure pump as the primary pressure source, and has no need for a buffer tank between membrane stages. The process was tested on an organic solution of polyethyleneglycol 400 (PEG-400) and PEG-2000 in acetonitrile, which is a challenging model as the flexible chains make it difficult to obtain 100% rejection of any PEG. Polyimide and polybenzimidazole membranes were screened for the cascade process. Using this process it was possible to increase the final yield of PEG-2000 from 59% to 94% while reducing the solvent intensity (solvent consumed per kg of product). The process has been analyzed using a process model developed to predict the cascade performance. It was found experimentally that the recycle ratio and the transmembrane pressure affect the process yield significantly, in agreement with the model predictions. Model analysis and experimental validation are presented.

3.2. Introduction

One of the major challenges for nanofiltration (NF) technology is insufficient separation between solutes[26]. NF membranes typically show a sigmoidal curve for rejection as a function of molecular size (Figure 3.1), so that feasible separation of compounds based on molecular size is only possible with large differences in molecular weight. Many opportunities to apply NF membranes exist in the pharmaceutical industry, and there are many successful applications of OSN technology. Despite this, insufficient discrimination between similar-sized species severely limits the industrial application of OSN when product purity is of high importance. In order to compete with conventional separation methods such as chromatography, adsorption, and crystallization, membranes must offer much better separation performance. To carry out solute fractionation using membranes, constant-volume diafiltration (CVD) is generally employed, which can be very effective in removing low molecular weight compounds. However, the use of CVD with a single membrane unit using currently available NF membranes results in a significant trade-off between yield and purity[115, 116].

To improve the separation performance, one might either: 1) develop better membranes with superior performance; or 2) modify the process configuration, for instance by using a membrane cascade. Much effort has been expended on the search for better membranes, mainly by trying to control pore size and pore size distribution[117-120].

In the NF range a typical membrane rejection profile exhibits a broad curve, with rejection rising slowly over a wide range of solute sizes, instead of an ideal sharp separation curve with an abrupt change in rejection (see Figure 3.1). In an attempt to explain this, a transport model by Bowen & Welfoot[49, 51, 53] was adapted, taking into account hindered diffusion to predict rejection of solutes at different pore sizes. The rejection was estimated as a function of solute radius for “perfect” membranes, i.e. membranes in which the pores are all cylindrical with uniform diameter. The resultant sigmoidal profile is quite close to the observed data[58], suggesting that sharp separations might be difficult to achieve, even if it was possible to fabricate membranes with uniform cylindrical nanopores.

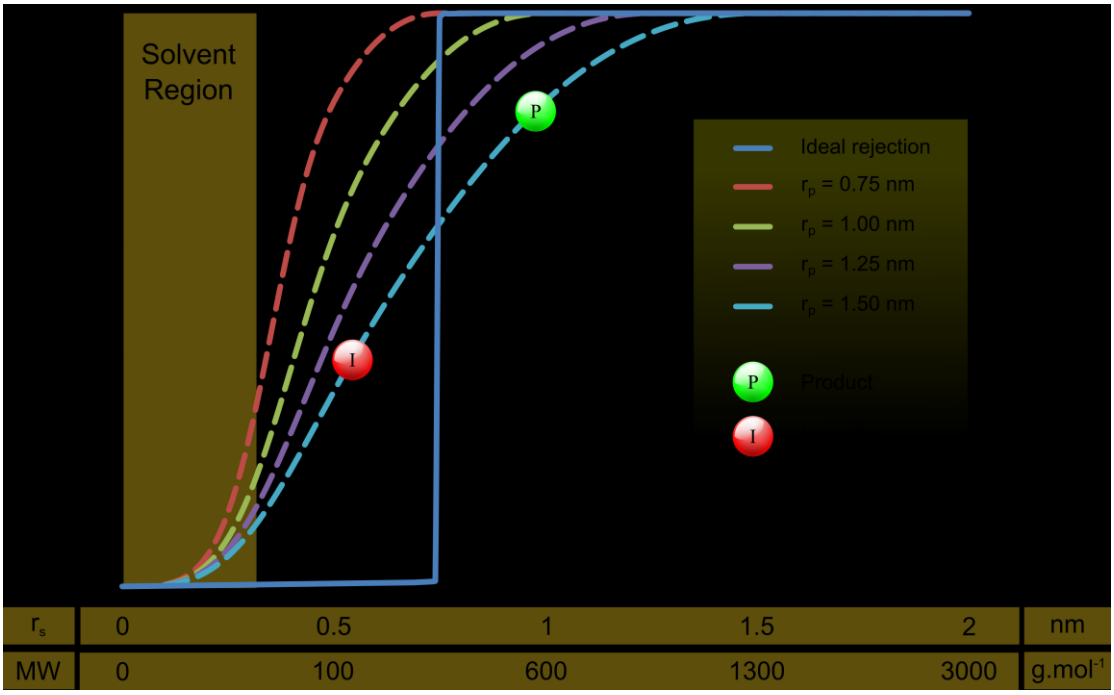


Figure 3.1. Calculation using the pore-flow model of the rejection of uncharged solutes by a membrane with uniform pore sizes (r_p) between 0.75 nm and 1.5 nm. This range covers molecular weights of most nanofiltration solutes (approximate MW shown). If the product and impurity solutes give indicated rejection values, the separation efficiency is too low to be practical due to broad rejection curve.

Since a near-ideal rejection profile seems difficult to obtain, it was sought to improve the membrane separation performance by using several membrane stages as a cascade. The concept of membrane cascades dates back to the 1940s when it was first applied for uranium enrichment [21]. Hwang [121, 122] then laid the foundations of cascade theory by applying the McCabe-Thiele method to the design of the counter-current membrane cascade. This work showed the potential and the advantages of a well-designed membrane cascade system, with the ability to achieve any desired solute fractionation. Since then different schemes have been proposed by many authors[123-128], mainly based on the counter-current recycling cascade configuration. In particular, Lightfoot and co-workers [129-131] developed the ideal membrane cascade theory for continuous solute fractionation in liquid solutions. However, most reports in the literature have been simulation-based or theoretical. Notable exceptions are several experimental reports by Ghosh and co-workers [116, 132], who validated the cascade concept for purification of proteins using ultrafiltration membranes.

In the field of NF most reports extrapolate single-stage experimental data to multi-stage membrane cascades[133-136]. The first experimental validation of solute fractionation using membrane cascades in OSN was by Siew *et al.* (2012) [137] who

successfully applied a 3-stage stripping cascade to concentrate valuable APIs while minimizing solvent consumption. The paucity of experimental work in the area may be due to the difficulty of cascade control. It was speculated by Lightfoot [130], and verified by Siew [137], that the biggest challenge in cascade implementation is the delicate control of interacting flows. Inadequate control results in reduced separation efficiency, and can even lead to worse performance than a single-stage system [132, 138]. In addition, with an increasing number of membrane stages, extra buffer tanks and pressure pumps are usually required, complicating the process and increasing the initial capital cost. Thus, the theoretical advantages of membrane cascades diminish rapidly with an increasing number of stages [133]. Therefore, for a membrane cascade system to be practical, the number of cascade stages must be minimized, the control of the system should be simple, and the system design should be easy to reconfigure for multiple campaigns. Simplicity and flexibility in process design should not be understated, as the versatility of equipment is considered vital to reducing capital expenditure in the pharmaceutical industry [139, 140].

In this Chapter, a new cascade process configuration is presented that operates with just a single pump as the pressure source and bypasses the buffer tank requirement between the membrane stages. A binary solution of PEG-400 (MW of 400 Da) and PEG-2000 (MW of 2000 Da) dissolved in acetonitrile solvent was used as the model mixture. This model solution was chosen as they are commonly used to characterize nanofiltration membranes; and also, they are available at much lower price compared to oligo solutes. In addition, separation of PEG mixtures is a challenging model. This is due to the flexibility of PEG chains which makes quite difficult to obtain 100% rejection of any one PEG.

A process model was developed which predicted that the principal process variables significantly affecting the separation efficiency should be the recycle ratio and permeate flux. The process model showed a good agreement with the experimental data. By employing a two-stage diafiltration process it was possible to increase the yield of PEG-2000 from 59% to 94% without compromising its final purity. Detailed analysis and experimental data are presented.

3.3. Experimental

3.3.1. Materials

Acetonitrile (MeCN), *N*,*N*-dimethylacetamide (DMAc), and isopropyl alcohol (IPA), were HPLC grade and used as supplied from *VWR*. PEG-400 and PEG-2000 were purchased from *Merck* and *Sigma*, respectively. Lenzing P84 polyimide powder and Celazole® S26 polybenzimidazole (PBI) solution (26 *wt*% polymer in DMAc containing 1.5 *wt*% LiCl) were purchased from *HP polymer GmbH* and *PBI Performance Products Inc*., respectively. Non-woven polyolefin Novatexx 2471 was from *Freudenberg Filtration Technologies*, Germany. Maleic acid (MA) was from *Sigma* and 1,6-hexanediamine (HDA) and α,α'-dibromo-*p*-xylene (DBX), were from *ACROS Organics* and *VWR*, respectively.

3.3.2. Preparation of Polyimide and Polybenzimidazole (PBI) Membranes

Polyimide membranes were prepared following the procedure described by See Toh *et al.* [44]. A dope solution was prepared by dissolving P84 polyimide (23 *wt*%) in DMF:dioxane at 2:1 ratio, containing 2 *wt*% maleic acid. Once a homogenous solution was obtained, it was cast on a polyolefin non-woven support using an adjustable casting knife height (*Elcometer Ltd*., UK) set at 300 µm. The cast film was immersed into a de-ionized (DI) water coagulation bath for 30 minutes to form the membrane. The membrane was then washed with IPA three times to remove residual water. Next, the membrane was cross-linked using a solution of 100 $g.L^{-1}$ HDA in IPA for 16 hours. After this, it was again washed with IPA three times to remove residual cross-linker. Finally, the membrane was conditioned with PEG-400:IPA (3:2 *v/v*) for 16 hours, then air-dried.

Four PBI dope solutions were prepared by diluting the Celazole® S26 solution to 17 *wt*%, 20 *wt*%, or to 22 *wt*% with DMAc (22 wt% solution was made twice to show reproducibility). The fabrication protocol is described in *Section 2.3.2*.

The compositions of the membranes prepared for this study are summarized in Table 3.I.

Table 3.I. Membrane compositions and preparation conditions

Membrane	Polymer Type	Polymer (*wt*%)	Dope Solvent	Additive	Cross-linker
M1	Polyimide	23	2:1 DMF:Dioxane	2 *wt*% MA	HDA
M2	PBI	17	DMAc	1.5 *wt*% LiCl	DBX
M3	PBI	20			
M4-A	PBI	22			
M4-B	PBI	22			

3.3.3. Membrane Screening

All five membranes in Table 3.I were screened against a test solution containing 1 $g.L^{-1}$ each of PEG-400 and PEG-2000 in MeCN. MeCN was chosen for its excellent ability to solvate PEG compounds. For each membrane a disc with an effective area of 51 cm^2 was loaded into a membrane cell (92 mL) with six retentate side ports and one permeate port. A typical set-up consists of an inlet port, a retentate port fitted with a back-pressure regulator, a pressure gauge port, a thermocouple port, and a permeate port. A schematic of the system used for membrane screening and diafiltration experiments is shown in Figure 3.2.

In both the single-stage and the two-stage diafiltration set-ups, a *Gilson* HPLC pump (Model 305) provided the flow, set at 30 $ml.min^{-1}$. The pressure of each cell was controlled using a back-pressure regulator, and a magnetic stirrer bar was placed inside each cell (stirred at 500 RPM) to maintain a constant hydrodynamic profile in the fluid in contact with the membrane. The feed tank volume was 100 ml, and the volume of each cell plus the associated tubing was approximately 100 ml.

All membranes were first washed with at least 2 L of pure MeCN at 10 bar to remove all the conditioning agents and to achieve a steady-state flux. Next, a test solution (100 ml) containing 1 $g.L^{-1}$ each of PEG-400 and PEG-2000 was pumped into the cell already containing pure solvent. The solution was circulated at different pressures and the permeate was recycled back into the feed until a steady-state was reached. At this point, and at different times thereafter, samples of both permeates and retentates (~1 mL) were taken for HPLC analysis to assess the membrane performance.

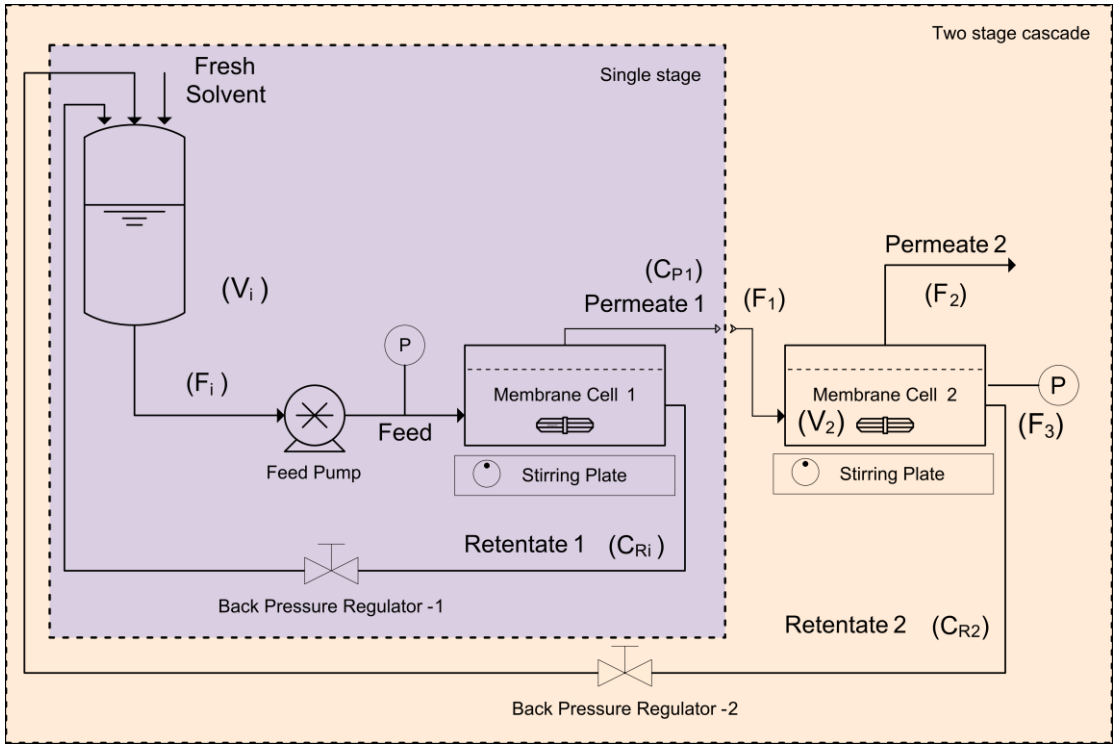


Figure 3.2. System diagrams of single-stage diafiltration and two-stage cascade diafiltration. For two-stage cascade diafiltration, the permeate from the first stage is directly connected to the feed of the second stage. The symbols in parentheses are the variables used in the process model (*Section 3.3.4*).

3.3.4. Process Modeling

The single-stage diafiltration system, as shown in Figure 3.2 (inner box), can be modeled by writing a mass balance around the system. Assuming that the system operates at a constant volume and it is perfectly mixed,

$$V\frac{dC_{R,i}}{dt} = -F \cdot C_{p,i} = J_v \cdot A \cdot C_{p,i} \qquad \text{(Eq. 3.1)}$$

where V (L) is the system volume, F is the permeate flow-rate ($L.hr^{-1}$), J_v ($L.m^{-2}.hr^{-1}$) is the membrane flux, A (m^2) is the membrane area, and $C_{R,i}$ and $C_{P,i}$ ($g.L^{-1}$) are the concentrations of species i in the retentate and permeate, respectively.

Defining the observed rejection of species *i* as,

$$R_{obs,i} = 1 - \frac{C_{p,i}}{C_{R,i}} \qquad \text{(Eq. 3.2)}$$

and substituting Eq. (3.2) into Eq. (3.1) yields,

$$\frac{dC_{R,i}}{dt} = -\left(\frac{1}{V}\right) J_v A\, C_{R,i}\left(1 - R_{obs,i}\right) \quad \text{(Eq. 3.3)}$$

This equation can be solved either numerically or analytically. When integrated analytically with appropriate boundary conditions, the following equation is obtained:

$$\frac{C_{r,i}}{C_{r,i,o}} = \exp\left[-\frac{J_v A t}{V}\,(1 - R_{obs})\right] = \exp[-diavolume\,(1 - R_{obs})] \quad \text{(Eq. 3.4)}$$

where *diavolume* represents the total volume of permeate collected relative to the initial system volume. This useful time-like dimensionless parameter allows different diafiltration systems to be compared.

In membrane diafiltrations, the solvent usually permeates faster than the solutes through the membrane. Consequently, there is a buildup of solute very near the membrane surface, resulting in concentration polarization effects [61]. The rejection was defined as "observed" in Eq. (3.2) because one consequence of concentration polarization is to make the observed rejection different from the real, or intrinsic rejection. However, for the purpose of this study, it was assumed that the effects of concentration polarization were negligible as the solutions used were quite dilute (0.1 *wt*%), and it was assumed that hydrodynamic turbulence generated at the membrane surface was enough to largely disrupt concentration polarization. In addition, osmotic pressure across the membrane was assumed negligible.

A similar analysis of the two-stage diafiltration can be solved numerically using MATLAB. As the two stages are interconnected, a total of four ordinary differential equations can be written for species *i* and *j* in stages 1 and 2.

$$\frac{dC_{R1,i}}{dt} = \left(\frac{1}{V_1}\right)\left[-F_1 C_{R1,i}\left(1 - R_{1,i}\right) + F_3 C_{R2,i}\right] \quad \text{(Eq. 3.5)}$$

$$\frac{dC_{R2,i}}{dt} = \left(\frac{1}{V_2}\right)\left[F_1 C_{R1,i}\left(1 - R_{1,i}\right) - F_2 C_{R2,i}\left(1 - R_{2,i}\right) - F_3 C_{R2,i}\right] \quad \text{(Eq. 3.6)}$$

$$\frac{dC_{R1,j}}{dt} = \left(\frac{1}{V_1}\right)\left[-F_1 C_{R1,j}\left(1 - R_{1,j}\right) + F_3 C_{R2,j}\right] \quad \text{(Eq. 3.7)}$$

$$\frac{dC_{R2,j}}{dt} = \left(\frac{1}{V_2}\right)\left[F_1 C_{R1,j}\left(1 - R_{1,j}\right) - F_2 C_{R2,j}\left(1 - R_{2,j}\right) - F_3 C_{R2,j}\right] \quad \text{(Eq. 3.8)}$$

where V_1 is the feed tank plus the first-stage volume, V_2 is the second-stage volume, and F_i (equal to $J_v \cdot A$) is the flow as shown in Figure 3.2 (outer box).

One important parameter, the recycle ratio (r_C), is defined as,

$$r_C = \frac{F_3}{F_1} = \frac{(B_1 \Delta P_1 - B_2 \Delta P_2)}{B_1 \Delta P_1} \quad \text{(Eq. 3.9)}$$

where ΔP_1 and ΔP_2 (bar) represent the trans-membrane pressure (TMP) through the first and second stages, respectively, and B_1 and B_2 represent the permeance ($L.m^{-2}.hr^{-1}.bar^{-1}$) of the first and second stage membranes, respectively.

The recycle ratio, r_C, is an independent variable under control because the flow rate through the first and second membranes can be controlled using the back-pressure valve at the retentate side of the second stage. Notably, the effect of r_C on the final yield and purity is significant and is discussed in the results section.

As the system volume does not always stay exactly constant, the concentration of the system deviates from the model. Thus, for final yield and purity calculations, final samples were taken and the final system volume was explicitly measured to obtain accurate data. Mass yield and purity of PEG-2000 were then calculated using the following equations,

$$\text{Yield (\%)} = \frac{M_{PEG-2000,final}}{M_{PEG-2000,initial}} \times 100 \quad \text{(Eq. 3.10)}$$

$$\text{Purity (\%)} = \frac{M_{PEG-2000,final}}{M_{PEG-2000,final} + M_{PEG-400,final}} \times 100 \quad \text{(Eq. 3.11)}$$

where M_i is the total mass in the entire system. All process modeling was carried out in MATLAB.

3.3.5. Single-Stage Diafiltration

Single-stage diafiltration was performed independently with M4-A and M4-B membranes using the configuration shown in Figure 3.2 (inner box). Initially, PEG test solution ($1 g.L^{-1}$ each PEG solute dissolved in 100ml MeCN) was circulated around the system at 10 bar and 22 ^{o}C. Once a steady-state concentration of the two PEG species in the retentate and permeate had been reached (confirmed by HPLC), a preparative diafiltration was performed at 10 bar. The system was maintained at a constant volume by adding the same volume of pure solvent into the system as permeated over the same time. Permeate and retentate samples were analyzed by HPLC at different times.

3.3.6. Two-Stage Diafiltration

Two-stage diafiltration using the configuration shown in Figure 3.2 was performed three times using two different batches of PBI 22 DBX membranes (M4-A and M4-B membranes): Firstly, using M4-A membranes with a recycle ratio (r_C) of 0.5; secondly, and under as near as possible the same conditions as before, using M4-B membranes with an r_C of 0.5; finally, again using M4-B membranes, but with an r_C of 0.17.

Without connecting the second membrane cell, the first-stage membrane was equilibrated with PEG test solution (1 $g.L^{-1}$ of each PEG solute) at 22 ^oC, while recirculating the permeate back into the feed tank, until a steady state was achieved. Once the PEG concentrations had become constant in the permeate and retentate, the permeate from the first stage was fed directly into the second cell (initially charged with pure solvent) as shown in Figure 3.2. To control the recycle ratio, the first stage was set at a higher pressure than that of the second stage. Permeate and retentate samples were analyzed by HPLC at intervals.

3.3.7. Analytical Methods

All samples were analyzed by HPLC using an *Agilent* 1100 Series system. The pump flow-rate was set at 1 $ml.min^{-1}$, the injection volume was 30 µL, the column temperature was 30 ^oC, and an ACE C18 RP column was fitted. The column was eluted with a gradient of MeOH and water buffered with 0.1 M ammonium acetate, pH 6.5. The eluent was monitored with an ELSD (evaporative light scattering detector, *Varian* 385-LC) detector, with the evaporation temperature set to 40 ^oC, nebulization temperature at 55 ^oC, and the nitrogen gas flow rate at 1.5 SLM. As the ELSD response varies exponentially with the mass concentration, calibration curves were prepared for both PEG-400 and PEG-2000.

3.4. Results and Discussion

3.4.1. Constant Volume Diafiltration (CVD) Parameters

It has been illustrated in Chapter 2 (please refer to Figure 2.3) that to achieve a clean and efficient separation using membrane diafiltration, two conditions need to be satisfied: 1) The difference in rejection between the two solutes needs to be wide; and 2) the rejection of the larger compound should be close to 100%. In other words, to obtain a high yield and purity separation, the bigger compound must have as close to 100% rejection as possible, and the smaller compound should exhibit as low rejection as possible. Correspondingly, the lower the rejection of the smaller molecule, the lower the solvent volume required to achieve the desired separation. For the purpose of this study the bigger compound, PEG-2000, was chosen as the marker to test the process.

3.4.2. Membrane Screening

Apart from rejection, permeability is often considered a critical variable. However, a high permeability is not always necessary or even desirable. In fact, especially in the pharmaceutical industry, it is often more important to achieve a high yield and level of purity, because complete retention of a particular solute is the main objective. Since there is always a trade-off between permeability and rejection, one must select the membrane to match it as closely as possible to the specific process requirements. As a rule of thumb, the rejection of the smaller compound should not exceed 80% for the process to be practical and feasible.

The performances of the membranes screened here are summarized in Table 3.II. Polyimide membrane M1 showed poor discrimination between the PEG test solutes, and exhibited inconsistent performance between coupons M1(1) and M1(2), and thus was discarded. On the other hand, polybenzimidazole (PBI) membranes M2 – M4 showed consistency and the expected trend. As the proportion of polymer in the dope increased, the resultant membrane's rejection increased and its permeability decreased correspondingly. This trend towards tighter membranes with higher polymer fraction has been observed previously [31].

Table 3.II. PEG separation performance of the membranes. Tests were conducted in MeCN at 10 bar at 22 °C. Two coupons per membrane batch were tested.

Membrane†	Rejection (%)*		Flux ($L.m^{-2}.hr^{-1}$)
	PEG-400	PEG-2000	
M1(1)	29 ± 10	79 ± 6	94 ± 9
M1(2)	10 ± 5	52 ± 2	17 ± 7
M2(1)	24 ± 3	83 ± 2	119 ± 8
M2(2)	6 ± 3	83 ± 2	127 ± 3
M3(1)	28 ± 5	89 ± 3	72 ± 5
M3(2)	22 ± 4	78 ± 12	85 ± 8
M4-A(1)	51 ± 2	92 ± 2	32 ± 2
M4-A(2)	51 ± 5	92 ± 0.2	22 ± 2
M4-B(1)	62 ± 2	94 ± 0.7	38 ± 0.8
M4-B(2)	68 ± 3	95 ± 0.7	29 ± 0.0

*† Number in parenthesis indicates different membrane coupon from the same batch. *Error values represent one standard deviation from the mean. Measurements were made at two different times (at least 3 hours apart) to show they are at steady state.*

As anticipated from the flexible conformation of PEG molecules, it was not possible to simultaneously obtain near 100% rejection of the desired PEG-2000 and low or medium rejection of PEG-400. Similarly to many other studies of nanofiltration (NF), as the membrane was made tighter, the rejection of the smaller compound rose in parallel with that of the larger one. Thus, if the membrane was made tight enough for the rejection of the larger species to approach 100%, then the rejection of the smaller one would also become high with reduced permeability. As a result, any separation based on that membrane would take too long and consume a very large amount of solvent. This trend is also apparent in Table 3.II, where the increase in rejection of PEG-400 with membrane tightness/polymer proportion is greater than the increase in the rejection of PEG-2000.

As a result of the screening, M4-A and M4-B membranes (both the same composition) were chosen to carry out the test separation as they had the highest rejection for PEG-2000, and the membranes showed consistent and reproducible behavior. With the data obtained from the membrane screening, the preparative diafiltration performance of M4-A and M4-B membranes could be predicted, and then compared to experiment. The performance of M4-A membranes is presented in the

main text and the replicate performance of M4-B membrane is included in Appendix C.

3.4.3. Single-Stage Diafiltration

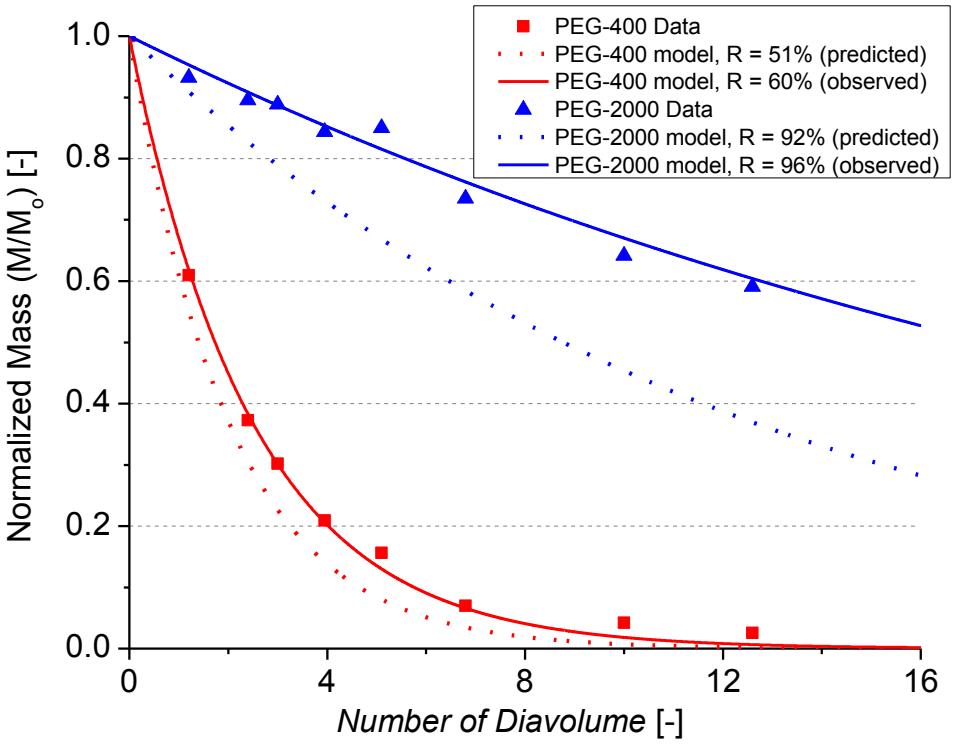


Figure 3.3. Single-stage CVD using M4-A(2) membrane. Dotted curve: Predicted solute mass in retentate using rejection from the screen. Solid curve: Best fit of model to experimental data. The differences in rejections between the screening results and the preparative CVD may be due to membrane aging. The yield of PEG-2000 after 13 *diavolumes* was 59%. The temperature stayed approximately constant at 22 ^{o}C.

Single-stage CVD was performed using M4-A(2) membrane, and the results are summarized in Figure 3.3 (data for M4-B compiled in Appendix C). The mass of each PEG remaining in the retentate followed the expected trend. However, the rejection of each compound determined by fitting Eq. (3.2) to the CVD data in Table 3.III (60% for PEG-400 and 96% for PEG-2000) was higher than the values measured during the membrane screening tests (51% and 92%, respectively). Such underestimation of the rejection values may be due to aging of the membrane, or to the concentration polarization effect.

Although the CVD rejection of PEG-2000 was high at 96%, its final yield was only 59% after 13 *diavolumes* of MeCN had permeated, with 98% purity. The observed curve for the mass of PEG-2000 remaining in the retentate very closely matches the predicted behaviour for a membrane with R = 95% in Figure 3.3. In common with the

experience of many others in the field of membrane separation, the limiting factor is the membrane performance itself, with insufficient separation even after screening and optimization. It is for this reason that membrane cascades were originally proposed to overcome this fundamental material limitation. However, as mentioned previously, very limited actual experimental data can be found in the literature.

This contrast between theory and experiment suggests that implementing a cascade process presents practical challenges. Most cascades employ a buffer tank and an extra pressure pump to give pressure at each stage. This poses a process control challenge, plus an extra equipment cost. It should also be noted that membrane performance is a function of flux. Consequently, it is important to maintain control of the flux for each membrane independently, otherwise poor control of the system can lead to even worse performance than a single-stage system [132, 138]

This control problem could be circumvented if neighbouring stages were connected directly to one another, with the permeate from the first membrane being fed directly into the second (Figure 3.2). With just a single high pressure pump to provide the pressure to the first membrane, in this design the pressure difference over each membrane is controlled by pressure relief valves linked back into the feed tank. In this simplified configuration, the problems of both delicate process control and the cost of additional equipment are avoided, as neither buffer tanks nor additional pumps are required. Also, the flux through each membrane can be semi-independently controlled simply by adjusting the settings of the pressure relief valves. As this configuration was tested in a lab scale with the necessary turbulence below the membrane provided by stirring, it is envisaged that in large-scale implementations of this configuration, a low-priced pump (i.e. a simple gear pump without pressure head) would be utilized for mixing via recycling the fluid around each stage.

3.4.4. Model Predictions and Effect of Recycle Ratio (r_C)

Prior to running the two-stage cascade experiment shown in Figure 3.2, the system was modeled using MATLAB by implementing Eq. (3.2) and (3.5) – (3.9). Process models can elucidate parameters that can potentially affect the yield. Two parameters were studied in detail: recycle ratio, r_C (defined in Eq. (3.9)), and operating pressure. r_C is an independent variable that can be controlled using the back-pressure regulators, and its value can be adjusted from zero to as high as the membrane can withstand. Using the flux and rejection values for M4-A obtained from membrane screening, the

simulated yield and purity of PEG-2000 after 12 *diavolumes* were plotted against r_C for the two-stage diafiltration process (Figure 3.4).

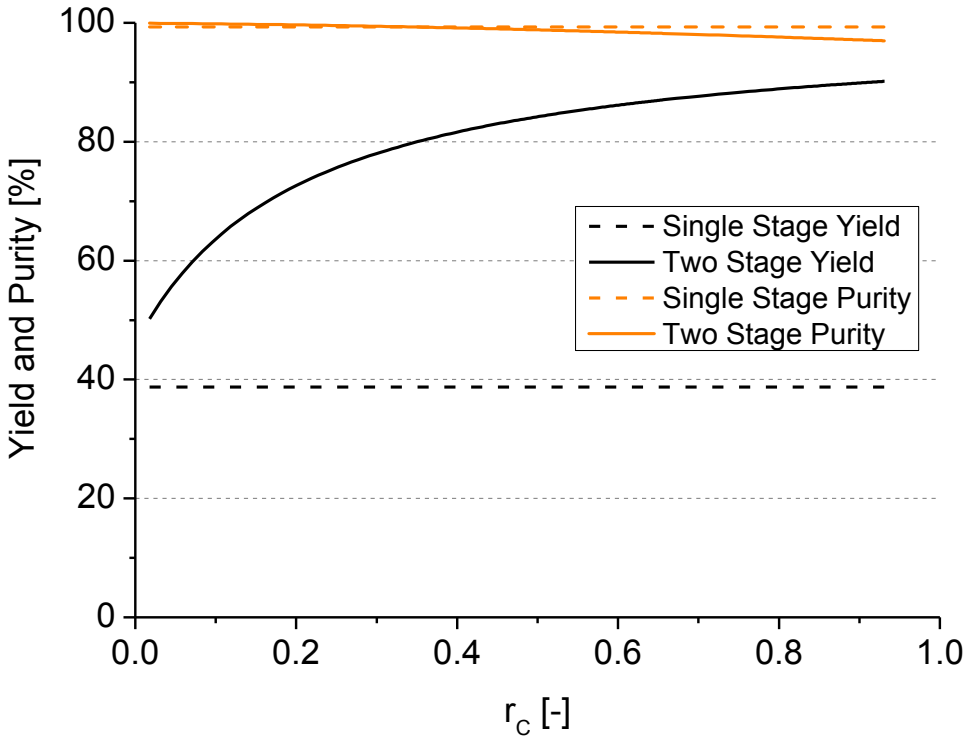


Figure 3.4. Modeled effect of recycle ratio, r_C, on the yield and purity of PEG-2000 using M4-A in a two-stage cascade after 12 *diavolumes*. The parameters were obtained from the screening experiment. For comparison, single-stage purity and yield after 12 *diavolumes* are indicated.

The two-stage yield curve is predicted to follow a saturation profile and, according to the model, the yield can be increased up to two-fold, depending on the recycle ratio. This compares very favorably with a single stage yield of only 38%, although there is a slight fall in purity with increasing r_C. The main reason for the dramatic improvement in yield with increasing recycle ratio is that the PEG concentration in the second stage is kept low, thus minimizing the yield loss through the second membrane. Without recycling, the PEG-400 and -2000 that permeate through the first stage accumulate in the second stage over time, which in turn permeate the second membrane lowering the yield.

On the other hand, the predicted purity hardly changes with rising recycle ratio. The slight decrease in purity with increasing r_C occurs because the concentration in the second stage is minimized and hence the impurity removal rate is slower. Therefore, two-stage CVD takes slightly more *diavolumes* to achieve the same purity as single-stage. The recycle ratio can be controlled mainly in two different ways:

either by adjusting the membrane areas of the first and second stages, or by adjusting the operating transmembrane pressures. It is usually more convenient to adjust transmembrane pressures than membrane areas so this method is employed in this study.

3.4.5. Effect of Operating Pressure

The effect of operating pressure on solute rejection has been studied extensively by many authors[51, 53, 60]. In NF, solute rejection is usually observed to increase with rising pressure. It is predicted in the proposed two-stage system that r_C should be maintained as high as possible (Figure 3.4). And in order to get $r_C > 0$, the flux through the first membrane must be higher than that through the second, and this difference in flux rises with r_C. To achieve this, the first membrane has to operate at higher pressure drop than the second. For this reason the effect of pressure, and hence of permeate flux, on rejection was studied (Figure 3.5).

When working with polymeric membranes, one must be aware of and avoid further membrane aging during diafiltration to ensure reproducible results. For every polymeric material and polymer composition, there exists an operable pressure range within which irreversible damage to the membrane does not occur. To verify that the membrane had not suffered irreversible aging, and that the performance remained constant after each increase in pressure, the pressure was then returned to 5 bar and the performance was re-evaluated, allowing the higher end of the applicable pressure range to be established. This revealed that the membrane performance was indeed repeatable within the tested pressure range up to 20 bar.

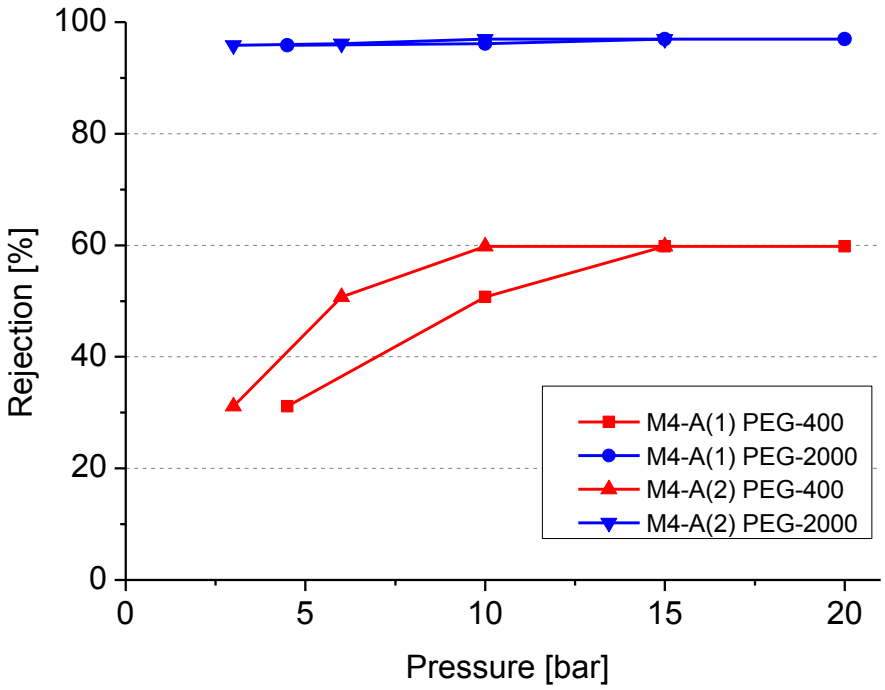


Figure 3.5. The change of PEG rejection with pressure in M4-A(1) and M4-A(2) membranes. PEG-400 rejection is a strong function of pressure, whereas PEG-2000 rejection is not.

It can be seen that the rejection of PEG-400 was strongly affected by the operating pressure until it plateaued at 60%, whereas the rejection of PEG-2000 stayed nearly constant over the tested pressure range. It can also be seen that the rejection of PEG-400 at 10 bar in the M4-A(2) membrane slightly increased over that measured in the screening experiment; this is assumed to be due to further aging during the single-stage diafiltration study.

It is clear from the data that to obtain the best separation between two solutes, the flux of the first membrane should be as high as possible to increase the recycle ratio (Figure 3.4), and the operating pressure should be kept low to widen the gap between the two solute rejections (Figure 3.5). At the same time, the process needs to be completed within a practical timescale. Thus, a balance must be struck in terms of operating conditions to optimize the yield and solvent consumption.

3.4.6. Two-Stage Cascade Diafiltration

To minimize any irreversible compaction of the membranes, the transmembrane pressures of both membranes were kept below 20 bar. Thus, the operating trans-membrane pressures were chosen to be 16 bar for the first stage, and 10 bar for the

second, corresponding to a r_C of 0.5. Consequently, the absolute pressures were 26 bar and 10 bar, respectively, which are high enough to allow the process to be completed within a practical time. The results from the two-stage diafiltration using M4-A membranes are summarized in Figure 3.6 (data for M4-B compiled in Appendix C). Concentration profiles of the first and second stage are shown in Figures 3.7a and 3.7b, respectively.

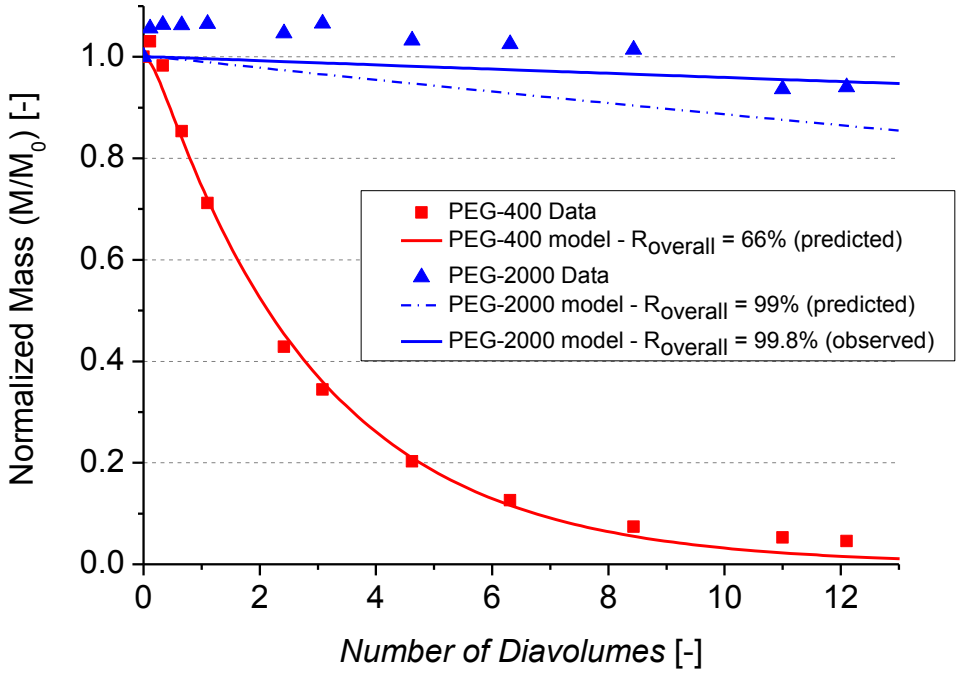


Figure 3.6. Total normalised mass of PEG-400 and -2000 during two-stage diafiltration using M4-A membranes, with recycle ratio, r_C = 0.5. Dotted curve: Predicted solute mass in the total retentate using rejection values from the screen. Solid curve: Best fit of model to PEG-2000 experimental data (PEG-400 is omitted for clarity). The yield of PEG-2000 was 94% at the same purity as from the single-stage diafiltration (i.e. 98%). The effective overall rejections of PEG-400 and PEG-2000 were 65.5% and 99.8%, respectively. Overall rejection values are back-calculated rejection for the entire system (including both first and second stage membranes).

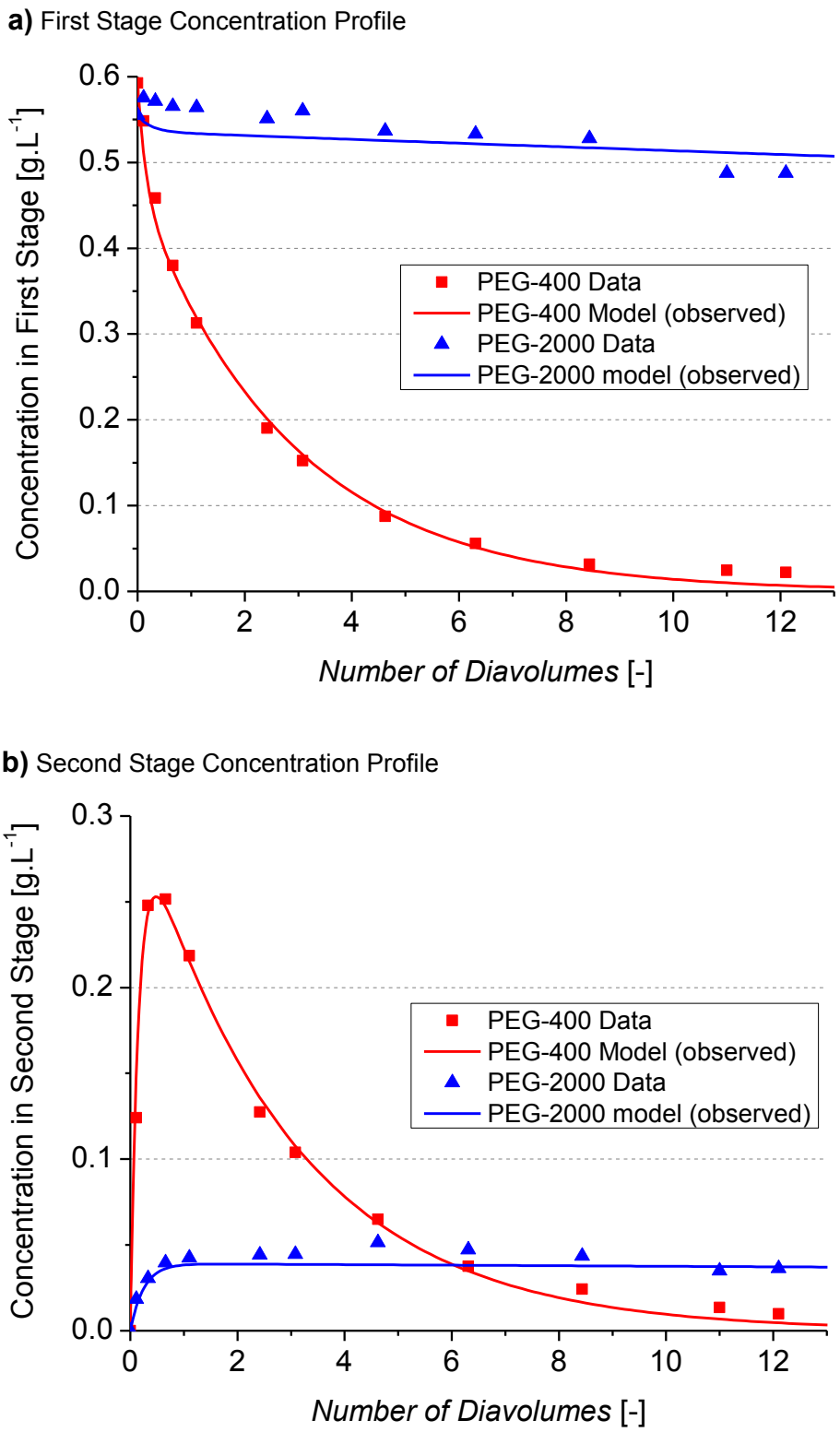


Figure 3.7. Retentate concentration profiles for individual stages during two-stage CVD, with the recycle ratio, r_C = 0.5: **a)** Profile of the first stage using M4-A(1); **b)** Profile of the second stage using M4-A(2).

Figures 3.6 and 3.7 show that the distribution of PEGs between each stage follows the expected trends. For instance, the initial spike of PEG-400 concentration in the

second stage followed by gradual decay, and the steadily low concentration of PEG-2000 in the second stage, were predicted by the model. The overall observed rejections of PEG-400 and PEG-2000 for the two-stage CVD cascade were back-calculated as 65.5% and 99.8%, respectively.

However, in Figure 3.6 it can be seen that the normalized mass of PEG-2000 goes over the value of 1 in the first 8 *diavolumes*. This blip was due to the difficulty of holding the system volume exactly constant, balancing solvent addition against permeate out. The system volume had actually decreased slightly from that at the beginning, causing the measured PEG-2000 concentrations to be marginally higher than the starting concentration for the first 8 *diavolumes* (Figure 3.7a). Only after the system volume had been increased to the original value (at around 9 *diavolumes*) did the normalised mass drop below unity. This distracting artefact was not observed during the single-stage diafiltration, indicating how relatively little PEG-2000 was lost from the two-stage system. By contrast, the final yield and purity calculation are not subject to such distortions because, unlike during the experiment, the final system volume and concentrations could be measured accurately.

The yield and purity comparison between the single and two-stage diafiltrations are shown in Figure 3.8 below.

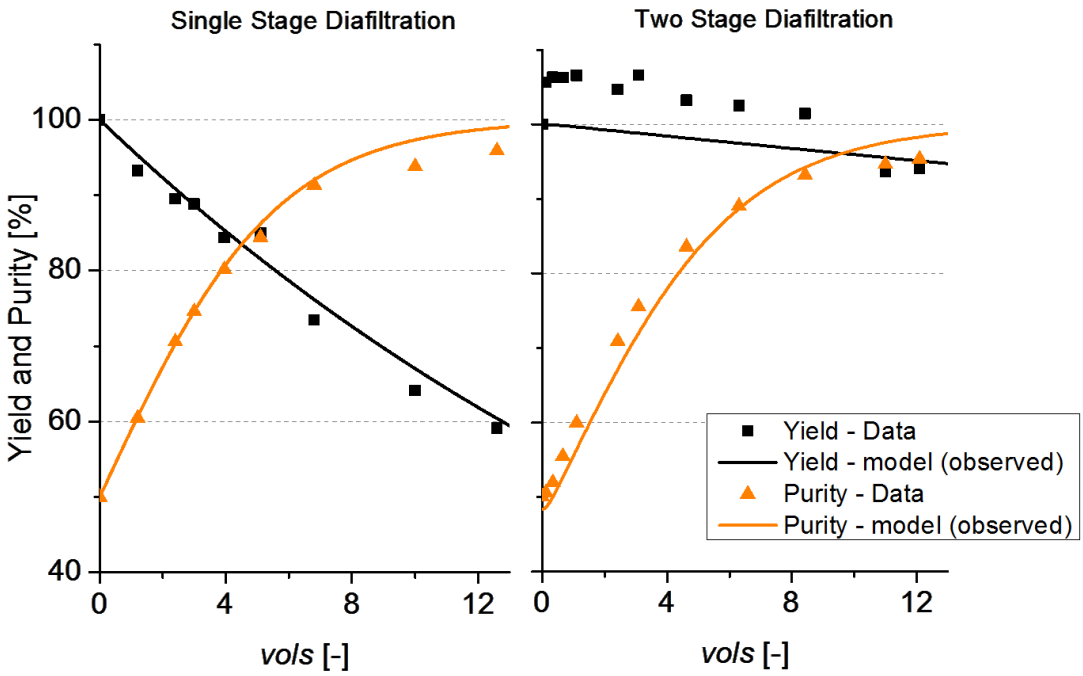


Figure 3.8. Comparison of PEG-2000 yield and purity between single- and two-stage diafiltrations over 12 *diavolumes (or vols)*. The yield increased from 59% to 94% at the purity of 98% at $r_C = 0.5$.

After 12 *diavolumes* CVD in the two-stage system the yield of PEG-2000 was 94% and the purity was 98%. For the same purity of PEG-2000 from the single-stage system, 12 *diavolumes* had also been permeated, but the yield was just 59%. It can be seen that the number of *diavolumes* required to reach 98% purity, within experimental error, was approximately the same in both single and two-stage systems. This is mainly because the rejection of PEG-400 had only increased from 51% in single-stage CVD to 66% (overall) in two-stage CVD, and the rate of PEG-400 removal for two rejection values is quite similar (as illustrated in Figure 2.3).

To increase confidence in the preceding data a new batch of PBI membrane, M4-B, was prepared, as nearly identical as possible to M4-A. Using M4-B in single stage CVD of a mixture of PEG-400 and -2000 the latter was isolated in 59% yield, at 98% purity after 13 *diavolumes*, and the rejections were 60% for PEG-400 and 96% for PEG-2000. When M4-B was used in another two-stage diafiltration, with $r_C = 0.5$ again, the yield increased to 88% (Appendix C) after 16 *diavolumes* to get the same 98% purity. This is a very similar performance to that of M4-A. In addition, when r_C was reduced from 0.5 to 0.17, the yield decreased from 88% to 74% as predicted. This was a consequence of a continuously rising concentration of PEG-2000 in the second stage, leading to much greater absolute mass permeation through the second stage (Appendix C). The performances of the two membranes have been summarized in Table 3.III.

Table 3.III. Summary of comparison between single-stage and two-stage diafiltration for M4-A and M4-B membranes. All values are given in percentages.

Mode	M4-A			M4-B		
	$R_{PEG-400}$	$R_{PEG-2000}$	Yield*	$R_{PEG-400}$	$R_{PEG-2000}$	Yield*
Single-Stage$	51	96	59	60	96	59
Two-Stage†	66	99.8	94	74	99.3	88

**At the same purity of 98%. $Data for M4-A(2) and M4-B(1). †Total of 12 vols for M4-A, 16 vols for M4-B was permeated, both at $r_C = 0.5$, overall rejection values are given which were back-calculated to fit the concentration profile. It represents the combined rejection of two membranes.*

In a more general comparison of single-stage and two-stage cascade CVD, the higher yield in the latter comes with a slightly greater solvent consumption. Firstly,

this is because adding a second stage increases the system volume, and therefore the amount of solvent per *diavolume* increases. Secondly, the two-stage cascade configuration inherently increases the rejection of every solute in the system, so the number of *diavolumes* required to wash out a compound must increase as well. However, it is worth noting that the amount of solvent index (solvent consumption per unit of product) is actually halved. The green-ness of membrane diafiltration processes will be discussed in further detail in Chapter 4. Nevertheless, in processes where yield is a greater priority (*e.g.* in the pharmaceutical industry) than solvent or plant costs, cascades should be preferable over single stage system.

Although the cascade configuration was tested on polymeric flat-sheet membranes using organic solvents, the process itself can be applied using any combination of membranes and can be rearranged in a way to suit the specific need.

3.5. Conclusions

Successful application of the membrane cascade concept to a constant volume diafiltration (CVD) platform has been demonstrated using organic solvent nanofiltration (OSN) membranes. A binary solution of PEG-400 and PEG-2000 in acetonitrile was used to test the process. This mixture was chosen due to the inherent difficulty of achieving a clean separation of flexible PEG molecules using nanofiltration (NF). Five membranes were fabricated and screened and a set of polybenzimidazole (PBI) membranes (M4-A, M4-B) was selected, based on their rejection performance. Diafiltration was performed using both single-stage and two-stage cascade processes. The yield of PEG-2000 was increased from 59% in the single stage CVD to 94% using the two-stage cascade process, while obtaining the same final purity. A process model was developed using MATLAB which predicted that the recycle ratio parameter (r_C) should affect the yield significantly, and this was proven correct experimentally. The process was repeated three times, twice with independently prepared PBI membranes and $r_C = 0.5$ to show repeatability, and once with $r_C = 0.17$ to demonstrate the significance of this parameter to the process yield. The operating pressure was also found to affect the solute rejection and final yield. The proposed cascade configuration achieves significant process intensification (PI) and promotes greener process by reducing the solvent intensity by a factor of two while boosting the process yield. In addition, as no extra pressure pump or buffer tank

is required, the control problem is much simplified without increasing capital costs, addressing the essential requirements of green process engineering. The simplicity and versatility of the new system overcomes the previously encountered limitations of the membrane cascade process, and it is envisaged that this system can be applied using any combination of membranes.

Imperial College London

Chapter 4

Membrane Cascade with Solvent Recovery: Pharmaceutical Separation Case Study

The low-yield challenge of LPOS platform was tackled in Chapter 3. In this chapter, the developed cascade was integrated with a solvent recovery unit to tackle the high solvent consumption challenge. Membrane diafiltration processes exhibit high E-factor compared to other conventional processes, mainly from the high solvent consumption. In this Chapter, an adsorptive solvent recovery unit is investigated to improve the environmental impact without losing the yield and purity profile. A pharmaceutical purification case study is presented.

4.1. Summary

The cascade configuration proposed in Chapter 3 improved the yield without compromising the product purity. Apart from the yield challenge, membrane processes suffer another severe challenge such as high solvent consumption, hindering their widespread application in the pharmaceutical and fine chemicals industries. In this Chapter, an efficient purification methodology employing the cascade configuration coupled to an adsorptive solvent recovery unit is investigated, addressing the solvent consumption challenge. The process has been validated on purification of an active pharmaceutical ingredient (API) from genotoxic impurity (GTI) using Organic Solvent Nanofiltration (OSN). The model system selected for study comprises roxithromycin macrolide antibiotic (Roxi) with 4-dimethylaminopyridine (DMAP) and ethyl tosylate (EtTS) as API and GTIs, respectively. This system was chosen to show the versatility of the proposed cascade, apart from separating PEG mixtures, in relevant application areas. By implementing the two-stage cascade configuration for membrane diafiltration, the process yield was again increased from 58% to 95% while maintaining less than 5 ppm GTI in the final solution. Through this yield enhancement, the membrane process has been "revamped" from an unfeasible process to a highly competitive unit operation when compared to other traditional processes. The advantage of size exclusion membranes over other separation techniques has been illustrated by the simultaneous removal of two GTIs from different chemical classes.

In addition, a solvent recovery step has been assessed using charcoal as a non-selective adsorbent, and it has been shown that pure solvent can be recovered from the permeate. Considering the costs of solvent, charcoal, and waste disposal, it was concluded that 70% solvent recovery is the cost-optimum point. Conventional single-stage diafiltration (SSD) and two-stage diafiltration (TSD) configurations were compared in terms of green metrics such as cost, mass and solvent intensity, and energy consumption. It was calculated that implementation of TSD, depending on the batch scale, can achieve up to 92% cost saving while reducing the mass and solvent intensity up to 73%. In addition, the advantage of adsorptive solvent recovery has been assessed revealing up to 96% energy reduction compared to distillation and a 70% reduction of CO_2 footprint.

4.2. Introduction

Developing sustainable and green processes has become an important priority for the pharmaceutical and fine chemical industries in response to the growing concerns of regulatory authorities with respect to environmental impact[141, 142]. At the same time, the removal of genotoxic impurities (GTIs) from active pharmaceutical ingredient (API) post-reaction mixtures has gained increasing attention due to the adverse health effects of GTIs. Strict pharmaceutical regulations call for impurity levels as low as few ppm[143]. It is well known that downstream separation processes account for as much as 80% of the total manufacturing costs [144, 145]. With profit margins growing thin, there is a huge drive for reducing both the cost and environmental impact via process intensification (PI). PI refers to a set of innovative principles in process and equipment design to achieve significant benefits in process efficiency, operating expenses, quality, and waste [146]. As an effective PI tool, membrane engineering has been recognized as one of the core technologies that provides green process engineering [147].

Conventional separation unit operations for API purification such as recrystallization, flash chromatography, and adsorption, are thoroughly described in the literature[103]. Recently emerging technologies, such as organic solvent nanofiltration (OSN) [12, 133] and molecularly imprinted polymers [140, 148], as well as their synergistic combination [149], have also been suggested for GTI removal.

With respect to pharmaceutical applications, OSN has a unique advantage in that it can perform molecular separations at ambient temperature[9], allowing many thermally sensitive compounds (APIs and catalysts) to be purified under mild conditions. Considering the many advantages of OSN, it has promising potential to develop much greener and economical processes in the pharmaceutical and fine chemicals industries. In fact, membrane processes have been chosen among the top 10 green engineering research areas by the ACS GCI Pharmaceutical Roundtable [142], and several green metrics using membranes, such as productivity-to-size (PS) ratio and modularity, have been proposed to facilitate compilation of data and comparison [146, 147, 150]. For example, it has been shown that membranes can offer a substantial increase in reaction conversion with reduced catalyst loading, while reducing the plant size for

hydrogen production[151]. Also, membranes have been successfully applied to crystallization processes to improve control and efficiency[152] .

Despite these promising potentials, membrane processes have been facing difficulties in acceptance by the pharmaceutical industry, difficulties such as: 1) difficult performance prediction resulting in extensive membrane screening to find a suitable membrane[58]; 2) ineffectively compiled literature on performance and applicability compared with the traditional operations[147]; 3) insufficient separation performance[26] resulting in unacceptable loss of product yield and/or purity (Discussed in Chapter 3); and 4) large solvent consumption[102]. Among the aforementioned reasons, the latter two are the main reasons limiting the OSN-based membrane processes from wide implementation in pharmaceutical manufacturing.

Chapter 3 discussed a new membrane cascade configuration that overcomes the previous yield and implementation challenges. In Chapter 4, the potential of an OSN membrane cascade is shown via an industrial application: removal of GTIs from APIs. Employing a two-stage membrane cascade configuration over single-stage diafiltration leads to a significant increase in API yield without compromising its purity. In addition, the initial membrane screening time is much reduced, or even eliminated, as the process offers much more versatility and buffers membrane performance.

Furthermore, Chapter 4 also addresses the second major challenge of membrane purification, its extensive solvent consumption. In order to comply with the high standards of API quality assurance, ultra-low GTI levels have to be achieved calling for a substantial amount of solvent. In order to minimize the solvent consumption – *i.e.* decrease the environmental impact and increase sustainability – an adsorption unit featuring charcoal was integrated in the process. Adsorption isotherms of the charcoal-GTI system have been studied in order to identify the isotherm behavior and optimal permeate-to-charcoal ratio for solvent recovery.

To critically assess the proposed configuration, the process economics as well as conventional green metrics such as mass and solvent intensity were evaluated. In addition, the energy consumption and carbon footprint of adsorption and distillation unit operations have been compared in detail. The simplicity and versatility of this process configuration is expected to boost membrane applications in industries where

membranes were formerly not competitive enough in terms of economics and sustainability.

4.3. Experimental

4.3.1. Materials

Acetonitrile (MeCN), *N*,*N*-dimethylacetamide (DMAc), methanol (MeOH) and isopropyl alcohol (IPA), were HPLC grade and used as supplied from *VWR*. Celazole® S26 polybenzimidazole (PBI) solution (26 *wt*% polymer in DMAc containing 1.5 *wt*% LiCl) was purchased from *PBI Performance Products Inc*. Non-woven polyolefin Novatexx 2471 was from *Freudenberg Filtration Technologies*, Germany. Ethyl tosylate (EtTS), 4-dimethylaminopyridine (DMAP) were purchased from *Sigma-Aldrich;* and PEG-400 and α,α'-dibromo-*p*-xylene (DBX) were purchased from *Merck* and *VWR*, respectively. Charcoal (YAO 20x45) and Roxithromycin samples were kindly provided by *Eurocarb* Ltd, UK, and *Hovione FarmaCiencia SA*, Portugal, respectively.

4.3.2. Preparation of Polybenzimidazole (PBI) Membranes

PBI dope solutions were prepared by diluting the Celazole® S26 solution to 22 *wt*% with DMAc. The fabrication protocol is described in *Section 2.3.2*.

4.3.3. Membrane Rejection Test

All PBI membranes were screened against a test solution containing 10 $kg.m^{-3}$ of Roxi and 1 $kg.m^{-3}$ (1000 ppm) each of DMAP and EtTS. For each membrane a disc with an effective area of 51 cm^2 was loaded into a membrane cell with six retentate side ports and one permeate port, and a volume of 92 ml. A typical set-up consists of an inlet port, a retentate port fitted with a back-pressure regulator, a pressure gauge port, a thermocouple port, and a permeate port. A schematic of the system used for membrane screening and diafiltration experiments is shown in Figure 4.1.

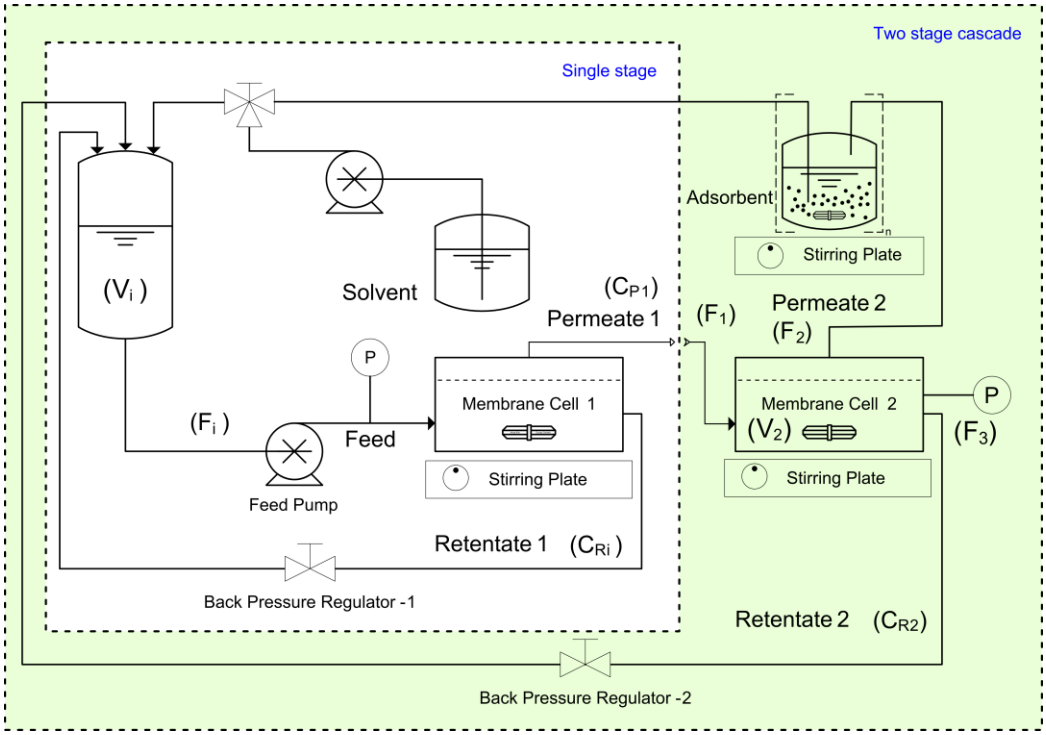


Figure 4.1. System diagrams of single-stage diafiltration and two-stage cascade diafiltration. For two-stage cascade diafiltration, the permeate from the first stage is directly connected to the feed of the second stage. The symbols in parentheses are the variables used in the process model (Appendix A).

In both the single-stage and the two-stage diafiltration set-ups, an HPLC pump (*Gilson* Model 305) provided the flow, set at 30 ml.min^{-1}. The pressure of each cell was controlled using a back-pressure regulator, and a magnetic stirrer bar was placed inside each cell (stirred at 500 RPM) to maintain a constant hydrodynamic profile in the fluid in contact with the membrane. The feed tank volume was 100 ml, and the volume of each cell plus the associated tubing was approximately 100 ml.

All membranes were first washed with at least 2 L of pure MeOH at 10 bar to remove all the conditioning agents and to achieve a steady-state flux. Next, a testing solution (10 kg.m^{-3} of Roxi and 1000 ppm each of DMAP and EtTS in MeOH) was circulated at different pressures and the permeate was recycled back into the feed until a steady-state was reached. At this point, and at different times thereafter, samples of both permeate and retentate were taken for HPLC analysis to assess the membrane performance.

4.3.4. Single Stage Diafiltration

Single-stage diafiltration was performed independently with two PBI membranes using the configuration shown in Figure 4.1. Initially, a test solution (10 kg.m^{-3} of

Roxi and 1000 ppm each of DMAP and EtTS in MeOH) was circulated around the system at 5 bar at 21 ^{o}C. Once steady-state concentration of all the species in the retentate and permeate had been reached, a preparative single stage diafiltration was performed at 5 bar. The system was maintained at a constant volume by adding the same volume of pure solvent into the system as permeated over the same time. Permeate and retentate samples were analyzed by HPLC at different times. The mass yield of Roxi was then calculated using the following equations,

$$\text{Yield } (\%) = \frac{M_{roxi,final}}{M_{roxi,initial}} \times 100 \qquad \text{(Eq. 4.1)}$$

4.3.5. Two Stage Diafiltration

The two-stage diafiltration using the configuration shown in Figure 4.1 was performed twice with a recycle ratio of 0.5 (r_C=0.5), defined in Eq. 3.9 in Chapter 3. The employed concentrations were 10 kg.m^{-3} of Roxi and 1000 ppm each of DMAP and EtTS dissolved in MeOH. Without connecting the second membrane cell, the first-stage membrane was equilibrated with a test solution at 21 ^{o}C, while recirculating the permeate back into the feed tank, until a steady state was achieved. Once the concentrations had become constant in the permeate and retentate, the permeate from the first stage was fed directly into the second cell (initially charged with pure solvent) as shown in Figure 4.1. To control the recycle ratio (r_C), the first stage and second stage transmembrane pressures were set at 15 and 5 bar, respectively. r_C is an semi-independent variable under control because the flow rate through the first and second membranes can be controlled using the back-pressure valve at the retentate side of the second stage. Permeate and retentate samples were analyzed by HPLC at different intervals.

4.3.6. Charcoal Isotherm Determination & Solvent Recovery

To obtain charcoal adsorption isotherm data, 500 ml solution containing 500 ppm of each GTI (DMAP and EtTS) was first prepared. The solution was split into five 100 ml solutions and the following amount of charcoal was added: 1g, 5g, 10g, 25g, and 40g. Each solution was stirred vigorously at 21±0.5 ^{o}C and samples were taken at various times (4-20 hrs) to confirm equilibrium was established.

Adsorption isotherms are typically described using the following equation,

$$q_e = \frac{(C_o - C_e)V}{m} \quad \text{(Eq. 4.2)}$$

where q_e refers to the amount of adsorbate in the adsorbent at equilibrium ($mg.g^{-1}$), C_o and C_e refer to the adsorbate initial concentration ($mg.L^{-1}$) and equilibrium concentration ($mg.L^{-1}$), respectively, V represents the solution volume (L), and m is the mass of the adsorbent (g).

Charcoal adsorption typically follows the Freundlich isotherm model[153], which may be written as the following:

$$q_e = K_F C_e^{1/n} \quad \text{(Eq. 4.3)}$$

where K_F and n are empirical constants representing the sorption capacity and sorption intensity, respectively. The experimental isotherm data will be further discussed later.

The amount of charcoal required to purify solvent from the permeate below the limit-of-detection (LOD, 1 ppm for DMAP, 3 ppm for EtTS) can be calculated by first equating two isotherm equations,

$$q_e = \frac{(C_o - C_e)V}{m} = K_F C_e^{\frac{1}{n}} \quad \text{(Eq. 4.4)}$$

solving for "m" yields the amount of charcoal required:

$$m = \frac{(C_o - C_e)V}{K_F C_e^{1/n}} \quad \text{(Eq. 4.5)}$$

where m represents the total amount of charcoal (kg) required to adsorb all of the GTIs in the solution. The calculation was based on the EtTS isotherm instead of the summation of two GTI isotherms. This is because the adsorption strength was weaker for EtTS compared to DMAP, and when EtTS was completely adsorbed, DMAP was also fully adsorbed (will be shown later).

To recover pure solvent from the permeate, each diavolume (300 ml) was collected separately and the calculated amount of activated charcoal was added. Each solution was stirred vigorously at 21±0.5 ^{o}C and samples were taken at various times (4-20hrs) until no more GTIs were detected in the supernatant. The recovered solvent was not re-used for the same experiment.

4.3.7. Analytical Methods

All samples were analyzed by HPLC using an *Agilent* 1100 Series system equipped with an UV detector and Varian 385-LC ELSD detector. The pump flow-rate was set at 1 $ml.min^{-1}$, the injection volume was 30 µL, the column temperature was 30 ^{o}C, and an ACE C18 RP column was fitted. The column was eluted with a gradient of MeOH and water buffered with 5 mM diethylammonium acetate, pH 6.5. The UV wavelength was set at 260 nm, the evaporation temperature was set to 40 ^{o}C, nebulization temperature at 55 ^{o}C, and the nitrogen gas flow rate was at 1.5 SLM. Calibration curves were made for roxi using ELSD, for DMAP and EtTS using UV.

4.4. Results and Discussion

The molecular weights of the GTIs (<200 Da) and APIs (>500 Da) fall in the nanofiltration MW range[8]. To carry out a fractionation of solutes using membranes, typically fractionating impurities from a product, a constant volume diafiltration (CVD) process is usually employed (discussed in *section* 2.3.3). In this particular system, hence, GTIs get pushed through the membrane as the APIs are retained, making OSN diafiltration a promising platform for API purification.

The unique ability of membranes to separate primarily based on molecular size is of particular advantage in API purification, since having two different classes of GTIs present in a crude API mixture is common[8] and with conventional technology often requires more than one unit operation to remove them separately. In this work, such advantage was exploited by removing two different chemical classes of GTIs (DMAP – arylamine, and EtTS - arylsulfonate) from API (roxythromycin) simultaneously in a single membrane diafiltration (Figure 4.2).

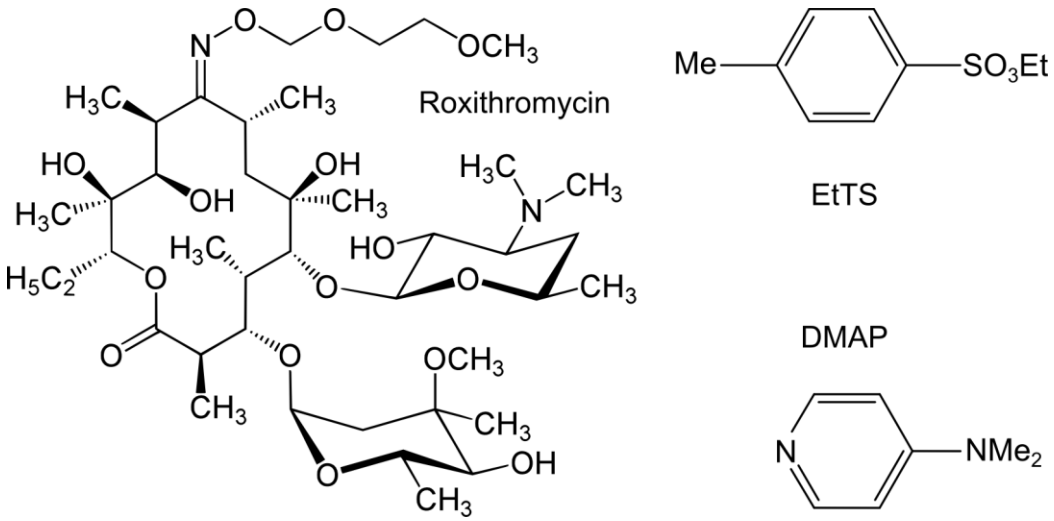


Figure 4.2. Chemical structure of the model compounds: roxythromycin (Roxi, 837 Da) API, ethyl tosylate (EtTS, 200 Da) and 4-dimethylaminopyridine (DMAP, 122 Da) GTI impurities.

To develop the process, a suitable membrane was first selected and tested at different transmembrane pressures, followed by single stage diafiltration and two stage cascade diafiltration experiments. Also, the effectiveness of charcoal with the tested GTIs was assessed. To test the process performance, the following concentrations were employed: 10 $kg.m^{-3}$ for API and 1 $kg.m^{-3}$ (1000 ppm) for each GTI[102]. All processes have been repeated twice and the error bars on the figures show the corresponding standard deviations. The recovered solvent was considered pure if the GTI levels were below their limit-of-detection (LOD).

4.4.1. Membrane Selection & Single Stage Diafiltration (SSD)

To identify a suitable membrane for API purification, a 22DBX PBI OSN membrane has been tested against the compounds of interest dissolved in methanol. However, as the solute rejections are functions of transmembrane pressure (*i.e.* flux)[62], the rejections have been measured at different pressures. The solute rejections and fluxes obtained at various pressures are shown in Table 4.I.

Table 4.I. Rejection and Flux Data at Different Transmembrane Pressures

Pressure (bar)	$\mathbf{R_{Roxi}}$	$\mathbf{R_{DMAP}}$ (%)	$\mathbf{R_{EtTS}}$	**Flux †** ($dm^3.m^{-2}.h^{-1}$)
5	93.5±0.3	10.5±0.7	14.9±0.2	14.0±2.1
10	95.2±0.2	14.3±3.2	19.2±4.7	24.7±4.2
15	94.9±0.2	15.7±2.3	20.6±3.9	39.7±6.2

† All measurements were made at 21± 0.5 °C. The average values of two membranes are reported with error bars indicating one standard deviation.

Table 4.I shows that the selected membrane shows wide difference in rejection between the API and GTIs, where API is highly retained by the membrane while GTIs easily pass through the membrane. It can also be seen that the change of API rejection with respect to the pressure is insignificant; however, the rejection of GTIs is dependent on the transmembrane pressure, up to 35% difference. Normally, 94% API rejections shown in Table 4.I are insufficient to obtain high yield after purification and further membrane screening would be necessary. However, to demonstrate that excessive membrane screening period is not required, the membrane was selected to test the advantages of cascade configuration. The single stage diafiltration (SSD) data obtained are presented in Figure 4.3.

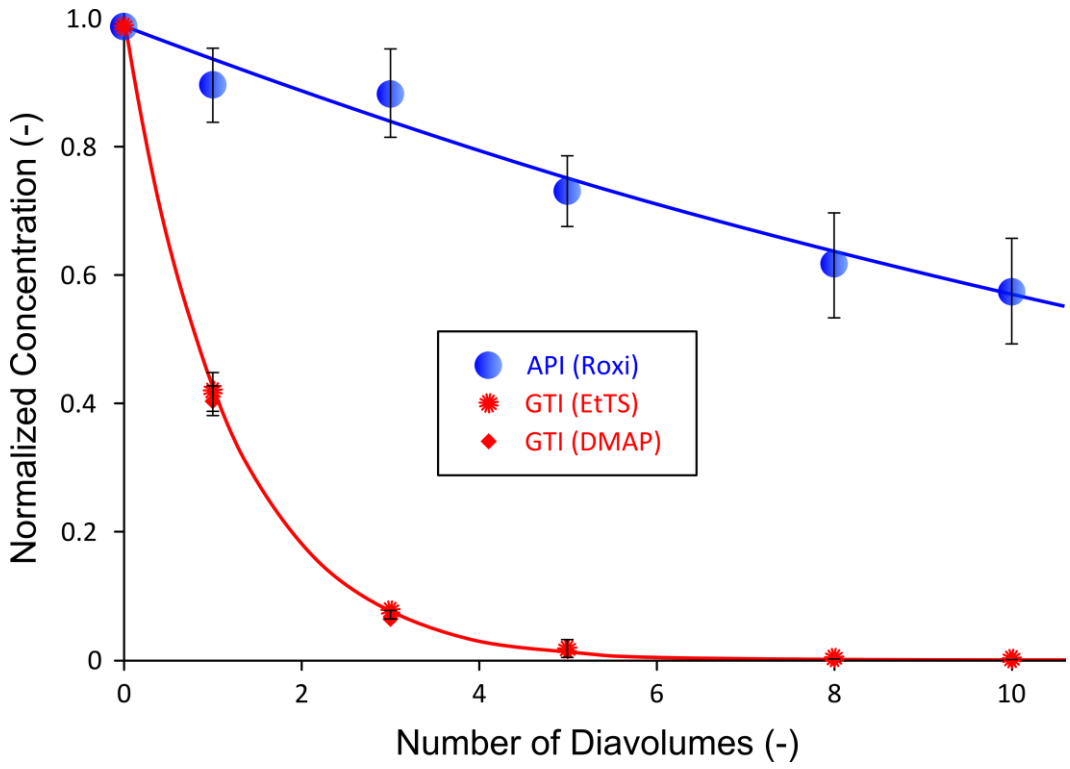


Figure 4.3. Single stage diafiltration (SSD) normalized concentration profile using PBI membranes. Both GTIs were removed at virtually the same rate. Less than 5 ppm GTI purity has been achieved after 10 diavolumes with final yield of 58%.

Figure 4.3 summarizes the SSD normalized concentration profile of the system using PBI membranes. The mass balance of all species fell within 4~6%. The concentration profiles of API and GTIs closely matched to model predictions simulated using rejection values from Table 4.I. It can be seen that even with the

moderately-high rejection of 94%, the yield of API after 10 *diavolumes* was only 58%. Given that APIs are high-value products, such a loss is unacceptable in industry.

Apart from the process yield, both GTIs showed similar rejections due to having similar molecular weights (122 and 200 $g.mol^{-1}$, respectively). As expected, they were removed at nearly the same rate and the final GTI concentration decreased to below 5 ppm, satisfying the typical target level of 10 ppm[102, 154]. Although the yield was low, the advantage of membrane processes over affinity-based purification technologies (e.g. resin, chromatography) was clearly demonstrated in this system: GTIs from different chemical classes can be removed simultaneously; usually affinity-based purifications would require specific selective agents for each chemical class of impurities[148, 155].

Nevertheless, the low API yield results in an unfeasible manufacturing process in terms of economics and sustainability. To address this low yield challenge, one might undertake a cumbersome screening period to find tighter membranes. However, this leads to higher GTI rejection as well, calling for even higher number of *diavolumes*. In addition, apart from limited availability of different types of commercial OSN membranes, it is often difficult to find the right membranes to meet the process demand. As an alternative to overcome such a challenge, the two-stage cascade configuration proposed in Chapter 3 can be employed.

4.4.2. Two Stage Diafiltration (TSD)

It has been shown in Chapter 3 that to achieve a high yield using the cascade configuration, the recycle ratio, which is defined as the retentate (F_{R2}) from the second stage over the feed into the second stage (F_{P1}), must be controlled carefully. The difference in yield can be up to two-fold depending on the chosen recycle ratio. After a thorough predictive simulation based on the rejection data in Table 4.I, an optimum operating condition has been chosen and implemented (See Experimental Section). The results from TSD are shown in Figure 4.4. The mass balance for all species closed within 1~5%.

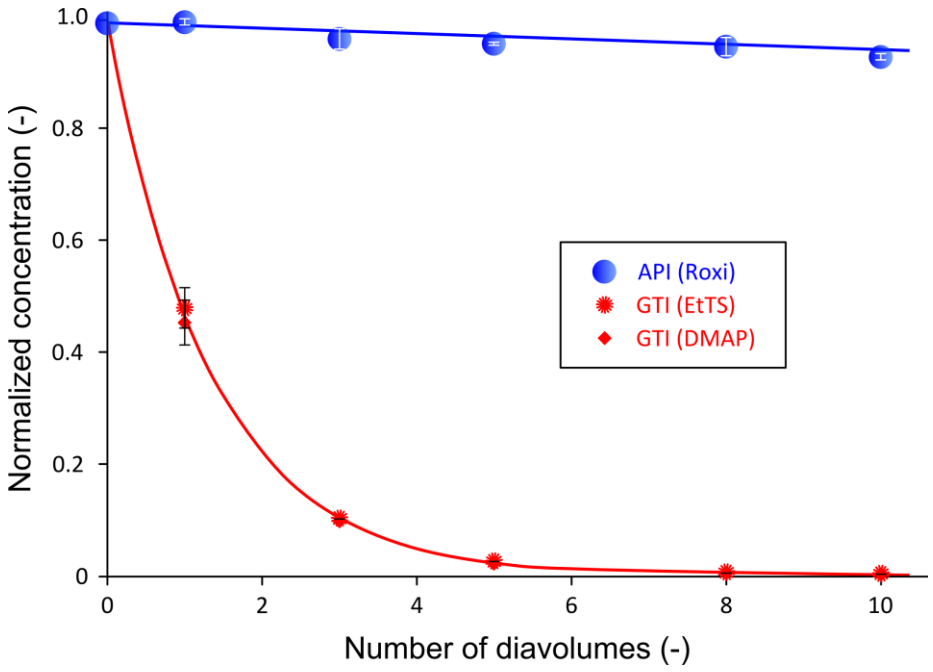


Figure 4.4. Two-stage diafiltration (TSD) normalized concentration profile using PBI membranes. Recycle ratio (r_C) was set at a value of 0.5. GTI concentrations less than 5 ppm were again achieved after 10 diavolumes with the final API yield of 95%, a substantial improvement from SSD yield of 58%.

Figure 4.4 illustrates a drastic improvement in final yield of API, from 58% to 95%, without compromising the final purity. By introducing the second stage and setting the recycle ratio at a value of 0.5 (r_C = 0.5), the actual loss of API through the membrane was considerably reduced, as predicted by the process model. The overall rejection of API (combined rejection of two stages) has increased from 94% in the SSD, to 99.5% in the TSD. On the other hand, although the overall rejections of GTIs have increased from 15% (SSD) to 25% (TSD), the rate of GTI permeation through the membrane remained high in accordance with the model prediction. Hence, the permeation of 10 *diavolumes* – the same as performed SSD – allowed the target impurity level of 10 ppm to be met. More precisely, GTI levels below 5 ppm have again been achieved, proving the benefit of two-stage membrane cascade configuration.

Although a set of non-commercial PBI membranes were used for this study, commercially available polyimide membranes have also shown excellent API purification performances[12], which can be applied to the proposed system. In addition, it should be stressed that the proposed process is not limited to polymeric membranes and to API purification applications but it can be applied with other types of membranes (ceramic, carbon membranes, etc) and to other applications (catalyst

recovery, membrane reactors, refinery industry, etc). The essence of the proposed cascade configuration lies in its simplicity and versatility. Also, the process is very straightforward to implement and control[20]. Furthermore, the system can be easily modeled, where the only required input parameters are the membrane permeability and solute rejections (discussed in Chapter 3). For example, depending on the product rejection, the process yield improvement in moving from SSD to TSD can be predicted as shown in Figure 4.5.

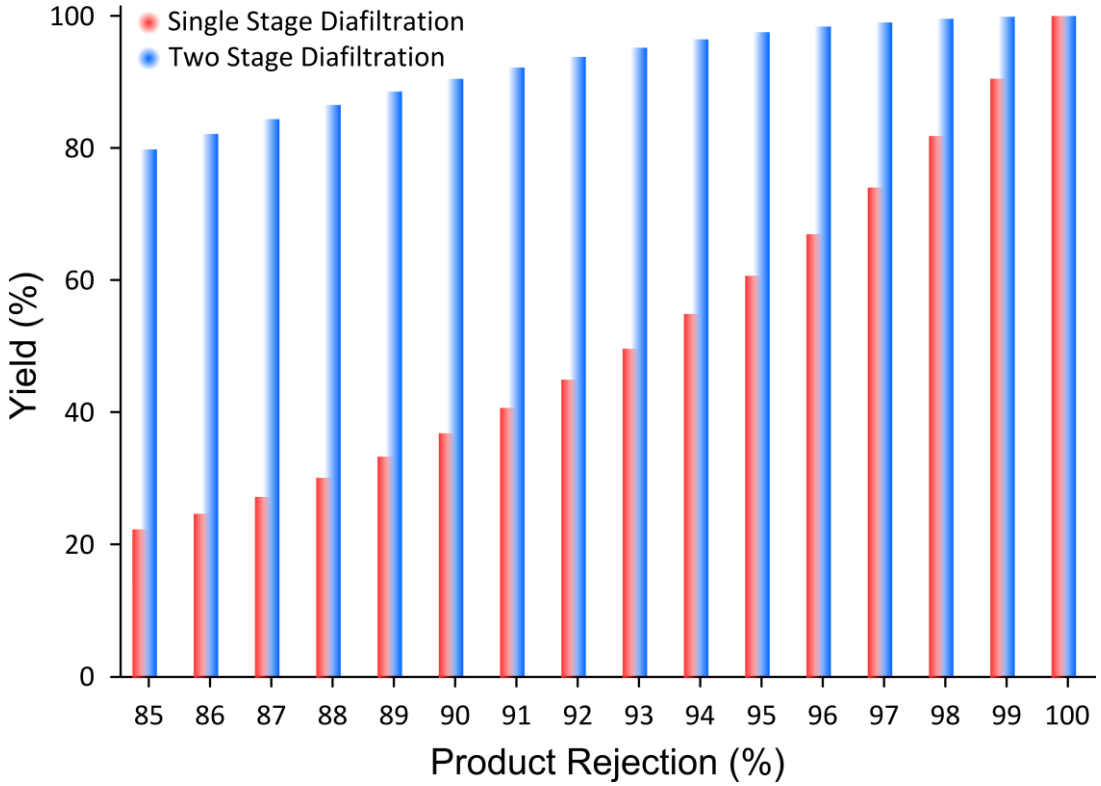


Figure 4.5. Predicted yield improvement after 10 diavolumes for different product rejection. The TSD configuration achieves significant yield improvement, overcoming the membrane limitation inherent in the SSD for rejection less than 99%. As long as the product rejection is above 90%, the process promises high product yield, making the process competitive to other traditional unit operations.

Figure 4.5 clearly illustrates the potential yield improvement through implementing the TSD system proposed in this work. For instance, when the membrane rejection of a product is 85%, SSD achieves a yield of only 22% after 10 *diavolumes*. However, when the TSD configuration is applied, the yield improves up to 80%, close to 4x improvement. Although the increase in yield is substantial, the yield of 80% is still unsatisfactory for high-value products. However, when the product rejection is 98%, the yield improves from 81% to 99.6% after 10 *diavolumes*. The implication of such yield improvement should not be understated. This difference in yield, undoubtedly, transforms the membrane process from “unfeasible” status to

an economically sustainable and viable process, and makes it highly competitive to other conventional processes. Hence, the TSD configuration provides substantial improvement relative to the SSD configuration. In addition, as long as the rejections of the impurities are less than 50%, it can be shown that the final product purity will not be compromised[156]. It is worth pointing out that most GTIs fall below 50% rejection on commonly available nanofiltration membranes[12], making the TSD configuration a competitive platform for API purification.

It is possible to extend the system to three or four-stage configuration which would increase the yield even further, and the model can also be generalized. However, the rejection increase of impurities mostly outweighs the yield gain and the system requires even higher *diavolumes*. Hence, the additional capital cost as well as the operation complexity must be carefully assessed before extending the cascade system.

With the yield challenge resolved, the process opens up new opportunities for integration with other unit operations. As the final permeate waste stream from the system mostly contains GTIs, the possibility of solvent recycle via adsorption can be exploited. Hence, the use of activated charcoal for solvent recovery has been assessed by adsorption of impurities.

4.4.3. Solvent Recovery – Adsorption Isotherm & Feasibility assessment

Activated charcoal is a widely used adsorbent with high adsorption capacity due to its high surface area[157]. It has been applied to API purification as part of an API recrystallization process, however the selectivity between the API and GTI was poor, resulting in relatively high API loss[102]. Combining membranes with different adsorbents has been reported previously[140, 158] and it was concluded that the major impediment to success was the API loss from the membrane stage. For the TSD configuration, the high GTI uptake of activated charcoal at low concentrations can be exploited for solvent recovery, as the permeate from the TSD system mostly contains only GTIs with negligible API. In order to determine the optimal permeate to charcoal ratio, the activated charcoal was first characterized using a conventional isotherm experiment.

The adsorption isotherms obtained for both GTIs are summarized in Figure 4.6.

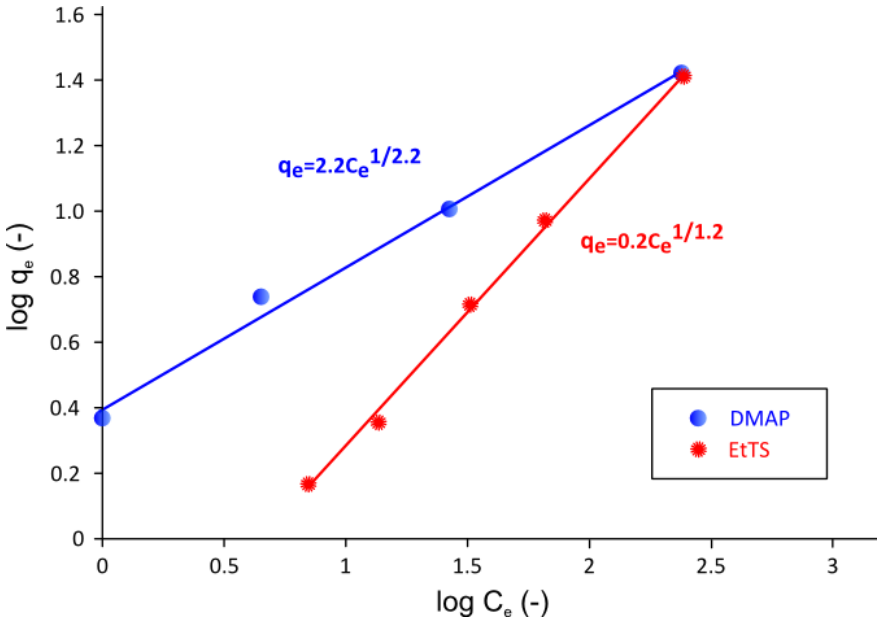


Figure 4.6. Log-log plot of adsorption Isotherm of GTIs on charcoal in methanol at 21°C. The Freundlich isotherm describes the adsorption behavior of two GTIs well.

As can be seen in Figure 4.6, when isotherm data are plotted in log q_e vs log C_e scale, a linear relationship can be obtained, indicating that the system follows the Freundlich isotherm[153] described in Eq. 4.3.

The Freundlich isotherm has been specifically developed to describe adsorption onto charcoal, where stronger binding sites are occupied first, followed by exponential decrease in adsorption energy until all sites are occupied[159]. One notable trend from Figure 4.6 is that the K_F value for EtTS is lower than that of DMAP, showing that the adsorption strength for EtTS is weaker than that of DMAP.

At this point, two important remarks in regard to the solvent recovery experiment must be stated clearly. First, the competition for adsorption sites between the two GTIs has not been taken into account because the objective was complete GTI adsorption, and the kinetics of adsorption was outside the scope of this study. Hence, a simple Freundlich model was sufficient to describe the system. Secondly, the actual solvent recovery experiment was carried out in a batch-wise mode, rather than continuous mode, to assess the feasibility of adsorptive solvent recovery. Each discrete *diavolume* from TSD experiments was collected separately and the necessary amount of charcoal was added and stirred until all GTIs were adsorbed to a level below the limit-of-detection (LOD) (Eq. 4.5).

The permeate concentration of each *diavolume* and the corresponding amount of charcoal required (cumulative) are shown in Figure 4.7a, and the efficacy of a typical charcoal adsorption is presented in Figure 4.7b.

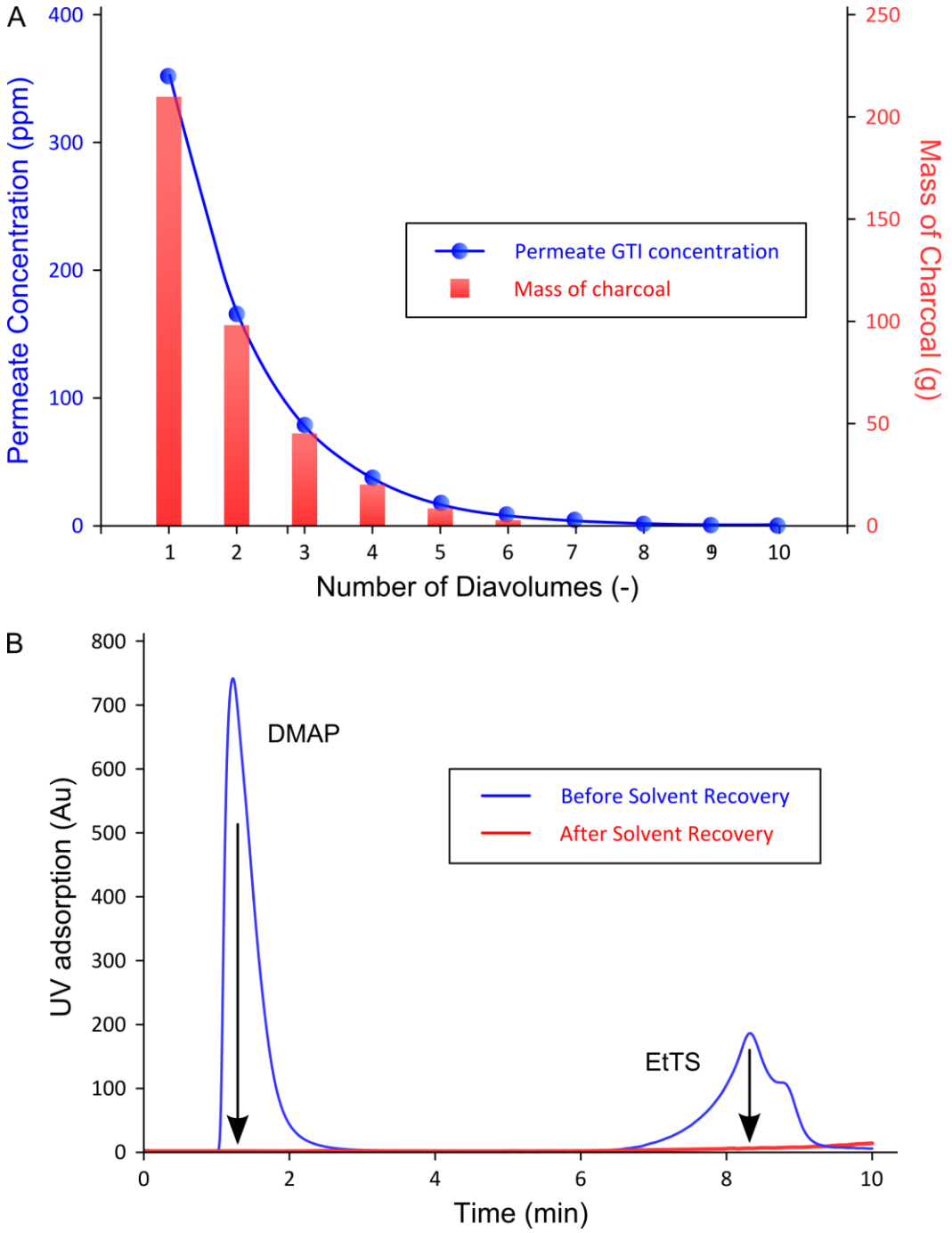


Figure 4.7. (**a**) GTI permeate concentration at each *diavolume* before adsorption and the respective amount of charcoal used to extract pure solvent. Approximately 90% of GTI permeate in the first three *diavolume*, requiring over 70% of the overall charcoal used. (**b**) A typical UV-HPLC chromatogram of crude permeate (1st *diavolume* data shown) and recovered solvent, which shows no remaining impurity (C_{GTI} < LOD). Arrows show the extent to which initial permeate GTI content is reduced via solvent recovery.

Figure 4.7b shows that the GTI adsorption to charcoal allowed the recovery of the permeate by yielding pure solvent with concentrations below LOD for both GTIs measured by UV-HPLC, *i.e.* 1 and 3 ppm for DMAP and EtTS, respectively. In addition, no API was detected in the supernatant after the GTI adsorption. The purity of the recovered solvent allows its reuse in the manufacturing process.

As expected from the TSD diafiltration data (Figure 4.4), it can be seen in Figure 4.7a that approximately 90% of the GTIs permeate through the membrane in the first three *diavolumes*. After the third *diavolume*, the remaining 10% of the GTIs permeate at much slower rate. Figure 4.7a also shows that over 70% of the required charcoal is used in the first three dia*volumes*, and it can also be seen that recycling the last *diavolume* takes the least amount of charcoal. This trend clearly suggests a potential for optimization. Hence, an economic analysis has been carried out in terms of cost of MeOH (£0.36 kg^{-1}), charcoal (£6 kg^{-1}), and waste disposal (£0.42 kg^{-1}), to optimize the solvent recovery amount, as shown in Figure 4.8. The used charcoal and untreated solvent were treated as solid and solvent waste, respectively.

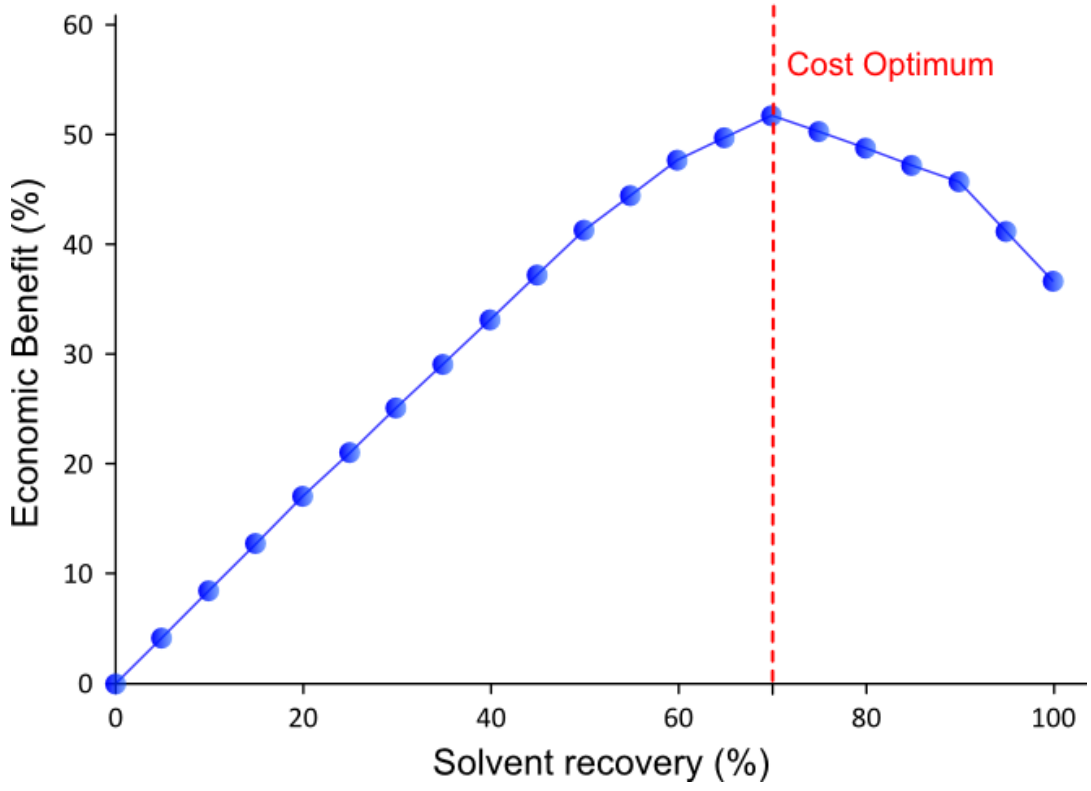


Figure 4.8. Calculated economic benefit from solvent recovery plotted versus percentage of solvent recovered curve shows an optimum for solvent recovery. The calculation is based on the cost of solvent, charcoal, and waste disposal.

For the purposes of calculation, it was assumed that the last permeate *diavolume* was recovered first and gradually progressed towards the first permeate *diavolume*. Hence, 10% solvent recovery means the last 10% of the permeate has been recycled, and so on. It can be seen in Figure 4.8 that the relative benefit from solvent recovery continuously increases until the maximum value at 70% solvent recovery. Then, the relative benefit decreases from the maximum value to recover the last 30% of the solvent, representing the first three *diavolumes*. From this point, the cost of charcoal and waste disposal overtakes the marginal gain obtained from recovering the solvent.

Also, the amount of solid waste generated from charcoal increases rapidly for the last 30% (discussed in the next section). Nevertheless, it is more economical to recover 100% solvent than to have no solvent recovery, as the cost of charcoal is quite inexpensive. Also, the optimum could easily be affected by the cost of solvent and charcoal.

Apart from this specific example, most API purification diafiltrations have shown similar permeate concentration profiles[12, 102] in which 90% of impurities are removed in the first three *diavolumes*. Therefore, it is expected that the cost optimum solvent recovery point implementing an adsorptive solvent recovery unit would often lie between 70-80%. Nevertheless, it is expected that 100% solvent recovery would be preferred when additional factors, *i.e.* handling, capital cost, and greenness aspects, are considered.

4.4.4. Economic & Green Metrics Analysis

Implementing a two-stage diafiltration process with a solvent recycle unit provides important process intensification of API purification. To assess the proposed process in more detail, the three processes described in this work, single-stage diafiltration (SSD), two-stage diafiltration (TSD), and two-stage diafiltration with solvent recovery (TSD+SR), are compared in terms of costs, mass and solvent intensity, energy consumption, and CO_2 output, which are the key process metrics[160].

As briefly mentioned in the previous section, the cost of API varies widely from £100 kg^{-1} to £100,000kg^{-1}**,** depending on the strength, dose, production scale, and type of the API. While the economic gain from solvent recovery mainly depends on the scale of API production, its ability to reduce the overall environmental impact of the process is mainly related to the solvent used and the amount of solvent recycled.

Hence, to make a reasonable comparison, the three processes are compared at different API prices. Furthermore, to compare implementing adsorption over distillation for solvent recovery, energy consumption and CO_2 intensity have been compared at 70% solvent recovery.

The magnitude of cost reduction at different API price is summarized in Figure 4.9. The parameters taken into account for the calculation are cost of API loss, solvent, charcoal, membrane module, and waste disposal.

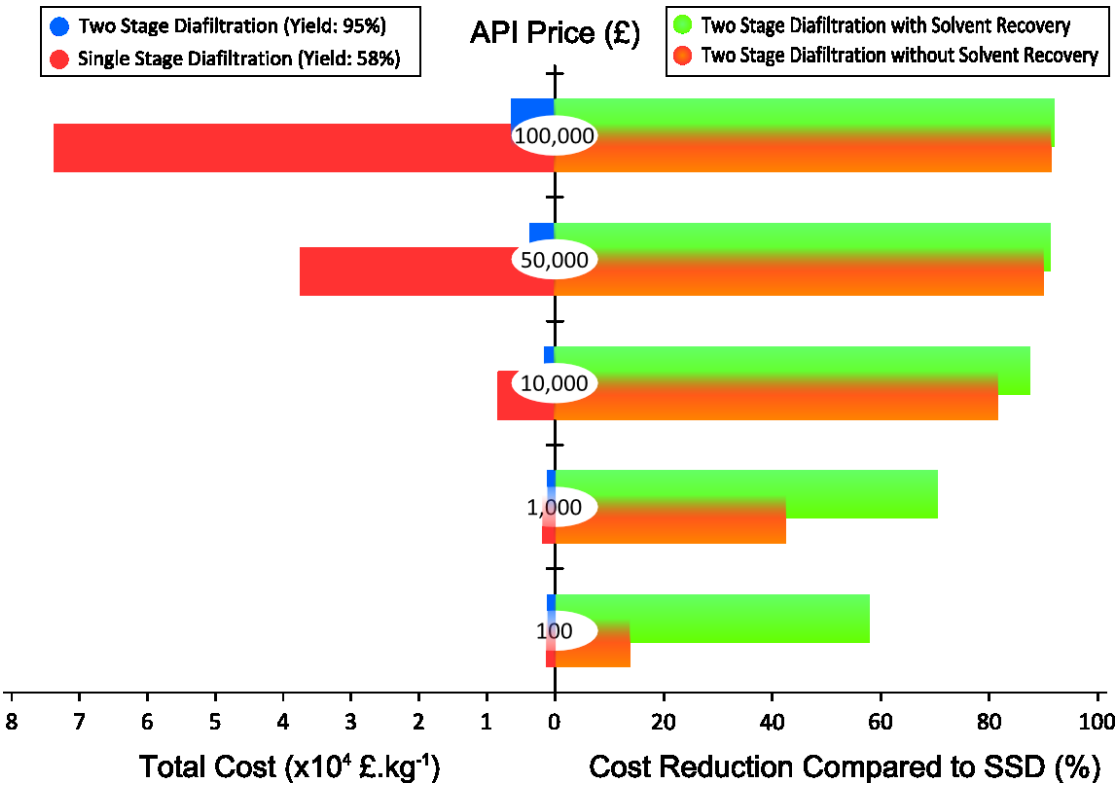


Figure 4.9. (left) Total purification cost per unit of API calculated for single-stage diafiltration (SSD) and two-stage diafiltration (TSD). The calculation includes the cost of API loss, solvent, membrane, charcoal, and waste disposal. **(right)** Summary of cost reduction for API purification compared to SSD by implementing TSD and TSD with 70% solvent recovery. The cost reduction is most significant when the cost of API is high. The difference between TSD and TSD+SR becomes considerable at lower API cost.

Figure 4.9 clearly illustrates that the separation cost is considerably reduced when the TSD process is implemented. At an API price of £100,000 kg^{-1}, the cost reduction can be as high as 92%. Also, as the price of API goes down, the cost reduction also goes down because the major factor for the cost reduction comes from the API loss. As the yield of SSD is only 58% compared to the TSD yield of 95%, the loss of API is substantially reduced in TSD, improving the economics of separation. In addition, TSD+SR always compare favorably over TSD. As can be seen in Figure 4.9, the gap

between TSD and TSD+SR gets wider as the price of API goes down. This trend arises because the cost of solvent and waste disposal becomes comparable relative to that of API loss as the price of API goes down, and recovering 70% of the solvent contributes significantly to the process economics. In all cases, TSD+SR achieves cost saving over conventional SSD, mainly through increasing the process yield of API and reducing the solvent consumption.

Apart from the separation cost, implementation of solvent recovery brings additional advantages from the green engineering perspective. Mass intensity and solvent intensity are two of the most commonly used process metrics to describe a particular process. Due to their inherent simplicity, they are being widely applied to compare different processes[141, 142]. They are defined as,

$$\text{Mass Intensity } (MI_i) = \frac{Mass\ of\ all\ materials\ used\ excluding\ water\ (kg)}{Mass\ of\ product\ i\ (kg)} \quad \text{(Eq. 4.6)}$$

$$\text{Solvent Intensity } (SI_i) = \frac{Mass\ of\ all\ solvents\ used\ excluding\ water\ (kg)}{Mass\ of\ product\ i\ (kg)} \quad \text{(Eq. 4.7)}$$

$$\text{Mass Intensity Ratio (MIR)} = \frac{MI_1}{MI_2} \quad \text{(Eq. 4.8)}$$

where MI_1 and MI_2 are mass intensity of two different processes for the purpose of comparison. Mass intensity ratio less than a value of 1 means MI_1 process is preferred, and vice versa.

A solvent recovery unit achieves visible improvement in process sustainability in terms of mass intensity (MI) and solvent intensity (SI) of the process, as shown in Figure 4.10.

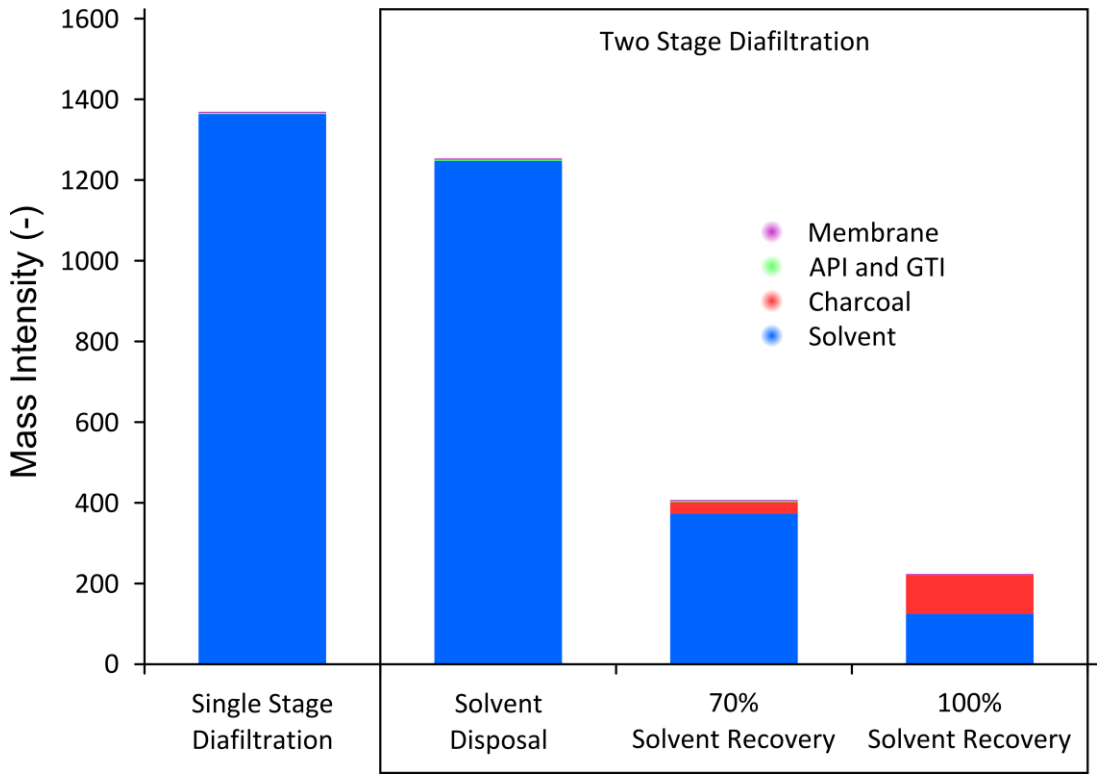


Figure 4.10. Mass Intensity (MI) comparison. The largest part of MI comes from solvent use. TSD achieves lower MI than SSD in all cases.

The results in Figure 4.10 show several interesting trends. First, compared to SSD, TSD and TSD+SR clearly achieve better MI. TSD without solvent recovery achieves 8% MI reduction, whereas TSD+70%SR and TSD+100%SR achieve 70% and 84% reduction in MI, respectively. It should be stressed that the overall system volume for TSD (consisting of first stage and second stage) is actually higher than SSD (consisting only of first stage), which means each given *diavolume* produces higher waste solvent for TSD. Nevertheless, it can be seen that the actual MI is lower because TSD achieves much higher yield, allowing lower overall solvent consumption compared to SSD. The mass intensity ratio of TSD to SSD was calculated to be 0.91, suggesting that TSD, without solvent recovery, is marginally preferred. Secondly, it can be seen in Figure 4.10 that solvent consumption accounts for most of the mass intensity. As pointed out earlier, this high solvent consumption is the major challenge of membrane diafiltration processes, where for both SSD and TSD without SR, the solvent contributes over 99.9% of the calculated MI. Hence, when solvent recovery is implemented, a considerable reduction in MI can be observed, making the process greener and more sustainable. It is also apparent that the solvent fraction is lower for TSD+SR, as the mass of charcoal adsorbent contributes to the MI. The calculated mass intensity ratios of TSD+70%SR and TSD+100%SR

were 0.29 and 0.16, respectively, approximately 4 times improvement. Lastly, the gain from recovering the last 30% of the solvent is relatively marginal as the solid waste becomes significant to the amount of solvent recovered. Nevertheless, the amount of solvent recovery depends on the type of application and hence a reasonable balance should be struck between the solvent recovery, charcoal consumption, and process operation.

MI values obtained in this study correlate well with other membrane diafiltration MI values reported in the literature[12, 102]. Also, it is interesting to compare MI values obtained in this work to the compiled MI data from seven major pharmaceutical companies on various processes and unit operations[161]. The compiled data from 2007 reported that the maximum, minimum, and median MI values of the drug manufacturing processes in development pipelines are 887, 23, and 120, respectively. In terms of MI, membrane processes (SSD and TSD) without solvent recovery are not very competitive. However, once the solvent recovery unit is implemented, the process MI falls within the range, albeit above the median value. This trend clearly indicates that in order for the membrane diafiltration unit to be competitive to conventional processes from a green engineering perspective, a solvent recovery unit must be implemented. However, it should be stressed that MI values can vary considerably depending on the operating concentration range. In this study, the concentration of API in the solution was 10 $kg.m^{-3}$, but it is also common to use up to 100 $kg.m^{-3}$ or higher, which would reduce the MI one order of magnitude.

Both the economic and environmental impacts of a solvent recovery unit depend on the solvent type as well as the recovery process itself, i.e. whether the solvent is recovered by adsorption or distillation. For instance, chlorinated solvents (*i.e.* DCM) or high-boiling-point solvents (*i.e.* DMF) would have different impacts in process sustainability and energy consumption[162, 163]. The current trend is to minimize chlorinated and high-boiling-point solvent consumption, and replace them with milder and nontoxic solvents[164]; however, there are still many cases where such solvents are required. Hence, a comparison between distillation and an adsorption unit in terms of energy consumption and CO_2 generation considering solvents used widely in chemical processes, is presented in Figure 4.11.

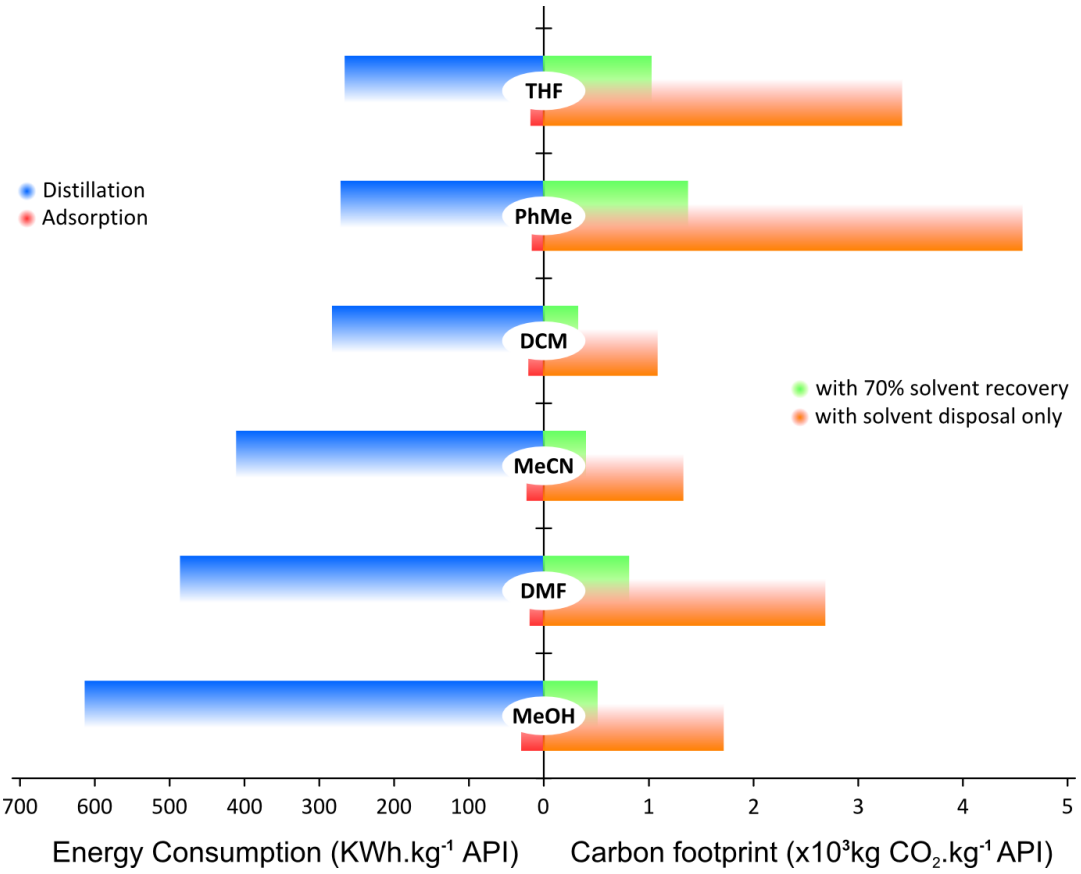


Figure 4.11. (left) Comparison of energy consumption for distillation and adsorption for solvent recovery for commonly used organic solvents; **(right)** Comparison of CO_2 footprint with and without solvent recovery.

Figure 4.11 shows the difference in energy consumption between distillation and adsorption unit operation for TSD with 70% solvent recovery. For distillation, the calculation takes into account the solvent heat capacity, and heat of vaporization and condensation; as for the adsorption process, heat of adsorption, stirring and vacuum filtration energy have been taken into account. For comparison purposes, all calculations have been normalized to the unit of API purified. Surprisingly, the energy required to recycle MeOH is higher than that for DMF using distillation. This rather unexpected trend arises because the basis of calculation was on the same *volume* of solvent for the same API crude concentration (10 $kg.m^{-3}$). Considering the density and molecular weight of each solvent, the energy required to evaporate the same *volume* of different solvents does not necessarily follow the order of boiling points. On the other hand, it can be seen that the energy required for adsorption process is 92 – 96% lower than that from distillation.

It is interesting to compare the difference in mass of waste to be removed through solvent recovery between SSD and TSD permeate. The total waste in the permeate for

SSD (total solute including API and GTI) is as high as 1.2 g waste per kg of solvent. On the contrary, the TSD configuration yields 4 times less waste in in the permeate, since much less API permeates through the membrane. Such a mass gain makes adsorption processes feasible for solvent recovery. In previous studies employing conventional SSD only distillation-based solvent recovery units were investigated[19]. The TSD processes coupled with an adsorptive solvent recovery unit presents a notable advantage in solvent and energy consumption.

Figure 4.11 also summarizes the CO_2 footprint of the process with and without solvent recycle. The calculation takes into account the amount CO_2 generated from incinerating the solvents as well as the associated carbon intensity from using steam and electricity for the solvent recovery unit. The main source of CO_2 comes from solvent incineration, where the carbon intensity contributions from using steam and electricity (taken as 204 and 369 kg of CO_2 per MWh, respectively) were less than 1% of the overall CO_2 footprint. Hence, there was a negligible difference in CO_2 reduction between distillation and adsorption. Although the comparison was made at 70% solvent recovery, the carbon footprint can be further reduced through a higher fraction of solvent recovery. For instance, a combined approach where the first three diavolumes are recovered by distillation and the rest by adsorption, can be explored to minimize the energy consumption and CO_2 footprint. Nevertheless, it is clear from Figure 4.11 that recovering solvent reduces the CO_2 footprint because not as much solvent is incinerated but recycled.

In summary, considering the cost (Figure 4.9), mass intensity (Figure 4.10), and energy consumption (Figure 4.11), the overall trend leads to a clear conclusion that a solvent recovery unit is strongly preferred for membrane diafiltration processes to secure a competitive edge in comparison to other separation technologies.

4.5. Conclusions

In this work, previous limitations faced by membrane processes have been successfully overcome through the application of a membrane cascade and solvent recovery. The proposed membrane cascade configuration was tested on a practical application: purifying an API product from two different classes of GTIs using an organic solvent nanofiltration (OSN) platform. In summary, the following conclusions can be drawn:

- A two-stage membrane cascade configuration has been proposed and applied which drastically increased the process yield (58% to 95%) without compromising its final purity (below 5 ppm GTI).
- The configuration allows much higher membrane versatility, as membranes with insufficient separation performance can be used to achieve high yields. This reduces the initial membrane-screening period, which is often the bottleneck stage for membrane process development.
- Removing two classes of GTIs in a single unit operation has shown the advantage of a size exclusion membrane process over affinity-based separations.
- The TSD process achieved significant cost saving up to 92% compared to conventional single stage diafiltration. Implementing a solvent recycle unit achieved 70% and 73% reduction in mass intensity (MI) and solvent intensity (SI), respectively.
- An adsorptive solvent recovery unit consumes 92 - 96% less energy compared to distillation.
- A solvent recovery unit is required to make membrane diafiltration processes competitive to conventional separation techniques.

The proposed membrane process can overcome the previous challenges of LPOS platform such as low product yield and high solvent consumption. Through the two-stage cascade configuration, it is expected that the membrane process achieves competitive yield and purity, which will be assessed in the next Chapter.

Imperial College London

Chapter 5

Process Intensification of Liquid-Phase Oligonucleotide Synthesis (LPOS) Platform Through Membrane Reactor and New Protecting Group Chemistry

Three of the key challenges of LPOS platform identified in Chapter 2 are tackled in this Chapter. The two-stage cascade configuration developed in Chapter 3 and 4 was implemented. A membrane reactor concept with new protecting group chemistry was applied to significantly simplify the overall process.

5.1. Summary

In Chapter 2, a scalable Liquid-Phase Oligonucleotide Synthesis (LPOS) platform using Organic Solvent Nanofiltration (OSN) separation technology has been proposed. In this Chapter, several innovations that improve the LPOS-OSN platform are discussed. Three main challenges of the LPOS-OSN platform — redundant solvent exchanges, incomplete removal of phosphoramidite monomers, and low yield — have been successfully overcome through a combination of chemical and process innovations. Notably, the use of a membrane reactor to combine the reaction and separation significantly simplified the overall process, eliminating the redundant solvent exchanges and reducing the number of unit operations by a third (from 9 to 3 unit operations per chain extension cycle). The bulky protection group, 4,4'-dimethoxytritylphenylmethyl ether (Dmtr, MW 302 Da), was replaced with a smaller methoxyisopropyl ether (MIP, MW 74 Da) protection, which freely permeates through the membrane, to better suit the LPOS platform. Excess phosphoramidite monomers were chemically modified to an anionic entity that can be removed using polybenzimidazole (PBI) membranes through ion-exchange mechanism. It was also shown that the ion-exchange capacity of the membranes can be amplified through an acid-doping step. The process yield was improved using a simplified cascade configuration developed in Chapter 3 and 4. It is envisaged that the proposed improvements to the LPOS platform can enhance its viability in the industry scale.

5.2. Introduction

The general definition of membranes, both polymeric and inorganic, is a semipermeable barrier that can selectively permeate and separate solutes. However, it has been investigated since 1970s to employ membranes not only as a separation unit, but combined advantageously with a chemical reaction(s) as a membrane reactor unit to either: (i) simplify the overall process, (ii) manipulate the reaction equilibrium, (iii) recycle valuable compounds (i.e. catalyst or reagents), and/or (iv) allow continuous processing, to list a few of many potential functions[165]. Membrane reactors have already been utilized in various applications such as biochemical, environmental, petrochemical, and pharmaceutical systems, with many commercial successes[166]. Its industrial applicability and perspective as a "multifunctional reactor" has huge potential for process intensification (PI) of chemical processes[30].

In this Chapter, a practical application of a membrane reactor is presented to improve the Liquid-Phase Oligonucleotide Synthesis (LPOS) platform proposed in Chapter 2. The growing oligos were anchored on a branched soluble support for step-wise chain extension reaction. Each chain extension cycle comprised of two reactions (chain extension and deprotection of 5'-*O*) and each reaction was followed by a membrane diafiltration (Figure 2.1). Polybenzimidazole (PBI) OSN membranes were employed as they can withstand various types of organic solvents including acids and bases, and have the capacity to separate solutes with nanometer precision[45]. Employing the proposed 4-step cycle LPOS-OSN platform, 9-mer oligoribonucleotides (RNA oligos) were successfully synthesized and it was shown to be competitive to the SPOS platform in terms of efficiency and economics, yet scalable.

However, several hurdles have been identified for the LPOS platform to become commercially feasible. The main practical issue from the process perspective was the need for multiple solvent exchanges in-between unit operations, illustrated in Figure 5.1a. For instance, the chain extension reaction was carried out in MeCN (or DMF-MeCN) whereas the deprotection reaction was carried out in DCM. Apart from the reaction, the actual membrane separation was done in MeOH-MeCN due to oligos' solubility requiring a mixture of solvents (H-bonding requirements). In addition, a separate precipitation step was required in diethyl ether (Et_2O) to remove the bulky

5'-*O* protecting group, *i.e.* 4,4'-dimethoxytriphenylmethyl ether (i.e. Dmtr, 302 Da) due to high rejection by the membranes.

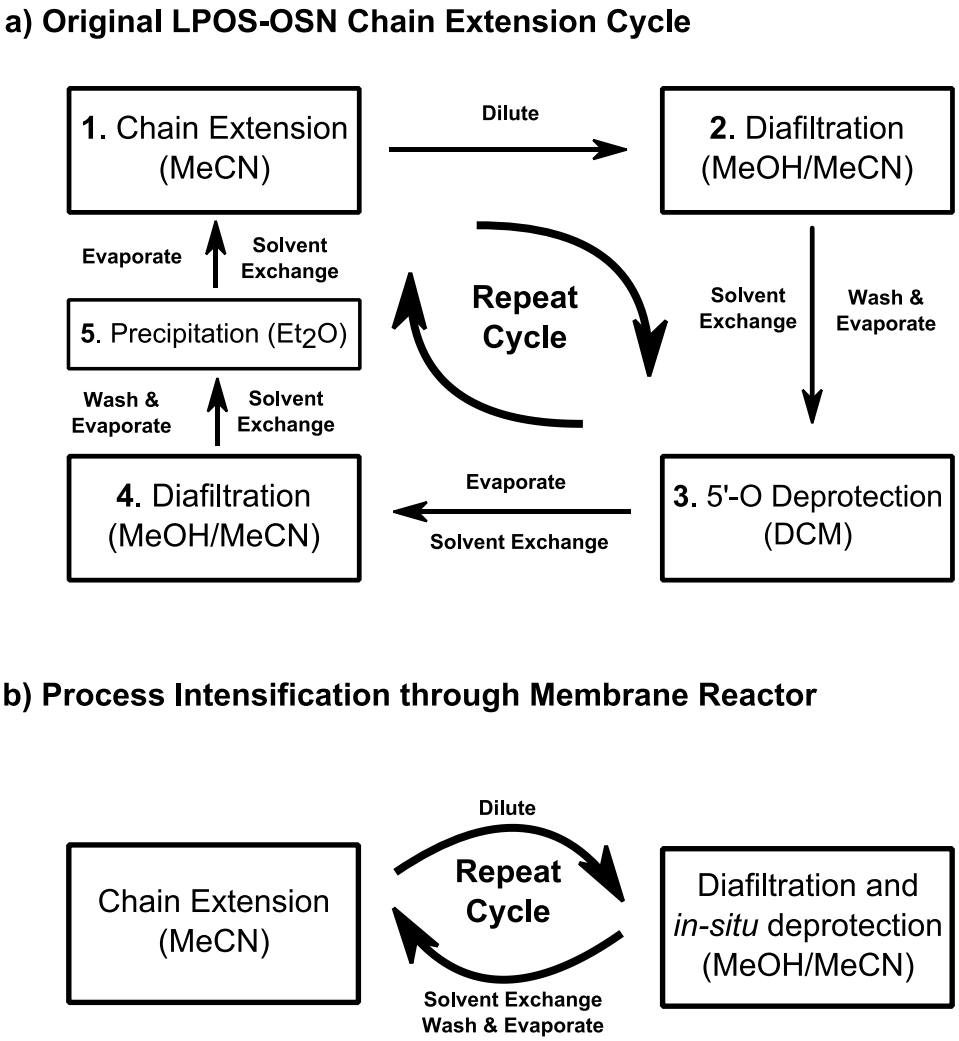


Figure 5.1. Concept diagram illustrating the potential improvement from the **a)** original LPOS-OSN process to the **b)** simplified process using a membrane reactor with MIP protecting group. Application of a membrane reactor should reduce the number of unit operations from 9 to 3 per chain extension cycle (counting each solvent exchange step).

Overall, total of 9 unit operations including 4 solvent exchange steps were required per chain extension. After assessing the overall process flow diagram, Dmtr protection was identified as the main root of the multiple solvent exchanges. Hence, it was envisaged that the process can be significantly simplified if the protecting group was replaced with a smaller yet effective protecting group which could pass the membrane easily. Hence, a methoxyisopropyl ether (*i.e.* MIP, 74 Da) protecting group proposed by Molina *et al.*[114] for oligo synthesis was adapted for this work. In combination with this, the concept of membrane reactor was applied to simplify the overall process even further, as illustrated in Figure 5.1b. Considering the fact that the

deprotection reaction is an equilibrium reaction, the use of membranes can advantageously combine the reaction and separation into one unit operation, shown in Figure 5.2.

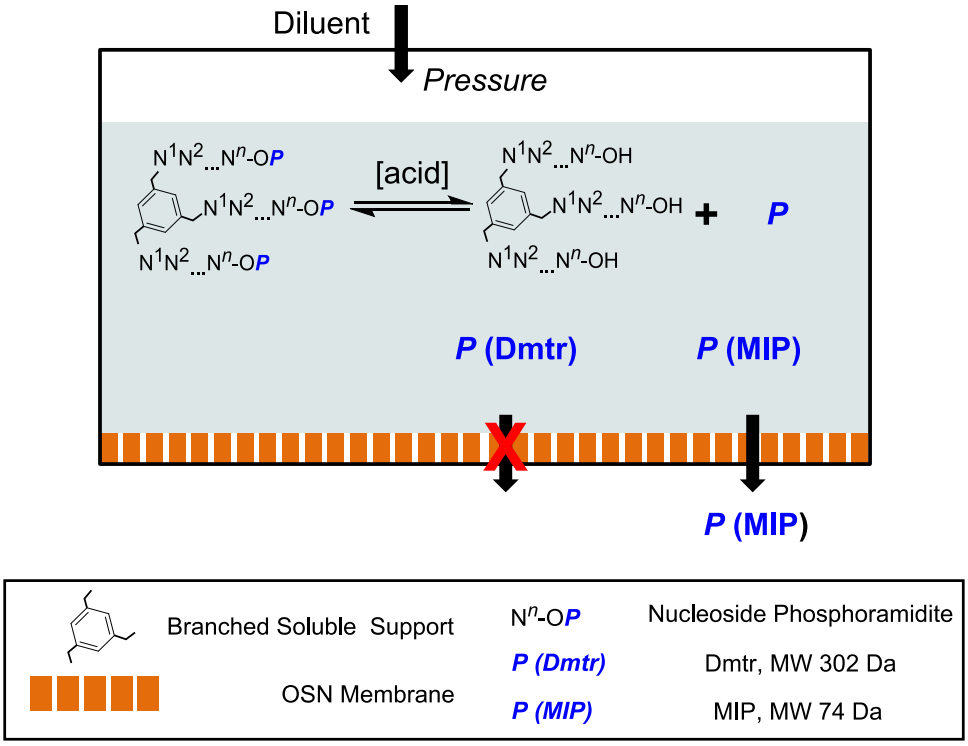


Figure 5.2. A concept diagram illustrating the use of membrane reactor for oligo synthesis. As the reaction is an equilibrium reaction, it can be pushed to completion by removing the compounds on the right-hand side of the equilibrium equation. However, the rejection of Dmtr group was too high to achieve 100% completion. The use of the smaller MIP group should allow 100% deprotection and purification, combining reaction and separation into one unit operation.

In this Chapter, it will be shown that the use of MIP protection combined with the membrane reactor unit improves the overall process dramatically, reducing the redundant solvent exchange unit operations.

Apart from the membrane reactor concept, two other challenges identified in Chapter 2 have been resolved and are reported here. The challenges were: (i) incomplete removal of excess monomers, and (ii) low process yield. The former challenge was solved by modifying the oligo synthesis chemistry coupled with membrane polymer modification through acid doping. It has been found that the PBI membranes exhibit both ion exchange and size exclusion properties, which were utilized appropriately. The latter challenge was tackled employing a membrane cascade configuration, which has been shown to improve the process yield without compromising the purity[156].

The chronological order in which each challenge was tackled is as follows: first, incomplete removal of excess monomers was solved; next, the protecting group was replaced with MIP and the membrane reactor was applied; finally, the rig was reconfgured into a cascade mode to improve the yield. For each challenge, a RNA oligo trimer (**UCC**) was synthesized with the modified protocol to illustrate the process improvement. The synthesized trimer oligos were cleaved from the support and their purities were compared to SPOS-prepared trimer.

5.3. Experimental

5.3.1. Materials

Acetonitrile (MeCN), methanol (MeOH), *N*,*N*-dimethylformamide (DMF), dichloromethane (DCM), *N*,*N*-dimethylacetamide (DMAc), diethyl ether (Et_2O) and isopropyl alcohol (IPA), were HPLC grade from *VWR, UK*. Anhydrous solvents were prepared by storing the solvents over baked 4Å molecular sieves. Celazole® S26 polybenzimidazole (PBI) solution (26 *wt*% polymer in DMAc containing 1.5 *wt*% LiCl) was purchased from *PBI Performance Products Inc, USA*. Non-woven polypropylene Novatexx 2471 was from *Freudenberg Filtration Technologies*, *Germany*. Polyethyleneglycol (PEG_{400}) and the crosslinker α,α'-dibromo-*p*-xylene (DBX) was purchased from *VWR, UK*. Nucleoside phosphoramidite building blocks were purchased from *Chemgene Corp., USA, Carbosynth Ltd, UK,* or *Fisher Scientific Ltd., UK*. Ethylthiotetrazole (ETT, 0.25M solution in MeCN, *Proligo*), phenylacetyl disulfide (PADS), 3*H*-1,2-benzodithiol-3-one (BDT), tetrabutylammonium fluoride trihydrate (TBAF), pyridine, pyrrole, choline chloride, tetramethylammonium chloride (TMA), and dichloroacetic acid (DCA) were bought from *Sigma-Aldrich, UK*. *tert*-Butyldimethylsilyl chloride (TBDMS-Cl) was purchased from *Tokyo Chemical Industry, Japan*, cyanoethyl *N,N*-diisopropyl phosphoamidochloridite was from *Toronto Research Chemicals, Canada*, *p*-toluenesulfonic acid monohydrate and 1.25M HCl in MeOH were purchased from *Fluka, UK*.

5.3.2. Membrane Fabrication and Membrane Diafiltration Rig

The membrane preparation protocol to fabricate 17wt% PBI cross-linked with DBX was the same as described previously in *Section 2.3.2*, adapted from the work of Valtcheva *et al.*[45]

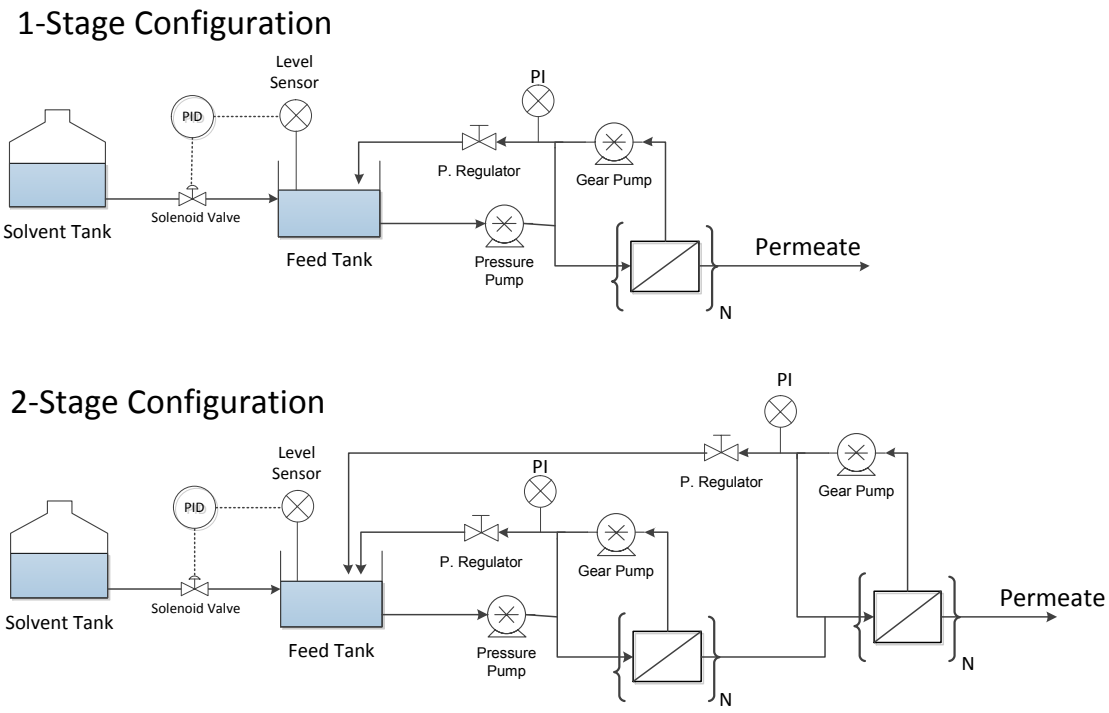


Figure 5.3. Membrane diafiltration rig schematics: 1-stage configuration is the conventional mode, whereas the 2-stage cascade configuration (N=4 per stage) is employed to improve the process yield.

Two different rig configurations were employed in this work: 1-stage, and 2-stage cascade configuration (Figure 5.3). The 1-stage configuration is the conventional diafiltration process employed in Chapter 2. On the other hand, the 2-stage cascade configuration[156] was employed to tackle the low-yield challenge identified in the LPOS-OSN process (discussed in *section 5.3.3*). For each stage (1st and 2nd stage), four membrane cells were connected in series, each cell containing a 51cm^2 membrane. Two gear pumps (1st stage: *Michael Smith Ltd.* GL Series, 2nd stage: *Cole-Palmer Ltd,* GB Series) provided flow-rates of 66 L.hr^{-1} to generate turbulence to minimize concentration polarization (build-up of solute concentration on the membrane surface, adversely affecting the performance). In contrast to the rig used in Chapter 2 where the pressure was controlled with nitrogen gas, the rig was reconfigured as a liquid-pressurized system using an HPLC pump (*Gilson* Model 305) and a back-pressure control valve. The operating rig pressure was between 5 and 10 bar. The feed tank was open to atmosphere, allowing easy and convenient level monitoring and control. The membrane purification experiment was operated in a constant-volume diafiltration (CVD) mode. The feed tank volume and each stage volume were 100 mL and 150 mL, respectively. Hence, the 1-stage configuration has a system volume of 250 mL and 2-stage has 400 mL.

The membrane permeance stayed constant approximately at 8 $L.m^{-2}.hr^{-1}.bar^{-1}$. The solvent mixture used for the purification experiment was 20% MeOH-MeCN. The temperature of the rig stayed constant at 21 ± 1 ^{o}C.

5.3.3. Oligonucleotide Synthesis Protocol

The overall oligos synthesis scheme, including the modifications made in this work, is summarized in Figure 5.4.

The initial loading and final purification procedures stayed the same as Chapter 2 (section 2.3.4.1). The chain extension cycle, however, has been modified in two ways: 1) conversion of phosphoramidite monomers to anionic species (discussed in Section 5.3.4.1); 2) the use of new MIP protection (discussed in Section 5.3.5.6).

5.3.4. Solving the First Challenge: Complete Removal of Excess Monomers

To avoid confusion, it is noted that this challenge was first tackled with commercially available 5'-*O*-Dmtr phosphoramidite monomers, and later applied to 5'-*O*-MIP phosphoramidite monomers. The procedures are discussed below.

5.3.4.1. Modification of Chain Extension Reaction Protocol

The growing oligonucleotidyl homostar (**4**, 45 μmol, 0.1g) and the 5'-*O*-Dmtr phosphoramidite monomers **11** (***P*** = Dmtr, 1.5 eq. per OH, 0.2 mmol, 162 mg) were dissolved in DMF (1 mL) and co-evaporated from dry MeCN (3 x 10 mL) under inert argon atmosphere. The mixture was then dissolved in 0.25M ETT in MeCN (3 eq. per OH, 0.4 mmols, 1.62 mL). After stirring for 0.5 hr, distilled water was added (2 eq. per OH, 0.135 mmols, 6 μL), followed by PADS (3 eq. per OH, 0.4 mmols, 123 mg) after 5 minutes. After 0.5 hr, BDT (3 eq. per OH, 0.4 mmols, 68 mg) was added, and stirring continued for another 0.5 hr. The crude mixture was then diluted to 20% MeOH-MeCN (100 mL) and charged to the membrane rig (containing 150 mL) shown in Figure 5.3. The addition of pyridine was employed in Chapter 2, which was deliberately omitted in this Chapter to avoid the membrane losing the anionic exchange capability (discussed in detail in Section 5.4.1.2). As mentioned in Chapter 2, the exact amount of reagents varied slightly due to the yield and chain extension conditions.

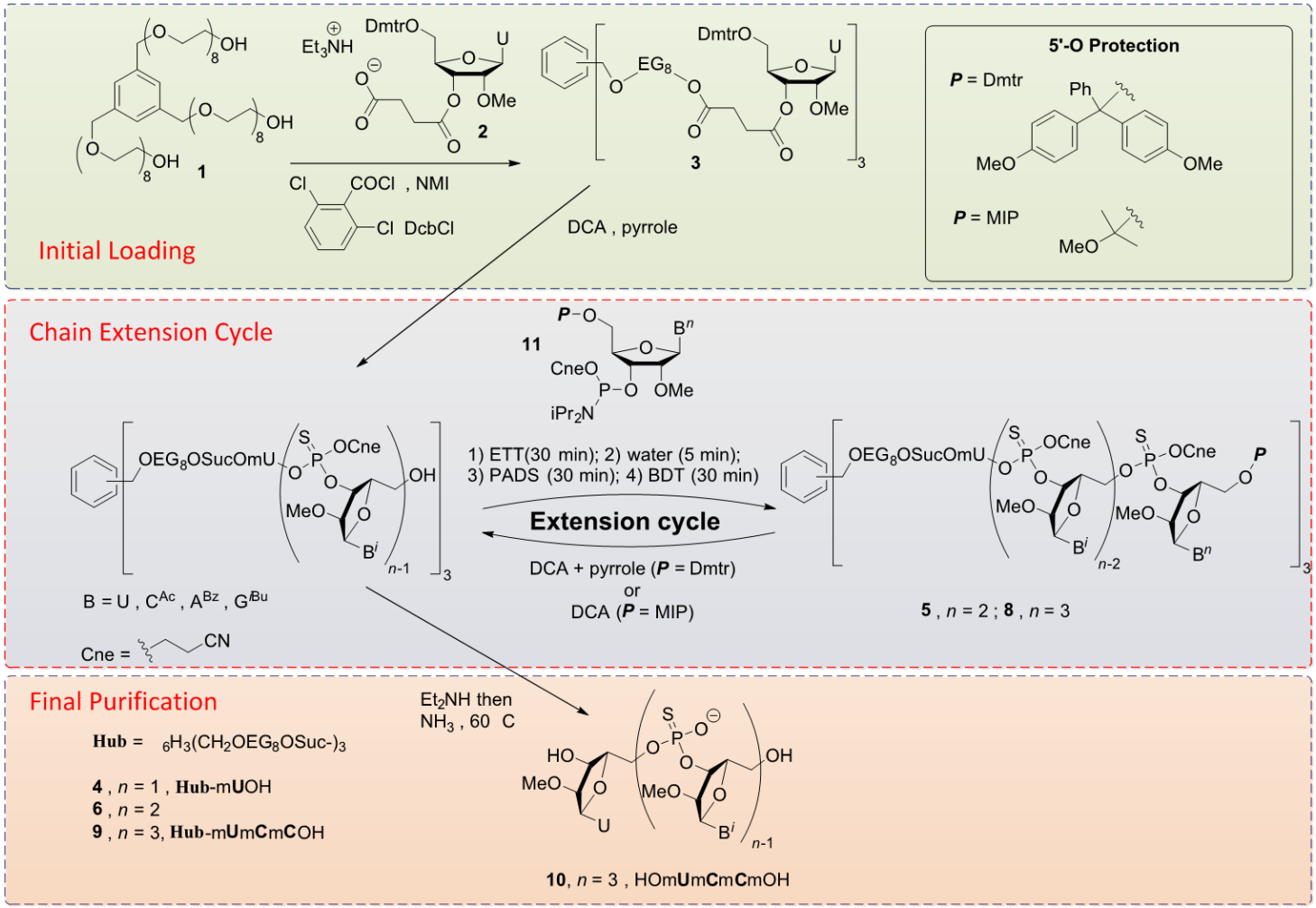


Figure 5.4. Overall chemistry scheme employed in this work: Initial loading and final purification procedures stayed the same as Chapter 2, but the chain extension cycle has been modified.

The remaining chain extension cycle procedure stayed the same as Chapter 2. A total of 13 *diavolumes* were given at 10 bar and 21 ^{o}C using 20% MeOH-MeCN after the chain extension reaction using the procedure described in 2.3.4.3. At the end of the CVD, the purified solution was washed out of the rig and evaporated to dryness *in vacuo*. The detritylation (deprotection of 5'-*O*-Dmtr) reaction was done in dry DCM (30 mL) with DCA (1*vol*%, 0.3 mL) and pyrrole (2*vol*%, 0.6 mL) under 30 minutes of stirring. For the second diafiltration, again at 10 bar and 21 ^{o}C, the first 5 *diavolumes* contained 1*vol*% pyridinium dichloroactate (Py.DCA) in 20%MeOH-MeCN (250 mL per diavolume), followed by 10 *diavolumes* with neat solvent (20%MeOH-MeCN). At the end of the CVD, the purified solution was washed out of the rig and evaporated to dryness *in vacuo*. This procedure is repeated twice to yield trinucleotidyl homostar (Hub-[*suc*-**U**p**U**p**C**-OH]$_3$) **9**.

5.3.4.2. Acid Doping of PBI Membranes

PBI membranes were doped with HCl by permeating 10 mmol.L^{-1} of HCl in 20% MeOH-MeCN solution (2L) through the membranes. Then, the rig was washed out with neat solvent mixture (at least 2L). Upon doping the membranes, trinucleotidyl homostar (Hub-[*suc*-**U**p**U**p**C**-OH]$_3$) **9** was synthesized using the same scale (**4**, 45 μmol, 0.1g) following the protocol explained in Section 5.3.4.1 using the doped membranes for membrane CVD.

5.3.5. Solving the Second Challenge: Bulky 5'-O Protection

5.3.5.1. Synthesis of 5'-O-MIP Phosphoramidite Monomer

The synthesis protocol for 5'-*O*-MIP-2'-*O*Me-cytidine (*N*-Ac) phosphoramidite was adapted from Molina et al.[114] and the synthesis scheme is illustrated in Figure 5.5.

A bulk-scale synthesis was carried out up to the 4th step to prepare 5'-*O*-MIP-3'-*O*H cytidine (*N*-acetyl) **12e** with 83% yield, and the last step was carried out in a small-scale prior to each oligo coupling reaction, as compound **12f** is much more sensitive to acid-catalyzed hydrolysis. The detailed synthesis protocol and characterization are compiled in Appendix D.

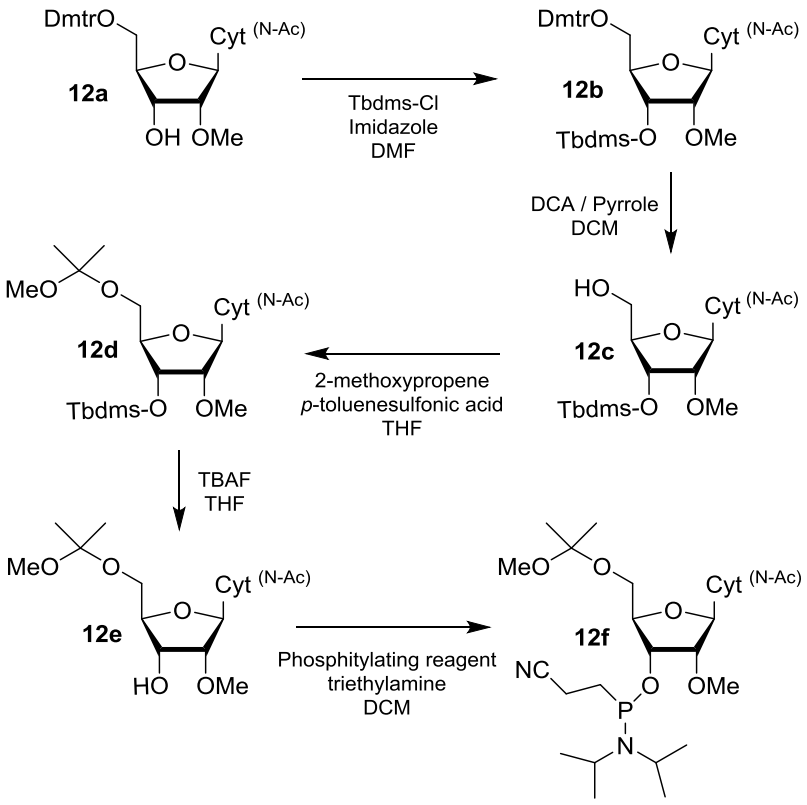


Figure 5.5. Synthesis protocol for 5'-*O*-MIP cytidine phosphoramidite. A bulk-scale synthesis was carried out until **12e**; the last step, phosphitylation to synthesize cytidine phosphoramidite **12f**, was carried out prior to each chain extension reaction.

5.3.5.2. Oligo synthesis with 5'-O-MIP

With the synthesized 5'-*O*-MIP cytidine (*N*-acetyl) phosphoramidite **12f**, trinucleotidyl homostar (Hub-[*suc*-**U**p**U**p**C**-OH]$_3$) **9** was prepared following the modified chain extension reaction described in Section 5.3.4.1 using the same scale (**4**, 45 µmol, 0.1g). This time, however, the deprotection procedure of 5'-*O*-MIP (deMIPylation) was modified to be applied in the membrane reactor, and will be described in *Section 5.3.5.4b*.

5.3.5.3. Deprotection Equilibrium Study (Effect of Solvent and Acid)

As the Dmtr group is the main 5'-*O* protection used for oligo synthesis; its deprotection mechanism and kinetics are thoroughly studied and reported in literature[167, 168]. Deprotection kinetics of the MIP group were investigated on **12e**. A solution containing 1g.L^{-1} of MIP solute was spiked with different amounts and types of acids, as summarized in Table 5.I. After a set amount of time, the reaction was quenched with Et_3N and the sample was analyzed using HPLC for the extension of deprotection.

5.3.5.4. In-situ Deprotection in the Rig: Concept of Membrane Reactor

The concept of membrane reactor was applied to both Dmtr and MIP protected dinucleotidyl homostar on 1-stage diafiltration rig (Figure 5.3), described in the following sections.

5.3.5.4a. 5'-O-Dmtr Deprotection

5'-*O*-Dmtr protected dinucleotidyl homostar **5** (0.08 mmols, 0.334g) was dissolved in 1*vol*% DCA-MeCN (2.5 mL DCA in 100 mL) and charged to the rig (containing 150 mL). Then, the rig was pressurized to 10 bar at 21 ^{o}C, and the first 5 *diavolumes* were permeated with 1*vol*% DCA-MeCN, followed by 10 *diavolumes* with neat MeCN. Samples were taken intermittently to assess the extent of deprotection. At the end of the CVD, the purified solution was washed out of the rig, and the solvent stripped off *in vacuo*.

5.3.5.4b. 5'-O-MIP deprotection

5'-*O*-MIP protected dinucleotidyl homostar **5** (0.07 mmols, 0.279g) was dissolved in 20% MeOH-MeCN (100 mL) and charged to the rig (containing 150 mL), pressurized up to 10 bar at 21 ^{o}C. The first 5 *diavolumes* were permeated with 0.01~0.15*vol*% DCA (0.6 mL per *diavolume*) and 0.02wt% of choline chloride (tetramethylammonium (TMA) chloride for 3-mer deprotection) in 20% MeOH-MeCN (250 mL per *diavolume*). An incremental amount of acids was added to drive the reaction to completion. The next 10 *diavolumes* were permeated with 20% MeOH-MeCN. Samples were taken intermittently to assess the extent of deprotection. At the end of the CVD, the purified solution was washed out of the rig, and the solvent stripped off *in vacuo*.

Table 5.I. Acid screening for MIP deprotection

Run	[MIP] ($g.L^{-1}$)	Solvent	Acid	[Acid]	Eq.	Effect
1	1	20% MeOH-MeCN	ETT	3.25 $g.L^{-1}$	10	Slow deprotection
2	1	20% MeOH-MeCN	HCl	2 *vol*%	10	Extremely fast deprotection, done in < 1 min
3	1	20% MeOH-MeCN	Hexafluo-ro IPA	0.26 *vol*%	10	No reaction
4	1	20% MeOH-MeCN	Acetic Acid	0.14 *vol*%	10	No reaction
5	1	20% MeOH-MeCN	TFA	0.1 *vol*%		Extremely fast deprotection, done in < 5 min
6	1	20% MeOH-MeCN	DCA	0.1 *vol*%		Extremely fast deprotection, done in < 5 min
7	1	20% MeOH-MeCN	TFA	0.01 *vol*%		Extremely fast deprotection, done in < 5 min
8	1	20% MeOH-MeCN	DCA	0.01 *vol*%		Moderate deprotection rate, 30min ~ 1 hr
9	1	MeCN	TFA	0.1 *vol*%		Extremely fast deprotection, done in < 5 min
10	1	MeCN	DCA	0.1 *vol*%		Moderate deprotection rate, 30 min ~ 1 hr

5.3.6. Solving the Third Challenge: Improving the Yield

The 2-stage cascade configuration shown in Figure 5.3 was employed to improve the process yield. With the modified method implementing the first two improvements (removal of monomers, replacement of 5'-*O*-protection) discussed in section 5.3.4 and 5.3.5, trinucleotidyl homostar (Hub-[*suc*-**U**p**U**p**C**-OH]$_3$) **9** was synthesized using the same scale (**4**, 45 μmol, 0.1g) and purified using the cascade rig. After each chain extension, the crude mixture was diluted to 20% MeOH-MeCN (100 mL) and charged to the cascade rig (containing 300 mL). Upon permeation of 13 diavolumes with 20% MeOH-MeCN, in-situ deMIPylation was carried out following the procedure described in 5.3.5.4b.

As discussed in Chapter 3, a crucial parameter to control in the cascade is the recycle ratio, which is defined as the flowrate of retentate from the second stage over the flowrate of permeate from the first stage (Eq. 3.9). In this work, the recycle ratio was set between 0.4-0.5 by operating the 1st stage and 2nd stage at 18 bar and 6 bar, respectively. The same number of *diavolumes* was used for both diafiltrations.

5.3.7. Global Deprotection and Final Purity Analysis

Total of four samples of synthesized trinucleotidyl homostar (Hub-[*suc*-**U**p**U**p**C**-OH]$_3$) **9** (*Section 5.3.4.1, 5.3.4.2, 5.3.5.2, and 5.3.6*) were cleaved from the support and characterized. The deprotection procedure is described in detail in section 2.3.4.4. The globally deprotected oligos have been analyzed by Dr. Glynn Williams offsite.

5.3.8. Analytical Methods

All samples were analyzed by HPLC using an *Agilent* 1100 Series system equipped with an UV detector and *Varian* 385-LC ELSD detector. The pump flow-rate was set at 1 ml.min^{-1}, the injection volume was 30 µL, the column temperature was 30 ^{o}C, and an ACE C18 RP column (*Hichrom Ltd*) was fitted. The column was eluted with a gradient of MeOH and water buffered with 100 mM ammonium acetate. The UV wavelength was set at 260 nm, the ELSD evaporation temperature was set to 40 ^{o}C, nebulization temperature at 55 ^{o}C, and the nitrogen gas flow rate was at 1.5 standard liters per minute.

NMR spectra were recorded on Brüker AV-400 or Brüker AV-500 spectrometers. Mass spectra were recorded on *Micromass* MALDI micro MX or *Micromass* LCT Premier (ESI) mass spectrometers.

5.4. Results and Discussion

To improve the logical flow of the Chapter, the current section is structured in a chronological order at which each challenge was resolved, with each succeeding challenge implementing the previous modifications: first, incomplete removal of excess phosphoramidite monomers was solved using 5'-*O*-Dmtr protected monomers (commercially available); next, the protecting group was replaced with MIP and the membrane reactor was applied; finally, the rig was reconfigured into a cascade mode to tackle the yield challenge.

5.4.1. Solving the First Challenge: Incomplete Removal of Excess Monomers

5.4.1.1. Effect of Water and BDT on Oligos Synthesis

The main challenge of the LPOS-OSN platform was to remove all the excess phosphoramidite (PA) monomers after each chain extension, where the excess PA monomers typically converted to four different types of compounds **(11a-d)**, as shown in Figure 5.6.

A typical post-reaction crude always contained two neutral species (**11a, 11b**) and two negatively charged species (**11c, 11d**), in variable molar ratios. Notably, despite the small

MW differences (~80 Da) between the neutral and charged species, it was observed that the neutral species are highly rejected (>90%) by PBI membranes whereas the anionic species freely passed through (< 50%). Although smaller reaction excess reagents such as PADS and ETT all permeated by a sieving mechanism, it was speculated in Chapter 2 that the transport of anionic PA monomers occurs through an ion exchange mechanism.

The formation of four different types of PA monomers is likely to arise due to the presence of reaction equilibrium prior to PADS addition. This observation is further supported by the fact that reducing the PADS excess from 10 to 3 eq. reduced the thioamidate **11a** amount to an undetectable level (discussed in Chapter 2).

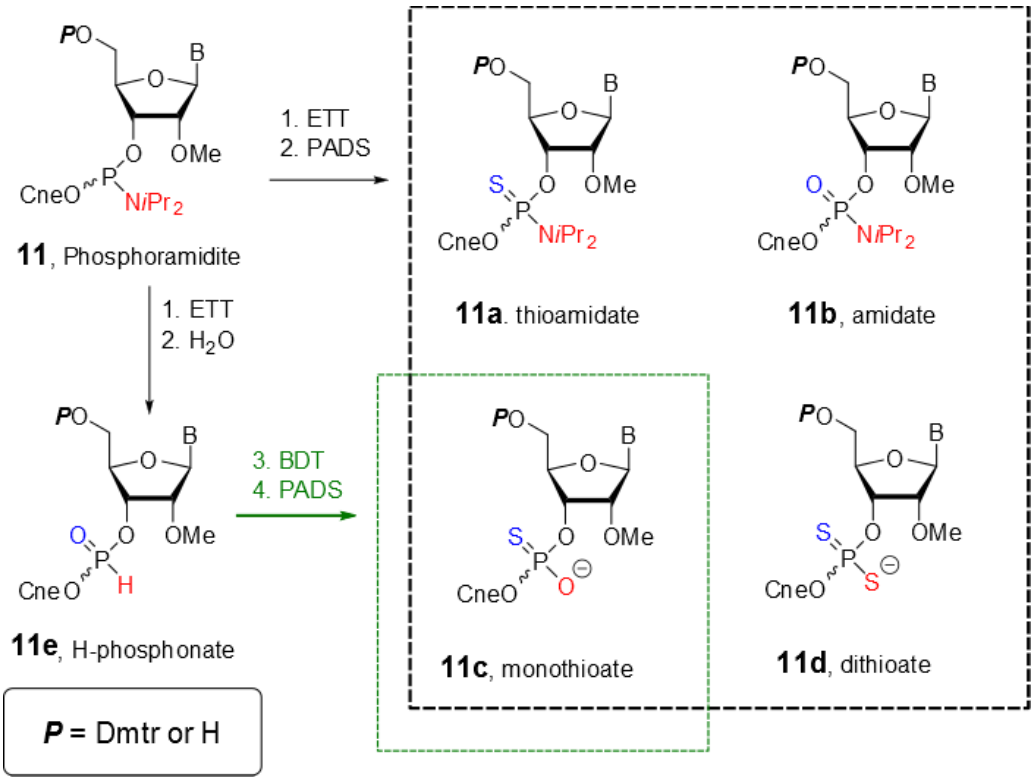


Figure 5.6. Four types of phosphoramidite (PA) monomers after chain extension (**11a-d**). The 5th type, H-phosphonate **11e**, is only generated when the phosphoramidite comes in contact with water. Conventional chain extension method in Chapter 2 generates all four types of PA monomers, shown in black box. With the modified protocol, adding water then BDT/PADS, converts all excess PA to monothioate **11c**, shown in green box.

It was reported by van der Marel *et al.*[169] that all PA monomers converts to H-phosphonate **11e** with the addition of water, which in turn can be converted to monothioate **11c** with BDT sulfurizing reagent. The protocol optimized by van der Marel *et al.*[169] was adapted in this work. Figure 5.7 summarizes the effect of water and BDT in terms of monomer formation after a chain extension reaction to dinucleotidyl homostar **5**.

It can be seen in Figure 5.7 that the new synthesis protocol works effectively. Compared to the original protocol (Figure 5.7a) that typically showed 3 different types of PA monomers (thioamidate **11a** not present), the addition of water effectively converts all the excess PA monomers to H-phosphonate **11e** (Figure 5.1b). Although the protocol reported in van der Marel *et al.* employed 20 eq. excess of water, it was experimentally determined that 2 eq. of water is just as effective (Appendix D). It was also determined that a co-evaporation step after water addition, to remove water, is not necessary.

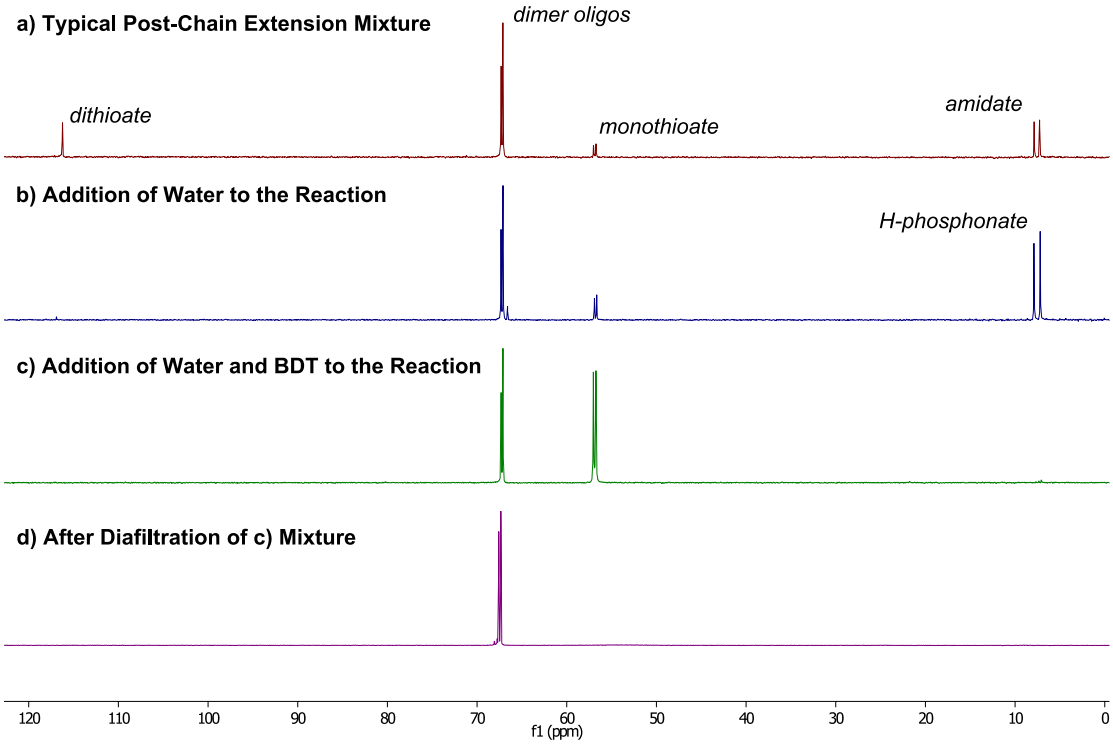


Figure 5.7. Stacked ^{31}P-NMR spectra to illustrate the effect of water and BDT. Addition of water hydrolyzes all the monomers to H-phosphonate **11e**. As the peak shift for H-phosphonate **11e** was the same with the amidate **11b** peak, ^{1}H NMR was used to identify the presence of H-phosphonate (Appendix D). Addition of BDT turns all the H-phosphonate into monothioate **11c**. Upon diafiltration after detritylation (***P*** = H), all monothioates were removed from the reaction mixture.

It was found that H-phosphonate **11e**, being a neutral species, also exhibited high rejection (>90%) similar to those of thioamidate **11a** and amidate **11b**. Upon the addition of BDT, all the H-phosphonates effectively converted to monothioate **11c** (Figure 5.7c), which permeated through the membrane (Figure 5.7d).

5.4.1.2. Effect of PBI Membrane Doping with Acid

It was initially observed that all the monothioates **11c** were permeating through the membrane with reliable repeatability. However, upon using the same membranes with the same procedure several times, the monothioate peak began to reappear in the ^{31}P-NMR of the retentate (Figure 5.8b). Initially puzzled by the results, it was soon realized that the PBI membrane can lose its anionic exchange capacity upon constant exposure to weak bases (*e.g.* pyridine which was used to quench the chain extension reaction), as illustrated in Figure 5.8a. Although the benzimidazole ring has a pKa value of 5.6 (conjugate acid) and pyridine has a value of 5.25 (conjugate acid), a large excess of pyridine and the polymeric nature of the beanzimidazole ring causes slow deprotonation of the PBI polymer backbone. Please note that only one benzimidazole ring was modified in the diagram (Figure 5.8a) to illustrate the concept. To resolve this phenomenon, the PBI membranes were doped with 10 mmol.L^{-1} HCl (MeOH-MeCN) to make the benzimidazole rings positively charged again. The stability of PBI membranes under such doping conditions have been shown in the work of Valtcheva *et al.*[45]

The effect of HCl doping on PBI membranes is illustrated in Figure 5.8c, as the monothioate **11c** peak completely disappeared from the crude after diafiltration. It has also been determined that as long as the PBI membranes are kept away from bases such as pyridine, the performance remains steady and effective. Together with this effect, a simple yet elegant trick of using water and BDT solved one of the main challenges in the LPOS-OSN synthesis platform. With the optimized protocol, a trimer oligo **10** was synthesized, and the purity and yield are assessed in Section 5.4.3.

5.4.2. Solving the Second Challenge: Bulky 5'-O-protection

Apart from the PA monomer removal challenge, a serious drawback of the LPOS-OSN platform has been the complicated process procedure requiring redundant solvent exchange steps. As shown in the flow diagram in Figure 5.1, each chain extension cycle has five main unit operations: (1) chain extension reaction in MeCN (or DMF-MeCN) followed by (2) diafiltration in MeOH-MeCN, then (3) detritylation reaction in DCM again followed by (4) diafiltration in MeOH-MeCN, and finally (5) oligo precipitation step in diethyl ether (Et_2O) to remove Dmtr-pyrrole. Hence, four solvent exchange steps are required per cycle (total of 9 unit operations per cycle). There are also several rig washing and solvent evaporation steps

in-between membrane diafiltrations. In addition, it should be noted that chlorinated solvents like DCM and flammable solvents like Et_2O are highly undesirable at large scale[102].

Clearly, the process is highly solvent-intensive and needs to be simplified to be more practical at large scale. Upon analyzing the flow diagram, it can be deduced that the main reason for 3 out of the 4 solvent exchange steps arises due to the use of Dmtr protection. The solvent exchange to (and from) DCM is to carry out the detritylation reaction, and the precipitation in Et_2O is to remove Dmtr-pyrrole since its bulkiness prevents permeation through the membranes.

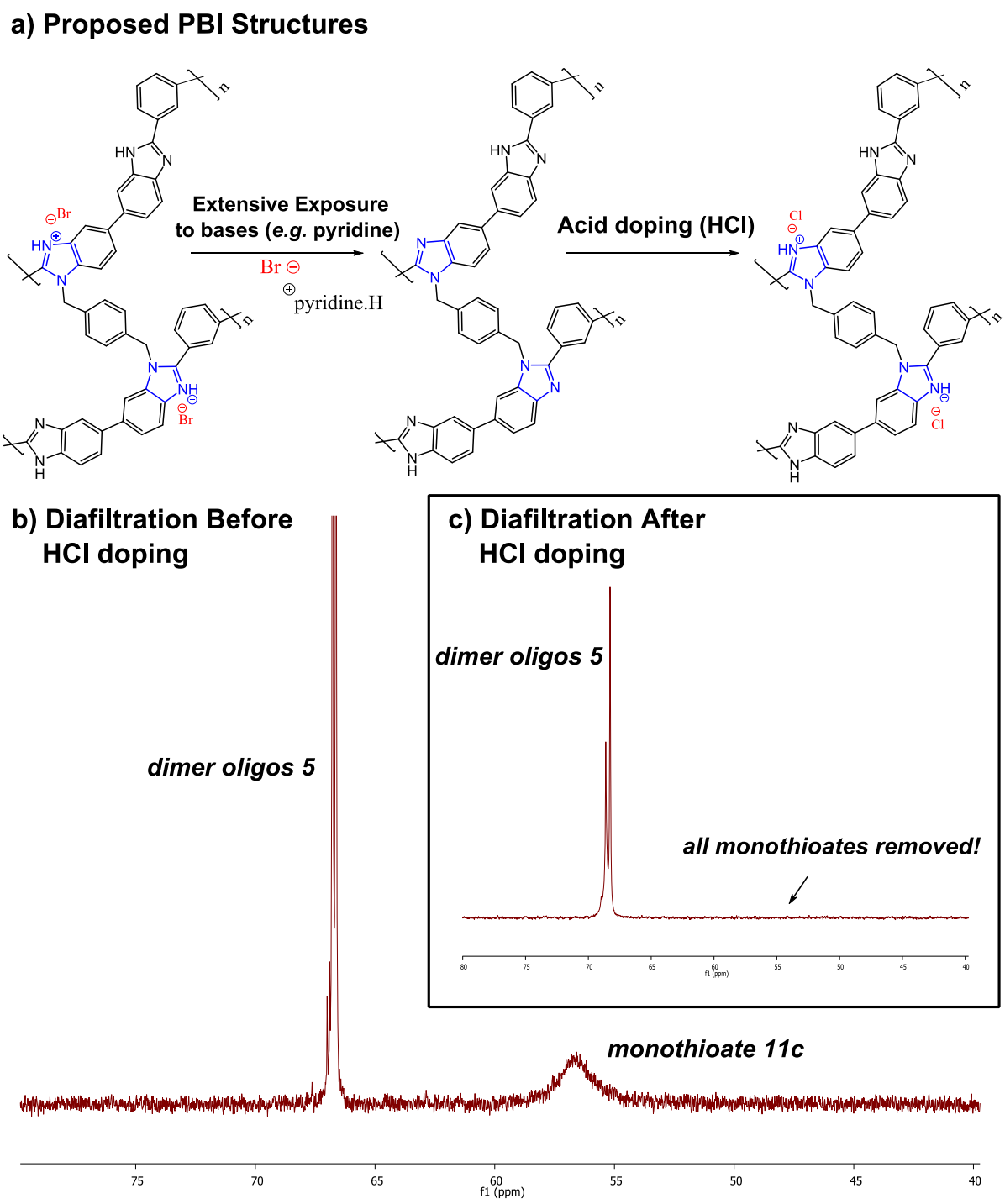


Figure 5.8. a) Speculated PBI polymer structures showing the effect of HCl doping, only one benzimidazole ring in the monomer is modified in the diagram to illustrate the concept. b) ^{31}P-NMR of retentate after diafiltration without HCl doping; c) ^{31}P-NMR of retentate after diafiltration with HCl doping.

One way to reduce the unit operations is to run the detritylation reaction in the diafiltration solvent, *i.e.* MeCN or MeOH-MeCN. However, because the detritylation reaction is an equilibrium reaction (Figure 5.2), a trap is necessary to capture the Dmtr cation which comes

off in the presence of acid. In Chapter 2, pyrrole was employed to drive the reaction to completion. The reaction has been found to work best in DCM and toluene[85] but has also been shown to proceed in MeCN[167], albeit more slowly. It was postulated that instead of using a trap to drive the reaction to completion, the membrane can participate in the reaction by selectively permeating Dmtr cation to drive the reaction *in-situ*. This membrane reactor concept would not only reduce the number of solvent exchange steps, but also eliminate the precipitation unit operation from the process (Figure 5.1b), achieving a significant process intensification.

To test this concept, dinucleotidyl homostar (5'-*O*-Dmtr) **5** was loaded onto the rig and 1*vol*% DCA in MeCN was fed for 5 *diavolumes* to commence the reaction *in-situ*. The results are shown in Figure 5.9a.

It can be seen that the detritylation reaction occurs inside the rig in MeCN. Figure 5.9a clearly shows that the reaction proceeds until the 5th *diavolume* (switched to neat solvent from this point). However, it can also be seen that the di-Dmtr dinucleotidyl homostar peak reappears after the 5th *diavolume* and the mono-Dmtr dimer peak grows bigger than that of detritylated dinucleotidyl homostar **6**. Hence, the reaction reverses after the 5th *diavolume* when the acid is removed. This observation suggests that the permeation of Dmtr cation through the membrane is too slow compared to that of DCA, and the Dmtr cation reattaches to the oligos as the solution acidity goes down. In addition, an unidentified peak near 28th minute in Figure 5.9a appears slowly, an impurity likely to be related with Dmtr group.

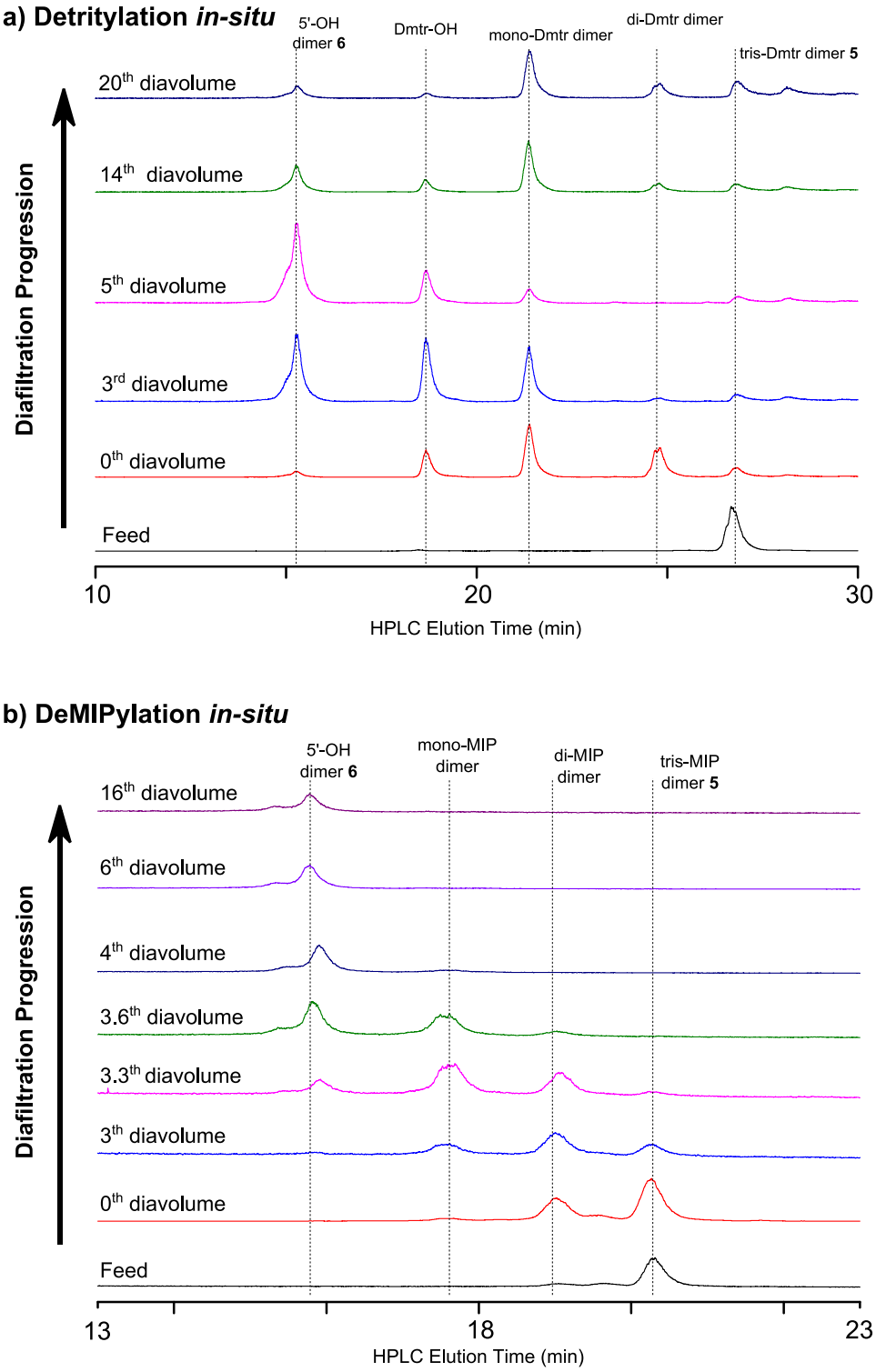


Figure 5.9. HPLC chromatogram summarizing the membrane reactor in action for: a) Dmtr protection and b) MIP protection. Dmtr deprotection reaction proceeds to 5th *diavolumes* but reverts back as the acid concentration decreases. MIP deprotection reaction reaches completion due to the small size of MIP.

An alternative way to tackle this challenge is to replace the 5'-*O*-protection with a smaller moiety. Dmtr protection has long been favored for the solid-phase process, mainly because

the cation generates an intense orange color which can be analyzed for the extent of deprotection. However, for LPOS-OSN purposes, its bulkiness is an undesired feature due to its high rejection by the membranes. Instead, a recent publication by Molina *et al.*[114] proposed a volatile 5'-*O* protection for oligo synthesis containing an acetal functional group (methoxyisopropyl, *i.e.* MIP, MW 74 Da). It has been reported that various types of phosphoramidite can be prepared. With its small size and synthesis efficacy, it was deemed to be an ideal candidate for Dmtr-group replacement.

Hence, a 5'-*O*-MIP cytidine phosphoramidite was synthesized following the procedure given by Molina *et al.*[114] With the new protecting group, it was expected that the deprotection reaction can proceed to completion in the rig *in-situ*, realizing the membrane reactor concept. Initial experiments for MIP deprotection were carried out employing HCl as an acid; however, prolonged exposure to HCl severely degraded the growing oligos. One identified degradation was the deprotection of the cytosine base (*N*-Ac), mainly because HCl is a strong acid which completely dissociates in solution.

An acid screening was carried out (Table 5.I) which showed that a dilute DCA solution (0.01~0.15*vol*%) results in a reasonable deprotection rate with weaker acidity in the rig compared to HCl. The progression of the deMIPylation reaction using DCA is captured in the HPLC, shown in Figure 5.9b. It can be seen that the reaction progresses until it reaches completion at the 4th *diavolume*. Contrary to the Dmtr protecting group, the reaction does not revert back. The actual deMIPylation reaction required more acid compared to the screening, as the crude containing dinucleotidyl homostar **5** buffered the acid to some extent. Deprotection of the cytosine base (*N*-Ac) was again detected by HPLC (bump in front of the product peak), but at a much lower extent. A possible remediation is to use benzoyl protection (instead of *N*-Ac) for the cytosine base instead, also commercially available with Dmtr protection. However, such deprotection should have negligible effect on the product quality or the subsequent chain extension.

The results in Figure 5.9 demonstrate that deprotection of 5'-*O*-MIP and purification of PA monomers can be done at the same time in one membrane diafiltration, as depicted in Figure 5.1b. This presents a significant improvement in terms of process time and economics, as the number of unit operations per chain extension cycle can be reduced by a third: 9 unit operations (including the solvent exchange) down to 3 per cycle. A further simplification may be possible by running the diafiltration with the reaction solvent, 1*vol*% DMF-MeCN,

and the membranes are found to be stable in such solvents[45]. However, it should be noted that 5'-*O*-MIP PA monomers are not commercially available at the moment, and appropriate logistics should be implemented to adapt this new protecting group for oligo synthesis.

Combining MIP protection and membrane reactor with the water and BDT protocol (Section 5.4.1), a trimer oligo **10** was synthesized successfully. The purity and yield is assessed in Section 5.4.3.

5.4.3. Effect of Cascade, Yield and Purity Analysis

As the nature of oligo synthesis requires repeated cycles (i.e. *n*-mer requires *n*-1 chain extension cycles), it is vital to achieve near quantitative yield in each cycle to achieve high overall yield, as described in Eq. 1.8.

For instance, with a chain extension yield of 95%, the overall yield to synthesize 23-mer oligos would be merely 32%. It was identified earlier on that the main source of yield loss comes from the membrane diafiltration. With the conventional single-stage diafiltration employed in Chapter 2, the yield loss in the first three cycles was close to 50%, mainly since the growing oligos were not completely retained by the membrane. The chain extension yield after 5-mer improved to an average of 95% per cycle, which is still lower than desired to achieve a feasible process.

It has been shown in Chapter 3 and 4 that employing a 2-stage membrane cascade configuration can, with an appropriate selection of recycle ratio (r_c) and operating pressure, improve the process yield without compromising the product purity. The proposed configuration was adapted in this work and the membrane rig was reconfigured to a 2-stage cascade mode (Figure 5.3). The yield improvement using the cascade for the 3-mer synthesis, with MIP protection, is illustrated in Figure 5.10. The r_c value was continuously adjusted between 0.4-0.5 by operating the first and second stages approximately at 18 bar and 6 bar, respectively.

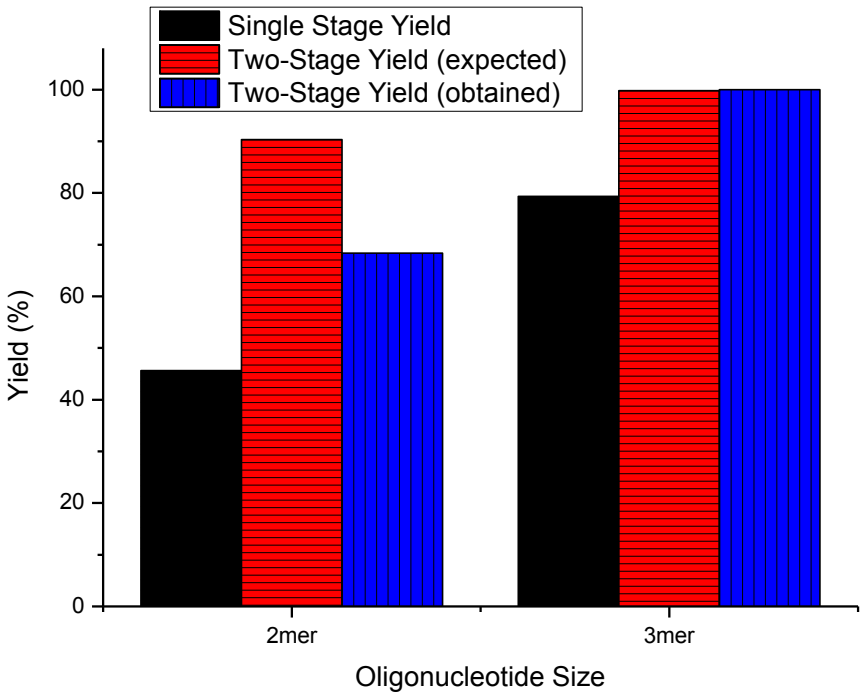


Figure 5.10. Yield improvement through 2-stage cascade configuration. 3-mer oligos was synthesized using MIP protection. The actual yield improvement in the 2-mer was lower than expected because a normal phase column was run on the final retentate. Nevertheless, the yield improved to near 100% in the 3-mer chain extension cycle.

It can be seen that the chain extension yield using the MIP protection was considerably lower than the yield obtained with the Dmtr protection, owing to the smaller MIP size leading to lower oligo rejections. In comparison to the yield shown in Figure 5.10, the 2-mer and 3-mer yields using Dmtr protection with single-stage diafiltration were 75% and 90%, respectively (Shown in Figure 2.11).

Apart from the difference in yield between MIP and Dmtr protected oligo synthesis, it can be seen in Figure 5.10 that the yield increases when the 2-stage cascade is employed, although not as much as expected. The discrepancy between the expected and obtained yield arose from an unexpected impurity collected in the final retentate. The final retentate, after 2-stage diafiltration, was contaminated with salt impurites (either choline chloride or TMA chloride). Considering the fact that the measured rejection of such salts is below 20%, it is yet unknown why the salt impurities remained behind after 15 *diavolumes*. A possible explanation is that the *captured* salts from the PBI membranes got leached out as the acid (DCA) got washed away. It should be noted that the addition of salts was not necessary to drive out the monothioates **11c** (R=H), and they were only added to obtain comparable results

with the Dmtr dataset. The addition of DCA alone would be sufficient to allow monothioates to permeate PBI membranes via ion exchange mechanism. To remove the salt impurities, the final retentate was purified using a normal-phase column (1 – 20% MeOH-Chloroform gradient). Most of the loss in yield is likely to have originated from this step. In the 3-mer stage, the final retentate was again contaminated with salt impurities, and was put through a normal-phase column again. This time, however, the obtained yield was close to the expected value, showing the advantage of 2-stage cascade. It is expected that from 3-mer onward, the chain extension cycle yield reaches up to 100%.

As pointed in Chapter 3 and 4, the advantage of the 2-stage cascade configuration is the ease of control and operation. The 2-stage configuration does not require additional control and can easily be automated. It is expected that the yield gain from the cascade outweighs the additional equipment cost. However, the intensive solvent usage of membrane diafiltration should not be left unnoticed as discussed in Chapter 4.

In summary, four 3-mer oligos were synthesized (**UCC**) in the following order: (i) with water and BDT protocol before HCl doping of PBI membranes, (ii) after HCl doping of PBI membranes, (iii) with 5'-*O*-MIP PA monomers, then (iv) with 2-stage cascade, with each trial implementing the preceding protocol. The first three 3-mers have been globally deprotected and their purity has been assessed and compared to the purity of SPOS synthesized 3-mer, summarized in Figure 5.11.

Several trends can be observed in Figure 5.11. First, the 3-mer prepared with Dmtr protection *prior* to HCl doping had the highest number of unknown impurity peaks with a purity of 68% (estimated via area integration). The peaks immediately to the left of the product 3-mer peak are likely to be two compounds: chain-extended monothioates **11c** not removed during the 2-mer chain extension cycle, and chain-extended mononucleosidyl homostar **4** that did *not* get chain extended during the 2-mer cycle, due to incomplete reaction.

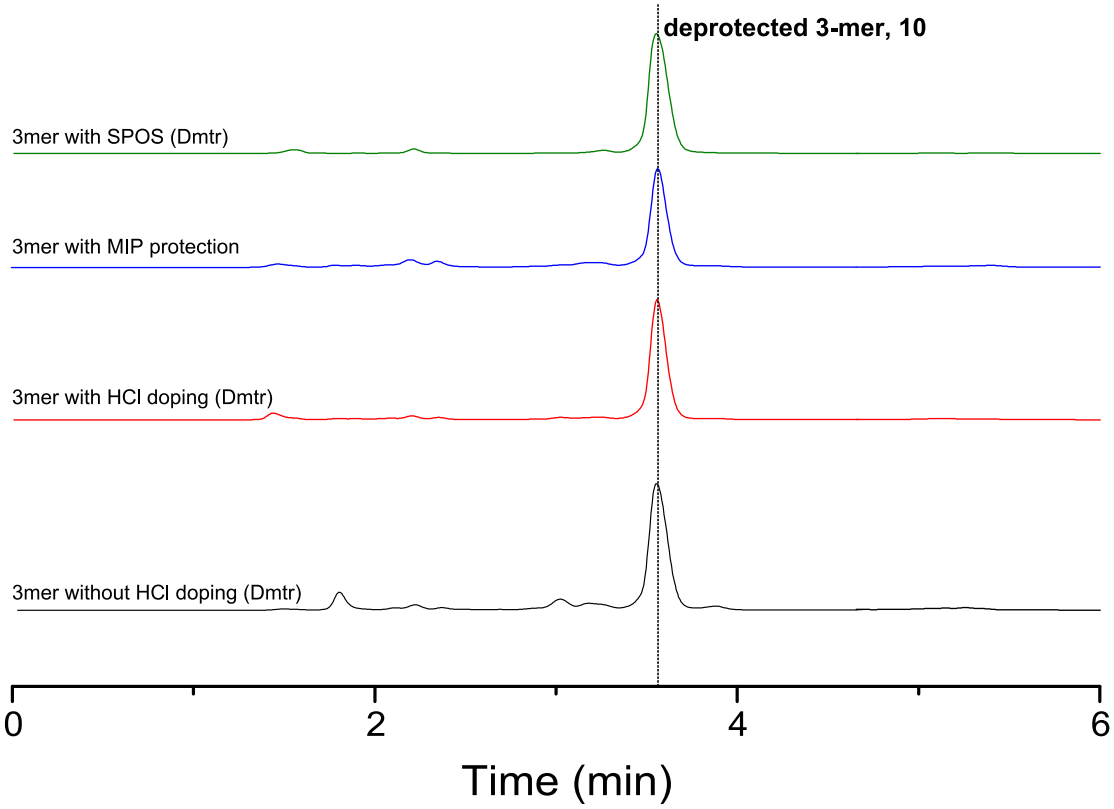


Figure 5.11. HPLC chromatogram of each 3-mer synthesized after global deprotection, compared to a SPOS-prepared 3-mer. 3-mer synthesized before the HCl doping shows the lowest purity, with peak profiles significantly different compared to the chromatogram of SPOS-prepared 3-mer.

Secondly, 3-mer prepared with Dmtr protection *after* HCl doping had 77% purity and showed a similar impurity profile compared to the 3-mer prepared by SPOS (92% purity). This purity improvement from 68% to 77% shows that HCl doping effectively removes the monothioates **11c**. A small bump to the left of the product peak is again likely to be the chain-extended mononucleosidyl homostar **4** that did *not* get chain extended in the previous step, as it is also present in the SPOS chromatogram. Thirdly, the 3-mer prepared with MIP protection also exhibited a similar impurity profile but had a relatively low purity of 64%. A visible difference between all LPOS-OSN prepared 3-mers and the SPOS-prepared 3-mer is the unidentified bump at 2.3 minutes, possibly monomer-related.

Overall, it is important to minimize the *n*-1 and *n*+1 impurities (peaks near the product peak), as these are the most difficult impurities to remove in the final purification step. Such impurities mainly arise due to incomplete chain extension or double chain extension, respectively. Hence, it can be concluded from the impurity profiles shown in Figure 5.11 that a 5'-*O* capping step after each chain extension reaction should be implemented to avoid *n*-1 impurities, and to improve the product purity. In addition, more comprehensive

characterization tools such as LC-MS need to be utilized to identify what exactly the main impurities are.

5.5. Conclusions

Three of the key challenges identified in the liquid-phase oligonucleotide synthesis (LPOS) platform have been overcome in this work. First, incomplete removal of phosphoramidite monomers was tackled by modifying the synthesis chemistry to effectively convert all excess monomers to an anionic species that can be selectively removed by PBI membranes through ion-exchange mechanism. It was found that doping the PBI membranes with acid improved its ion-exchange capability, ensuring complete removal of anionic phosphoramidite monomers.

Secondly, replacing the bulky Dmtr 5'-*O* protection group with a much smaller MIP protection group simplified the overall process significantly. A membrane reactor concept was applied by carrying out the 5'-*O* deprotection in the rig *in-situ*, reducing the number of unit operations from 9 to 3 per each chain extension cycle, achieving significant process intensification. In addition, undesirable solvents such as DCM and Et_2O were eliminated, and impractical solvent exchange steps were avoided reducing the overall solvent consumption. It should be stressed that the membrane diafiltration process is still a highly solvent-intensive operation. With the environmental impact becoming a significant priority within chemical industries, an appropriate measure to reduce the overall solvent consumption needs to be developed. The process can be further simplified by running the diafiltration using the same solvent as the reaction solvent, 1% DMF-MeCN, combining the entire chain extension cycle into a single-unit process. Finally, the low yield challenge faced by the LPOS-OSN platform (also by membrane processes in general) was tackled through the use of a membrane cascade. Although the observed yield improvements were not as high as expected due to the contamination with salt impurities, it guides the right direction for the LPOS-OSN platform. Nevertheless, with the proposed solutions in this work, the LPOS-OSN process can be a highly competitive and *scalable* platform for oligonucleotide synthesis.

Imperial College London

Chapter 6

Conclusions, Critical Assessment, and Future Direction

The main findings and conclusions of this thesis are summarized. The overall quality and weaknesses of the work are critically assessed, and future directions to further improve the proposed LPOS platform and OSN are suggested.

6.1. Overall Conclusions

This project began with the aim of developing a scalable oligonucleotide (oligos) manufacturing platform in liquid phase to augment the current mainstream, solid-phase platform. The core concept was to attach a *soluble* polymeric support to the growing oligos in homogeneous liquid-phase to facilitate downstream separation. OSN technology was identified as a suitable separation unit to purify growing oligos from the excess reagents, as OSN membranes can discriminate molecules primarily based on their molecular size in organic media. By tuning the size of the soluble support and membrane separation capacity, it was postulated that cumbersome oligo purification could be made simpler.

Initial attempts using linear PEG support demonstrated that the concept itself is feasible, but proved that it requires simultaneous optimization of chemistry, membrane, and process design. It was recognized early on that branching the soluble support has many advantages such as higher membrane retention as well as increased oligos loading. Hence, a branched monodispersed PEG support was synthesized and employed. After screening different types of OSN membranes, polybenzimidazole (PBI) membrane cross-linked with dibromoxylene (DBX) was selected as the most suitable due to its reproducibility and chemical stability.

The general synthesis protocol of oligos, iterative chain extension strategy, was adapted in this work. Each chain extension cycle is composed of two sets of reactions and two membrane purifications (via constant-volume diafiltration mode, CVD). The first set of reactions, chain extension and sulfurization, was carried out in MeCN or DMF-MeCN solvent, whereas the second set of reaction, detritylation, was done in DCM. In both membrane CVDs, MeOH-MeCN mixture was used to ensure growing oligos were well-solvated.

After chain extension reaction and sulfurization, excess phosphoramidite monomer converted to four different types of compounds: two neutral species (amidate and thioamidate) and two anionic species (monothioate and dithioate). Interestingly, the anionic species freely permeated through the PBI membranes but the neutral species, despite having similar MW, were highly rejected by the membranes. It was observed that addition of small organic salts, *i.e.* dichloroacetic acid or pyridinium dichloroacetate, facilitates the transport of anionic monomers through the PBI membranes. Hence, it was hypothesized that the transport occurs via ion-exchange mechanism whereby the anionic monomers hop through the immobile cations in the PBI backbone (benzimidazolium ring).

At the end of each chain extension cycle, the main remaining impurity was Dmtr-pyrrole along with traces of neutral monomers, which were deliberately removed by precipitating out the product in Et_2O. After each step, the growing oligos were characterized using HPLC, NMR, and MS; such capability to characterize the product adds a unique advantage to the LPOS platform. With the developed platform, 5-mer and 9-mer 2'-*O*Me phosphorothioate oligoribonucleotides have been successfully synthesized and characterized. An economic analysis showed that the main cost factor is, as expected, the phosphoramidite monomers, and also that it is crucial to implement a solvent recovery unit to minimize the overall cost, as the membrane diafiltration is a highly solvent-intensive operation. Although the process has shown its feasibility in liquid-phase, the yield and purity of the final oligos was considerably lower compared to the identical oligos synthesized via SPOS.

Several challenges were identified with the developed platform, they were: 1) incomplete removal of excess monomers, 2) multiple solvent exchanges in-between unit operations and the need for a precipitation step, and 3) low process yield and purity. It is absolutely essential to completely remove excess monomers, as they could get chain extended in the subsequent step, generating *n*-1 impurities. Fortunately, a fascinating work reported by van der Marel *et al.*[169] was adapted to convert all phosphoramidite monomers to anionic monothioates with 3*H*-1,2-benzodithiol-3-one (BDT) sulfurizing reagent; the monothioates freely permeated through the PBI membranes. This simple and effective trick solved one of the most problematic challenges. It was also found that doping the PBI membranes with acid (*i.e.* HCl) enhances their ion-exchange capacity, allowing monothioates to permeate even faster.

From the practical perspective, the number of solvent exchanges and unit operations had to be reduced to achieve a feasible and competitive process (the second challenge). It was identified that the main villain behind multiple solvent exchange steps was the bulky Dmtr protecting group (MW 302 Da). For instance, the detritylation reaction best works in DCM, and the reason for the precipitation step in Et_2O was to remove Dmtr-pyrrole. Hence, the Dmtr group was replaced with a smaller MIP group (MW 74 Da) which can be deprotected in the diafiltration solvent (MeOH-MeCN) and freely permeate through the membrane, eliminating the need for precipitation step. In addition, by running the deprotection reaction inside the membrane diafiltration rig *in-situ*, the reaction and separation was combined into a single membrane reactor unit operation. By applying the membrane reactor concept, it was possible to reduce the number of unit operations from 9 to 3 per chain extension cycle, with

only one solvent exchange step per cycle. However, the final oligo (**UCC** trimer) purity using MIP protected phosphoramidite monomers was lower than oligo prepared using commercial Dmtr-protected monomers.

The third challenge, low process yield and purity, was tackled using a 2-stage membrane cascade configuration that was developed during this project. It is critical to maintain quantitative yield for each step to achieve a high overall yield (arithmetic demon). Unfortunately, the yield improvement of oligos was not as high as expected due to an unexpected contamination by salt impurities in the final retentate, requiring an additional purification step using normal-phase chromatography. Nevertheless, the yield has improved a lot and it approached near quantitative yield at trimer level. It should be noted that the purity has improved significantly after overcoming the first challenge (monomer removal). However, replacing the Dmtr protection with MIP again lowered the purity, mainly because the MIP-protected monomers are not commercially available in high purity and they were synthesized in the lab. Apart from the monomer-related impurities, other sources of impurities come from prolonged exposure to other reagents compared to SPOS as well as long exposure time inside the steel-framed membrane rig.

A 2-stage membrane cascade system was developed and proposed in this work to overcome the inherent limitation of membrane processes in general. It was shown using a pore-flow transport model that in nanofiltration range between 100 – 2000 Da, it is difficult to achieve clean and sharp separations between solutes purely based on molecular size, resulting in low yield and purity. One possible solution is to use the modular nature of membranes and modify the process configuration into cascades. The cascade configuration proposed in this work operates using a single pressure pump without any need for buffer tank in-between membrane stages, simplifying the process control and allowing easy integration into other unit operations. The configuration was first tested on a mixture of PEG (PEG-400, PEG-2000) solution on PBI 22DBX membrane which showed that the yield of PEG-2000 increases from 59% to 94% without compromising the final purity. It was theoretically shown, and experimentally validated, that the recycle ratio and the transmembrane pressure affect the overall yield significantly.

The 2-stage cascade configuration was taken a step further by implementing an adsorptive solvent recovery unit to tackle both low yield and high solvent consumption challenges. The process was tested to purify an active pharmaceutical ingredient (API, roxithromycin

antibiotic) from two potential genotoxic impurities (GTIs, 4-dimethylaminopyridine and ethyl tosylate). Both GTIs were removed simultaneously to less than 5 ppm level. On the other hand, by implementing a 2-stage cascade, the yield of API was increased from 58% to 95% while maintaining the same purity. It was shown that the membrane CVD operation is highly solvent-intensive with an unacceptable E-factor. Hence, as the permeate stream from the 2-stage cascade contains mostly GTIs, an adsorptive solvent recovery unit using charcoal (activated carbon) was investigated which demonstrated that pure solvent can be recovered from the permeate. An economic analysis revealed that implementation of 2-stage cascade can achieve up to 92% cost reduction while reducing the mass and solvent intensity up to 73%. Through such yield enhancement and solvent consumption reduction, the membrane processes, combined with a solvent recovery unit, have been shown to be highly competitive unit operation compared to other traditional operations.

6.2. Critical Assessment and Future Direction

In this work, a scalable liquid-phase oligonucleotide synthesis (LPOS) platform using OSN separation technology has been proposed. Although the proposed process has shown its potential, it still needs to go through continuous improvements and optimizations. Several important points are discussed as follows.

First of all, although the membrane process is considered as a scalable technology, actual viability of LPOS platform in large scale operation must be shown experimentally, in terms of both technical and economic feasibility. Notably, the economic analysis done in Chapter 2 did not include the labor and operation cost, which could be a significant cost factor to the overall economics.

Secondly, one of the crucial considerations during this process research project was the technical practicality of the process at large scale. For instance, the number of solvent exchange steps required for the process described in Chapter 2 did not seem practical at all. Fortunately, the number of unit operations was drastically reduced in Chapter 5 with a new protecting group and the use of membrane reactor. However, ideally, the entire process should proceed in a single vessel which combines both reaction and separation. Theoretically, this can be done in DMF solvent where all the relevant reactions can be carried out. Unfortunately, and ironically, using DMF in lab scale was not practical due to its high boiling point, making the oligo analysis difficult (over 2L of solvent had to be evaporated completely

after each diafiltration for characterization). Nevertheless, a push to simplify the process into a single-solvent system is the right direction forward.

Thirdly, a more systematic approach to tune the support MW and membrane MWCO should be employed. PBI membranes were selected in this work mainly due to their excellent chemical and mechanical stability in all oligo synthesis conditions, as well as their reliable reproducibility. However, their actual separation performance, in parallel with the size of polymer support, has not yet been optimized. It should be emphasized that increasing the support size to enhance its rejection comes at a cost of decreased oligo loading (mmol of oligos per g of support) and increased solution viscosity. Hence, an optimization should focus on to minimize the support MW while increasing the bulkiness of the support, and improving the separation performance of membranes.

Fourthly, the oligo purity must be improved. Undoubtedly, understanding impurity profiles is a time-consuming and labor-intensive task. Notably, many impurities have already been identified for the SPOS platform[1], which are likely to be present in the LPOS platform as well. A thorough analysis is encouraged to reduce the impurities and improve the oligo purity. It has been shown in Chapter 5 that replacing the Dmtr protection with MIP group brings enormous process simplification benefits. However, although preparation of MIP-protected monomers is relatively straightforward and efficient, they are not commercially available at the moment, which is likely to become a hindering factor at large scale. Appropriate logistics should be considered and implemented to use MIP-protected monomers at large scale. A possible alternative is to find a membrane that permeates Dmtr group; however, further work to run detritylation reaction in the diafiltration solvent should be simultaneously explored.

Lastly, PBI OSN membranes must be scaled up and fabricated into membrane modules. It is not an easy task to fabricate flat sheet membranes into modules, especially for OSN membranes, as all the wetted parts (spacers, O-rings, adhesives, backing) must be solvent-resistant materials.

Apart from developing a LPOS platform, another main objective of this project was to understand and narrow the gap between membrane science in academia and membrane technology used in industry. Throughout the process development work, several limitations of the OSN technology have been identified that hinder its widespread use in industry.

First of all, the number of available OSN membranes is severely limited. Currently available commercial OSN membranes are mostly polyimide membranes; OSN membranes made out of PAN (polyacrylonitrile)[170], PIM-1 (polymers of intrinsic microporosity)[36], and PEEK (polyetheretherketine)[171] materials have been reported which are yet to be commercialized. PBI membranes developed by Valtcheva *et al.*[45] were chosen in this work for its excellent chemical stability and reproducibility rather than their separation performance. As different applications call for different requirements, it seems unlikely that any one type of membrane can be the solution-for-all. Availability of many types of membranes that cover wide range of solvent systems and separation requirements would be necessary for industry to gain more confidence in the OSN technology.

Secondly, the performance prediction of OSN membranes is weak. At the moment, it takes preliminary experience with OSN membranes to have a rough guess at their performance. Hence, developing an application around the OSN technology can become a time-consuming process, a risk that industry is reluctant to take. There are two fronts on which this challenge might be tackled. The first front is to compile the performances of OSN membranes in more accessible format to attract and guide end-users. Albeit time-consuming work, OSN membranes should be standardized and tested in many different solvents and pressures to give a rough guide for membrane selection. The second front is to develop predictive tools, building from fundamental ground up. However, as discussed in Chapter 1, predicting OSN membrane performance is an overwhelming task, particularly for polymeric membranes, due to the different degrees of solvent-membrane interactions. Nevertheless, this is an intellectual challenge that must be resolved in academia to give more confidence in membrane technology to end-users.

Thirdly, it should be recognized by membrane researchers that it is difficult to fabricate an ideal membrane with perfect performance. Rather, membranes should be synergistically implemented into existing processes to exploit their true potential. More emphasis should be placed on the process development aspect through application-driven projects. Also, improving mass transfer coefficients within membrane modules should be considered as important as fabricating high flux membranes.

In summary, albeit several challenges still need to be met, the field of OSN technology has improved tremendously in the past decade, and many potentially lucrative applications exist that are waiting to be tapped.

As a concluding remark, it is sincerely hoped that this work contributes to the field of membrane science, OSN technology in particular, to bring the membrane technology closer to the real-world applications, and also, the LPOS-OSN platform proposed in this work to be improved upon and widely applied in the field of oligo therapeutics.

References

1. Y.S. Sanghvi, A status update of modified oligonucleotides for chemotherapeutics applications, *Curr. Protoc. Nucleic Acid Chem.,* **2011**, 4.1. 1-4.1. 22.

2. C.B. Reese, Q. Song, The H-phosphonate approach to the solution phase synthesis of linear and cyclic oligoribonucleotides, *Nucleic Acids Res.,* **1999,** *27*, 963.

3. I. Adamo, C. Dueymes, A. Schönberger, A.E. Navarro, A. Meyer, M. Lange, J.L. Imbach, F. Link, F. Morvan, J.J. Vasseur, Solution Phase Synthesis of Phosphorothioate Oligonucleotides Using a Solid Supported Acyl Chloride with H Phosphonate Chemistry, *Eur. J. Org. Chem.,* **2006**, 436-448.

4. G. Bonora, R. Rossin, S. Zaramella, D. Cole, A. Eleuteri, V. Ravikumar, A liquid-phase process suitable for large-scale synthesis of phosphorothioate oligonucleotides, *Org. Process Res. Dev.,* **2000,** *4*, 225-231.

5. C.-H. Chen, W.-Y. Chen, Y.-C. Chen, M.-J. Lee, C.-D. Huang, K. Chanda, C.-M. Sun, Convergent Solution Phase Synthesis of Chimeric Oligonucleotides by a 2+2 and 3+3 Phosphoramidite Strategy, *Aust. J. Chem.,* **2010,** *63*, 227-235.

6. G.M. Bonora, C.L. Scremin, F.P. Colonna, A. Garbesi, HELP (high efficiency liquid phase) new oligonucleotide synthesis on soluble polymeric support, *Nucleic Acids Res.,* **1990,** *18*, 3155.

7. V. Kungurtsev, J. Laakkonen, A.G. Molina, P. Virta, Solution-Phase Synthesis of Short Oligo-2′-deoxyribonucleotides by Using Clustered Nucleosides as a Soluble Support, *Eur. J. Org. Chem.,* **2013**, 6687-6693.

8. M.C. de Koning, A.B.T. Ghisaidoobe, H.I. Duynstee, P.B.W. Ten Kortenaar, D.V. Filippov, G.A. van der Marel, Simple and efficient solution-phase synthesis of oligonucleotides using extractive work-up, *Org. Process Res. Dev.,* **2006,** *10*, 1238-1245.

9. P. Vandezande, L.E.M. Gevers, I.F.J. Vankelecom, Solvent resistant nanofiltration: separating on a molecular level, *Chem. Soc. Rev.,* **2008,** *37*, 365-405.

10. Y.H. See-Toh, M. Silva, A. Livingston, Controlling molecular weight cut-off curves for highly solvent stable organic solvent nanofiltration (OSN) membranes, *J. Membr. Sci.,* **2008,** *324*, 220-232.

11. E.M. Rundquist, C.J. Pink, A. Livingston, Organic Solvent Nanofiltration; a Potential Alternative to Distillation for Solvent Recovery from Crystallisation Mother Liquors, *Green Chem.,* **2012**.

12. G. Székely, J. Bandarra, W. Heggie, B. Sellergren, F.C. Ferreira, Organic solvent nanofiltration: A platform for removal of genotoxins from active pharmaceutical ingredients, *J. Membr. Sci.,* **2011,** *381*, 21-33.

13. A.P.B. Ribeiro, J.M.L.N. de Moura, L.A.G. Gonçalves, J.C.C. Petrus, L.A. Viotto, Solvent recovery from soybean oil/hexane miscella by polymeric membranes, *J. Membr. Sci.,* **2006,** *282*, 328-336.

14. D.F. Stamatialis, N. Stafie, K. Buadu, M. Hempenius, M. Wessling, Observations on the permeation performance of solvent resistant nanofiltration membranes, *J. Membr. Sci.,* **2006,** *279*, 424-433.

15. L.S. White, A.R. Nitsch, Solvent recovery from lube oil filtrates with a polyimide membrane, *J. Membr. Sci.,* **2000,** *179*, 267-274.

16. L.S. White, Development of large-scale applications in organic solvent nanofiltration and pervaporation for chemical and refining processes, *J. Membr. Sci.,* **2006,** *286*, 26-35.

17. A. Buekenhoudt, H. Beckers, D. Ormerod, M. Bulut, P. Vandezande, R. Vleeschouwers, Solvent Based Membrane Nanofiltration for Process Intensification, *Chem. Ing. Tech.,* **2013,** *85*, 1243-1247.

18. K. Li, Ceramic membranes for separation and reaction. *Wiley Online Library*, 2007.

19. M. Spear, Separations in Flux. *Chem. Process.,* 2006.

20. S. Adler, E. Beaver, P. Bryan, S. Robinson, J. Watson, Vision 2020: 2000 Separations Roadmap, *AIChE J.,* **2000**.

21. M. Mulder, Basic principles of membrane technology. *Springer*, 1996.

22. R. Baker, Membrane technology and applications. *John Wiley & Sons*, 2012.

23. T.J. Leahy, M. Sullivan, Validation of bacterial retention capabilities of membrane filters, *Pharm. Technol,* **1978,** *2*, 64-75.

24. J.-L.J. Maubois, G.P. Mocquot, L.J. Vassal, Preparation of cheese using ultrafiltration, **1980**, US patent 4,205,090.

25. S. Sourirajan, Reverse osmosis. *London, UK: Logos Press Ltd.*, 1970.

26. B. Van der Bruggen, M. Mänttäri, M. Nyström, Drawbacks of applying nanofiltration and how to avoid them: A review, *Sep. Purif. Technol.,* **2008,** *63*, 251-263.

27. A. Boam, A. Nozari, Fine chemical: OSN-a lower energy alternative, *Filtr. & Separat.,* **2006,** *43*, 46-48.

28. A. Tsoukala, L. Peeva, A.G. Livingston, H.-R. Bjørsvik, Separation of Reaction Product and Palladium Catalyst after a Heck Coupling Reaction by means of Organic Solvent Nanofiltration, *ChemSusChem,* **2012,** *5*, 188-193.

29. J.C.T. Lin, A.G. Livingston, Nanofiltration membrane cascade for continuous solvent exchange, *Chem. Eng. Sci.,* **2007,** *62*, 2728-2736.

30. A. Stankiewicz, Reactive separations for process intensification: an industrial perspective, *Chem. Eng. Process. Process Intensif.,* **2003,** *42*, 137-144.

31. Y.H. See-Toh, F.C. Ferreira, A.G. Livingston, The influence of membrane formation parameters on the functional performance of organic solvent nanofiltration membranes, *J. Membr. Sci.,* **2007,** *299*, 236-250.

32. M. Bulut, L.E.M. Gevers, J.S. Paul, I.F.J. Vankelecom, P.A. Jacobs, Directed development of high-performance membranes via high-throughput and combinatorial strategies, *J. Comb. Chem.,* **2006,** *8*, 168-173.

33. K. Gupta, Synthesis and evaluation of aromatic polyamide membranes for desalination in reverse osmosis technique, *J. Appl. Polym. Sci.,* **1997,** *66*, 643-653.

34. W.R. Bowen, T.A. Doneva, H.B. Yin, Separation of humic acid from a model surface water with PSU/SPEEK blend UF/NF membranes, *J. Membr. Sci.,* **2002,** *206*, 417-429.

35. J. Wang, Z. Yue, J.S. Ince, J. Economy, Preparation of nanofiltration membranes from polyacrylonitrile ultrafiltration membranes, *J. Membr. Sci.,* **2006,** *286*, 333-341.

36. D. Fritsch, P. Merten, K. Heinrich, M. Lazar, M. Priske, High performance organic solvent nanofiltration membranes: Development and thorough testing of thin film composite membranes made of polymers of intrinsic microporosity (PIMs), *J. Membr. Sci.,* **2012,** *401–402*, 222-231.

37. R.R. Nair, H.A. Wu, P.N. Jayaram, I.V. Grigorieva, A.K. Geim, Unimpeded Permeation of Water Through Helium-Leak–Tight Graphene-Based Membranes, *Science,* **2012,** *335*, 442-444.

38. S. Karan, S. Samitsu, X. Peng, K. Kurashima, I. Ichinose, Ultrafast Viscous Permeation of Organic Solvents Through Diamond-Like Carbon Nanosheets, *Science,* **2012,** *335*, 444-447.

39. K. Keizer, R.J.R. Uhlhorn, T.J. Burggraaf, Gas separation using inorganic membranes. *Membr. Sci. Technol.*, **1995**, 2, 553-588.

40. H. Vinh-Thang, S. Kaliaguine, Predictive Models for Mixed-Matrix Membrane Performance: A Review, *Chem. Rev. (Washington, DC, U. S.),* **2013,** *113*, 4980-5028.

41. A.F. Ismail, L.P. Yean, Review on the development of defect-free and ultrathin-skinned asymmetric membranes for gas separation through manipulation of phase inversion and rheological factors, *J. Appl. Polym. Sci.,* **2003,** *88*, 442-451.

42. M.F. Jimenez Solomon, Y. Bhole, A.G. Livingston, High flux membranes for organic solvent nanofiltration (OSN)—Interfacial polymerization with solvent activation, *J. Membr. Sci.,* **2012,** *423–424*, 371-382.

43. M.F. Jimenez Solomon, Y. Bhole, A.G. Livingston, High flux hydrophobic membranes for organic solvent nanofiltration (OSN)—Interfacial polymerization, surface modification and solvent activation, *J. Membr. Sci.,* **2013,** *434*, 193-203.

44. Y.H. See Toh, F.W. Lim, A.G. Livingston, Polymeric membranes for nanofiltration in polar aprotic solvents, *J. Membr. Sci.,* **2007,** *301*, 3-10.

45. I.B. Valtcheva, S.C. Kumbharkar, J.F. Kim, Y. Bhole, A.G. Livingston, Beyond polyimide: Crosslinked polybenzimidazole membranes for organic solvent nanofiltration (OSN) in harsh environments, *J. Membr. Sci.,* **2014,** *457*, 62-72.

46. Y. See Toh, X. Loh, K. Li, A. Bismarck, A. Livingston, In search of a standard method for the characterisation of organic solvent nanofiltration membranes, *J. Membr. Sci.,* **2007,** *291*, 120-125.

47. J. Micovic, K. Werth, P. Lutze, Hybrid separations combining distillation and organic solvent nanofiltration for separation of wide boiling mixtures, *Chem. Eng. Res. Des.,* **2014**.

48. J.G. Wijmans, R.W. Baker, The solution-diffusion model: a review, *J. Membr. Sci.,* **1995,** *107*, 1-21.

49. W. Deen, Hindered transport of large molecules in liquid-filled pores, *AIChE J.,* **1987,** *33*, 1409-1425.

50. E. Smit, M.H.V. Mulder, C.A. Smolders, H. Karrenbeld, J. van Eerden, D. Feil, Modelling of the diffusion of carbon dioxide in polyimide matrices by computer simulation, *J. Membr. Sci.,* **1992,** *73*, 247-257.

51. W.R. Bowen, J.S. Welfoot, Modelling the performance of membrane nanofiltration—critical assessment and model development, *Chem. Eng. Sci.,* **2002,** *57*, 1121-1137.

52. W.R. Bowen, H. Mukhtar, Characterisation and prediction of separation performance of nanofiltration membranes, *J. Membr. Sci.,* **1996,** *112*, 263-274.

53. W.R. Bowen, J.S. Welfoot, Modelling of membrane nanofiltration—pore size distribution effects, *Chem. Eng. Sci.,* **2002,** *57*, 1393-1407.

54. E. Nagy, E. Kulcsár, A. Nagy, Membrane mass transport by nanofiltration: Coupled effect of the polarization and membrane layers, *J. Membr. Sci.,* **2011,** *368*, 215-222.

55. D.o.R. Machado, D. Hasson, R. Semiat, Effect of solvent properties on permeate flow through nanofiltration membranes. Part I: investigation of parameters affecting solvent flux, *J. Membr. Sci.,* **1999,** *163*, 93-102.

56. E.S. Tarleton, J.P. Robinson, S.J. Smith, J.J.W. Na, New experimental measurements of solvent induced swelling in nanofiltration membranes, *J. Membr. Sci.,* **2005,** *261*, 129-135.

57. P. Marchetti, A. Butté, A.G. Livingston, An improved phenomenological model for prediction of solvent permeation through ceramic NF and UF membranes, *J. Membr. Sci.,* **2012,** *415–416*, 444-458.

58. J. Stawikowska, J.F. Kim, A.G. Livingston, Pore-flow calculations based on pore size distributions in polyimide membranes determined by a nanoprobe imaging technique, *Chem. Eng. Sci.,* **2013,** *97*, 81-95.

59. D. Peshev, A.G. Livingston, OSN Designer, a tool for predicting organic solvent nanofiltration technology performance using Aspen One, MATLAB and CAPE OPEN, *Chem. Eng. Sci.,* **2013,** *104*, 975-987.

60. L.G. Peeva, E. Gibbins, S.S. Luthra, L.S. White, R.P. Stateva, A.G. Livingston, Effect of concentration polarisation and osmotic pressure on flux in organic solvent nanofiltration, *J. Membr. Sci.,* **2004,** *236*, 121-136.

61. S. Sablani, M. Goosen, R. Al-Belushi, M. Wilf, Concentration polarization in ultrafiltration and reverse osmosis: a critical review, *Desalination,* **2001,** *141*, 269-289.

62. P. Aimar, R. Field, Limiting flux in membrane separations: a model based on the viscosity dependency of the mass transfer coefficient, *Chem. Eng. Sci.,* **1992,** *47*, 579-586.

63. X. Yang, R. Wang, A.G. Fane, C.Y. Tang, I. Wenten, Membrane module design and dynamic shear-induced techniques to enhance liquid separation by hollow fiber modules: a review, *Desalin. Water Treat.,* **2013,** *51*, 3604-3627.

64. Evonik, http://duramem.evonik.com/product/duramem-puramem/en/Pages/default.aspx, last accessed: January, 2014

65. SolSep, http://www.solsep.com/, last accessed: January 2014

66. P. Sehn, E. Zhao, J. Johnson, M. Hallan, M. Peery, Design, Development, and Field Testing of Sixteen Inch Diameter RO Modules in a Waste Water Reuse Application, *Water Pract. Technol.,* **2009,** *4*.

67. J.D. Watson, F.H.C. Crick, Molecular structure of nucleic acids, *Nature,* **1953,** *171*, 737-738.

68. M. Behlke, E. Devor, Chemical synthesis of oligonucleotides, *Integr. DNA Technol.,* **2005**.

69. Y. Fichou, C. Férec, The potential of oligonucleotides for therapeutic applications, *Trends Biotechnol.,* **2006,** *24*, 563-570.

70. A. Michelson, A.R. Todd, Nucleotides part XXXII. Synthesis of a dithymidine dinucleotide containing a 3 : 5 -internucleotidic linkage, *J. Chem. Soc.,* **1955**, 2632-2638.

71. V.A. Efimov, A.L. Kalinkina, O.G. Chakhmakhcheva, T.S. Hill, K. Jayaraman, New efficient sulfurizing reagents for the preparation of oligodeoxyribonucleotide phosphorothioate analogues, *Nucleic Acids Res.,* **1995,** *23*, 4029.

72. M.V. Rao, C.B. Reese, Dibenzoyl tetrasulphide-A rapid sulphur transfer agent in the synthesis of phosphorothioate analogues of oligonucleotides, *Tetrahedron Lett.,* **1992,** *33*, 4839-4842.

73. C. Stein, J.L. Tonkinson, L. Yakubov, Phosphorothioate oligodeoxynucleotides--anti-sense inhibitors of gene expression?, *Pharmacol. Ther.,* **1991,** *52*, 365-384.

74. S.M. Ryan, G. Mantovani, X. Wang, D.M. Haddleton, D.J. Brayden, Advances in PEGylation of important biotech molecules: delivery aspects, *Expert Opin. Drug Del.,* **2008,** *5*, 371-383.

75. H. Schaller, G. Weimann, B. Lerch, H. Khorana, Studies on polynucleotides. XXIV. The stepwise synthesis of specific deoxyribopolynucleotides (4). Protected derivatives of deoxyribonucleosides and new syntheses of deoxyribonucleoside-3 phosphates, *J. Am. Chem. Soc,* **1963,** *85*, 3821-3827.

76. M. Smith, D. Rammler, I. Goldberg, H. Khorana, Synthesis of uridylyl-(3'<< 5')-Uridine and uridylyl-(3'K5')-adenosine, *J. Am. Chem. Soc,* **1961,** *84*, 430-440.

77. E.L. Brown, R. Belagaje, M.J. Ryan, H. Gobind Khorana, Chemical synthesis and cloning of a tyrosine tRNA gene, *Methods Enzymol.,* **1979,** *68*, 109-151.

78. C. Reese, Oligo-and poly-nucleotides: 50 years of chemical synthesis, *Org. Biomol. Chem.,* **2005,** *3*, 3851-3868.

79. R. Hogrefe, T.L. BioTechnologies, A short history of oligonucleotide synthesis, *Trilink Biotechnol.,* **2006**.

80. R.L. Letsinger, P.S. Miller, Nucleotide chemistry. XIV. Protecting groups for nucleosides used in synthesizing oligonucleotides, *J. Am. Chem. Soc.,* **1969,** *91*, 3356-3359.

81. R.L. Letsinger, K.K. Ogilvie, Nucleotide chemistry. XIII. Synthesis of oligothymidylates via phosphotriester intermediates, *J. Am. Chem. Soc.,* **1969,** *91*, 3350-3355.

82. R.L. Letsinger, W.B. Lunsford, Synthesis of thymidine oligonucleotides by phosphite triester intermediates, *J. Am. Chem. Soc.,* **1976,** *98*, 3655-3661.

83. S. Beaucage, M. Caruthers, Deoxynucleoside phosphoramidites--A new class of key intermediates for deoxypolynucleotide synthesis, *Tetrahedron Lett.,* **1981,** *22*, 1859-1862.

84. Y.S. Sanghvi, Z. Guo, H.M. Pfundheller, A. Converso, Improved process for the preparation of nucleosidic phosphoramidites using a safer and cheaper activator, *Org. Process Res. Dev.,* **2000,** *4*, 175-181.

85. A.H. Krotz, R.L. Carty, A.N. Scozzari, D.L. Cole, V.T. Ravikumar, Large-scale synthesis of antisense oligonucleotides without chlorinated solvents, *Org. Process Res. Dev.,* **2000,** *4*, 190-193.

86. R. Hall, A. Todd, R. Webb, 644. Nucleotides. Part XLI. Mixed anhydrides as intermediates in the synthesis of dinucleoside phosphates, *J. Chem. Soc.,* **1957**, 3291-3296.

87. B.C. Froehler, P.G. Ng, M.D. Matteucci, Synthesis of DNA via deoxynudeoside H-phosphonate Intermediates, *Nucleic Acids Res.,* **1986,** *14*, 5399.

88. C. Dreef, C. Dreef-Tromp, G. van der Marel, J. van Boom, A Convenient Approach Towards the Conversion of H-Phosphonate and H-Phosphonothioate Diesters into Phosphoro (di) thioate Derivatives, *Synlett,* **1990,** *1990*, 481-483.

89. C.B. Reese, H. Yan, Solution phase synthesis of ISIS 2922 (Vitravene) by the modified H-phosphonate approach, *J. Chem. Soc., Perkin Trans. 1,* **2002**, 2619-2633.

90. I. Lebedeva, L. Benimetskaya, C. Stein, M. Vilenchik, Cellular delivery of antisense oligonucleotides, *Eur. J. Pharm. Biopharm.,* **2000,** *50*, 101-119.

91. A. Fire, S.Q. Xu, M.K. Montgomery, S.A. Kostas, S.E. Driver, C.C. Mello, Potent and specific genetic interference by double-stranded RNA in Caenorhabditis elegans, *Nature,* **1998,** *391*, 806-811.

92. C. Stein, Y. Cheng, Antisense oligonucleotides as therapeutic agents--is the bullet really magical?, *Science,* **1993,** *261*, 1004.

93. A.K. Vaishnaw, J. Gollob, C. Gamba-Vitalo, R. Hutabarat, D. Sah, R. Meyers, T. de Fougerolles, J. Maraganore, A status report on RNAi therapeutics, *Silence,* **2010,** *1*, 1-13.

94. A.D. Branch, A good antisense molecule is hard to find, *Trends Biochem. Sci.,* **1998,** *23*, 45-50.

95. A. Akinc, W. Querbes, S. De, J. Qin, M. Frank-Kamenetsky, K.N. Jayaprakash, M. Jayaraman, K.G. Rajeev, W.L. Cantley, J.R. Dorkin, Targeted delivery of RNAi therapeutics with endogenous and exogenous ligand-based mechanisms, *Mol. Ther.,* **2010,** *18*, 1357-1364.

96. M.A. Maier, M. Jayaraman, S. Matsuda, J. Liu, S. Barros, W. Querbes, Y.K. Tam, S.M. Ansell, V. Kumar, J. Qin, Biodegradable lipids enabling rapidly eliminated lipid nanoparticles for systemic delivery of RNAi therapeutics, *Mol. Ther.,* **2013,** *21*, 1570-1578.

97. A.R. Lajmi, L. Schwartz, Y.S. Sanghvi, Membrane purification of an antisense oligonucleotide, *Org. Process Res. Dev.,* **2004,** *8*, 651-657.

98. L. Andersson, L. Blomberg, M. Flegel, L. Lepsa, B. Nilsson, M. Verlander, Large scale synthesis of peptides, *Peptide Science,* **2000,** *55*, 227-250.

99. S. So, L.G. Peeva, E.W. Tate, R.J. Leatherbarrow, A.G. Livingston, Organic Solvent Nanofiltration: A New Paradigm in Peptide Synthesis, *Org. Process Res. Dev.,* **2010,** *14*, 1313-1325.

100. U. Tedebark, A. Scozzari, O. Werbitzky, D. Capaldi, L. Holmberg, Industrial-Scale Manufacturing of a Possible Oligonucleotide Cargo CPP-Based Drug, *Methods Mol. Biol.,* **2011,** *683*, 505-524.

101. E. Bayer, M. Mutter, Liquid phase synthesis of peptides, *Nature (London, U. K.),* **1972,** *237*, 512-513.

102. G. Székely, M. Gil, B. Sellergren, W. Heggie, F.C. Ferreira, Environmental and economic analysis for selection and engineering sustainable API degenotoxification processes, *Green Chem.,* **2013,** *15*, 210-225.

103. B.P. Chekal, A.M. Campeta, Y.A. Abramov, N. Feeder, P.P. Glynn, R.W. McLaughlin, P.A. Meenan, R.A. Singer, The challenges of developing an API crystallization process

for a complex polymorphic and highly solvating system. part I, *Org. Process Res. Dev.,* **2009,** *13*, 1327-1337.

104. S. So, L.G. Peeva, E.W. Tate, R.J. Leatherbarrowb, A.G. Livingston, Membrane enhanced peptide synthesis, *Chem. Commun. (Cambridge, U. K.),* **2010,** *46*, 2808-2810.

105. Q.L. Lu, A. Rabinowitz, Y.C. Chen, T. Yokota, H. Yin, J. Alter, A. Jadoon, G. Bou-Gharios, T. Partridge, Systemic delivery of antisense oligoribonucleotide restores dystrophin expression in body-wide skeletal muscles, *Proc. Natl. Acad. Sci. U. S. A.,* **2005,** *102*, 198-203.

106. S. Beaucage, Solid-phase synthesis of siRNA oligonucleotides, *Curr. Opin. Drug Discovery Dev.,* **2008,** *11*, 203.

107. G. Székely, M. Schaepertoens, P.R. Gaffney, A.G. Livingston, Iterative synthesis of monodisperse PEG homostars and linear heterobifunctional PEG, *Polym. Chem.,* **2014**.

108. R.C. Vasconcelos. Organic solvent nanofiltration in the synthesis of DNA oligonucleotides and heterobifunctional polymers. *Ph.D Dissertation*, Imperial College London, London, 2011.

109. F. Zheng, C. Li, Q. Yuan, F. Vriesekoop, Influence of molecular shape on the retention of small molecules by solvent resistant nanofiltration (SRNF) membranes: A suitable molecular size parameter, *J. Membr. Sci.,* **2008,** *318*, 114-122.

110. C. Xie, M. Staszak, J. Quatroche, C. Sturgill, V. Khau, M. Martinelli, Nucleosidic Phosphoramidite Synthesis via Phosphitylation: Activator Selection and Process Development, *Org. Process Res. Dev,* **2005,** *9*, 730-737.

111. IBA, http://www.iba-lifesciences.com/ last accessed: January, 2014

112. EuroFins_MWG_Operon, http://www.operon.com/ last accessed: January 2014

113. Invitrogen, http://www.lifetechnologies.com/ last accessed: January 2014

114. M. Alejandro Gimenez, K. Vyacheslav, V. Pasi, L. Harri, Acetylated and Methylated β-Cyclodextrins as Viable Soluble Supports for the Synthesis of Short 2'-Oligodeoxyribonucleotides in Solution, *Molecules,* **2012,** *17*, 12102-12120.

115. P. Barker, R. Alsop, G. Vlachogiannis, Fractionation, purification and concentration of dextran solutions by ultrafiltration, *J. Membr. Sci.,* **1984,** *20*, 79-91.

116. K. Mohanty, R. Ghosh, Novel tangential-flow countercurrent cascade ultrafiltration configuration for continuous purification of humanized monoclonal antibody, *J. Membr. Sci.,* **2008,** *307*, 117-125.

117. Z. Xu, L. Yu, L. Han, Polymer-nanoinorganic particles composite membranes: a brief overview, *Front. Chem. Eng. China,* **2009,** *3*, 318-329.

118. T.C.T. Pham, H.S. Kim, K.B. Yoon, Growth of uniformly oriented silica MFI and BEA zeolite films on substrates, *Science,* **2011,** *334*, 1533-1538.

119. M. Tsapatsis, Toward High-Throughput Zeolite Membranes, *Science,* **2011,** *334*, 767-768.

120. J.L.C. Rowsell, O.M. Yaghi, Metal–organic frameworks: a new class of porous materials, *Microporous Mesoporous Mater.,* **2004,** *73*, 3-14.

121. S.T. Hwang, K. Kammermeyer, Operating lines in cascade separation of binary mixtures, *Can. J. Chem. Eng.,* **1965,** *43*, 36-39.

122. S.T. Hwang, K. Kammermeyer, A. Weissberger, Membranes in separations. *Wiley New York*, 1975; Vol. 7.

123. R. Pathare, R. Agrawal, Design of membrane cascades for gas separation, *J. Membr. Sci.,* **2010,** *364*, 263-277.

124. R. Agrawal, Membrane cascade schemes for multicomponent gas separation, *Ind. Eng. Chem. Res.,* **1996,** *35*, 3607-3617.

125. N. Laguntsov, E. Gruzdev, E. Kosykh, V.Y. Kozhevnickov, The use of recycle permeator systems for gas mixture separation, *J. Membr. Sci.,* **1992,** *67*, 15-28.

126. O. Masayoshi, T. Morisue, O. Ozaki, T. Miyauchi, Gas separation performance of tapered cascade with membrane, *J. Nucl. Sci. Technol.,* **1978,** *15*, 411-420.

127. F. Maskan, D.E. Wiley, L.P.M. Johnston, D.J. Clements, Optimal design of reverse osmosis module networks, *AIChE J.,* **2000,** *46*, 946-954.

128. F. McCandless, S. Herbst, Counter-current recycle membrane cascades for the separation of the boron isotopes in BF3, *J. Membr. Sci.,* **1990,** *54*, 307-319.

129. E. Lightfoot, Can membrane cascades replace chromatography? Adapting binary ideal cascade theory of systems of two solutes in a single solvent, *Sep. Sci. Technol.,* **2005,** *40*, 739-756.

130. E.N. Lightfoot, T.W. Root, J. L O'Dell, Emergence of ideal membrane cascades for downstream processing, *Biotechnol. Prog.,* **2008,** *24*, 599-605.

131. E.N. Lightfoot Jr, Membrane cascade-based separation, **2006**, US 7141171 B2.

132. M. Mayani, C.D.M. Filipe, R. Ghosh, Cascade ultrafiltration systems—Integrated processes for purification and concentration of lysozyme, *J. Membr. Sci.,* **2010,** *347*, 150-158.

133. J. Vanneste, D. Ormerod, G. Theys, D. Van Gool, B. Van Camp, S. Darvishmanesh, B. Van der Bruggen, Towards high resolution membrane-based pharmaceutical separations, *J. Chem. Technol. Biotechnol.,* **2012,** *88*, 98-108.

134. J. Vanneste, S. De Ron, S. Vandecruys, S.A. Soare, S. Darvishmanesh, B. Van der Bruggen, Techno-economic evaluation of membrane cascades relative to simulated moving bed chromatography for the purification of mono-and oligosaccharides, *Sep. Purif. Technol.,* **2011,** *80*, 600-609.

135. A. Caus, S. Vanderhaegen, L. Braeken, B. Van der Bruggen, Integrated nanofiltration cascades with low salt rejection for complete removal of pesticides in drinking water production, *Desalination,* **2009,** *241*, 111-117.

136. A. Caus, L. Braeken, K. Boussu, B. Van der Bruggen, The use of integrated countercurrent nanofiltration cascades for advanced separations, *J. Chem. Technol. Biotechnol.,* **2009,** *84*, 391-398.

137. W.E. Siew, A.G. Livingston, C. Ates, A. Merschaert, Continuous solute fractionation with membrane cascades – A high productivity alternative to diafiltration, *Sep. Purif. Technol.,* **2013,** *102*, 1-14.

138. R. Ghosh, Novel cascade ultrafiltration configuration for continuous, high-resolution protein–protein fractionation: a simulation study, *J. Membr. Sci.,* **2003,** *226*, 85-99.

139. D.M. Roberge, L. Ducry, N. Bieler, P. Cretton, B. Zimmermann, Microreactor technology: A revolution for the fine chemical and pharmaceutical industries?, *Chem. Eng. Technol.,* **2005,** *28*, 318-323.

140. G. Székely, J. Bandarra, W. Heggie, F.C. Ferreira, B. Sellergren, Design, preparation and characterization of novel molecularly imprinted polymers for removal of potentially genotoxic 1,3-diisopropylurea from API solutions, *Sep. Purif. Technol.,* **2012,** *86*, 190-198.

141. C. Jiménez-González, D.J.C. Constable, C.S. Ponder, Evaluating the "greenness" of chemical processes and products in the pharmaceutical industry--a green metrics primer., *Chem. Soc. Rev.,* **2012,** *41*, 1485-98.

142. C. Jiménez-González, P. Poechlauer, Q.B. Broxterman, B.-S. Yang, D. am Ende, J. Baird, C. Bertsch, R.E. Hannah, P. Dell'Orco, H. Noorman, S. Yee, R. Reintjens, A. Wells, V. Massonneau, J. Manley, Key Green Engineering Research Areas for Sustainable Manufacturing: A Perspective from Pharmaceutical and Fine Chemicals Manufacturers, *Org. Process Res. Dev,* **2011,** *15*, 900-911.

143. EMEA, *Limits of Genotoxic Impurities*, 2006, EMEA/CHMP/QWP/251334/2006

144. M. Degerman, N. Jakobsson, B. Nilsson, Designing Robust Preparative Purification Processes with High Performance, *Chem. Eng. Technol.,* **2008,** *31*, 875-882.

145. T. Winkelnkemper, G. Schembecker, Purification performance index and separation cost indicator for experimentally based systematic downstream process development, *Sep. Purif. Technol.,* **2010,** *72*, 34-39.

146. E. Drioli, A.I. Stankiewicz, F. Macedonio, Membrane engineering in process intensification—An overview, *J. Membr. Sci.,* **2011,** *380*, 1-8.

147. E. Drioli, A. Brunetti, G. Di Profio, G. Barbieri, Process intensification strategies and membrane engineering, *Green Chem.,* **2012,** *14*, 1561.

148. G. Székely, E. Fritz, J. Bandarra, W. Heggie, B. Sellergren, Removal of potentially genotoxic acetamide and arylsulfonate impurities from crude drugs by molecular imprinting., *J. Chromatogr. A.,* **2012,** *1240*, 52-8.

149. G. Székely, J. Bandarra, W. Heggie, B. Sellergren, F.C. Ferreira, A hybrid approach to reach stringent low genotoxic impurity contents in active pharmaceutical ingredients: Combining molecularly imprinted polymers and organic solvent nanofiltration for removal of 1,3-diisopropylurea, *Sep. Purif. Technol.,* **2012,** *86*, 79-87.

150. A. Criscuoli, E. Drioli, New metrics for evaluating the performance of membrane operations in the logic of process intensification, *Ind. Eng. Chem. Res.,* **2007,** *46*, 2268-2271.

151. A. Brunetti, G. Barbieri, E. Drioli, Upgrading of a syngas mixture for pure hydrogen production in a Pd–Ag membrane reactor, *Chem. Eng. Sci.,* **2009,** *64*, 3448-3454.

152. E. Curcio, A. Criscuoli, E. Drioli, Membrane crystallizers, *Ind. Eng. Chem. Res.,* **2001,** *40*, 2679-2684.

153. H.M.F. Freundlich, Over the adsorption in solution, *J. Phys. Chem,* **1906,** *57*, 385-470.

154. R. Kecili, J. Billing, M. Leeman, D. Nivhede, B. Sellergren, A. Rees, E. Yilmaz, Selective scavenging of the genotoxic impurity methyl p-toluenesulfonate from pharmaceutical formulations, *Sep. Purif. Technol.,* **2013,** *103*, 173-179.

155. C. Lee, R. Helmy, C. Strulson, J. Plewa, E. Kolodziej, V. Antonucci, B. Mao, C.J. Welch, Z. Ge, M.A. Al-sayah, Removal of electrophilic potential genotoxic impurities using nucleophilic reactive resins, *Org. Process Res. Dev.,* **2010,** *14*, 1021-1026.

156. J.F. Kim, A.M. Freitas da Silva, I.B. Valtcheva, A.G. Livingston, When the membrane is not enough: A simplified membrane cascade using Organic Solvent Nanofiltration (OSN), *Sep. Purif. Technol.,* **2013,** *116*, 277-286.

157. G. Alberti, V. Amendola, M. Pesavento, R. Biesuz, Beyond the synthesis of novel solid phases: Review on modelling of sorption phenomena, *Coord. Chem. Rev.,* **2012,** *256*, 28-45.

158. C. Pink, H.-t. Wong, F.C. Ferreira, A.G. Livingston, Organic solvent nanofiltration and adsorbents; a hybrid approach to achieve ultra low palladium contamination of post coupling reaction products, *Org. Process Res. Dev.,* **2008,** *12*, 589-595.

159. K.Y. Foo, B.H. Hameed, Insights into the modeling of adsorption isotherm systems, *Chem. Eng. J.,* **2010,** *156*, 2-10.

160. A. Lapkin, D.J.C. Constable, Green Chemistry Metrics: Measuring and Monitoring Sustainable Processes. *John Wiley & Sons, Ltd*, 2008.

161. J. Kindervater, J. Manley, R. Henderson, Lessons learned through measuring green chemistry performance – The pharmaceutical experience, *ACS Green Chem. Inst.,* **2007**.

162. R. Gani, C. Jiménez-González, D.J.C. Constable, Method for selection of solvents for promotion of organic reactions, *Comput. Chem. Eng.,* **2005,** *29*, 1661-1676.

163. R.K. Henderson, C. Jiménez-González, D.J.C. Constable, S.R. Alston, G.G.a. Inglis, G. Fisher, J. Sherwood, S.P. Binks, A.D. Curzons, Expanding GSK's solvent selection guide – embedding sustainability into solvent selection starting at medicinal chemistry, *Green Chem.,* **2011,** *13*, 854.

164. D.J.C. Constable, C. Jimenez-gonzalez, R.K. Henderson, Perspective on Solvent Use in the Pharmaceutical Industry, *Org. Process. Res. Dev.,* **2007,** *11*, 133-137.

165. K.K. Sirkar, P.V. Shanbhag, A.S. Kovvali, Membrane in a Reactor: A Functional Perspective, *Ind. Eng. Chem. Res.,* **1999,** *38*, 3715-3737.

166. I.F. Vankelecom, Polymeric membranes in catalytic reactors, *Chem. Rev. (Washington, DC, U. S.),* **2002,** *102*, 3779-3810.

167. C.H. Paul, A.T. Royappa, Acid binding and detritylation during oligonucleotide synthesis, *Nucleic Acids Res.,* **1996,** *24*, 3048-3052.

168. M.A. Russell, A.P. Laws, J.H. Atherton, M.I. Page, The kinetics and mechanism of the acid-catalysed detritylation of nucleotides in non-aqueous solution, *Org. Biomol. Chem.,* **2009,** *7*, 52-57.

169. A.B. Ghisaidoobe, M.C. de Koning, H.I. Duynstee, P.B. Ten Kortenaar, H.S. Overkleeft, D.V. Filippov, G.A. van der Marel, A two-step sulfurization for efficient solution-phase synthesis of phosphorothioate oligonucleotides, *Tetrahedron Lett.,* **2008,** *49*, 3129-3132.

170. A.V. Volkov, V.V. Parashchuk, D.F. Stamatialis, V.S. Khotimsky, V.V. Volkov, M. Wessling, High permeable PTMSP/PAN composite membranes for solvent nanofiltration, *J. Membr. Sci.,* **2009,** *333*, 88-93.

171. K. Hendrix, M. Van Eynde, G. Koeckelberghs, I.F.J. Vankelecom, Crosslinking of modified poly(ether ether ketone) membranes for use in solvent resistant nanofiltration, *J. Membr. Sci.,* **2013,** *447*, 212-221.